This electronic thesis or dissertation has been downloaded from the King's Research Portal at https://kclpure.kcl.ac.uk/portal/



Optimising combinatorial microbicide delivery for prevention of colorectal HIV infection

Swedrowska, Magda

Awarding institution:
King's College London

The copyright of this thesis rests with the author and no quotation from it or information derived from it may be published without proper acknowledgement.

END USER LICENCE AGREEMENT



Unless another licence is stated on the immediately following page this work is licensed

under a Creative Commons Attribution-NonCommercial-NoDerivatives 4.0 International

licence. https://creativecommons.org/licenses/by-nc-nd/4.0/

You are free to copy, distribute and transmit the work

Under the following conditions:

- Attribution: You must attribute the work in the manner specified by the author (but not in any way that suggests that they endorse you or your use of the work).
- Non Commercial: You may not use this work for commercial purposes.
- No Derivative Works - You may not alter, transform, or build upon this work.

Any of these conditions can be waived if you receive permission from the author. Your fair dealings and other rights are in no way affected by the above.

Take down policy

If you believe that this document breaches copyright please contact librarypure@kcl.ac.uk providing details, and we will remove access to the work immediately and investigate your claim.

Download date: 08. Oct. 2023

Optimising combinatorial microbicide delivery for prevention of colorectal HIV infection

Magda Swędrowska

A thesis submitted to King's College London in partial fulfilment for the degree of

Doctor of Philosophy

Supervisors:

Prof. Benjamin Forbes

Prof. Charles Kelly



Institute of Pharmaceutical Science

Faculty of Life Sciences & Medicine

King's College London

Abstract

A combination of antiretroviral drugs, tenofovir, dapivirine and darunavir, provide enhanced antiviral activity compared to a single agent when tested *in-vitro*. However, the impact of co-formulation on drug absorption after topical delivery to the colorectal mucosa is unclear, and methods are required to screen for drug-drug interactions. The main aim of this project was to establish methods to determine drug transport mechanisms and interactions of three antiretroviral drugs for colorectal topical delivery to permit the rational composition of an optimized formulation.

The first stage of the project focused on developing and optimizing a colorectal model for studying drug permeability across *in-vitro* and *ex-vivo* models, which comprised of a Caco-2 cell line and colorectal tissue mucosal segments, respectively. Once experimental conditions were optimized, the permeability of tenofovir, dapivirine and darunavir were measured experimentally. Selected inhibitors and substrates of ABC-efflux pump transporters were used to establish the mechanism of drug transport. Furthermore, drugs were co-formulated and tested for drug-drug interactions, cross reaction between transporters and effect on net drug transport across the monolayer. An *in-silico* screening was also performed to identify the potential for molecular interactions of tenofovir, dapivirine and darunavir with the P-glycoprotein transporter.

The combination of *in-vitro*, *ex-vivo* and *in-silico* studies for tenofovir and darunavir showed that tenofovir is passively paracellularly transported across the epithelium, whereas darunavir is transported transcellularly and is a substrate for P-gp and MRP2 transporters. Dapivirine did not exhibit any active transport in the *in-vitro* model, although it showed very strong binding affinity to P-gp structure in the *in-silico* model. The permeability of the compounds ranked in accordance with their lipophilicity: tenofovir < darunavir < dapivirine. Co-administration of the ARV drugs did not influence the permeability or intracellular accumulation of the individual drugs. Film formulations containing darunavir were tested and demonstrated drug release and uptake by epithelial cells showing potential for further development as a protective microbicide formulation for the prevention of colorectal transmission of human immunodeficiency virus.

Acknowledgments

I would like to thank my supervisor Ben Forbes, without whom this thesis would not have been possible and for believing in my potential, even before the start of this PhD. I would like to especially thank him for his support, encouragement and letting me take responsibility for my project.

I would also like to thank my second supervisor Professor Charles Kelly and all collaborators- Dr Khondaker Miraz Rahman, Dr Shirin Jamshidi and Dr Julia Mantaj for helping me in carrying out all the research. I would like to thank Dr Abhinav Kumar for his support that he gave me and for being always available and helpful.

I would like to thank my friends and colleagues from King's College London, QMUL and Erasmus students for all their support and motivation over the last few years. My time would not be the same without you all. I would most of all like to thank, James and my family for all of their support they gave me throughout this work.

List of Publications

Publications:

Kumar A, Dailey LA, Swedrowska M, Siow R, Mann G, Vizcay-Barrena G, Arno M, Mudway I, Forbes B. Quantifying the magnitude of the oxygen artefact inherent in culturing airway cells under atmospheric oxygen versus physiological levels. FEBS Letter. 2016, 2, 258-269.

Chua H, Hauet Richer N, Swedrowska M, Ingham S, Tomlin S, Forbes B. Dissolution of intact, divided and crushed circadin tablets: Prolonged vs. Immediate release of melatonin. Pharmaceutics 2016, 8, 1-11.

Swedrowska M, Ingham S, Tomlin S, Forbes B. Crushing of melatonin tablets for safe and reliable delivery via adult and pediatric nasogastric tubes. Pharmaceutics (manuscript in preparation).

Swedrowska M, Jamshidi S, Kumar A, Charles K, Rahman KM, Forbes B. *In-silico, in-vitro* and *ex-vivo* screening of drug-drug transporter interactions in an antiretroviral drug combination for prevention of colorectal HIV transmission. Molecular Pharmaceutics (manuscript submitted).

Talks and Presentations:

Swedrowska M, Kumar A, Charles K, Forbes B. Optimising topical delivery for prevention of colorectal HIV infection. APS-PharmSci2015, 2015, Nothingam, UK.

Swedrowska M, Kumar A, Charles K, Forbes B. Transport characteristics of antiretroviral drugs- single agents, double and triple combinations in Caco-2 cells. HIV R4P 2014 Cape Town International Conference, 2014, Cape Town, SA.

Swedrowska M, Kumar A, Charles K, Forbes B. Tissue Permeability and drug-drug interactions of darunavir in intact rabbit colorectal tissue. MOTIF Consortium meeting, 2014, Paris, France.

Swedrowska M, Kumar A, Charles K, Forbes B. Can microbicide transport be modified by rectal gel formulation? APS-PharmSci2013, 2013, Edinburgh, UK.

Table of Contents

Abstract ..... **II**

Acknowledgments ..... **III**

List of Publications ..... **IV**

Table of Contents ..... **V**

List of Figures ..... **X**

List of Tables ..... **XV**

List of Abbreviations ..... **XVII**

Chapter One: Introduction **1**

1.1. Microbicides for prevention of HIV transmission **2**

1.1.1 Microbicidal agents and formulations 2

1.1.2 Mechanism of action of antiretroviral drugs 4

1.1.3 Combination-based microbicide formulations 6

1.2. Colorectal anatomy and challenges in colorectal drug delivery. 7

1.2.1 Function of the colorectal epithelium 7

1.2.2 Paracellular route of absorption 9

1.2.3 Transcellular route of absorption 11

1.2.4 Active transport 13

1.2.5 Models for studying the colorectal absorption of drugs 21

1.3. Role of protein transporters in antiretroviral drugs absorption **28**

1.3.1 Tenofovir 30

1.3.2 Dapivirine 34

1.3.3 Darunavir 35

1.4. Aim and scope of the thesis **38**

Chapter Two: Materials and Methods.....39

2.1. Materials and Reagents.....40

2.2. Optimising Caco-2 cell model culture conditions.....43

2.2.1. Cell culture conditions.....43

2.2.2. Cell layer morphology and protein expression.....43

2.2.3. Cell-based assays for evaluating compounds toxicity.....47

2.2.4. Test solutions.....49

2.2.5. Data and statistical analysis.....49

2.3. Drug transport across Caco-2 cell monolayers.....50

2.3.1. Measurement of apparent permeability.....50

2.3.2. Test solutions.....52

2.3.3. Sample analysis.....52

2.3.4. Transepithelial electrical resistance (TER).....52

2.3.5. Transport data analysis.....53

2.3.6. Drug uptake studies.....54

2.3.7. Total Protein measurements.....54

2.3.8. Enzyme linked Immunosorbent assay (ELISA).....55

2.3.9. Data and statistical analysis.....56

2.4. The effect of film formulation on drug transport across Caco-2 cell monolayers.....57

2.4.1. Validation of a sensitive liquid chromatographic tandem mass spectrometer (LC-MS/MS) assay for darunavir.....57

2.4.2. Method verification.....58

2.4.3. Data and statistical analysis.....60

2.4.4. Dissolution profile of darunavir in a film formulation.....60

2.5. Drug transport across colorectal tissue segments.....63

2.5.1. Animal welfare.....63

2.5.2. Tissue preparation 63
2.5.3. Krebs solution 64
2.5.4. Test solutions 64
2.5.5. ARV drug permeability across colo-rectal tissue segments 65
2.5.6. Data and statistical analysis 65
2.6. *In-silico* modelling of ARV drug binding to P-glycoprotein 66
2.6.1. Molecular docking of ligands with P-glycoprotein 66
2.6.2. Molecular Dynamics simulations of P-gp in complex with compounds 67
Chapter Three: Results 69
3.1. Optimizing *in-vitro* model conditions 70
3.1.1. Characterisation of Caco-2 cells 70
3.1.2. Cell layer morphology, protein expression and barrier properties 71
3.1.3. Cell based assays for evaluating compound toxicity 75
3.1.4. Cell viability and membrane damage 76
3.1.5. Caco-2 cell permeability and P-gp transporter activity 83
3.2. Tenofovir, dapivirine and darunavir transport across Caco-2 cell monolayers 89
3.2.1. Tenofovir transport across Caco-2 cell monolayers 89
3.2.2. Dapivirine transport across Caco-2 cell monolayers 94
3.2.3. Darunavir transport across Caco-2 cell monolayers 100
3.2.4. Effect of co-administrations of tenofovir, dapivirine and darunavir on permeability in Caco-2 cell monolayers 108
3.2.5. Permeability of tenofovir and darunavir in inflamed Caco-2 cell monolayers and the effect of film formulations on secretion of selected interleukins 114

3.3. Effect of formulations on ARV permeability in Caco-2 cell monolayers 117

3.3.1. Effect of GRAS excipients used in formulation on modulating tenofovir, dapivirine and darunavir permeability across Caco-2 cell monolayers 117

3.3.2. The impact of prototype formulations on drug absorption across Caco-2 cell monolayers 121

3.4. Permeability of tenofovir and darunavir in *ex-vivo* colorectal tissue 129

3.5. Molecular docking of ligands with P-glycoprotein 135

3.5.1. Molecular docking of mannitol and digoxin with P-glycoprotein ... 135

3.5.2. Molecular docking of tenofovir, darunavir and dapivirine with P-glycoprotein 137

3.5.3. Molecular dynamics simulation of P-gp in complex with mannitol and digoxin 139

3.5.4. Molecular dynamics simulation of P-gp in complex with dapivirine and darunavir 142

Chapter Four: Discussion 147

4.1. General discussion 148

4.2. Tenofovir, dapivirine and darunavir transport across Caco-2 cell monolayers. 150

4.3. Screening the impact of co-formulation on ARV drug absorption across Caco-2 cell monolayers 165

4.4. Tissue permeability and drug-drug interactions of tenofovir and darunavir in intact *ex-vivo* colorectal tissue 171

4.5. Molecular docking of ligands with P-glycoprotein 173

Chapter Five: Conclusion & Future Work 176

5.1. Conclusion 177

5.2. Future work 179

Bibliography 181

List of Figures

Figure 1. Mechanism of antiretroviral drugs targeting the viral life cycle of HIV. 5

Figure 2. Schematic diagram of passive and active transport across cell membrane. 8

Figure 3. A schematic figure showing the thickness of the mucus across gastrointestinal t tract (o- outer loose mucus layer, s- firmly adherent mucus layer). 9

Figure 4. Schematic structure of crystal structure of P-gp transporter protein. 17

Figure 5. Structure of tenofovir disoproxil fumarate and its metabolites. 31

Figure 6. Structure of darunavir and its metabolites. 37

Figure 7. Schematic diagram of the set-up of Western blot sandwich. 45

Figure 8. Schematic diagram of the Transwell and the staining of tight junction protein ZO-1 on Caco-2 cells after 21 days in culture 50

Figure 9. Schematic diagram of experimental system to study drug transport in Caco-2 cell model. 51

Figure 10. Schematic diagram of experimental system for studying drug transport in the presence of inhibitor (or formulation excipients). 52

Figure 11. Schematic diagram of dissolution and permeation process in the Transwell®. 62

Figure 12. Schematic diagram of mounting colorectal tissue segments to vertical diffusion chambers. 64

Figure 13. Caco-2 cells grown on Transwell inserts after: a) day 2 × 100 magnification, b) day 2 × 400 magnification, c) day 3 × 200 magnification and d) day 13 × 200 magnification. 70

Figure 14. Protein expression of MDR1/ P-gp, MRP-2 and BCRP 71

Figure 15. The staining of tight junction protein ZO-1 on Caco-2 cells after 21 days in culture. 72

Figure 16. The variation of transepithelial electrical resistance (TER) with days in culture for Caco-2 cells. 73

Figure 17. The relationship between Caco-2 cell number vs. absorbance measured using the MTT assay. 75

Figure 18. Relationship of cellular metabolic activity versus increasing concentration of DMSO (0.1 - 5%) after 24 h of DMSO exposure to Caco-2 cells at day 2 in culture. 76

Figure 19. The effect of 24 h exposure of varying concentration of digoxin on the viability of Caco-2 cells..... 77

Figure 20. The correlation between cellular LDH release and metabolic activity from Caco-2 cells at 14^{th} day of culture after exposure to Digoxin for 24 h..... 78

Figure 21. The effect of different concentration of tenofovir on Caco-2 cells (at 2^{nd}, 7^{th} and 14^{th} day of culture) after 24 h of exposure to drug..... 79

Figure 22. The effect of different concentrations of dapivirine on Caco-2 cells (cultured for 2, 7, or 14 days) after 24 h of exposure..... 80

Figure 23. The correlation between cellular LDH release and metabolic activity of Caco-2 cells cultured for 2 (orange), 7 (green) or 14 (blue) days and exposed to Digoxin for 24 h. 81

Figure 24. The effect of different concentration of Darunavir on Caco-2 cells (cultured for 2, 7, or 14 days) after 24 h of exposure. 82

Figure 25. Flux of a) Digoxin 10 µM b) C^{14}-Mannitol with respect to time in both apical-to-basolateral (red line) and basolateral-to-apical (blue line) directions across Caco-2 cell monolayers. 83

Figure 26. Permeability of mannitol and digoxin..... 84

Figure 27. Effect of co-administering varying concentration of a) verapamil 0.2 – 10 µM b) CsA 0.2 – 10 µM on the absorptive and secretory permeability of digoxin 10 µM across Caco-2 cell monolayers. 86

Figure 28. Effect of varying concentration of a) verapamil 0.0001 – 10 µM, b) CsA 0.0001 – 10 µM on the accumulation of digoxin 10 µM by Caco-2 cells..... 86

Figure 29. Efflux ratio measured in Caco-2 cell monolayers for digoxin 10 µM and digoxin 10 µM in the presence of: PEG 200 1% (v/v), PEG 400 1% (v/v), PEG 200 1% (v/v) with verapamil 10 µM and PEG 400 1% (v/v) with verapamil 10 µM... 88

Figure 30. Maintenance of TER during tenofovir exposure and tenofovir flux across Caco-2 cell monolayers. 90

Figure 31. Permeability of varying concentration of tenofovir (0.1 - 100 µM)..... 92

Figure 32. Influence of transporter inhibitors on tenofovir permeability and cell uptake. 93
Figure 33. Permeability of varying concentration of dapivirine in the presence of different transport solutions. 96
Figure 34. Maintenance of TER during dapivirine exposure and dapivirine flux across Caco-2 cell monolayers. 97
Figure 35. Permeability of varying concentrations of dapivirine (0.1 - 10 µM) 98
Figure 36. Influence of transporter inhibitors on the permeability of dapivirine 10 µM across Caco-2 cell monolayers. 99
Figure 37. Effect of transporter inhibitors on the accumulation of dapivirine 10 µM by Caco-2 cells in 48-well plates after 21 days in culture. 100
Figure 38. Maintenance of TER during darunavir exposure and darunavir flux across Caco-2 cell monolayers. 101
Figure 39. Permeability of darunavir 0.1 - 100 µM. 103
Figure 40. Influence of P-gp transporter inhibitors on darunavir permeability. 104
Figure 41. Influence of MRP-2 and BCRP transporter inhibitors on darunavir permeability. 106
Figure 42. Influence of transporter inhibitors on darunavir permeability. 106
Figure 43. Effect of transporter inhibitors on the accumulation of darunavir 10 µM by Caco-2 cells. 107
Figure 44. Drug transport of tenofovir in double combinations. 109
Figure 45. Drug transport of tenofovir in triple combination. 109
Figure 46. Drug transport of Dapivirine in double combinations. 110
Figure 47. Drug transport of dapivirine in triple combination. 110
Figure 48. Drug transport of darunavir in double combinations. 111
Figure 49. Drug transport of darunavir in triple combination. 112
Figure 50. Intracellular accumulation of individual ARVs drugs when co-formulated into double combinations. 113
Figure 51. IL-8 secretion by Caco-2 cell monolayers exposed IL-1 β (inflammatory stimuli) in range of concentrations between 0.1 and 25 ng/ml IL-1 β. 115
Figure 52. Permeability of tenofovir and darunavir across Caco-2 cells after being exposed to inflammatory stimuli. 116

Figure 53. Influence of excipients on tenofovir 100 µM permeability..... 118
Figure 54. Influence of excipients on dapivirine 10 µM permeability..... 119
Figure 55. Influence of excipients on darunavir 10 µM permeability.. 120
Figure 56. Calibration curve for darunavir in the range of 0.01 – 10 µg/mL..... 121
Figure 57. The effect of the film formulations (containing darunavir (blue bars) and placebo film (red bars) - 0.0314 cm^2 film) immersed in different volumes at the apical side of the membrane on Caco-2 cell viability. 124
Figure 58. The variation of TER measurements in the presence of darunavir and placebo film immersed in 100 µL HBBS at the apical side of the membrane across Caco-2 cell monolayers.. 125
Figure 59. The variation of TER measurements in the presence of darunavir and placebo film immersed in 500 µL HBBS at the apical side of the membrane across Caco-2 cell monolayers. 125
Figure 60. Dissolution and transfer of darunavir from film formulations (0.148 mg darunavir in 0.196 cm^2 film in 0, 28, 100 and 500 µL of HBSS solution) across Caco-2 cell monolayers or across cell-free system after placement at the apical side of the monolayer in the Transwell diffusion system. 126
Figure 61. Dissolution and transfer of darunavir from a film formulations; 0.148 mg darunavir in 0.196 cm^2 film or 0.0237 mg darunavir loaded in 0.0314 cm^2 film immersed in 500 µL of HBSS solution in a Transwell diffusion system across Caco-2 cell monolayers or across cell-free system for 180 min time period..... 127
Figure 62. Dissolution and transfer of darunavir from a film formulations; 0.148 mg darunavir in 0.196 cm^2 film immersed in 500 µL of HBSS solution in the absence and in the presence of verapamil 100 µM and bromosulphalein 50 µM in a Transwell diffusion system across Caco-2 cell monolayers or across cell-free system. 128
Figure 63. Electrical parameters in guinea-pig, rat and rabbit colorectal tissue segments. 130
Figure 64. Mannitol and tenofovir transport across rat colorectal tissue segments. 132
Figure 65. Tenofovir permeability in colo-rectal tissue segments..... 133
Figure 66. Darunavir transport across rabbit tissue segments.. 134

Figure 67. Docking of mannitol (negative control; non-P-gp substrate) and digoxin (positive control; P-gp substrate) in yellow colour to a modelled P-gp transporter protein. 135

Figure 68. Docking of tenofovir, darunavir and dapivirine (in yellow colour) to a P-gp efflux pump. 137

Figure 69. Drug - P-gp transporter complexes in the transmembrane domain after MD simulation and the most important interactions determined by the 50 ns molecular simulation (a) mannitol, (b) digoxin. 140

Figure 70. Most important interaction after 50 ns MD stimulation between a) mannitol b) digoxin and P-gp efflux pump. 141

Figure 71. Drug - P-gp transporter complexes in the transmembrane domain after MD simulation and the most important interactions determined by the 50 ns molecular simulation (a) dapivirine, (b) darunavir. 143

Figure 72. Most important interaction after 50 ns MD stimulation between a) darunavir b) dapivirine and P-gp efflux pump. 144

Figure 73. Time dependence of root-mean-square deviation (RMSD) (Å) of P-gp for the backbone atoms in the course of MD simulations in the complexes and ligand-free protein. 145

Figure 74. Atomic positional fluctuations (Å) of Cα atoms in the ligand-bound systems compared with the ligand-free P-gp. 145

Figure 75. Fluctuations in the hydrogen bond distance between Dapivirine NH1 and Ser-693, during 50 ns MD trajectories. 146

Figure 76. Fluctuations in hydrogen bond distance between Darunavir O1 and Tyr-274, during 50 ns MD trajectories 146

Figure 77. The absorptive permeability of tenofovir, darunavir and dapivirine in the context of reported permeability of drugs in Caco-2 monolayers in similar experiments as a function of octanol-water partition coefficients. 155

List of Tables

Table 1. Electrical characteristic of epithelial tissues and cells [50]. 11

Table 2. Kinetic interaction between antiretroviral drugs and drug transporters, with K_m and IC_{50} provided in brackets where known. 14

Table 3. Advantages and disadvantages using different methods for drug transport. 22

Table 4. Comparison between different colorectal cell lines. 25

Table 5. Effect of transport inhibitor CsA and select protease inhibitors (PIs) on the bidirectional permeation of TDF and TFV across MDCKII-MDR1 and Caco-2 cells. 33

Table 6. TER values of Caco-2 cells (21 days in culture) after exposure to different media in the apical and basolateral chamber for 120 min.. 74

Table 7. Total recovery of mannitol and digoxin after 2h incubation period at the apical side of Caco-2 cell monolayers. 84

Table 8. Acceptance criteria for drug transport assay. 85

Table 9. Recovery of mannitol and varying concentrations of tenofovir after 120 min absorptive or secretory permeability assays across Caco-2 cell monolayers 91

Table 10. Recovery of dapivirine and mannitol after 2 h absorptive permeability assay in Caco-2 cells in the presence of different transport medium in the receiver chamber 95

Table 11. Recovery of mannitol and darunavir after absorptive and secretory permeability assays in Caco-2 cell monolayers 102

Table 12. The intra and inter-day variation at the range of concentrations of darunavir tested for LC-MS/MS system. 122

Table 13. Apparent permeability coefficient (P_{app}), efflux ratio and recovery of ^{14}C-mannitol, digoxin 10 µM and digoxin 10 µM in the presence of Verapamil 100 µM across guinea-pig, rat and rabbit colorectal mucosal segments. 131

Table 14. Gold molecular docking the best 10 poses for mannitol and digoxin in TMDs domain. 136

Table 15. Gold molecular docking the best 10 poses for tenofovir, darunavir and dapivirine in TMDs domain..... 138

Table 16. Average energy contributions to form of mannitol and digoxin complexes with P-gp..... 139

Table 17. Average energy contributions to form of dapivirine and darunavir complexes with P-gp..... 142

List of Abbreviations

A-B	Apical to basolateral
ABC	ATP-binding cassette
ANOVA	Analysis of variance
API	Active pharmaceutical ingredient
ARV	Antiretroviral
ATP	Adenosine triphosphate
B-A	Basolateral to apical
BCRP	Breast cancer resistance protein
BSA	Bovine serum albumin
C_0	Initial concentration
Caco-2	Epithelial cell line derived from human colonic carcinoma
CPM	Counts per minute
CV	Coefficient of variance
CYP	Cytochrome
DMSO	Dimethyl sulfoxide
ELISA	Enzyme-linked immunosorbent assay
FBS	Fetal bovine serum
FDA	Food and drug administration
GOLD	Genetic optimization of ligand docking
GRAS	Generally recognised as safe
HAART	Highly active anti-retroviral therapy
HBSS	Hank's balanced salt solution
HIV	Human immunodeficiency virus
IC_{50}	Half maximal inhibitory concentration
LC-MS/MS	Liquid chromatography-tandem-mass spectroscopy

LDH	Lactate dehydrogenase
LOD	Limit of detection
log P	Log of the partition coefficient
LOQ	Limit of quantification
MRP	Multidrug resistance associated protein
MSM	Men who have sex with men
NBD	Nucleotide binding domain
NHP	Nonhuman primate
NNRTI	Non-nucleoside reverse transcriptase inhibitor
P_{app}	Apparent permeability
PBS	Phosphotate buffered saline
PEG	Polyethylene glycol
P-gp	P-glycoprotein
PI	Protease inhibitor
R^2	Regression correlation coefficient
SD	Standard deviation
SEM	Standard error of the mean
TER	Transepithelial electron microscopy
TMD	Transmembrane domain
ZO	Zonula occludens

Chapter One
Introduction

1.1. Microbicides for prevention of HIV transmission

Microbicides are compounds intended to prevent or significantly reduce sexual transmission of human immunodeficiency virus (HIV) infection [1]. The need for anti-HIV microbicides arises from the continuing HIV epidemic. According to UNAIDS 2015 report; an estimated 36.7 million people worldwide are living with HIV and each year approximately 2.1 million people become newly infected with HIV [2].To date, research into developing efficient and safe microbicides has been largely focused on the products designed to prevent vaginal transmission of HIV. However, the risk of HIV transmission during anal intercourse is about 18-fold greater than during vaginal intercourse [3]. The rate of HIV infection among men who have sex with men (MSM) represents the largest group of new HIV infection in North America, Australia and Western Europe. Additionally anal intercourse remains a significant problem driving the heterosexual epidemics in sub-Saharan Africa and often these cases are underreported [4]. The use of highly active antiretroviral therapy (HAART) has greatly improved treatment options for HIV, however is not curative and prospects for an HIV vaccine seem ever distant [5], [6]. Other methods of preventing the spread of HIV, including behavioural changes, condom usage and male circumcision, have had limited success [7]. Thus, attention is now focusing on developing microbicides for topical colorectal application which would restrict or minimize the transmission of HIV infection.

1.1.1 Microbicidal agents and formulations

Microbicides can be applied topically in the rectum or vagina in a variety of formulations e.g. vaginal ring, capsule, suppository, film or gel [8]. They are designed to deliver compounds over prolonged periods of time (vaginal ring) or be used around the time of sexual intercourse, applied on a daily basis (film and gel). Microbicides have been typically classified as non-specific and specific. Compared to the several choices for vaginal delivery of microbicides agents, current topical rectal microbicides are more likely to take the form of gels, enema-like products and suppositories. To date, rectal microbicide research is in the early phase of clinical studies. The first rectal microbicide studies evaluated the rectal safety of gels that were being developed as vaginal microbicides [9]. Early generation

microbicides are classed as non-specific agents that variously interfere with virus entry, fusion or binding but not with HIV cycle in host cells [10]. Non-specific microbicides that have been tested clinically include surfactants and pH modifiers, although they failed to demonstrate efficacy in clinical trials even after promising data from *in-vitro* studies. The first rectal microbicide to enter safety studies was Nonoxynol-9 (N-9), a detergent-based spermicide. The *in-vitro* studies conducted with N-9 showed efficacy through destruction of the HIV-1 lipid membrane. The first study, by Tabet and co-workers demonstrated that use of N-9 caused only mild rectal histological changes in samples that were collected after 12 hours of exposure to the microbicide [11]. In contrast, Phillips and colleagues [12] showed that 15 minutes of exposure to N-9 was insufficient to prevent HIV infection and caused rapid exfoliation of the rectal epithelium, potentially leading to higher rates of infection [13]. These findings reflected the timing of sample collection, because rectal epithelial reconstruction can occur within 1-8 hours after exposure to N-9 [12]. Other non-specific microbicides were based on low pH, i.e. pH 4.5 like vaginal environment, which inactivates HIV. However, this type of microbicide could not be used for colorectal delivery as the pH of colorectum is 7.4 and lowering the pH to 4.5 with application of microbicide would lead to epithelial damage [14].

The next-generation of microbicides contained more specific anti-retroviral drugs (ARV) which prevent main stages in HIV replication; such as protease inhibitors (PIs), (non-) nucleoside reverse transcriptase inhibitors ((N)NRTIs) and entry inhibitors, which brought promising results in clinical trials [15]. However, the only ARVs which have been evaluated in clinical studies for rectal microbicides are a NNRTI, UC781, and a nucleotide inhibitor tenofovir (TFV). The first generation of ARV rectal microbicides included only one active pharmaceutical ingredient (API), but there is increasing interest in developing combination microbicide formulations containing two or three drugs. Recent studies have mainly focused on NNRTIs (UC781 and dapivirine (TMC120)) or nucleotides (TFV). Protease inhibitors, such as darunavir, are also being considered as candidate rectal microbicides [16], [17]. The first rectal microbicide product which underwent a phase 1 safety trial was non-nucleoside reverse transcriptase inhibitor UC781. UC781 has activity against a wide range of subtype HIV-1 isolates and binds tightly

to HIV-1 reverse transcriptase. In a study, conducted at the University of California at Los Angeles a vaginal product, UC781 gel in two different concentrations 0.1% and 0.25%, was used rectally and found to be highly acceptable to participants and safe by every index used. An interesting feature of the study was that the evaluation of intestinal tissue explants exposed to UC781 *in-vivo* resisted HIV infection and did not exhibit any change in the colorectal mucosa after product exposure. However, the further development of UC781 did not proceed, because of problems with stability and solubility of ARV agent [18].

Promising preclinical results were evaluated, after developing new 'reduced glycerin' formulations of tenofovir (RG-TFV) 1% gel. Dezzutti et al. found that the new gel induced less rectal mucosal damage than the original formulation of TFV 1% gel used for vaginal administration and the reduction in glycerin compared to the original formulations did not affect activity against HIV or drug release. Overall this study suggested that new formulation of TFV should be advanced to Phase 2 rectal microbicide development and moreover it brings hope that it can be used as a dual compartment gel (for rectal and vaginal use) [19].

1.1.2 Mechanism of action of antiretroviral drugs

The viral life cycle is well known (**Error! Reference source not found.**) h owever the exact process of viral transmission *in-vivo* remains uncertain. The first point, at which microbicides could prevent initial transmission of the HIV-1, is when virus crosses the mucosal epithelium in rectum. Topical microbicides have a limited period of time in which to block the infection. A study by Hu J. et al. in a nonhuman primate (NHP) model showed that 30-60 min was sufficient to establish an infection after exposure to an infectious virus [6]. At this stage the virus attaches to target cells, so this time period is critical for prevention of initial infection by drugs which act as entry inhibitors. After the early infection is established an initial foci forms during the next 16-72 h within the mucosal epithelium. During this phase of infection, topical microbicides containing integrase inhibitors and reverse transcriptase that target pre-integration steps in the viral lifecycle could inhibit the establishment of such foci. Local viral replication is followed by dissemination of virus into regional lymph nodes; at this point systemic infection is established. The local expansion could be prevented by protease inhibitors which are able to inhibit

production of virus from the initial foci of infection. Efficient and safe microbicide prevention of transmission requires the delivery of appropriate drugs at a suitable concentration to these important target sites [13].

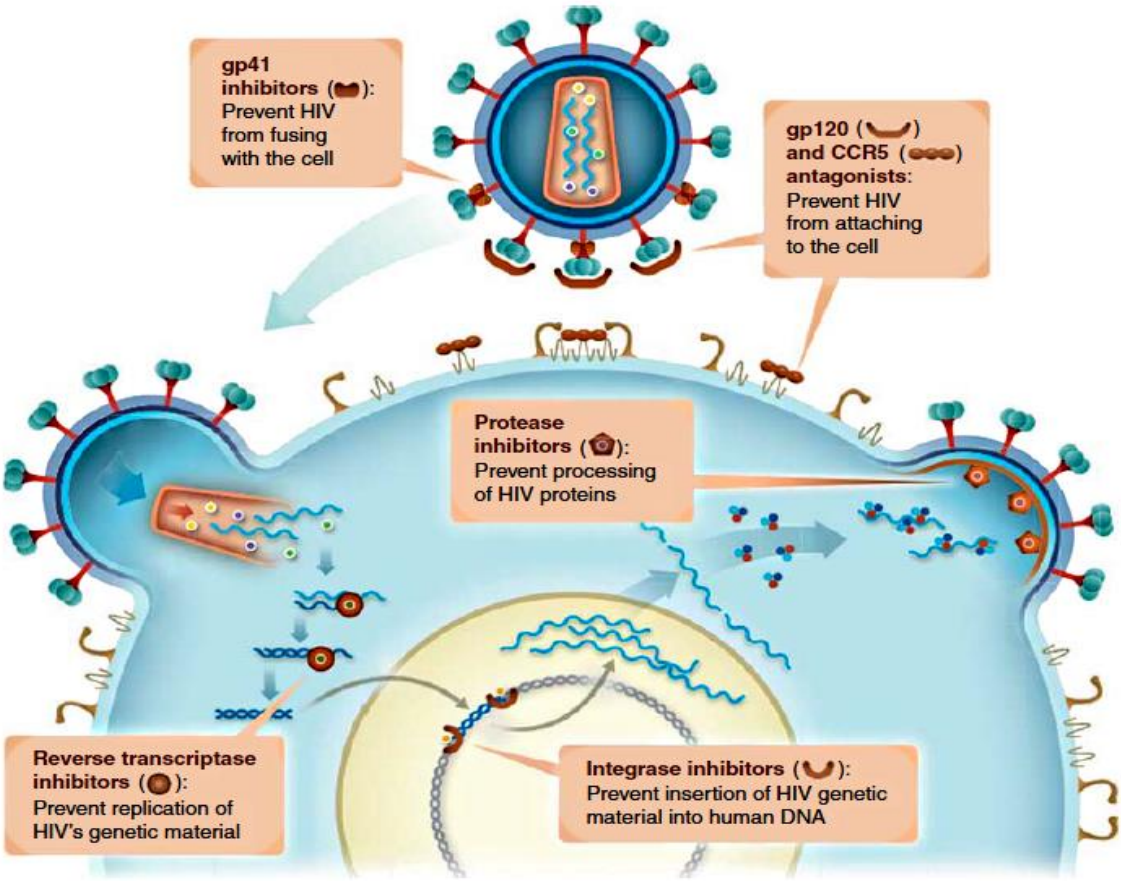


Figure 1. Mechanism of antiretroviral drugs targeting the viral life cycle of HIV [13].

1.1.3 Combination-based microbicide formulations

Development of effective next-generation topical microbicides for colorectal application should focus on combination-based microbicides. The strategy of mucosal application of microbicides containing a single ARV is compromised by increasing problems of drug resistance strains. Around 10-20% of new infections in the developed world are caused by strains resistant to at least one of three (PIs, NNRTIs, NRTIs) main types of ARV drugs [20]. The potential for resistance to arise from topical use of a single drug containing microbicide remains theoretical, but should be considered in development programmes. The combination of two-three drugs with different mechanism of actions is less likely to give rise to resistant strains. In addition, ARV combinations may have synergistic or additive activity and reduce the IC_{50} compared to the IC_{50} values of the individual drugs; i.e. provide more potent activity against HIV. In addition, combination-based microbicides that interfere with different stages in the transmission process and the viral life cycle may provide a better chance of protection. However, practical issues, hinder the development of combination-based microbicide. Co-formulating multiple ARV agents to provide two or three drugs are combined in the same product brings the concern about stability and drug-drug interactions [13], [21].

1.2. Colorectal anatomy and challenges in colorectal drug delivery

The rectal tract is more vulnerable to HIV transmission than the vaginal compartment on account of differences in immunology and histology [22]. The rectum is the posterior part of the large intestine and extends over 12-19 cm distally. The surface area of the rectum is approximately 200-400 cm^2 and the rectal environment has a neutral pH around 7.4-8 [16], [23]. In contrast to the multiple layers of stratified squamous epithelium present in female genital tract, which constitute an important physical barrier to HIV infection, the rectal mucosa has a single layer of columnar epithelium which separates the lumen from the lamina propria [24]. The rectal epithelium does not contain a traditional receptor for HIV-1, but the subepithelial tissue contains multiple viral targets. Columnar epithelium cells present in the colorectum do not express CD4, however they express CXCR4, which makes them susceptible to CD4-independent HIV-1 infection. Additionally, the rectum is populated with lymphoid tissues that contains specialized microfold cells (M cells), that are capable of binding and presenting the infecting virus to the underlying organized lymphoid tissue. The lamina propria is also densely populated with cells that are susceptible to HIV infection such as macrophages, dendritic cells and T cells that express CD4, CXCR4 and CCR5 [22], [25]. Differences in the physiological and anatomical characteristics between vaginal and rectal tract require a rectal microbicide to protect a higher number of potential target cells over a larger area.

1.2.1 Function of the colorectal epithelium

For absorption in the colorectal region of the intestine, a solute needs to pass mucosal surface that is composed of mucus (firmly and loosely adherent mucus layers), single layer of columnar epithelial cells, underlying lamina proporia and muscular mucosa before it reaches blood vessels and the systemic circulation [26]. Columnar epithelial cells create a barrier between the internal milieu and external environment and for most compounds it provides the predominant resistance to absorption. Molecules can be transport across the epithelium via two different routes, through paracellular or transcellular pathways. Tight junctions seal the

paracellular gaps between epithelial cells and create the gates that regulate paracellular transport (passive movement between adjoining cells) of solutes and water across epithelium [27]. Then transcellular pathway involves passive or active movement across cell membranes, including passage via specific transport channels (Figure 2) [28].

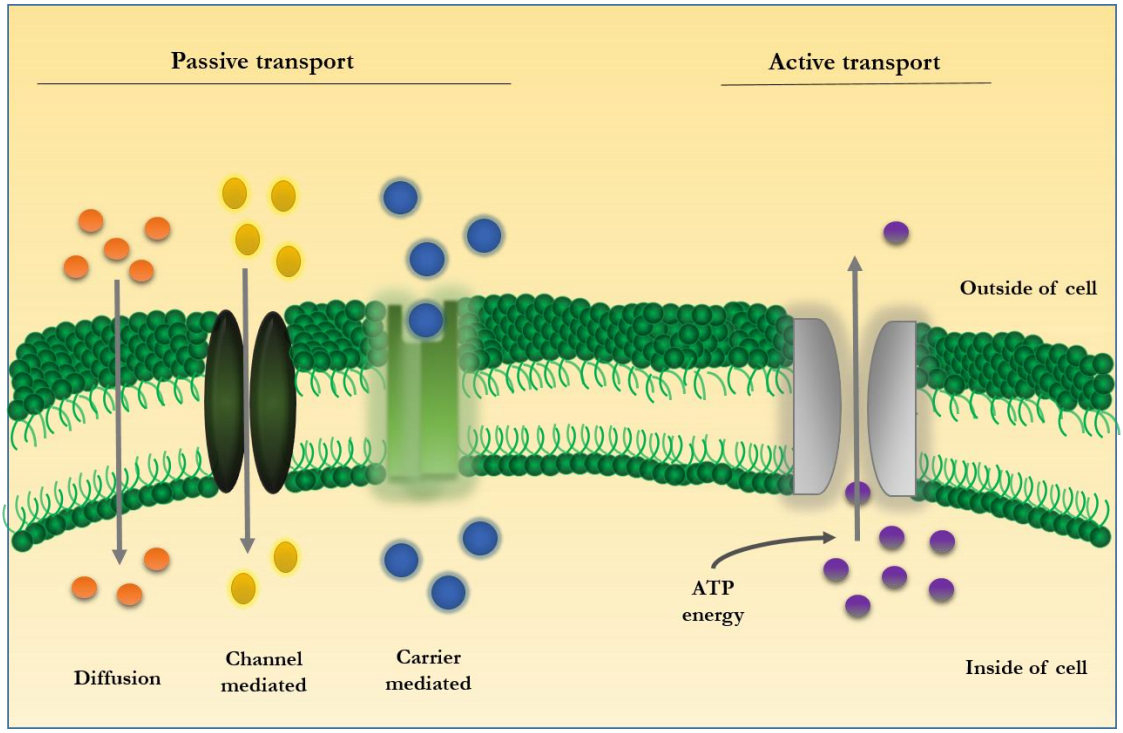


Figure 2. Schematic diagram of passive and active transport across cell membrane.

Specialized columnar epithelial cells (goblet cells) and sub-epithelial glands are present in the epithelial lining and are responsible for secreting the mucus that lines the epithelial surface [28]. The layer of mucus gel that provides a barrier between the lumen and underlying epithelium is secreted throughout gastrointestinal system from the stomach to the rectum (Figure 3) [29]. However, the specific protective function and properties of mucus may differ between different parts of gastrointestinal tract [30], [31]. It has been shown by Holm and colleagues that the mucus layer in the rat colon was the thickest and is composed of two layers: an outer 'loose' layer that can be easily aspirated and an inner mucus layer that is firmly adherent to the epithelium [32]. Moreover, the thickness of the mucus layer increases from ascending colon to the rectum where it reaches up to 285 µm in height [33].

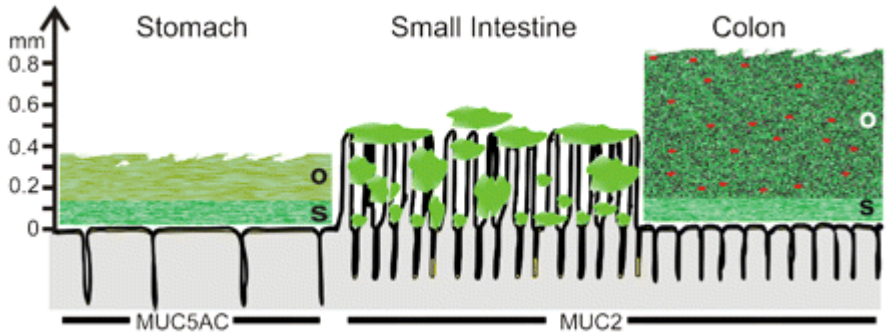


Figure 3. A schematic figure showing the thickness of the mucus across gastrointestinal tract (o- outer loose mucus layer, s- firmly adherent mucus layer) [31].

Mucus is mostly comprised of glycoproteins called mucins, water, lipids and electrolytes and plays an important role as a potential site for binding and drug interaction [34]. Mucus is linked to the apical membrane by the glycocalyx that is covalently bound to the brush membrane and is a component of unstirred water layer [35]. This layer hinders diffusion and may adversely affect the absorption of molecules according to the solubility, lipophilicity and size of the diffusing compound [30]. It was demonstrated by Wikman and colleagues that the permeability rate of hydrophobic compound- testosterone across HT29-H cells with mucus was slower as compared to the absorption when the mucus layer was removed from the monolayers [36].

1.2.2 Paracellular route of absorption

The transport of molecules by paracellular route is regulated by tight junctions and is limited by the size of the intercellular pores (radius between 10-50 Å) that excludes compounds with molecular with a radius > 15 Å from uptake via this route [37]. Small hydrophilic compounds (ions, water, weak electrolytes etc.) use paracellular route as their main mechanism of transepithelial transport, with transfer in both directions via diffusion according to the concentration gradient. Tight junctions are only one of the three components of junctional complexes that connect epithelial cells, which also possess adherens junctions and desmosomes which provide mechanical links between adjacent cells [38]. However, tight junctions have the major function in intercellular sealing and are responsible for 1) regulating the barrier afforded by the gaps between cells 2) providing separation

between compositionally distinct apical and basolateral cell membrane surface [39]. Tight junctions are very complex structure that is composed of cytoplasmic plague proteins; zona occludens 1, 2, 3 (ZO-1, ZO-2, ZO-3), 7H6 and cingulin and transmembrane proteins: claudin and occludin amongst others [40], [41].

The tightness of the intercellular junctions and integrity of the monolayer are measured in *in-vitro* models by electrical resistance and by measuring the flux of paracellular route markers (e.g. mannitol, rantidine and lucifer yellow) and may vary between different epithelial cells and their functionality in the system (Table 1) [42], [43]. Electrical resistance varies between 'leaky' and 'tight' junctions present in epithelium by even more than 10^5 fold. For instance, transepithelial resistance in the 'leaky' proximal tube approaches only 6 $\Omega \cdot cm^2$, whereas 'tight' junctions in urinary bladder mean that resistance reaches more than 300,000 $\Omega \cdot cm^2$ [27], [44], [45].

The tightness of intracellular junctions can be modulated by absorption/penetration enhancers to increase the absorption of drugs with low permeability [46]. These enhancers can be divided into two groups. The first generation open tight junctions through secondary affect as they do not act directly on tight junctions components (e.g. oleic acid which targets the cell membrane, sodium caprate which targets phospoliphase C or EDTA which depletes extracellular Ca^{2+} leading to activation of protein kinase C resulting in contraction of actin filaments that modulate the opening of the tight junctions). The second generation target specific elements of tight junctions such as the occludin peptide or C-CPE to target Claudin-4 [46], [47], [48], [49].

Table 1. Electrical characteristic of epithelial tissues and cells [50].

	Species	TER Ω · cm²	Reference
Tissues			
Ileum	Human (*ex-vivo)*	~50	[51]
Jejunum	Human (*ex-vivo)*	23 - 40	[52]
Colon	Human (*ex-vivo)*	12 - 69	[53]
Ileum	Rabbit	115	[54]
Distal colon	Rabbit	730	[54]
Jejunum	Rat	67	[54]
Cell lines			
Caco-2	Human colon	>500	[55], [56]
Caco-2 and HT-29-MTX	Human colon	110 - 185	[55]
HT-29-MTX	Human colon	25	[57]
MDCK	Dog	60 - 4000	[58], [59]
IEC-18	Rat	50 - 100 Ω cm²	[60], [61]

1.2.3 Transcellular route of absorption

Most compounds pass across biological membranes by passive diffusion, dictated by the concentration gradient, described by Fick's first law of diffusion [62]. The process of diffusion occurs when the molecule concentration on one side of the cell membrane is higher than on the other side. It can be effected by two different mechanisms- either compound uptake into the apical cell membrane followed by lateral diffusion within the membrane into basolateral membrane of the cell or diffusion across the apical membrane followed by compound entry into the cytoplasm before exit from the cell by traversing the basolateral membrane [63] [64]. Passive diffusion can be affected by the physiochemical characteristics of the molecule and also interaction with the cellular barrier. There are three physiochemical properties that largely determine the extent of passive absorption

of the molecule; molecular size, lipophilicity (log P or log D) and polarity (hydrogen bonding, charge) [64]. Lipinski and colleagues described these limiting factors using the 'rule of five':

- molecular weight is less than 500,
- compounds lipophilicity- log P is less than 5,
- no more than 10 hydrogen bond acceptors (the sum of nitrogen and oxygen groups in molecule),
- no more than 5 hydrogen bonds (the sum of amine and hydroxyl groups in molecule),

and compounds that comply with these criteria are more likely to be membrane permeable (this rule excludes molecules that are actively transported through cell membranes by carrier-mediated transporters) [65]. This means that only small (e.g. CO_2 and O_2), hydrophobic (e.g. benzene) and polar but uncharged molecules (e.g. ethanol and H_2O) are able to diffuse across a phospholipid bilayer [66].

Transcytosis (e.g. pinocytosis) is the passive transcellular transport of compounds from apical to basolateral cell membrane via a mechanism comparable to phagocytosis. Only molecules such as peptide antigens, vitamin B_{12} that are excluded from other transport routes are transported via this pathway [67]. Compounds are captured in vesicles, formed by invagination of the apical cell surface, which are transported across the cytoplasm and fuse with basolateral cell membrane. The transport vesicles contain proteolytic enzymes and as a consequence most proteins are degraded during the transport across cell membrane [67], [68]. However, within the intestinal epithelium, specialized M-cells are present which have a lower proteolytic activity in their vesicles and provide a more effective pathway for transport of molecules intended for oral vaccination. Unfortunately, the total count of M-cells in intestinal monolayer is very low, which reduces the chance of using this mechanism as a potential route for drug absorption [69].

1.2.4 Active transport

Cell membranes contain membrane transport proteins that create a pathway for molecules such as sugars, amino acids, ions, nucleotides to pass across cell membrane without coming into immediate contact with hydrophobic lipid bilayer [70]. Each of the membrane transport proteins is responsible for a transport of a particular class of compounds. Transmembrane proteins can be divided into two major groups: channel proteins and carrier proteins [66]. Channel proteins create aqueous pores that once open (simultaneously open to intracellular and extracellular space) allow molecules such as inorganic ions to pass passively through the cell membrane [70]. Whereas, protein transporters (ABC and SLC transporters) have specific binding sites and outer or inner gates that can be opened to allow active or passive transport. Active transport mediated by protein transporters requires a contribution of metabolic energy such as an ion gradient or ATP hydrolysis (to ADP and P_i) and to enable directional transport of molecules in an energetically antagonistic direction [71], [72]. A review of literature has highlighted that many ARV drugs used as microbicides are substrates for drug transporters (Table 2).

Table 2. Kinetic interaction between antiretroviral drugs and drug transporters, with K_m and IC_{50} provided in brackets where known [73], [74], [75], [76], [77], [78].

	ABC Transporters		SLC transporters	
	Substrate	**Inhibitor (IC_{50})**	**Substrate (K_M)**	**Inhibitor (IC_{50})**
Protease inhibitors(PIs)				
Atazanavir	P-gp MRP1 MRP2	P-gp (24.9 µM) MRP1 BCRP (69.1µM)		OATP2B1 (3.9µM)
Darunavir	P-gp	P-gp (33µM)	OATP1A2, OATP1B1	OATP2B1 (26µM)
Lopinavir	P-gp MRP1 MRP2	P-gp (1.7µM, 5.5µM) BCRP (7.7µM, 5.7µM)	OATP1A2 OATP1B1	OATP1B1 (0.1µM) OATP1B3 (0.5µM) OATP2B1 (0.72µM)
Nucleoside/Nucleotide Reverse Transcriptase Inhibitors (NRTIs)				
Tenofovir DF	P-gp	P-gp (>500µM)		
Tenofovir	P-gp? BCRP? MRP4?	MRP1 (500µM) MRP2? MRP3?	OAT1 (22.3µM) OAT3	
Emtricitabine	MRP1	P-gp (1.7mM) MRP1 MRP2 MRP3		
Non-Nucleoside Reverse Transcriptase Inhibitors (NNRTIs)				
Etravirenz		P-gp		
Efavirenz		P-gp BCRP (20.6µM) MRP1 MRP2 MRP3		

ABC transporters

In the human genome it has been recognized that the 48 genes which encode ABC transporters that are divided into seven subfamilies (A-G) and then further divide into subgroups [79]. The ABC superfamily is one of the largest family of proteins and includes several efflux drug transporters such as multi drug resistance-associated proteins (MRPs), P-glycoprotein (P-gp) and breast cancer resistance protein (BCRP) [80]. These efflux pumps can limit of the availability of antiretroviral drugs at several viral target sites. ABC efflux proteins are able to transport a range of different compounds including amino acids, lipids and drugs [73].

ABC transporters contain four domains- two transmembrane domains (TMDs) and two (ATP-binding) nucleotide binding domains (NBDs). However, transporters from ABCG subfamily (such as BCRP) consist only of two domains (one TMDs and one NBDs) and need to create dimers to form the full transporter. The nucleotide binding domains play an important role in binding ATP and the energy obtained from hydrolysis is used to transport compounds through transmembrane domains across cell membrane. NBD's domains are located in the cytoplasm and have hydrophilic properties. The transmembrane domains are located across a membrane and consists of 5-10 membrane-spanning α-helices that have specific binding sites for substrates or pathway through which substrate can be translocated. Recognition of many compounds occurs in multiple overlapping binding sites [80], [81]. NBDs are closely linked to each other, as well as with the transmembrane domains. In each of conserved NBDs there are two sequence motifs, Walker A and Walker B, and located between them is a third motif that is typical only for ABC superfamily, called signature C [82]. The lysine residue in the Walker A is responsible for interacting with the β-phosphate of ATP, whereas the Walker B binds with magnesium ions through its aspartic acid residue. The signature C motif plays an important role in recognition, binding and hydrolysis of ATP [83], [84].

P-glycoprotein

P-glycoprotein is encoded by the ABCB1 gene and stands out among the ABC transporters by showing the strongest activity for the widest variety of molecules [80]. P-gp substrates includes anticancer drugs (for example Vinca alkaloids, anthracyclines, taxanes, anthracenes), calcium-channel blockers (verapamil, azidopine), cardiac glycosides (digoxin), fluorescent dyes (rhodamine 123, H33342, calcein-AM) and it has been demonstrated that all HIV protease inhibitors are substrate for P-gp [80], [85]. P-gp protein can be detected in many tissue types with high levels of expression in the transport epithelia of the small and large intestine, liver, pancreas, adrenal gland, kidney and also is present in blood-brain barriers [80], [86]. The major role of the protein is either restricting the gastrointestinal absorption of substrate molecules, eliminating metabolites into the intestinal lumen or urine, or inhibiting the drug entry from the blood to the brain or to the fetus. Schinkel and colleagues demonstrated that a lack of P-gp expression in knockout mice did not influence their health and fertility unless the mice where challenged with P-gp substrates (for example, vinblastine) which resulted in increased accumulation of the drug in tissues and reduced drug elimination causing neurotoxicity [87].

P-gp is a 170-kDa single polypeptide (full transporter) with two transmembrane domains, each with six TM segments and two nucleotide binding domains (Figure 4) [88]. In 1997, Rosenberg and colleagues were first to clarify the structure of P-gp transporter by using electron microscopy and image analysis to show that the protein has a central region with an opening towards outer side of the membrane and a closed structure at the cytoplasmic side of the membrane [89]. The proposed structure was supported by Aller et all that demonstrated an X-ray structure (medium resolution 3.8-4.4 Å) of P-glycoprotein and possible drug-binding pockets [90]. The crystal structure of P-gp transporter was obtained from *Mus Musculus* and shows 87% sequence identity to human P-gp [90].

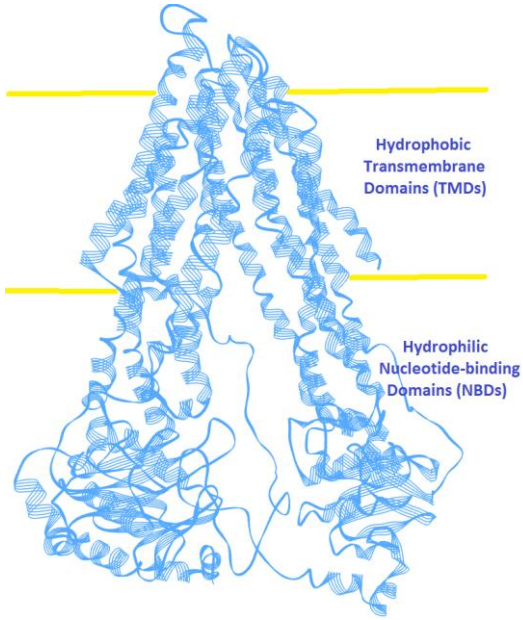


Figure 4. Schematic structure of crystal structure of P-gp transporter protein.

The P-gp crystal structure gave some important information and it has been shown by Senior et al that the transport of one molecule (substrate) needs the hydrolysis of two molecules of ATP, occurring one after the other [91]. P-gp exhibits diverse and polyspecific drug-binding nature and simultaneously is able to bind to two drug molecules [92]. To date, it has been very difficult to completely characterize the specific substrates for P-gp transporter because many of P-gp identified substrates do not fit into general classifications [93]. The most common properties of P-gp substrates are: large organic molecules (200 - 1900 Da), aromatic ring, hydrophobic, either neutral or positively charged (N atom), 2 or 3 electron donor groups with a distance of 2.5 - 4.6 Å [94]. Substrate binding is mainly by Van der Waals forces, π-π stacking or by hydrophobic interactions into drug-binding pocket in the transmembrane domain of P-gp. This stimulates ATP hydrolysis leading to conformational changes that transfer the substrate to the extracellular space. This process is followed up by the second ATP hydrolysis that is necessary to "re-start" the P-gp protein to be able to bind a substrate again [90], [95]. Binding of substrates to the ligand of the transporter occurs with different affinities, which are specific for each drug.

MRPs

Multidrug resistance-associated protein (MRP) is a part of ABCC subfamily of ABC protein family. The ABCC subfamily consists of 13 different members, nine of them are related to MRPs (MRP1-MRP6 (ABCC1-ABCC6) to MRP7-MRP9 (ABCC10-ABCC12)) [96], [97]. The structure of the MRP1 transporter exhibits homology to P-gp structure, with the exception of containing an additional an amino (N)-terminal TMDs (extension of five-membrane spanning domain) that is linked to the main core by a cytoplasmic region [98]. The same structure was found in MRP2, MRP3, MRP6 and MRP7, whereas other (MRP4, MRP5, MRP8 and MRP9) do not possess the N-terminal domain although they still contain the cytoplasmic linker that is specific for the MRPs subfamily [99], [100], [101].

Members of MRP subfamily show diverse expression in human body; MRP1 is widely present in all human tissues, MRP2 is detectable in intestine, kidney and liver, MRP3 in intestine, liver, kidney, adrenal glands and pancreas, MRP4 in intestine, lung, ovary, prostate, pancreas and testis, MRP5 is present in almost all tissues and MRP6 in liver and kidney, MRP7 can be detected in all tissues with higher expression in the pancreas, MRP8 is ubiquitously present in human tissues and also MRP9 is present in many human tissues [97], [102], [103]. Amongst the MRP subfamily, only the MRP2 transporter is expressed on the apical side of the cell membranes, for example in enterocytes and hepatocytes [99], [104].

MRPs members display an extremely wide substrate specificity that overlaps moderately with the substrate specification of P-gp, however additionally MRPs are able to transport organic anions and other metabolic products that are not substrates for P-gp [80]. MRP1 is able to transport neutrally charged molecules, anionic hydrophobic natural compounds, leukotriene C4, glutathione and other conjugates of these compounds. MRP2 is able to transport similar molecules to MRP1 including non-bile salt organic anions [97]. MRP3 exports bile acid molecules, glutathione, glucoronate and sulphate conjugates [105]. MRP4 and MRP 5 show resistance towards organic anions and nucleotide analogues [80], [102]. Many of the ARV drugs belonging to PI (atazanavir, ritonavir, indinavir, etc) and NRTI

(emtricitabine) classes are substrates for MRP, mostly MRP1 and MRP2 but also for MRP3, MRP4 and MRP5 [73].

BCRP

Breast cancer resistance protein (BCRP) was originally identified in a multidrug resistance human breast cancer cell line, MCF-7/AdrvVp [106]. The protein belongs to the ABCG subfamily (ABCG2) and is a half transporter (one TMD and one NBD) that has an ATP-binding segment at the amino-terminal end of ligand and six transmembrane domains. BCRP is present normally in the intestine, lymphocytes, brain endothelium and liver and contributes to drug resistance in some cancer cells. BCRP is a 75-kDa membrane protein for which an increasingly wide range of substrates have been identified since the transporters discovery in 1998 [106], [107]. BCRP can transport both negatively and positively charged compounds and substrates include: anticancer agents (mitoxantrone, topotecan, and irinotecan), many NRTIs drugs (didanosine, zidovudine, and lamivudine), fluorescent dyes (H33342) and many more. The substrate specificity of BCRP transporter is overlaps moderately with P-gp and the MRP transporters [81], [107].

SLC transporters

The human solute carrier (SLC) transporters are classified into 52 families with 395 membrane-bound members [108]. Members of SLC superfamily are divided into families based on the sum of detected and predicted transmembrane α-helices (approx. 10-14 segments) and homology in sequence (shares at least 20% similarity with one of the members of the family) [109], [110]. SLC transporters use secondary-active transport such as symporters, antiporters and uniporters, for which the movement of the substrate (ions or solutes) is driven by an energy coupling process such as an ion/ or voltage gradient. Symporters transport solutes and ions in the same direction, antiporters move solutes and ions in opposite directions, whereas uniporters transport only one substrate, either a solute or an ion [111], [112]. SLC proteins are able to transport a diverse range of substrates including organic and inorganic ions, which vary from very strict molecular requirements for substrates

(for example SLC7 family) to transporters that can transport a very broad range of substrates (for example OATs) [108]. In the human intestinal tissue different families of SLC transporter proteins are present including the following (with specific transporters in brackets):SLC15A1 (PepT1), SLCO1A2 (OATP-A, OATP1A2), SLC22A4 and SLC22A5 (OCTN1 and OCTN2), SLCO2B1 (OATP-B, OATP2B1) which are expressed variably over the total length of the intestinal tract [113], [114]. Several SLC families (such as OATPs, OATs, OCTs, ENTs and CNTs) are known to transport antiretroviral drugs (e.g. ritonavir, nelfinavir, zidovudine, saquinavir, lopinavir, etc.) and have an important role in their intestinal absorption [73].

1.2.5 Models for studying the colorectal absorption of drugs

The transport of the compounds through colorectal membrane may be affected by many factors as the physicochemical properties of drugs (molecular weight, solubility, partition coefficient, pKa, particle size, aggregates, hydrogen bonding, polar surface area, etc.) and the physiological environment (membrane permeability, pH in lumen and at the mucosal surface, surface area, expression of transporter protein, enzymes, presence of mucus, food and food composition, etc.) [115]. As a result of the complexity of the absorption process in human there is no ideal model that possesses all the properties necessary to mimic the colorectal membranes in humans. Instead it's necessary to use complimentary models to screen/predict drug transport before developing an optimized formulation that can be tested in human clinical trials. Methods used pre-clinically include; *in-silico* screening, physicochemical predictive model, intestinal rings or sacs, cell-based model, excised segments from different animals or humans in the Ussing chamber, *in situ* and *in-vitro* intestinal perfusions and animal-based studies [115], [116]. The complexity of the main methods, advantages and disadvantages for the evaluation of drug transport have been summarized in Table 3.

Table 3. Advantages and disadvantages using different methods for drug transport [115].

Absorption model	Number of experiments/ animals	Complexity vs *in-vivo*	Advantages and disadvantages
Physicochemical properties / synthetic membrane	Low	low ↓	'Rule of five', no animals involved, only transcellular pathway can be predicted, no active transport
Intestinal rings	High to intermediate		Incorporates unspecific binding, non-directed transport, animal and human tissue, viability of tissue limited to 10-20 min
Everted sacs	Intermediate		Limited stirring conditions, evaluates directed transport, animal and human tissue, viability of the tissue limited to 30 min
Cell lines	Intermediate		Very easy to use, no animal/human donor used, good stirring conditions, directed transport, human and animal cell lines, expression of transporters, mucus, tightness of tight junction might be higher, different drug appearance rate
Ussing chamber	Intermediate to low		Easily stirred and oxygenated, directed transport, viability of tissue around 2-3 h, animal and human tissue (may be from 'other' experiments), different drug appearance rate.
Intestinal perfusions	Low	high	Complex method, good stirring and oxygenation, directed transport, disappearance rate, anaesthesia, requires animal use

In-silico modelling, apart from reducing the time of traditional *in-vitro* and *in-vivo* methods, provides molecular details about drug (ligand) interactions with protein transporters (target). More recently, molecular docking studies have helped in developing inhibitors of carbonic anhydrase, aldose reductase and HIV-1 integrase [117], [118]. Molecular docking is used to estimate the binding affinity of a ligand towards a specific protein based on the molecular properties of a compound and the target structure. The docking studies aim to find the preferred conformation of the drug at the binding site of the protein. As a preliminary screen, for example, docking studies can be performed to understand most probable sites that are involved in drug binding to P-gp structure and estimate the likelihood of P-gp efflux influencing the transport of compounds. Docking studies involve visual analysis and docking scores performed by both blind (Smina molecular docking) and 'force field'-based methods (GOLD molecular docking). Blind Smina molecular docking allows full flexibility of the protein and full flexibility of the ligand and shows the most probable binding domain of the compounds to the P-gp protein structure, whereas GOLD docking allows only partial flexibility of P-gp structure (i.e., the docking domain of the protein is specified) and full flexibility of a ligand. Docking scores in GOLD are ranked using a force field scoring that includes the contribution of Van der Waals forces, hydrophobic interactions and number of hydrogen bonds. Aller and co-workers reported a crystal structure of the P-gp transporter which can be used to dock the structures of ligands (e.g. mannitol, digoxin, tenofovir, dapivirine and darunavir) [90].

Tissue explants from the colorectum are frequently used to assess anti-HIV agents and formulations during early development. In this model tissue explants are collected using endoscopy or harvested from surgical resection specimens. Tissue explants can be exposed to ARV agent and evaluated for toxicity. However, tissue explants have many limitations, including profound architectural deterioration within 24 hours of collection, which means that experiments can only proceed within this time period. Further consideration is that the clinical history of the tissue explant is unknown, as is pre-surgical exposure to hormone therapy, immune cell recruitment and inter-donor variability. Despite the limitations of this model,

explants can provide important preliminary efficacy and safety data on a microbicide agent before testing in animal models [119].

In-vitro models to study drug transport across the colorectal epithelium do not have the morphological and functional properties of normal adult human epithelial layer. The development of a primary human cell culture system to represent the rectal epithelium has been limited, because the cells are difficult to culture and have limited viability. The most commonly used *in-vitro* model for studying drug disposition and transport across the colorectal epithelium are cell lines (Table 4). The comparison of epithelial layer and transporter gene expression in the human colorectum with different colorectal cell lines (e.g. SW837, SW1463, HRA-16, etc.) has shown that Caco-2 cell line is the most suitable model for the study of the drug transport [120]. Caco-2 cells are human adenocarcinoma cell-derived and have been widely used as a model of the human intestinal epithelium. Previous studies have shown that the transport of low molecular weight drugs in the Caco-2 model correlates with absorption after rectal administration to rabbits in the absence or presence of permeability enhancers [113]. This data indicates a relationship that is predictive of the permeability of small protein, peptide and organic molecules in the rectum based on the permeability across Caco-2 monolayers, indicating that Caco-2 monolayers are a suitable model for predicting colorectal drug permeability [121].

Table 4. Comparison between different colorectal cell lines.

Caco-2	MDCK	HT-29	T-84	IEC-18
Origin				
Human epithelial colorectal adenocarcinoma cell line	Kidney cell line derived from dog	Human colon adenocarcinoma cell line	Human colon carcinoma cell line	Intestinal cell line derived from rat
Morphology				
• Well differentiated • Heterogeneous population • Protein expression • Tight junctions • CYP450 enzymes present	• Cell monolayer • Differentiated cells • Low expression of P-gp	• Undifferentiated cells • Form multilayer • Absence of tight junctions and polarity	• Poorly differentiated cells	• Not well differentiated cells • Leaky paracellular pathway
P_{app} of Mannitol				
In the range of 10^{-7} cm/s	0.5×10^{-6} cm/s	-	-	8.3×10^{-6} cm/s
TER				
>300 – 500 Ω cm^2	4000 Ω cm^2 (strain 1) 300 Ω cm^2 (strain 2)	<100 Ω cm^2	>1000 Ω cm^2	50 - 100 Ω cm^2
Applications				
• Drug permeability screening • Identifying transport mechanism	• Passive transport studies	• Paracellular drug transport • Drug transport across mucous	• Ion transport studies	• Good model to study small intestinal epithelial permeability of hydrophilic molecules
Advantages				
• Most used cell line for testing intestinal drug permeability • Good reproducibility, easy to maintain and robust • Functional property of human intestinal cells	• Commonly used	• Contain goblet cells secreting mucous	• Comparable cell phenotype to colonic crypt	• Good model to study permeability of hydrophilic compounds

Caco-2	MDCK	HT-29	T-84	IEC-18
Limitations				
• Absent of goblet cells secreting mucous	• Not for active and efflux studies	• Multilayer of cells	• Not applicable for drug transport studies	• Not applicable to study mediated transport of compounds
Reference				
[120], [122], [123], [124]	[58], [59]	[36], [125], [126]	[125], [127]	[60], [61]

Characteristics of Caco-2 monolayer

Caco-2 cells differentiate slowly to form a confluent epithelial cell monolayer. The Caco-2 cell monolayer forms a polarized single columnar cell barrier with microvilli on the apical membrane and tight junctions between cells. The tight junctions developed between adjacent cells restrict free transepithelial drug diffusion via the paracellular route. Small hydrophilic molecules, such as water, weak electrolytes and ions, are principally absorbed by this pathway, whereas more lipophilic drugs are predominately transported transcellularly across the mucosa. This transport includes uptake across the apical membrane, transfer through the cytoplasm and release across the basolateral membrane. These cells express transporters for amino acids, glucose, nucleosides, vitamin B12, protein carriers and oligopeptide transporter. Hence, Caco-2 cell monolayer model may be used to measure net drug permeability resulting from both transcellular and paracellular routes of absorption [128], [129], [130].

Drug transporters in Caco-2 monolayer

Efflux transporters, including the ATP-binding cassette (ABC) transporters (P-glycoprotein), multidrug resistance-associated protein 2 (MRP2) and the breast cancer resistance protein (BCRP) play a crucial role in the transport of drugs across Caco-2 monolayers and are responsible for drug absorption, distribution and elimination. In addition, the Caco-2 cell apical membrane features transporters that

are influx transporters and facilitate drug absorption, exemplified by the monocarboxylic acid transporter 1 (MCT1), organic anion-transporting polypeptide 2B1 (OATP-B), H^+/di-tripeptide transporter (PEPT1), organic cation/carnitine transporter (OCTN2) and the apical Na^+- dependent bile acid transporter (ASBT). On the basolateral membrane of Caco-2 cells, the efflux transporters which have been detected are organic solute transporters (OSTα-OSTβ), mRNAs of MRP4, MRP6 and both mRNA and protein of MRP3. Basolateral transporters transport the intracellular solutes serosally, thereby improving the absorption of drugs [131], [122].

1.3. Role of protein transporters in antiretroviral drugs absorption

The importance of drug transporters in cell and tissue compartments and their role in the disposition of several antiretroviral drugs is becoming increasingly recognised. However, transporter influence on drug disposition needs further investigation to inform new strategies for optimising the delivery of preventive microbicide agents to the rectal tissue. All the ARV drug families used in HAART therapy, besides entry inhibitors, need to enter the cell to reach their site of action [132].

Antiretroviral pharmacotherapy in the rectum for prevention of HIV transmission is a new research area. The distribution and role of drug transporters in this region remains to be clarified. To date, disposition of ARVs has been assessed with respect to the intestine to evaluate the effect of transporters on the systemic absorption of orally delivered ARVs [132]. Englund and colleagues have reported the expression of drug transporters along the human intestinal tract, including nine transporters (P-gp, BCRP, MRP2, MRP3, PEPT1, MCT1, OATPB, OCTN2, OCT1) that are expressed by the colonic epithelium. Comparing the colon and small intestine, some transporters such as MCT1, OCTN2 and MRP3 were differentially expressed [113]. Human transporters, i.e. ABC transporter and SLC transporters, can play a major role in the disposition of ARVs and control the level of drug entry in the cell, by uptake or efflux of drug molecules [132].

Many of ARV drugs are inhibitors and/or inducers or substrates of ABC transporters and can affect the transport of each other when administered together [73]. Previous *in-vivo* and *in-vitro* studies have demonstrated that all HIV protease inhibitors are substrates of P-gp [133]. Additionally, P-gp contributes in the transport of NRTIs such as abacavir and tenofovir disoproxil fumarate (TDF). As P-gp is an efflux transporter it could significantly reduce the absorption of TDF from intestinal tract reducing therapeutic efficiency [134].

ARV efflux and uptake is crucial to understand drug disposition and response, drug-drug interaction and drug toxicity. The combinations of

antiretroviral drugs proposed for use in topical microbicides may cause drug-drug interactions, resulting in toxic drug concentration or drug-induced toxicities [73]. Antiretroviral drug-drug interactions are very complex and involve competition for intracellular enzymes needed for drug activation and a combination of drug-induced effects, such as transient, toxicity and long-term changes in the activity and/or expression of drug transporters [135].

As discussed above, many of PIs and NNRTIs agents such as lopinavir or ritonavir are potent to inhibit P-gp transport; however some of them like ritonavir, amprenavir, lopinavir, nelfinavir induce P-gp expression after long-term exposure. Thus, induction and inhibition of P-gp may also contribute in drug-drug interactions [73]. Clinical studies, had shown that ritonavir increases the bioavailability and plasma exposure of darunavir (14-fold), atazanavir (238%), tripanavir (11-fold), fosamprenavir (400% increace in C_{min}) and it is recommended as a boosting agent with all PI ARV [136]. Combined ARV such as lopinavir/ritonavir significantly increase the plasma concentration of saquinavir and atazanavir, but decrease darunavir levels. This observation by Vishnuvardhan et al. suggests that combined ARV agents may induce PI metabolism and/or P-gp-mediated efflux. Additionally, co-administration of fosamprenavir and lopinavir/ritonavir resulted in a 2-fold decrease in the amprenavir and lopinavir C_{min} [137]. An earlier study showed that marovic is a high-affinity substrate for P-gp transporter (efflux ratio > 10) and when administered with combined PI ARV (darunavir, atazanvir) maraviroc plasma levels increase 3.5-10 fold. However, efavinarez reduces the AUC of maraviroc by 45%, but this effect is reversed if saquinavir/ritonavir or lopinavir/ritonavir is added [78]. Drug-drug interactions can occur between PIs and NRTIs commonly combined in first line HAART agents. For example, administration of PIs such as darunavir, atazanavir, lopinavir/ritonavir with TDF results in 25-37% increase in TDF exposure. *In-vitro* studies suggest that the enhanced bioavailability may be caused by interaction between P-gp transporters and/or OAT1 and OAT3 transporters [134].

1.3.1 Tenofovir

Tenofovir (TFV, 9-[9(R)-2-(phosphonomethoxy)propyl]adenine; PMPA) is an acyclic nucleotide phosphonate analogue with activity against hepatitis B virus and human immunodeficiency virus with an IC_{50} of 100 nM. The compound terminates HIV transcription from RNA to DNA before integration into the host cell genome and prevents initial cellular infection by targeting a phase in the HIV life cycle before genome integration. Tenfovir is approved by Food and Drug Administration (FDA) for the treatment of HIV infection and it is currently recommended as first line therapy in adults [138]. There are a number of advantages to the use of tenofovir in HIV therapy, including a lower rate of resistance development, minimal cytoxicity, long half-life, additive or synergistic activity when combined with certain other antiretroviral drugs and better side-effect profiles when compared to the older drugs [139]. However, the chemistry of tenofovir is complex and the resultant physicochemical properties determine the passive permeability across the epithelium and interaction with transporters.

Tenofovir has an amphiprotic nature with the potential to act as a weak base and an acid. The nitrogen group on the imidazole ring is a weak base, whereas the amine group (NH_2) group bound to the pyrimidine ring is able to accept a proton (NH_3^+). The H_2PO_3 is able to donate one or two protons thus making it a weak acid. At physiological pH (pH 7.35-7.45), the molecule is expected to be both negatively charged as a mixture of $H_2PO_3^-$ and HPO_3^{2-} and positively charged (NH_3^+). The aqueous solubility of tenofovir is around 13.4 mg/ml at 25°C.

As tenofovir is not well absorbed from the intestine due its hydrophilic nature, an ester prodrug, tenofovir disoproxil fumarate (TDF), was developed to enhance oral bioavailability. In TDF, the two negative charges of tenofovir are replaced by two isoproiipyloxycarbonyloxymethyl moieties, which increases the lipophilicity of the prodrug and thus an increase its permeation across membrane. Once TDF has reaches the circulation it is rapidly degraded to tenofovir(mono)ester by carboxylesterases or chemical hydrolysis and further is converted to tenofovir by phosphodiesterases (Figure 5). Tenofovir is eliminated unchanged in urine [140].

In contrast to the oral dosage form which contains TDF, a topical gel has been developed to contain 1% (w/w) tenofovir in the non-prodrug form [14].

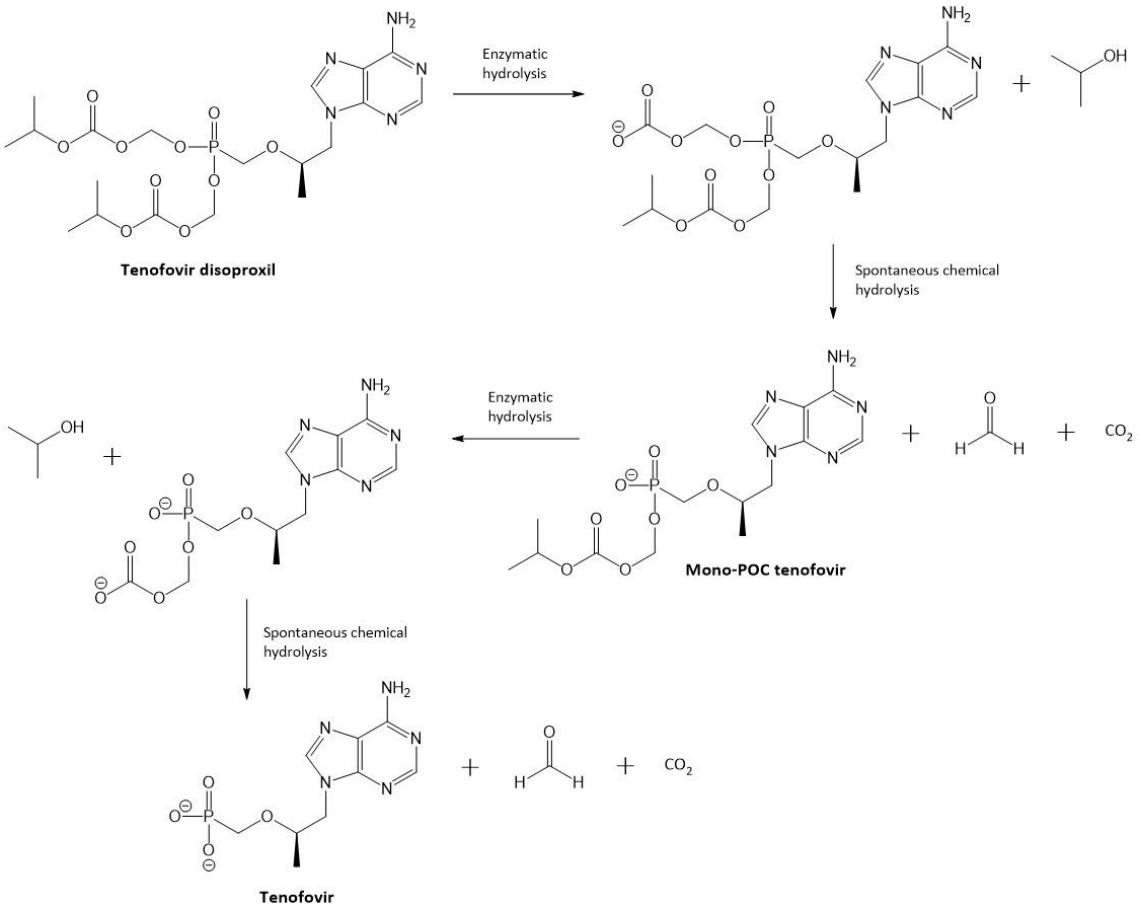


Figure 5. Structure of tenofovir disoproxil fumarate and its metabolites [140].

Drug transport across a mucosa is the product of a complicated interplay between transport and metabolism. *In-vitro* studies suggest than neither TDF nor tenofovir is a substrate, inhibitor or inducer of CYP enzymes, which suggests a low potential for clinically important drug-drug interactions with drugs that are substrates or inhibitors/inducers of those enzymes [141]. Previous studies have shown that TDF is a substrate for one or more intestinal efflux transport pump, and that the efflux transporter P-gp is at least partly responsible for this phenomenon. In contrast, the transport of tenofovir has been reported to be facilitated by human organic anion transporter (hOAT) types 1 and 3. Human organic anion transporter types belong to superfamily that mediates transmembrane transport of amphipathic exogenous and endogenous organic

compounds. An apical efflux system responsible for transporting tenofovir out of intracellular space has been reported, but is not well characterized. This transport of tenofovir is facilitated by multidrug-resistant protein type 4 (MRP4), which acts as an efflux pump and is highly expressed in the apical membranes of proximal tubules, liver and rectal tissue. P-gp is also expressed on the apical membrane, but recent findings have indicated that tenofovir is not a substrate for P-gp [74], [142].

The interaction with efflux transporters and drug-drug interactions of TDF and tenofovir from studies using cell lines have been summarised in Table 5. Moreover, *in-vivo* and *in-vitro* studies have suggest that transport across Caco-2 intestinal mucosal monolayers and Madin-Darby canine kidney cells stably transfected with the human MDR1 gene (MDCKII-MDR1), intestinal absorption in rats and uptake into PBMCs were all considerably greater for TDV than for tenofovir [143].

Table 5. Effect of transport inhibitor CsA and select protease inhibitors (PIs) on the bidirectional permeation of TDF and TFV across MDCKII-MDR1 and Caco-2 cells.

Substrate	Inhibitor	Conc. [μM]	Cell line	P_{app} A-B $\times 10^{-6}$	P_{app} B-A $\times 10^{-6}$	Efflux Ratio	Reference
TDF	none	10	MDCKII-MDR1	0.4	15	34	[134]
	CsA	10	MDCKII-MDR1	2.8	2.5	0.9	
	DRV	20	MDCKII-MDR1	0.4	13.2	33	
	IDV	20	MDCKII-MDR1	0.46	13.3	29	
	APV	20	MDCKII-MDR1	0.57	13.5	24	
	SQV	20	MDCKII-MDR1	0.5	11	22	
	ATV	20	MDCKII-MDR1	0.75	11.9	16	
	RTV	20	MDCKII-MDR1	2.5	11	4.4	
	LPV	20	MDCKII-MDR1	1.5	6.4	4.4	
	NFV	20	MDCKII-MDR1	1.4	6	4.3	
TDF	none	50	Caco-2	0.9	11.8	13	[134]
	CsA	10	Caco-2	1.2	2.2	1.7	
	DFP	2	Caco-2	2.2	19	8.4	
	IDV	20	Caco-2	1	7.5	7.5	
	APV	20	Caco-2	1.2	5.9	4.9	
	SQV	20	Caco-2	1.5	4.2	2.8	
	ATV	20	Caco-2	1.5	3	2	
	LPV	20	Caco-2	2.2	3.5	1.6	
	RTV	20	Caco-2	2.5	3.5	1.4	
Tenofovir	none	50	Caco-2	0.3	0.43	1.4	[74]
	CsA	10	Caco-2	0.48	0.6	1.3	

1.3.2 Dapivirine

Dapivirine (TMC120; 4-[[4-[2,4,6-trimethylphenyl)amino]-2-pyrimidinyl]-amino]-benzonitrile) is a non-nucleoside reverse transcriptase inhibitor (NNRTI) currently being tested in the clinical trials as a potential topical anti-HIV microbicide formulation [10].

In the first instance, Dapivirine was developed as an oral therapeutic and brought promising results in clinical studies showing high potency against HIV-1 virus. However, further on based on its potent activity, chemical and physical properties and favourable safety profile (poor systemic bioavailability), dapivirine development was focused on a topical microbicide for prevention of HIV virus [144]. Dapivirine has been developed into nanoparticle formulation, film formulation, a gel that is currently in early stage of clinical trials and one of the most successful vaginal ring formulations that in 2012 was advanced into Phase III clinical trials [145], [146].

Dapivirine acts as a non-competitive inhibitor that links with high affinity to a hydrophobic binding pocket of HIV-1 reverse transcriptase enzyme, affecting the enzyme activity and blocking virus replication. Dapivirine has shown to inhibit NNRTI- resistant viruses, wild type HIV-1 viruses and African isolates of HIV-1 (subtype C virus). However, dapivirine is not active against HIV-2 reverse transciptase [144]. It was demonstrated that dapivirine prevented systemic infection in a hu-SCId mouse model infected with HIV-1 strains at concentration of 0.7 µg/mL (2.25 µM) [147]. Dapivirine's high binding affinity to reverse transcriptase allows it to inhibit both cell free and cell associated virus [10]. It has been shown that over a 1 h incubation period with dapivirine, HEC-1A human vaginal epithelial cells accumulated 56% of the compound from the administered concentration [15].

Dapivirine is a highly lipophilic compound with partition coefficient (log P) equal to 5.27 at pH 9 [144]. Compound is practically insoluble in water, although solubility might be increased insignificantly by lowering the pH to 1 to induce ionization of the compound. Dapivirine is moderately soluble in propylene glycol and in polyethylene glycol 400 [144]. Dapivirine pKa is 5.8 suggesting that is a weak

base caused by pyrimidinyl amino group. Dapivirine is stable at room temperature up to 98°C and has a half-life around 12-14 h in human [144].

1.3.3 Darunavir

Darunavir is used as an ethanolate salt (TMC114, [(1S,2R)-3-[[(4aminophenyl)sulfonyl](2-methylpropyl)amino]-2-hydroxy-1-(phenylmethyl)propyl]-carbamic acid (3R,3aS,6aR)-hexahydrofuro[2,3-*b*]furan-3-yl ester monoethanolate) and is a protease inhibitor [148] which is highly active against resistance and wild-type strains of HIV virus [149]. Darunavir inhibits dimerization of HIV-1 virus protease that reduces proteolytic activity and leads to termination of HIV-1 virus replication [150]. Additionally, darunavir prevents HIV maturation by inhibiting the cleavage of virus gag-pol and gag polyproteins [151]. Darunavir has very low cytotoxicity and was designed to bind to HIV-1 protease by fitting tightly to the substrate envelope with very high affinity with dissociation constant (K_d) equal to 4.5×10^{-12} mol/L [149], [152]. In 2006, darunavir was approved by the FDA for use in antiretroviral treatment of HIV infection in naïve adults and patients with HIV strains resistant to at least one of the other protease inhibitors [153]. As darunavir is metabolized by cytochrome P450 isozyme 3A (CYP3A) it's recommended to co-administer it with a CYP3A inhibitor, ritonavir (dose 600/100 mg twice a day), to enhance oral absorption and significantly increases the plasma concentration of darunavir [154], [155].

Darunavir is a lipophilic compound with logP equal to 3.94 ± 0.57 [156]. The solubility of darunavir in water at 20°C is 0.15 mg/mL [148]. Darunavir consists of two tetrahydrofuranyl (bis-THF) groups that are fused to each other and one sulphonamide isostere [157]. King et al have shown that the bis-THF group is responsible for additional interactions with Asp29 (the crucial amino acid of HIV protease) that results in >100 times stronger binding with HIV protease compare to other ARV drugs (e.g. amprenavir) that contain only one of the THF moieties. Additionally, darunavir forms at least six hydrogen bonds with wild-type HIV protease and mostly these interactions are with main-chain atoms at the bottom of the HIV protease active binding site [151].

After oral administration, darunavir is adsorbed from the intestine, reaching peak plasma concentration after 2.5-4.0 h [158]. The absolute oral bioavailability for darunavir administrated alone is 37%, but once is co-administrated with ritonavir this increases to 82% [148].The bioavailability of darunavir taken orally with food can be improved by 30%, which has been attributed to the increased solubility of darunavir in the presence of the food [159]. This dependence has been described previously with other protease inhibitors, for example atanazavir, nelfinavir, saquinavir that were co-administered with food [160]. The composition of meal does not influence darunavir absorption [159]. Darunavir is about 95% bound with high affinity to human plasma protein, especially to α1-acid glycoprotein (AAG) and to albumin [161]. In the presence of low dose ritonavir, darunavir is eliminated with a terminal elimination half-life of 15 h (range 12.7-21.0 h) [158], [162]. Darunavir and its metabolites in predominately eliminated in faeces (80%) and in urine (14%) [162].

The absorptive permeability of darunavir across Caco-2 cell monolayers is intermediate-to-high, which is usually associated with passive transcellular transport. It has been reported by Lachau-Durand et.al. that the ratio of secretory/absorptive transport decreases with darunavir concentration indicating the saturation of an active transport component [163]. Permeability in Caco-2 cell monolayers and in *MDR1* gene-transfected renal LLC-PK1 cells in the presence of varying inhibitors demonstrating that darunavir is a P-gp substrate and most probably MRP2, OATP-A and/or OATP-B are involved in the transport of darunavir [76]. Additionally, darunavir exhibited P-gp inhibitory properties with IC_{50} equal to 32.9 µM [163].

Darunavir is metabolized by hepatic and intestinal cytochrome P450 (CYP) enzymes, mainly by CYP 3A4 which contributed significantly to the oxidative metabolism of the tested compound *in-vitro*. Three major metabolites of darunavir have been identified: M23 (by aliphatic hydroxylation), M19 (by carbamate hydrolysis) and M29 (by aromatic hydroxylation) plus three secondary metabolites; M6 and M27, M28 (by alicyclic hydroxylation) (Figure 6) [164], [162]. It has been shown that major metabolites were at least 10-fold less effective towards wild-type virus than the parent drug, darunavir [165]. The metabolic pathways from *in-vivo*

studies in humans, rats and dogs were consistent with results obtained from *in-vitro* studies. Apart from being a substrate for CYP3A4, darunavir is also an inhibitor with inhibitory constant (K_i) equal to 0.40 µmol/L [162].

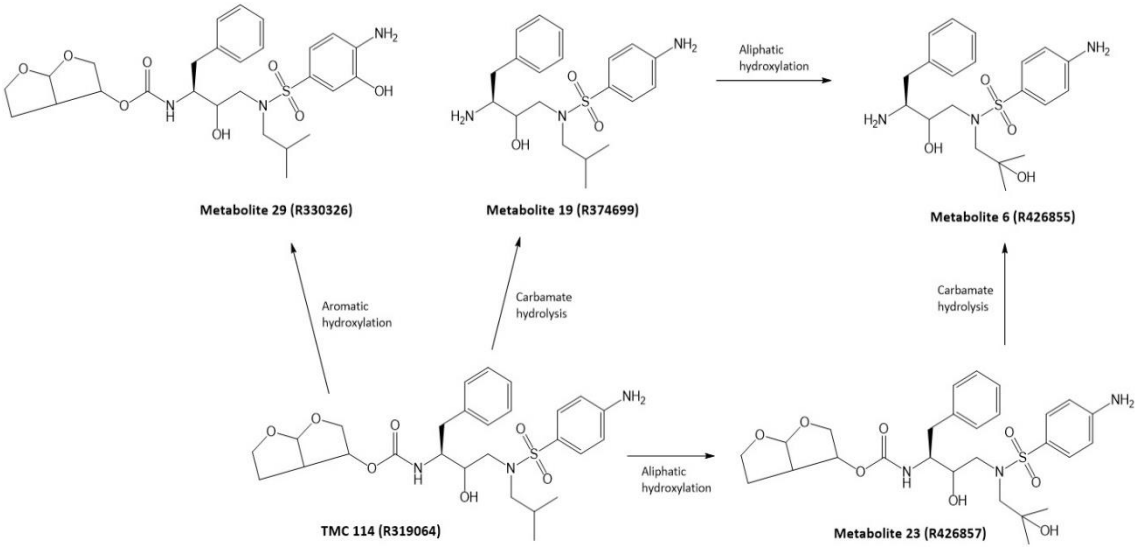


Figure 6. Structure of darunavir and its metabolites [164].

1.4. Aim and scope of the thesis

Microbicide formulations for colorectal delivery have been proposed for prevention of sexually transmitted HIV infection. Combinations of antiretroviral drugs, tenofovir, darunavir and dapivirine have shown to provide enhanced antiretroviral activity compared to single agents when tested *in-vitro* [166]. However, the impact of co-formulation on drug absorption after delivery to the colorectal mucosa is currently unclear, and methods are required to screen drug-transporter, drug-drug and drug-formulation interactions of biopharmaceutical relevance. The primary aim of this thesis was to investigate the permeability of tenofovir, dapivirine and darunavir across colorectal epithelium (using cell-based and tissue-based models), discern any role of transporters in regulating absorption using the selective inhibitors and explore the effect of co-administering the microbicidal agents and excipients on drug transport.

The specific objectives of this thesis were as follows:

1. To assess permeability of tenofovir, dapivirine and darunavir and to determine any potential interactions with ABC transporters using Caco-2 cell monolayers.
2. To screen for drug-drug transporter interactions for tenofovir, darunavir and dapivirine in combination and transport modification by potential formulation excipients and a prototype darunavir film formulation.
3. To compare the transport of tenofovir and darunavir in Caco-2 cells to permeability in the excised colorectal tissue segments of animal species used in pre-clinical drug development.
4. To characterise the molecular interactions of tenofovir, dapivirine and darunavir with P-gp efflux pump using *in-silico* screening.

Chapter Two
Materials and Methods

2.1. Materials and Reagents

[^{14}C]-dapivirine (Moravek Biochemicals, USA)

[^{14}C]-darunavir (Moravek Biochemicals, USA)

[^{14}C]-mannitol (Perkin Elmer, Wokingham, UK)

[^{14}C]-tenofovir (Moravek Biochemicals, USA)

[^{3}H]-digoxin (Perkin Elmer, Wokingham, UK)

[^{3}H]-mannitol (Perkin Elmer, Wokingham, UK)

3-(4,5-dimethylthiazol-2-yl)-2,5-diphenyltetrazolium bromide (MTT) (Sigma-Aldrich Company Ltd., Gillingham, UK)

4-(2-hydroxyethyl) piperazine-1-ethanesulfonic acid (HEPES) (Sigma-Aldrich Company Ltd., Gillingham, UK)

Albumin standard (Sigma-Aldrich Company Ltd., Gillingham, UK)

Anti- BCRP antibody (Abcam, Cambridge, UK)

Anti- MRP2 antibody (Abcam, Cambridge, UK)

Anti- P-glycoprotein antibody (Abcam, Cambridge, UK)

Bicinchoninic acid assay kit (BCA) (Sigma-Aldrich Company Ltd., Gillingham, UK)

Caco-2 cell line (American Type Tissue Culture, Rockville, USA)

Calcium chloride dehydrate (Sigma-Aldrich Company Ltd., Gillingham, UK)

Cell culture apparatus, plates, flasks (Corning Costar Corporation, USA)

D-(+)-Glucose (Sigma-Aldrich Company Ltd., Gillingham, UK)

Dapivirine (Selleckchem, Suffolk, UK)

Darunavir (Janssen R&D Ireland, Cork, Ireland)

Darunavir film formulation batch number,

Digoxin (Sigma-Aldrich Company Ltd., Gillingham, UK)

Dimethyl sulfoxide (DMSO) (Sigma-Aldrich Company Ltd., Gillingham, UK)

Dulbecco's modified Eagle's medium (DMEM) (Sigma-Aldrich Company Ltd., Gillingham, UK)

ELISA Ready-SET-Go!® (eBioscience, Lutterworth, UK)

Epithelial Voltohmeter (World Precision Instruments, High Wycombe, UK)

Fetal bovine serum (FBS) (Sigma-Aldrich Company Ltd., Gillingham, UK)

Hanks' Balanced Salt Solution (HBSS) (Sigma-Aldrich Company Ltd., Gillingham, UK)

HPLC grade methanol (Fisher Scientific LTD, Loughborough, UK)

HPLC grade water (Fisher Scientific LTD, Loughborough, UK)

Human IL-10 ELISA Ready-SET-Go!® (eBioscience, Lutterworth, UK).

Human IL-6 ELISA Ready-SET-Go!® (eBioscience, Lutterworth, UK).

Human IL-8 ELISA Ready-SET-Go!® (eBioscience, Lutterworth, UK).

Human Tumor necrosis factor-alpha (TNFα) (eBioscience, Lutterworth, UK).

Lactate dehydrogenase (LDH) (G-Biosciences, Lutterworth, UK).

L-glutamine, gentamicin (50 mg/ml) (Sigma-Aldrich Company Ltd., Gillingham, UK)

Magnesium sulphate (Sigma-Aldrich Company Ltd., Gillingham, UK)

Non-essential amino acids (Sigma-Aldrich Company Ltd., Gillingham, UK)

Penicillin-streptomycin (10,000 units penicillin and 10 mg streptomycin/ml) (Sigma-Aldrich Company Ltd., Gillingham, UK)

Phosphate-buffered saline solution (PBS) (Sigma-Aldrich Company Ltd., Gillingham, UK)

Placebo film formulation (Particle Sciences, Bethlehem, USA)

Poloxamer 407 (Sigma-Aldrich Company Ltd., Gillingham, UK)

Potassium chloride (Sigma-Aldrich Company Ltd., Gillingham, UK)

Potassium dihydrogen phosphate (Sigma-Aldrich Company Ltd., Gillingham, UK)

Scintillation cocktail (StarScint, Perkin Elmer, Wokingham, UK)

Sodium bicarbonate (Sigma-Aldrich Company Ltd., Gillingham, UK)

Sodium chloride (Sigma-Aldrich Company Ltd., Gillingham, UK)

Tenofovir (Gilead Sciences, Foster City, USA)

Transwell® 12-well plates (1.13cm^2, 0.4 µm pore size, polycarbonate membrane), (Corning Costar Corporation, USA)

Triton® X-100 (Sigma-Aldrich Company Ltd., Gillingham, UK)

Trypan blue (Sigma-Aldrich Company Ltd., Gillingham, UK)

Trypsin- EDTA (2.5 g/l trypsin, 0.5 g/l EDTA) (Sigma-Aldrich Company Ltd., Gillingham, UK)

α-tocopherol (vit.E) (Sigma-Aldrich Company Ltd., Gillingham, UK)

2.2. Optimising Caco-2 cell model culture conditions

2.2.1. Cell culture conditions

Cell maintenance

Caco-2 cells were grown in 162 cm^2 cell culture flasks at 37 ° C in 95% air, 5% CO_2. The cells were cultured in Dulbecco's Minimal Essential Medium Eagle's (DMEM), supplemented with 10% v/v fetal bovine serum, 1% v/v L-glutamine, 1% v/v nonessential amino acid, 0.1% v/v gentamicin. Medium was changed every 2 to 3 days. All processes were carried out using appropriate precautions and techniques for cell culture, using a Class II Flow cabinet.

Subculture

When approximately 80-90% confluent, cells were detached with 0.25% trypsin-EDTA. The trypsin was inactivated by addition of medium containing FBS. To avoid selecting for subpopulation, 100% of the cells were detached at each passaging procedure. The process took 5-15 min, the cells were regularly inspected. The cells were collected by centrifugation and the pellet was resuspended in medium. A 100 µL sample was taken from the cell suspension and combined with 100 µL trypan blue; this was mixed for 1-2 min, then suspended cell density was counted using Haemocytometer. The quantity of cells was calculated and the required cell concentration for subculturing was made.

2.2.2. Cell layer morphology and protein expression

Confocal microscopy

Caco-2 cell layers were stained for ZO-1 on day 21 in culture, to visualise expression of the tight junction protein. A solution containing 0.2% triton X-100 in 100 mM KCl, 3 mM $MgCl_2$, 1 mM $CaCl_2$, 200 mM Sucrose and 10 mM HEPES was applied to the cells for 2 min. The cell layers were washed three times in PBS and fixed for 20 min using freshly prepared 3% paraformaldehyde. The cells were washed three times with PBS and prepared for staining by permeabilization with 1% Triton X-100/0.5% PBS for 5 min. Cells were washed twice with PBS and once

with BLOTTO, and then were incubated overnight at 4°C with rabbit anti-zona occludens-1 (ZO-1; 12 µg/ml; Zymed, Cambridge BioScience, Cambridge, UK) in PBS containing 1% (w/v) BLOTTO. Cells were washed three times with PBS. Staining was visualized by incubation with AlexaFluor 488 chicken anti-rabbit IgG (10 µg/ml; Invitrogen) in PBS containing 1% BLOTTO for 60 min at room temperature. The cell layer was washed again four times. The membrane was cut from the support plastic and mounted on a microscope slide using one drop of Prolog Gold antifade reagent with DAPI. The slides were kept at room temperature overnight and viewed within one week using a Leica DMIR E2 confocal microscope (Leica Microsystems, Milton Keynes, UK). Fluorescent emissions from DAPI (λ_{ex}= 205nm, λ_{em}= 510-570 nm) were collected using separate channels at a magnification of × 40. Images obtained from each scan were pseudo-coloured blue (DAPI) and green (ZO-1), then overlapped afterwards to obtain a multi-coloured composite image.

Western blot

Cell pellets were snap-frozen by liquid nitrogen then lysed with RIPA plus buffer (150 mM NaCl, 5 mM EDTA, 1 % (v/v) NP-40, 50 mM Tris HCl, 0.1 % (v/v) SDS, 0.5 % (w/v) sodium deoxycholate, phosphatase and protease inhibitor added to 100 ml deionized water). The cell/ tissue lysates were transferred into Eppendorf tubes and centrifuged at 13,000 rpm in a Sigma 1-14 Microcentrifuge (Appleton Woods, Birmingham, UK) to obtain the cell pellet. A protein assay was carried out to determine the total protein concentration in each sample to ensure the approximately same amount of total protein is loaded onto the gel. Each sample was diluted with RIPA plus buffer by 1:5 and 1:10 dilutions. Albumin standards were prepared by serial dilution starting from 1.0 mg/ml to 0 mg/ml and used as a control. The albumin standards 5 µl and each of the samples (5 µl) were pipetted into a 96-well plate with three replicates per sample. A mixture (25 µl) composed of Protein Assay Solution A and Solution B (both Pierce TM BCA Protein Assay Kit) were added to each well and the samples were mixed. Afterwards, 200 µl of Solution B were pipetted into each well and the samples were mixed again. The plate was incubated in the dark for 15-30 min was read at 750 nm using a spectrophotometer (Wallac Victor 2, 1420 Multilabel Counter, PerkinElmer,

Hopkinton, USA). The total protein concentration in each sample was calculated according to the albumin standard curve.

For protein separation, an appropriate volume of RIPA plus buffer was added to each sample to make up a volume of 50 µl and boiled 1:1 with Laemmli sample buffer (Sigma-Aldrich, UK) for 5 min at 100°C. Samples (30 µl; equivalent to 30 µg total protein) were loaded onto 4-12% NuPage gels (Invitrogen, Paisley, UK) and protein separation was performed at 200 V for 50 min in 1X MOPS running buffer (Invitrogen, Paisley, UK). Then, the gel was soaked in Cathode buffer (450 ml deionized water, 50 ml methanol, 1.51 g Tris and 1.5 g Glycine) and moved into a Hybond-ECL nitrocellulose membrane (Amersham Biosciences, Buckinghamshire, UK) as described below. The nitrocellulose membrane was soaked for 2 min in deionised water and then transferred into Anode Buffer II (1.51 g Tris, 50 ml Methanol, 450 ml water). Quick Draw Filter paper (Bio Rad, UK) was soaked in appropriate buffer and a sandwich was built as shown in Figure 7 in the Trans-Blot® SD Semi-Dry Transfer Cell (Bio-Rad, Hertfordshire, UK).

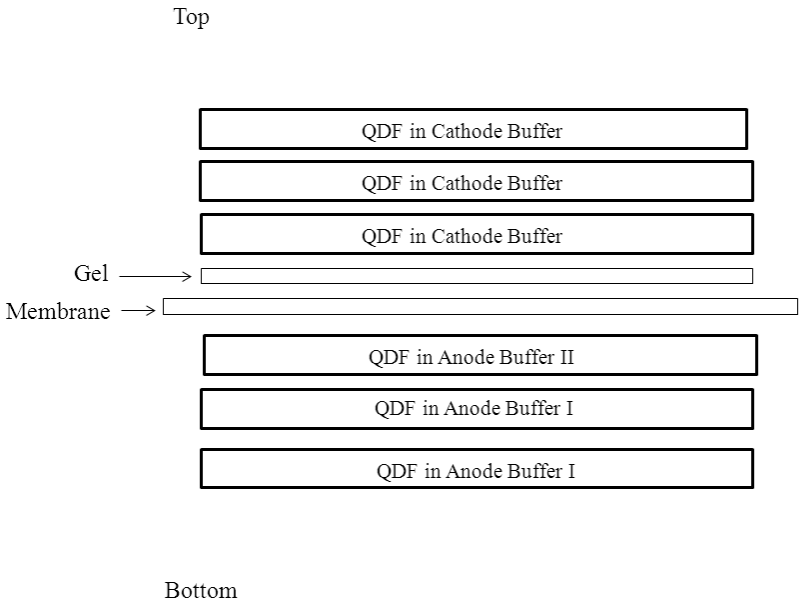


Figure 7. Schematic diagram of the set-up of Western blot sandwich.

Once all the layers were set up, transfer was performed at 19 V for 36 min. After the transfer was finished the membrane was blocked for at least one hour using a MTBST solution containing 5 g of milk powder (5 %) in 100 ml TBS and 50 µl Triton-X 100 (0.05 % (v/v)). The membrane was incubated overnight with primary antibodies rabbit monoclonal anti-P glycoprotein, anti-MRP2, or anti-BCRP (Abcam, Cambridge, UK) diluted 1:250 and rabbit monoclonal anti-α-tubulin (Abcam, Cambridge, UK) diluted 1:1000 in MTBST at 4°C on a rolling platform. Following a wash with MTBST solution, the membrane was blocked for two hours in MTBST solution. This was followed by the addition of goat-anti-rabbit IgG (conjugated to HRP, diluted 1:1000 in MTBST solution for 1 h at room temperature. The membrane was washed in MTBST solution for 5 min, twice in TBST solution for 5 min and finally in TBS solution for 5 min before visualised using electrochemiluminescent (ECL) detection kit (GE Healthcare Life Sciences, Buckinghamshire, UK). The antibodies were removed using Restore™ western blot stripping buffer (Thermo Scientific, Loughborough, UK) and re-probed using α-tubulin. Afterwards, the secondary antibody was re-applied and the ECL detection repeated to determine if any binding was present. Images were digitally captured, alternatively, blots were captured using traditional X-ray film development.

Film development was performed in a dark room. The ECL detection kit was applied onto the nitrocellulose membrane and placed in a developing cassette. The blot was closed with a thin film covered by an X-ray film (Amersham Hyperfilm ECL, GE Healthcare). The cassette was closed for 1 min to press the membrane to the film. The cassette was opened carefully, the film was placed directly into the film developer solution (Sigma Carestream Kodak autoradiobiography GBX developer/replenisher, Sigma Aldrich, UK) and developed until protein bands appeared. Once bands were visible the film was transferred into the fixation solution (Sigma Carestream Kodak autoradiobiography GBX fixer, Sigma Aldrich, UK) for ~ 5 min and finally placed in deionized water for a wash. The films were air-dried overnight and scanned.

2.2.3. Cell-based assays for evaluating compounds toxicity

Calibration curve: cell number

The 3-(4,5-dimethylthiazol-2-yl)-2,5-diphenyltetrazolium bromide (MTT) assay was used to assess the effects of exogenously applied compounds on Caco-2 cell metabolism. Caco-2 cells were plated at a range of seeding densities from 150 to 40,000 cells/well in 10% DMEM in a 96-well plate. The plates were incubated under standard conditions and assayed after 48 h, 7 or 14 days. The cell culture medium was removed and replaced with fresh cell culture medium (200 µl), then 50 µl of MTT solution (5 mg/ml in PBS) was added to each well. After 4 h the medium was removed by gentle inversion and tapping onto paper. Any formazan crystals generated within the adherent cell layers were solublised using 100 µl of a surfactant solution (10% v/v SDS in DMF: water (1:1)). Upon complete solubilization of the crystals by incubating overnight, the absorbance of each well was measured by spectrophotometry using a wavelength of 570 nm and correcting for background absorbance using a wavelength of 650 nm. A calibration curve was produced by plotting absorbance as a function of cell number/well, and the calibration curve obtained from cells seeded under two different cell culture conditions were compared.

Cell viability assay using MTT

The effect of different concentration of DMSO (0.1 – 5%) and different test agents (0.001 – 500 µM) was measured as a reduction in metabolic activity using the (MTT) assay. Cells were seeded in a 96-well plate and, after 48 h, 7 days and 14 days were exposed to 100 µL of DMSO (0.1 – 5%) or drugs at varying concentrations suspended in 2% FBS in DMEM solution incubated for 24 hours. After the exposure period, the medium was aspirated and replaced by 200 µl fresh 2% DMEM. MTT (50 µl; 5 mg/mL) was added to the wells and the plate was incubated for further 4 h. The medium was removed and the resulting intracellular formazon crystals were dissolved over 24 h in 100 µl of 10% SDS prepared in 1:1 water:DMF, after which the absorbance from the solubilized formazan was measured spectrophotometrically at an absorbance wavelength of 560 nm.

The relative cell viability (% viability) was calculated as follows:

$$\text{Viability (\%)} = \frac{A-S}{CM-S} \times 100 \qquad \textbf{Equation 1.}$$

Where A is the absorbance obtained for each concentration of the test drug, S is the absorbance obtained for positive control (1% v/v Triton-X) and CM is the absorbance obtained for untreated cells (negative control, DMEM alone). The latter reading was defined as 100 % cell viability.

Membrane damage study using LDH

Cells were seeded in 96-well plate and, after 24-48 h, were exposed to 100 µL of varying concentrations of tested drugs (0.001 - 500 µM) or DMEM alone (negative control) and incubated at for 2 and 24 h. The LDH assay was performed according to the manufacturer's guidelines (Pierce LDH Cytotoxicity Assay Kit). After the exposure period, 50 µl of supernatant from each well was removed into a new 96-well plate and 50 µl of reconstituted reaction mixture was immediately added to each well. The plate was covered in foil and put on a shaker for thorough mixing at 37 ˚C. After mixing for 30 min, the plate was removed and 50 µl of stop solution was added to all wells. The absorbance of the wells was measured by spectrophotometry (SpectraMax, UK) at an absorbance wavelength of 490 nm, using a reference wavelength of 680 nm.

All samples, positive and negative controls are run in triplicate. The relative cell LDH release (% LDH release) was calculated as follows:

$$\text{LDH release (\%)} = \frac{A-CM}{S-CM} \times 100 \qquad \textbf{Equation 2.}$$

Where A is the absorbance obtained for each concentration of the test substance, CM is the absorbance obtained for untreated cells (negative control) and S is the absorbance obtained for positive control (1% v/v Triton-X). The latter reading was defined as 100% LDH release.

2.2.4. Test solutions

Tested compounds were dissolved in DMSO and reconstituted with HBSS. The final tenofovir concentration was up to 500 µM, dapivirine was up to 100 µM, darunavir was up to 500 µM and digoxin up to 500 µM in solutions containing a final concentration of 1% v/v DMSO. All experiments were performed at 37 ° C.

2.2.5. Data and statistical analysis

Data analysis was performed using Microsoft Excel 2013. Statistical data was analysed using GraphPad Prism® (Version 5.01 for Microsoft Windows, GraphPad Software, San Diego, CA, USA). Data represent mean ± standard deviation from at least three independent studies, each performed in triplicate.

2.3. Drug transport across Caco-2 cell monolayers

2.3.1. Measurement of apparent permeability

For permeability studies, the cells were seeded at a density of 2×10^5 cells/well on the porous polycarbonate membrane inserts of the Transwell system, with a 12 mm diameter, pore size of 0.4 µm and a surface area of 1.12 cm^2. These cells were provided with fresh growth medium three times a week until the time of use. The cell layers were used between 21-28 days of culture. On the day of the experiment, the cell culture medium (DMEM supplemented with 10% FBS, 1% L-glutamine, 1% penicillin/streptomycin, and 1% non-essential amino acids) was removed and warm transport medium (HBSS supplemented with 10 mM HEPES, pH 7.4) at 37 °C was added: 0.5 mL to the apical chamber and 1.5 mL to the basolateral chamber. In some permeability studies, the transport medium for the receiver chamber was supplemented to enhance drug solubility by the addition of 0.2% (w/v) Poloxamer 407 or 0.1% (w/v) α – tocopherol or 4 % (w/v) BSA.

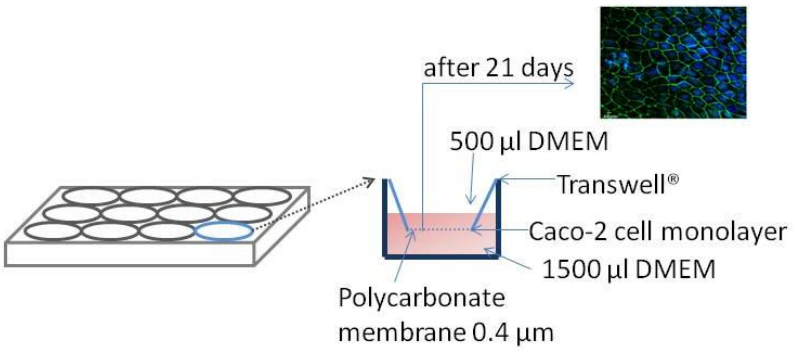


Figure 8. Schematic diagram of the Transwell and the staining of tight junction protein ZO-1 on Caco-2 cells after 21 days in culture.

In drug-drug interactions studies, the transport medium also contained transporter inhibitors or ARV drugs or excipients. Both chambers (donor and receiver chambers) were pre-incubated for 30 min with transport medium containing the appropriate inhibitor or ARV drugs to saturate any transporter binding sites.

For absorptive permeability, the experiment was initiated by adding 520 µL of the drug-containing test solution to the apical (donor) chamber of the inserts and 1520 µL of transport medium to the basolateral (receiver) chamber. For secretory permeability, the experiment was initiated by adding 1520 µL of the drug-containing test solution to the basolateral (donor) chamber and 520 µL of transport medium to the apical (receiver) chamber.

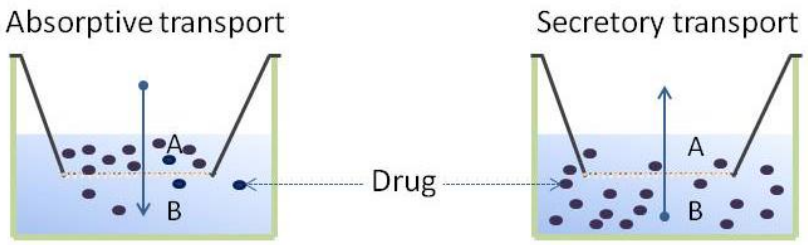


Figure 9. Schematic diagram of experimental system to study drug transport in Caco-2 cell model.

Within 1 min of starting the experiment, 20 µL of the test solution from both sides of chambers were removed and the donor concentration (C_0) was measured. Samples were withdrawn from the receiver chamber (apical chamber – 200 µL, basolateral chamber - 600 µL) at 30, 60 and 90 min. The volume withdrawn was replaced immediately with 200 (apical chamber) or 600 (basolateral chamber) µL preheated fresh transport medium. The sampled drug was corrected for in the calculation of drug flux. After each sampling time point the Transwell plate was returned to the 37 ° C incubator where it was under stirring conditions. The plates were agitated (50 rpm) on a Gyrotory Shaker-Model G2 (New Brunswick Scientific Co., Hertfordshire, UK). After 120 min, 200 or 600 µL samples were removed from

both the receiver and donor chamber. The integrity of the monolayer was confirmed by measuring the permeability of mannitol, a paracellular marker compound (^{3}H-mannitol or ^{14}C-mannitol) and transepithelial electrical resistance (TER).

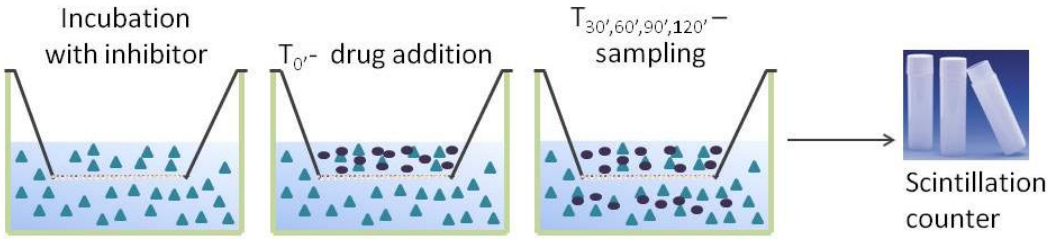


Figure 10. Schematic diagram of experimental system for studying drug transport in the presence of inhibitor (or formulation excipients).

2.3.2. Test solutions

Antiretroviral drugs were dissolved in DMSO and reconstituted with HBSS to generate the maximum concentration stock solution. The final tenofovir concentration was 0.1-100 µM, dapivirine was 0.1-10 µM and darunavir was in the range of 0.1-100 µM. Different drug concentrations were prepared by serial dilution and adjusted to have a final concentration of 1% v/v DMSO. All experiments were performed at 37 ° C. The cell layers were shaken at 50 rpm.

2.3.3. Sample analysis

Radiolabelled samples were analysed using a Beckman Coulter LS6000TA (Beckman Coulter™, Bucks, UK) dual scintillation counter, counted for 5 min per sample after addition approximately 4 mL of StarScint scintillation cocktail.

2.3.4. Transepithelial electrical resistance (TER)

The integrity of the monolayer was confirmed by taking TER readings before and after experiment using an EVOM™ epithelial voltohmmeter equipped with silver 'chopstick' electrodes. The volumes of pre-warmed (37 ° C) transport medium, 500 µL in the apical and 1500 µL in the basolateral chambers, were used to gently replace the cell culture medium in the apical and basolateral chamber. The cell layers were allowed to equilibrate for at least 30 min before measuring TER. When

the electrode set was immersed in the transport medium; the resistance reading was obtained. The resistance of monolayer was determined by subtracting the resistance of a cell-free membrane support (previously determined) from the total resistance of the system including the cell layer (Equation 3).

$$\text{Resistance}_{(\text{cell monolayer})} = \text{resistance}_{(\text{membrane support + cell monolayer})} - \text{resistance}_{(\text{membrane support})}$$

Equation 3.

The resistance (Ω) obtained is inversely dependent upon the area (cm^2) of the tissue. As a result, the product of the resistance and area was calculated (cm^2). In this study, all cell monolayers used had a TER greater than 1400 Ω cm^2.

2.3.5. Transport data analysis

The apparent permeability coefficient (Papp. cm/s) for the radiolabeled solute was calculated according to equation 4, derived from Fick's first law:

$$P_{app} = dQ/dt \times (1/C_0.A)$$ **Equation 4.**

Where dQ/dt is the gradient of the slop of flux versus time (µmoles/s), C_0 is the initial drug concentration applied in the donor chamber (µmoles/cm^3) and A is the surface area of the Transwell® filter (cm^2).

The total mass balance of compounds presented to cell layers was monitored using equation 5, to ensure that drug losses were accounted for. Recovered compound was the sum of residual compound in donor chamber, compound in the receiver chamber (corrected for sampling) and compound associated with the cell layer.

$$\text{Mass balance} = \text{Compound}_{(\text{recovered})}/\text{Compound}_{(\text{initial concentration})} \times 100\ \%$$

Equation 5.

2.3.6. Drug uptake studies

Drug uptake experiments were performed using transport medium. Caco-2 cells were seeded at density 1 × 10^4 cells/ well on 48-well plates and were used between 21-28 days of culture. Caco-2 cell monolayers were pre-incubated with drug-free transport medium for 30 min at 37 ˚ C which was replaced at t = 0 with transport medium containing 0.1 µCi/mL ^{14}C-tenofovir, ^{14}C-dapivirine or ^{14}C-darunavir supplemented with unlabelled tenofovir, dapivirine or darunavir, respectively, to obtain the desired concentration. In inhibition studies, a specific concentration of the inhibitor was added to the transport medium at the pre-incubation stage and included in the transport medium during the uptake experiment.

To measure drug uptake, the transport medium was removed and the cells were washed twice with ice-cold PBS and solubilised in 1% Triton X 100 at 37 ˚ C for 30 min. Cells from each well were collected, mixed with approximately 4 mL of StarScint scintillation cocktail and the total radioactivity was measured using a Beckman Coulter How was this to total cellular protein content per well, which was measured in each well using a Protein Assay kit using bovine serum albumin as the standard.

2.3.7. Total Protein measurements

Total protein was measured by reaction with bicinchoninic acid (BCA) and 4 % copper (II) sulphate [167]. This method is based on the reduction of Cu^{2+} by proteins in an alkaline medium, with the highly sensitive and selective colourimetric detection of Cu^{+} using BCA. The chelation of two molecules of BCA with each Cu^{1+} ion forms a purple coloured product that exhibits a strong absorbance that is linear with protein concentration. The protein assay was performed according to manufacturer's guidelines (Pierce™ BCA Protein Assay Kit). At the end of uptake studies, 10 µl of cell homogenate (cells solubilised in 1% Triton X 100 for at least 30 min) from each well was removed and placed into a new 96-well plate and 200 µl of reagent mixture was added immediately to each well. The plate was incubated at 37 ˚ C for 30 min. The absorbance was then read on a spectrophotometer set at a wavelength of 562 nm.

2.3.8. Enzyme linked Immunosorbent assay (ELISA)

Caco-2 cells were grown on Transwells for 21-28th days as described previously and the effect of drugs or formulations on cell inflammatory responses was investigated by measuring chemokine release using ELISA. The use of Transwell inserts allows access to both apical and basolateral sides of the cell layers, respectively representing the lumen and lamina propria of the intestinal epithelium. Before applying test solutions, the Caco-2 cell monolayers were washed twice with PBS. Caco-2 cells were treated with inflammatory stimuli consisting of IL-1β 1-25 ng/ml, LPS 1-10 µg/ml in DMEM containing 1% (v/v) FBS or cell culture medium (negative control) applied for 24 h. Additionally, the effect of the ARV drugs and darunavir/ placebo film formulation on Caco-2 cells inflammatory responses was assessed by applying test solutions to either apical or basolateral side and incubated for 2 h. Samples of were collected from the apical and basolateral chambers and measured using ELISA.

Supernatants were collected post-challenge and centrifuge at 1500 rpm for 10 min to remove extracellular particles. Cytokine concentrations were measured using Human IL-10 ELISA Ready-SET-Go!®, Human IL-8 ELISA Ready-SET-Go!®, Human IL-6 ELISA Ready-SET-Go!® and Human Tumor necrosis factor-alpha (TNFα) ELISA Ready-SET-Go!® were purchased from eBioscience (San Diego, CA) and the ELISA assay was performed according to manufacturer's guidelines.

Interleukin secretions were quantified using a reference standard curve provided with the kit. Results were expressed in relative terms to the negative control (untreated cells) to obtain comparison between groups.

2.3.9. Data and statistical analysis

Data analysis was performed using Microsoft Excel 2013. Statistical data was analysed using GraphPad Prism® (Version 5.01 for Microsoft Windows, GraphPad Software, San Diego, CA, USA). Standard one-way analysis of Varience (ANOVA) was used to compare TER readings (before and after transport studies) and mean values for apparent permeability (secretory to absorptive efflux). To compare absorptive, secretory and intracellular concentrations in the presence of inhibitors to the control condition (no inhibitor), a one-way Anova with Dunnett's post-test was used and considered significant for $p \leq 0.05$. Data represent mean ± standard deviation from at least three independent studies, each performed in triplicate.

2.4. The effect of film formulation on drug transport across Caco-2 cell monolayers

2.4.1. Validation of a sensitive liquid chromatographic tandem mass spectrometer (LC-MS/MS) assay for darunavir

Sample preparation

A liquid-liquid extraction method, using the organic solvent methyl-tert-butyl ether (MTBE) was used to prepare all samples (i.e. to validate assay, the instrument and to analysis of samples from the experiments). Darunavir stock solution (1 mg/mL) and internal standard (darunavir-^{13}C6, 1 mg/mL) were prepared in 100% methanol. The calibration series (seven-point calibration curve) were prepared by diluting the darunavir stock solution in HBSS, to achieve a concentration range of 0.1-20 µg/mL. 200 µL of each darunavir concentration, 200 µL of HBSS and 100 µL of internal standard were added into seven different glass centrifuge tubes. A blank, quality controls and samples were prepared by adding 200 µL of HBSS or quality control solutions or samples instead of darunavir solution. All tubes were vortexed for approximately 1 min, prior to addition of 1 M Ammonia solution (pH 9.2) and vortexed again for 1 min. Next, 5 mL of MTBE was added to each of the tubes and placed into rotation mixer (Rotator SB3) for 30 min at 40 rpm, followed by centrifugation for 5 min at 3500 rpm. Using a Pasteur pipette, the organic layer (top) was transferred into new centrifuge tubes and evaporated to dryness, under nitrogen gas (TurboVap® LV Evaporator, Zymark, UK) set at 50°C for 30-50 min, followed by reconstitution with 200 µL DS2 (dilution solvent- 0.1% formic acid in 70 % acetonitrile).

LC-MS/MS analysis of darunavir

Analysis of darunavir was performed using a Micromass Quattro-LC-SRM (Hewlett Packard series 110, UK) triple quadrupole mass spectrometer. The signals were optimized by injecting 2 µg/mL solution of darunavir and internal standard in DS2, using a HP1 100 LC infusion pump and a collision energy set to 15 V. A gradient mobile phase was used consisting of solvent A (5 mM Ammonium formate in HPLC-grade water) and solvent B (5 MM Ammonium formate in 95 % (v/v) HPLC-grade acetonitrile), at a flow rate of 200 µL/min and with MS detection of darunavir daughter ion at 392.06 m/z and 436.00 m/z with retention time of 2.2 min, and internal standard (darunavir-13C6) daughter ion t 398.00 m/z with retention time of 2.2 min. The LC system column was Thermo Hypersil Gold aQ 150×2.1 mm 3µ (ThermoScientific, Hempstead, UK). Peak integration was processed using MassLynx software. Calibration curves were plotted as a mean response (ratio of darunavir area to internal standard area) using a weighted (1/x) linear regression model with seven concentration points.

2.4.2. Method verification

Once all the conditions were established, the method was verified by calculating linearity, precision and accuracy accordingly to FDA recommendations [168].

Linearity

To determine linearity, the regression line was calculated using peak area against compound concentration. Linearity of the peak area was determined by triplicate injections of each of the seven calibration standards.

Intra-day precision

For calculating intra-day precision, a single set of the calibration standard series were prepared and analysed three times in triplicates on day one. The percentage coefficient of variation (% CV) was calculated for each of the concentration levels (n=9) to estimate the precision of the assay.

Inter-day precision

For inter-day precision, three calibration standard series were freshly prepared, each on a different day. The % CV of the data from these three independent calibration curves was calculated.

Limits of detection and quantification (LOD and LOQ)

The limit of detection (LOD) and limit of quantifications (LOQ) were determined using Equation 6 and 7, respectively. The limit of detection is defined as the lowest amount of a component that can be identified in the sample, but not necessary quantitated.

The limit of quantification is defined by the lowest quantity of an analyte that can be quantified with suitable accuracy and precision.

$$LOD = Y_B + 3S_B \qquad \textbf{Equation 6.}$$

$$LOQ = Y_B + 10S_B \qquad \textbf{Equation 7.}$$

Where, Y_B is the intercept obtained from the linear regression equation and S_B is the standard error of the Y estimate obtained from the linear regression.

Accuracy

The accuracy of the assay was determined by measuring a known concentration of darunavir and calculating the measured concentration from the standard calibration curve. To calculate the accuracy the experimental value is compared to the actual concentration using equation 8.

$$\text{Accuracy} = (T/A) \times 100 \qquad \textbf{Equation 8.}$$

Where, T is the theoretical sample concentration and A is the actual sample concentration.

2.4.3. Data and statistical analysis

Data analysis was performed using Microsoft Excel 2013. Statistical data was analysed using GraphPad Prism® (Version 5.01 for Microsoft Windows, GraphPad Software, San Diego, CA, USA). The dissolution profile of darunavir from each film was expressed at the cumulative % darunavir dissolved in the receiver chamber over the initial % darunavir recovered from the transwell membrane, as a function of time. One-way analysis of variance (ANOVA) was used to compare mean values for the dissolution profile of darunavir in different conditions and TER values before and after the experiment. To compare the dissolution profile of darunavir in the presence of inhibitor or tenofovir to the control condition (no inhibitor), a one-way Anova with Dunnett's post-test was used and considered significant for $p \leq 0.05$. Data represent mean ± standard deviation from at least three independent studies, each performed in triplicate.

2.4.4. Dissolution profile of darunavir in a film formulation

Film formulations were prepared by Particle Sciences (Bethlehem, USA). For preparation of darunavir-based dissolving films, micronized darunavir (0.57%) was added to a mixture of Tween 80 (0.55%) and water (91.499%, Ricca) and homogenized for 10 min using a probe homogenizer. Polyethylene oxide (PEO)-10 (1.10%, Dow) and PEO WSR-301 (0.055%, Dow) were added and mixed for 30

min. Polyethylene glycol (PEG) 1000 (0.916%, EMS) was then added and mixed for another 30 min using a mechanical stirrer. Once homogeneous, hydroxypropylmethylcellulose (HPMC) E50 (5.310%, Ashland Chemical) was added to the above dispersion and stirred by mechanical mixer for an additional 120 min, followed by bath sonication of the dispersion for 30 min to remove any entrained air. The dispersion was coated onto release paper at slow speed using a Coatema Easycoater, set for 1400 mm wet thickness, and then dried at 37°C. The following films were evaluated:

1) Darunavir film formulation batch number FID #3626; B32.5 - B32.4 [1.5 × 1.5 cm^2], drug loading 6.15 % contained 1.7 mg of Darunavir.
2) Darunavir Placebo Film batch number FID #3874; B32.2 - 32.3 [1.5 × 1.5 cm^2], placebo film samples.

To test the dissolution profile of different formulations at an *in-vitro* mucosal surface, Caco-2 cells were grown as described above for permeability studies. Caco-2 cells were used between 21-28 days of culture. To test the dissolution profile for cell-free system, the membrane inserts of the Transwell system were used without cell monolayer at the apical side.

To measure the dissolution profile of darunavir from the film formulation and transfer across Caco-2 cell monolayer or cell-free inserts, each film was cut using hole puncher with final surface area of 0.196 cm^2 and 0.0314 cm^2 and contained:

- Darunavir, drug loading 6.15% contained 0.148 mg and 0.0237 mg of darunavir, respectively.

The inserts with cell layers and cell-free were pre-incubated for 30 min with fresh transport medium. For absorptive permeability, the experiment was initiated by adding 500, 100, 28 or 0 µL of the test solution to the apical chamber of the inserts with 1500 µL transport medium in the basolateral chamber. In drug-drug interactions studies, the transport medium also contained transporter inhibitors. Both chamber were pre-incubated for 30 min with transport medium containing appropriate inhibitor to saturate any transporter binding sites.

At the start of the experiment, the film formulation under investigation was placed carefully on the top of the cell layer using forceps and a TER reading was taken within 2 min.

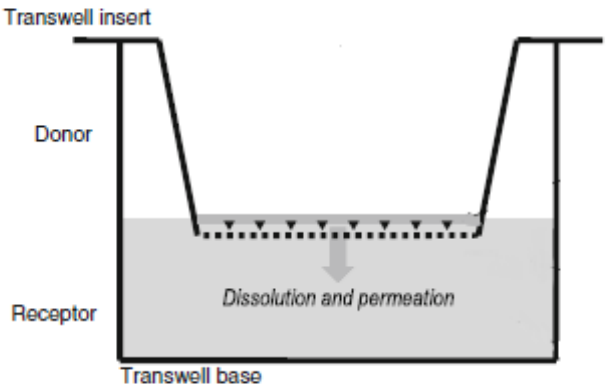


Figure 11. Schematic diagram of dissolution and permeation process in the Transwell®. The net effect of these processes was observed as drug appearance in the receiver chamber.

At intervals, the Transwell insert was moved to a new well containing fresh transport medium, thereby simplifying the sampling of the receiver fluid and ensuring that sink conditions were maintained. After each sampling time point, the Transwell plate was returned to the 37 ˚C incubator and placed under stirring conditions (50 rpm). After the last time point, samples from apical and basolateral chambers were collected and Transwell insert were placed in new well containing 1500 µL methanol (basolateral chamber) and 500 µL methanol were added to apical side. After 120 min, samples were collected, analysed and where used to calculate recovery of the drug. All samples were collected into Eppendorf tubes and analysed for darunavir concentration using LC MS/MS system. The integrity of the cell monolayer was measured by taking TER readings before and after each experiment using an EVOM™ epithelial voltohmmeter.

2.5. Drug transport across colorectal tissue segments

2.5.1. Animal welfare

All *ex-vivo* experiments were conducted with tissue derived from animals culled for different experimental purposes under the project licenses of the United Kingdom Home Office in accordance with the United Kingdom Animal Scientific Procedures Act, 1986). These 'unwanted' tissues were obtained freshly from different researchers at King's College London.

2.5.2. Tissue preparation

Excised Segments – Male Wistar guinea-pigs, Male Wistar rats and Male New Zealand white rabbits were used. Excision of colo-rectal tissue was performed under terminal anaesthesia and the last 10 cm of intestine was removed. Intestine was carefully washed with cold Krebs solution and transferred to a beaker with oxygenated (95%O_2/ 5%CO_2) ice cold Kreb's buffer. All segments were cut along their mesenteric border and the muscularis externa was removed using blunt dissection. Care was taken to avoid Peyer's patches. The stripped colo-rectum mucosae were mounted in modified Ussing Chambers (Harvard Apparatus, Cambridge, UK) containing oxygenated 37 $^{\circ}$C transport buffer solutions and tissue was allowed to recover for 30 min. The effective exposed area of the tissues was 0.2 cm^2. The modified Ussing Chamber system includes six chambers, a 12-channel gas manifold and a heat block to control the temperature. Vertical chambers allow to use electrodes to measure voltage potential and transmembrane electrical resistance.

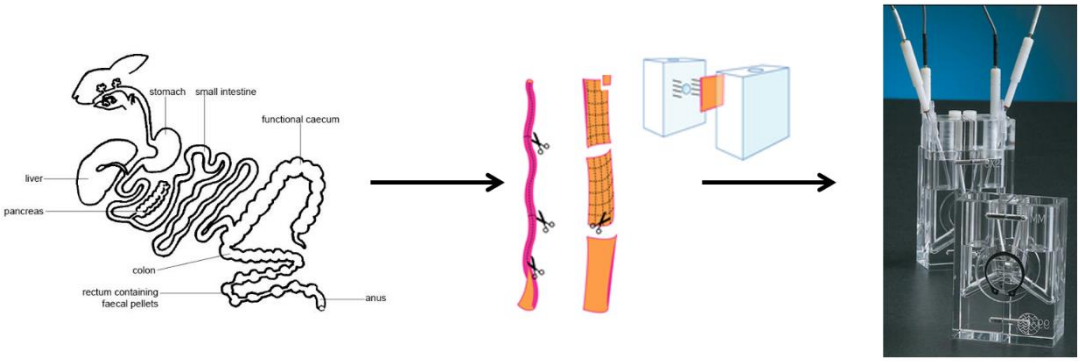


Figure 12. Schematic diagram of mounting colorectal tissue segments to vertical diffusion chambers.

Before an experiment Ussing Chambers were assembled and adjusted for background resistance and potential difference. The viability of the tissue was monitored by measuring potential difference (PD). In addition to the electrical monitoring, the low permeability, fluid phase marker compound mannitol was included in every experiment as a control for the integrity of the tissue.

2.5.3. Krebs solution

Krebs solution was composed of: 1.2 mM magnesium sulphate, 1.2 mM potassium dihydrogen phosphate, 2.5 mM calcium chloride dehydrate, 4.7 mM potassium chloride, 11.1 mM D-glucose, 25 mM sodium bicarbonate and 118 mM sodium chloride made up to volume in de-ionised water.

2.5.4. Test solutions

Drugs of interest were dissolved in DMSO and required concentrations were produced by reconstituting in Krebs solution. Each of the drugs was in radiochemical form to allow sensitive detection of drug transport: C^{14}-mannitol, H^{3}-mannitol, H^{3}-digoxin, C-^{14}-tenofovir and C^{14}-darunavir. To achieve the necessary concentrations, non-radioactive drugs were used. The final tenofovir concentration was 100 µM, darunavir 10 µM and Digoxin 40 µM in 1% DMSO v/v. All solutions were prepared before start of experiment and all experiments were performed at 37°C.

2.5.5. ARV drug permeability across colo-rectal tissue segments

The P_{app} for all compounds was determined in three independent experiments. The tissue was allowed to recover for 30 min, bathed bilaterally with 0.35 mL of Krebs solution and gassed continuously with 95% CO_2/5% O_2 at pH 7.4 maintained at 37°C to produce physiological stability. The experiments were started by removing Krebs solution from both sides and drug-containing Krebs solution was added into the donor compartment and Krebs solution into the receiver compartment. Samples, 20 µL, from both donor and receiver side of each chamber were taken and considered as time zero (for assessment of initial concentration and background radioactivity, respectively). Each 15 min, 100 µL samples were taken from the receiver compartment and replaced with fresh Kreb's buffer up to 60 min. At the end of the experiment, 100 µL samples were again taken from both the donor and receiver chambers. All samples were collected into scintillation vials, mixed with 4 mL of scintillation fluid and analysed a Beckman Coulter LS6000TA (Beckman Coulter™, Bucks, UK).

2.5.6. Data and statistical analysis

Data analysis was performed using Microsoft Excel 2013. Statistical data was analysed using GraphPad Prism® (Version 5.01 for Microsoft Windows, GraphPad Software, San Diego, CA, USA). To compare absorptive and secretory permeability in the presence of inhibitors to the control condition (no inhibitor), a one-way Anova with Dunnett's post-test was used and considered significant for $p \leq 0.05$. Data represent mean ± standard deviation from at least three independent studies, each performed in triplicate.

2.6. *In-silico* modelling of ARV drug binding to P-glycoprotein

2.6.1. Molecular docking of ligands with P-glycoprotein

Coordinates of the P-gp efflux pump were obtained from the P-gp crystal structure from *Mus Musculus* (PDB ID 3G61, 4.35 Å resolution) reported by Aller S.G. et al [90]. The ligands were generated by Chem3D 15.0 software. All the structures were minimised using the AMBER 12.0 package program. Molecular docking protocols were used in order to predict the binding site and affinities for a number of ligands. The relationship between the binding affinity of the ligands under study and the docking score was used for the comparison of the binding energies and affinities of all the diverse ligands to the P-gp efflux pump. Molecular docking was performed to generate several distinct binding orientations and binding affinities for each binding mode. Subsequently, the binding modes that showed the lowest binding free energy were considered as the most favourable binding modes.

AutoDock SMINA was used for the molecular docking of the ligands to the efflux pump structures to find the best binding pocket by exploring all probable binding cavities in the protein. Then the GOLD (Genetic Optimization of Ligand Docking) molecular docking method was applied for the docking of the ligands into the SMINA-located best binding site for performing flexible molecular docking and determining more precise and evaluated energies and scores. Based on the fitness function scores and ligand binding positions, the best-docked poses for each ligand were selected. The fitness function score of poses, generated using the GOLD program that has the highest GOLD fitness energy reveals the best-docked pose for each system was determined by analysing the fitness function score of poses (GOLD fitness energy) which was generated using the GOLD docking program.

The Genetic algorithm (GA) is used in GOLD ligand docking to examine the ligand conformational flexibility along with the partial flexibility of the protein [169]. The maximum number of runs was set to 20 for each compound and the default parameters were selected (100 population size, 5 for the number of islands, 100,000 number of operations and 2 for the niche size). Default cut off values of 2.5Å (dH-X) for hydrogen bonds and 4.0 Å for van-der-Waals distance were used.

When the solutions attained RMSD values within 1.5 Å, GA docking was terminated.

2.6.2. Molecular Dynamics simulations of P-gp in complex with compounds

The best poses of mannitol, digoxin, tenofovir, dapivirine and darunavir located in transmembrane domains of P-gp efflux pump were selected to provide the corresponding complex of each ligand with P-gp to run MD simulations combined with MM-PBSA/MM-GBSA calculation. A simulation for ligand-free P-gp was run as a control. All the MD simulations were carried out using the AMBER 12.0 package. Each system was solvated using an octahedral box of TIP3P water molecules. Periodic boundary conditions and the particle-mesh Ewald (PME) method were employed in all of the simulations [170]. During each simulation, all bonds in which the hydrogen atom was present were considered fixed and all other bonds were constrained to their equilibrium values by applying the SHAKE algorithm [171] . The force fields parameters for the ligands were generated by using the ANTECHAMBER module of the AMBER program.

A cut off radius of 12Å was used for the ligand-free proteins and complexes. Each of two minimization phases were performed in two stages. In the first phase, ions and all water molecules were minimized for 500 cycles of steepest descent followed by 500 cycles of conjugate gradient minimization. Afterwards, the systems were minimized for a total of 2500 cycles without restraint wherein 1000 cycles of steepest descent were followed by 1500 cycles of conjugate gradient minimization. After minimisations, the systems were heated for 500 ps while the temperature was raised from 0 to 300 K, and then equilibration was performed without a restraint for 100 ps while the temperature was kept at 300 K. Sampling of reasonable configurations was conducted by running a 50 ns simulation with a 2 fs time step at 300 K and 1 atm pressure. A constant temperature was maintained by applying the Langevin algorithm while the pressure was controlled by the isotropic position scaling protocol used in AMBER [172]. All histidines were protonated at their δ-nitrogen atoms.

To perform MM-PBSA/MM-GBSA calculations, 10 snapshots were collected from the last 100 ps of simulations of protein-ligand complexes for post processing analysis. The gas-phase interaction energy between the protein and the ligand ΔE_{MM} was the sum of electrostatic and van der Waals interaction energies. The solvation free energy ΔG_{sol} was the sum of the polar (ΔG_{PB}) and non-polar (ΔG_{SA}) parts. The ΔG_{PB} term was calculated by solving the finite-difference Poisson-Boltzmann equation using the internal PBSA program. The SCALE value was set to 5. The Parse radii were employed for all atoms [173]. The solvent probe radius was set at 1.4 Å (with the radii in the prm top files). MM-PBSA running was performed with the PBSA module (PROC=2). The value of the exterior dielectric constant was set at 80, and the solute dielectric constant was set at 1 [174]. The nonpolar contribution was determined on the basis of the solvent accessible surface area (SASA) using the LCPO method [175], $\Delta G_{SA}=0.04356\times\Delta SASA$ and CAVITY-OFFSET set at -1.008.

In the MM-GBSA calculations, like the MM-PBSA calculations, the gas-phase interaction energy (ΔE_{MM}) and the non-polar (ΔG_{SA}) part of the solvation energy were calculated. The electrostatic solvation energy in ΔG_{GB} was calculated by using GB models [176]. A value of 80 was used for the exterior dielectric constant, and a value of 1 was used for the solute dielectric constant for comparison. The binding free energies were calculated by using both the MM-PBSA and the MM-GBSA methods.

* Molecular docking was performed by Dr Jamshidi Shirin.

Chapter Three
Results

3.1. Optimizing *in-vitro* model conditions

3.1.1. Characterisation of Caco-2 cells

Caco-2 cells grew well in flasks with medium containing 10 per cent serum and after reaching 80 per cent confluency the cells were passaged at a 1:6 ratio into new flasks for further culture or were seeded on Transwell membranes or 96-well plates for drug permeability/uptake experiments (Figure 13). Cells were checked regularly by light microscopy. This cell line, for all experiments was cultured and tested between passage numbers 54-64.

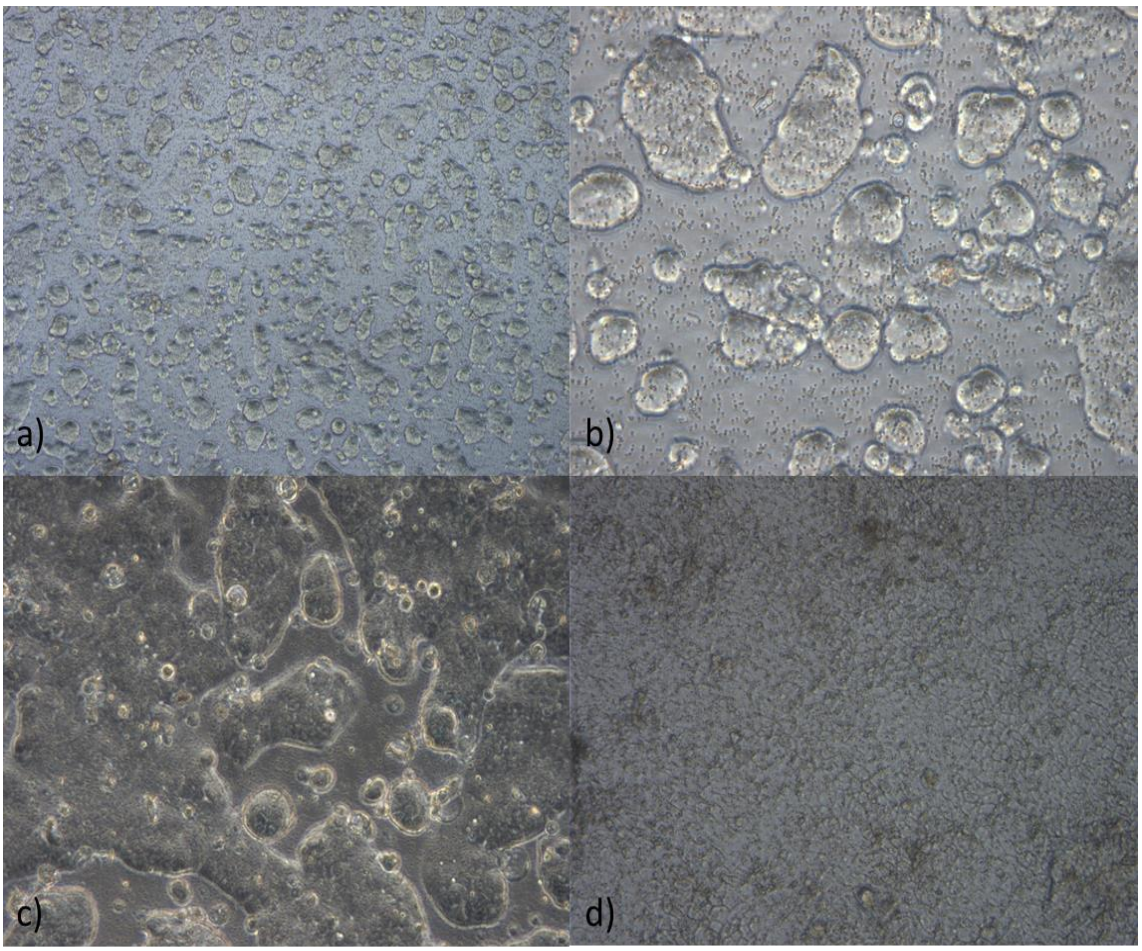


Figure 13. Caco-2 cells grown on Transwell inserts after: a) day 2 × 100 magnification, b) day 2 × 400 magnification, c) day 3 × 200 magnification and d) day 13 × 200 magnification. Spaces where the layer was incomplete were present at day 2 and day 3, on day 13 the layer was continuous.

3.1.2. Cell layer morphology, protein expression and barrier properties

To determine the presence of P-gp, MRP-2 and BCRP protein expression in Caco-2 cells and rabbit colorectal mucosal segments, cell and tissue lysates were analysed via Western blot using monoclonal anti-P Glycoprotein antibody (EPR10364), monoclonal anti-MRP2 antibody (EPR10997(2)) and monoclonal anti-BCRP/ABCG2 antibody (EPR2099(2)) as the primary antibodies, respectively. Caco-2 cells and rabbit tissue colorectal mucosal segments, showed immunoreactions as densely stained bands in the molecular weight range of 141 kDa, 174 kDa and 72 kDa indicating the presence of P-gp, MRP-2 and BCRP, respectively (Figure 14).

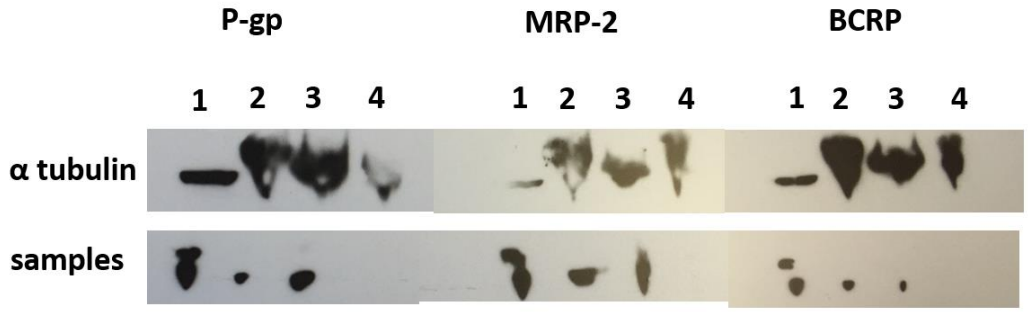


Figure 14. Protein expression of MDR1/ P-gp, MRP-2 and BCRP in samples: 1- Caco-2 cells, 2-rabbir colorectal tissue segments (sample 1), 3- rabbit colorectal tissue segment (sample 2), 4-negative control. Caco-2 cells were cultured in T-flasks and collected after reaching confluency at passage number p58.

In preparation for transport studies cells were grown for 21-28 days on the inserts to provide time for them to differentiate fully. Confocal microscopy revealed the presence of tight junction protein ZO-1 in the 21-day Caco-2 monolayer (Figure 15).

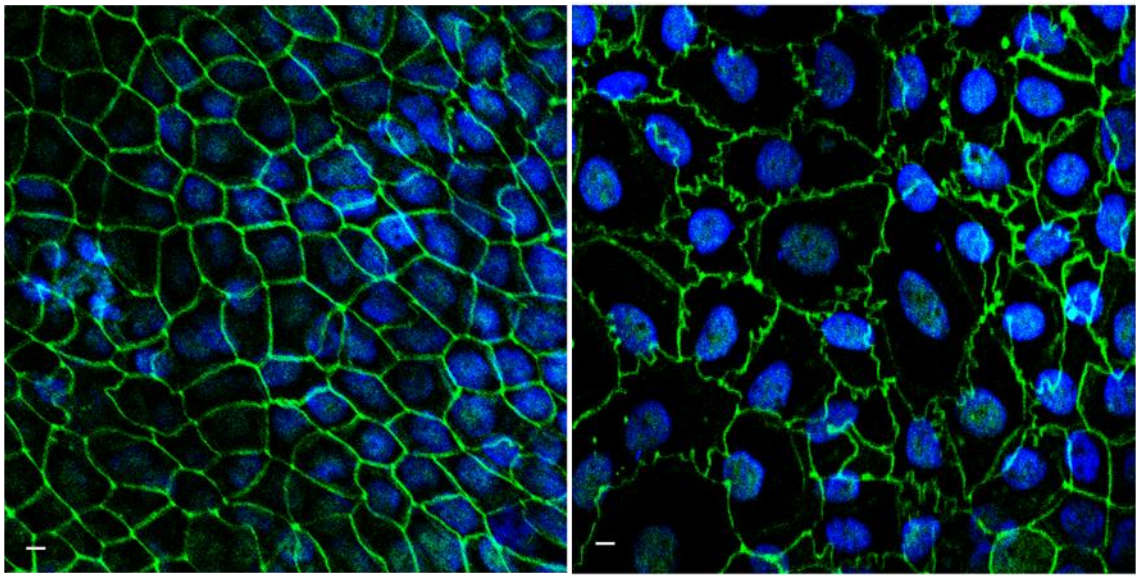


Figure 15. The staining of tight junction protein ZO-1 on Caco-2 cells after 21 days in culture. The imaging was performed on Caco-2 monolayers grown on two separate Transwell® inserts and using two different solutions: a) BLOTTO solution, b) BSA solution. Note: Blue DAPI green ZO-1, tight junction protein, magnification 63×, scale bar 10 µm.

Caco-2 cell monolayer development was monitored by TER measurements (Figure 16). With increasing days of culture the TER reached higher values, the greatest increase in resistance was observed from the third day to the seventh day. The TER for Caco-2 cells increased up to 1650 ± 120 Ω cm^2 on the 21st day of culture. This cell line was cultured over 54-64 passage number, possibly explaining higher TER values compared to those reported for cultures at earlier passage number. To calculate TER, the resistance of a cell-free insert was subtracted from the resistance measured for cell monolayers on inserts. Measurement of cell-free inserts in control experiments over several weeks showed a consistent value of 110 ± 15 Ω cm^2, n ≥ 200.

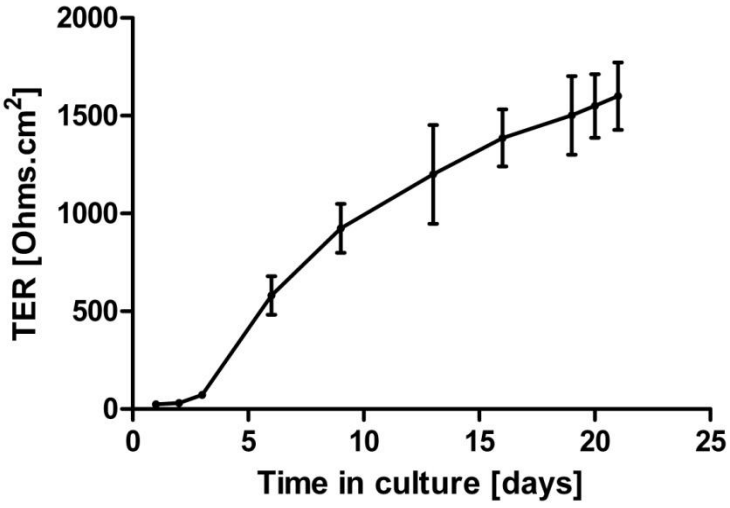


Figure 16. The variation of transepithelial electrical resistance (TER) with days in culture for Caco-2 cells. Data represents mean ± SD, n=10

Additionally, a simple experiment was performed to test whether the differences in TER resulted from short exposures to different media such as those to be used in determining drug permeability. Using caco-2 cells at day 21, TER was monitored over a 120 min exposure to HBSS or HBSS with 1% DMSO with the different solutions applied to the apical and basolateral chamber. It was observed that at no time point during exposure to the different solutions were measurements of TER statistically different for the transport media compared to the control (complete cell culture medium) (Table 6).

Table 6. TER values of Caco-2 cells (21 days in culture) after exposure to different media in the apical and basolateral chamber for 120 min. Data represents n=3, mean ± SD.

Culture condition	**TER at day 21 (Ω cm²)**
DMEM	1520 ± 136
HBSS	1498 ± 134
HBSS + 1% DMSO	1490 ± 101

3.1.3. Cell based assays for evaluating compound toxicity

MTT assay response versus cell number

The metabolic activity of Caco-2 cells following culture at varying seeding densities in cell culture medium for 48 h was measured using the MTT assay. A linear relationship was observed for absorbance vs. seeding density over the range of 1000 – 40000 cells/well. The coefficient of determination (R^2) value for absorbance versus Caco-2 cell relationship was greater than 0.9963 (Figure 17). This determined that over this range of cell seeding density the MTT assay was sensitive to cell number (as a surrogate for cell metabolic activity) and for further experiments utilising the MTT assay, cells were seeded at a density of 10000 cells/well.

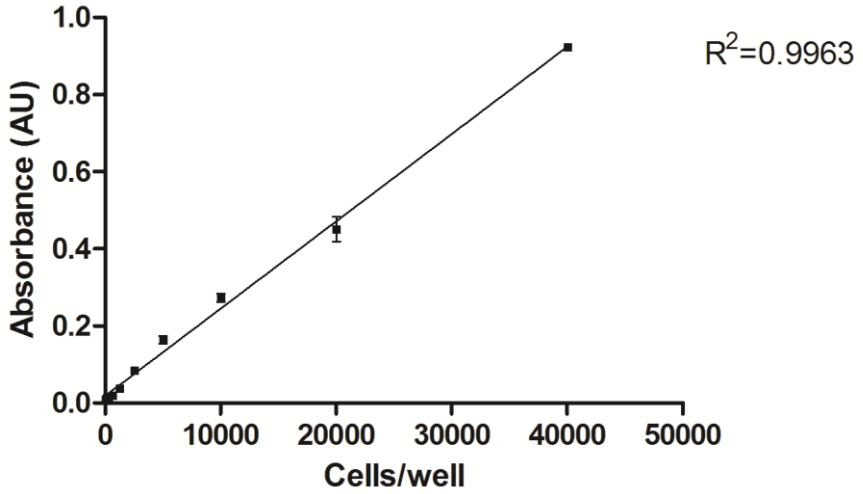


Figure 17. The relationship between Caco-2 cell number vs. absorbance measured using the MTT assay. Data represent mean ± SD, n=4; each experiment performed in triplicate.

3.1.4. Cell viability and membrane damage

To determine experimental conditions for further experiments by assessing the biocompatibility of test reagents at the concentrations to be used, cell viability assay and membrane damage was evaluated using different concentrations of DMSO, Digoxin and the ARV drugs under investigation.

Effect of DMSO on MTT assay response

Caco-2 cells were cultures for 48 h, then exposed for 24 h to varying concentration of DMSO. The cell viability after 24 h of exposure was unaffected by DMSO concentrations between 0 - 1%. The highest concentration of DMSO (5%) used reduced cell viability by 53% (Figure 18). In further experiments, the DMSO concentration used in the test solutions did not exceed more than 1%.

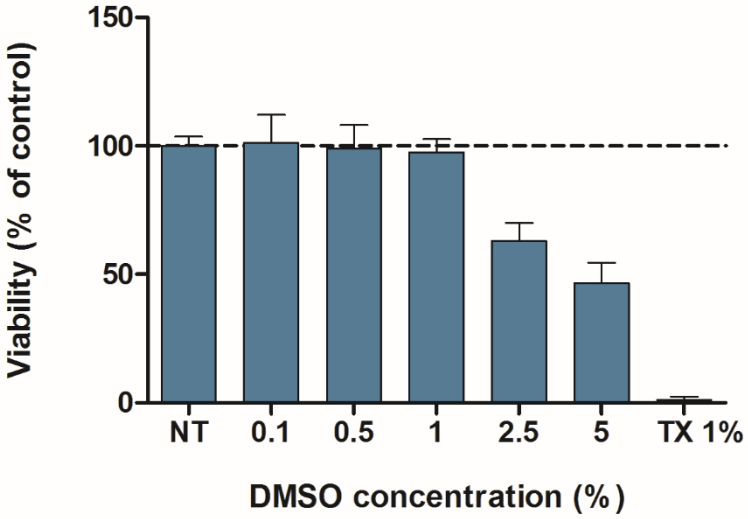


Figure 18. Relationship of cellular metabolic activity versus increasing concentration of DMSO (0.1 - 5%) after 24 h of DMSO exposure to Caco-2 cells at day 2 in culture (NT- non treated cells, TX 1%- cells treated with Triton-X 1% (v/v)). The product of cell metabolic activity was measured spectrophotometrically at 560nm. Data represent mean ± SD, n=3; each experiment was performed in triplicate.

Selection of digoxin concentration for transport studies

Caco-2 cells were exposed for 24 hours to varying concentration of digoxin at the 14th day of culture (Caco-2 cells monolayer appeared to be complete). Digoxin showed a dose-dependent toxicity profile (Figure 19). The highest concentration of Digoxin decreased cell viability by 51.5% compared to control. Digoxin concentration in the range of 0 to 15.7 µM, showed a reduction of 7% in cell viability, which was not statistically different compared to control. The LDH release was 10.5 ± 0.6 % at the maximum digoxin concentration, whereas at the lower concentration in the range of 8.8 – 15.7 µM, LDH release was only 0.08 and 2%, respectively. LDH release after exposure to digoxin showed a negative correlation with effects in the cell viability (MTT) assay with Pearson's correlation coefficient of value -0.96 (Figure 20). To ensure that further transport experiments were performed in non-toxic conditions, digoxin at 10 µM concentration was used for transport experiments.

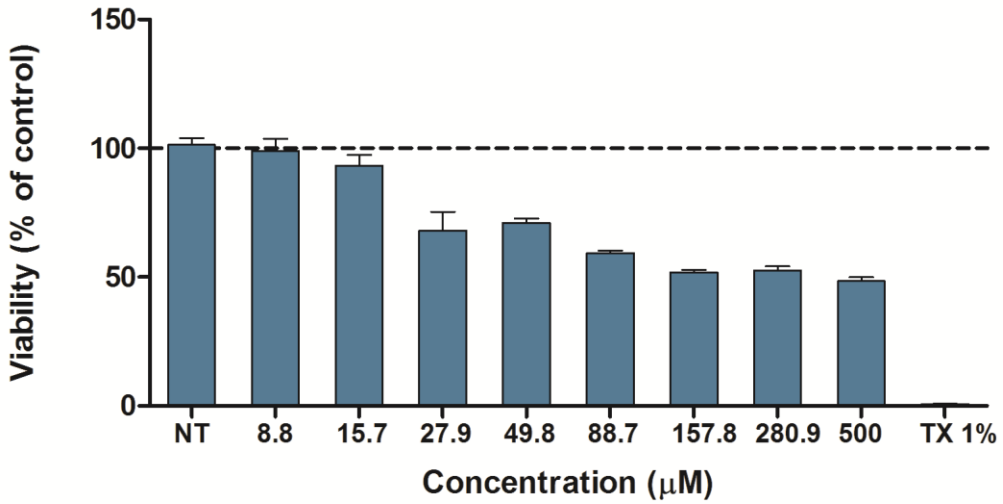


Figure 19. The effect of 24 h exposure of varying concentration of digoxin on the viability of Caco-2 cells (14th day of culture, NT- non treated cells, TX 1%- cells treated with Triton-X 1% (v/v)**).** Viability was calculated as a percentage of the control (cells with medium only). The data represent the mean ± SD, n=3; each done in triplicate.

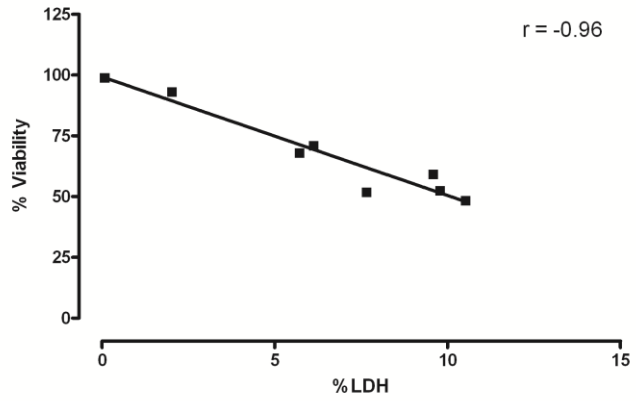


Figure 20. The correlation between cellular LDH release and metabolic activity from Caco-2 cells at 14th day of culture after exposure to Digoxin for 24 h. The data represent the mean, n=3; each experiment was performed in triplicate, r-Pearson correlation.

Selection of tenofovir concentration for transport studies

The biocompatibility of tenofovir with Caco-2 cells was tested by MTT assay and LDH assay at varying concentrations at different days of cell culture, including 2, 7 and 14 days. When cells were exposed to tenofovir for 24 h, tenofovir did not show any significant toxicity at any of the concentrations tested or at any of the different days of Caco-2 cell culture (Figure 21).

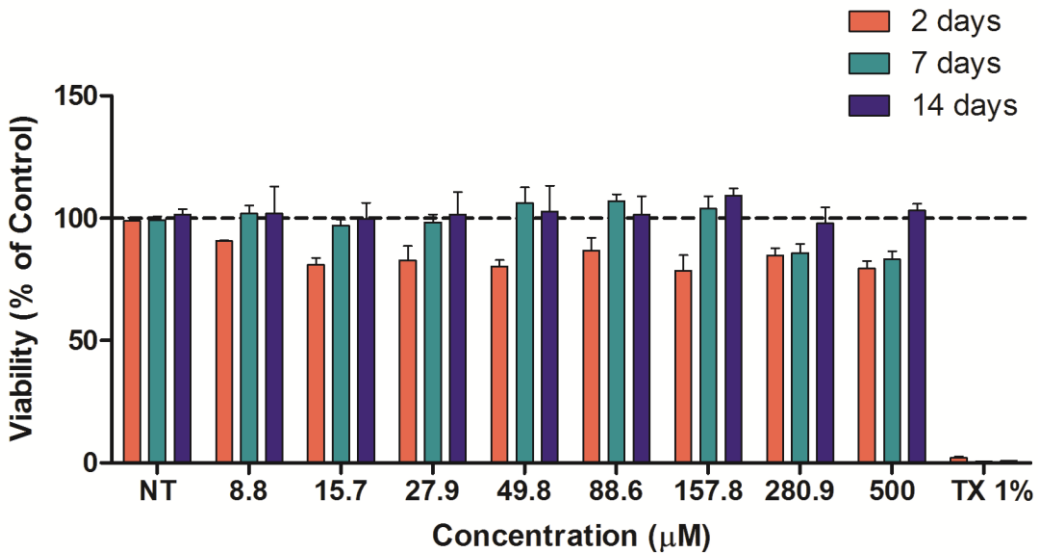


Figure 21. The effect of different concentration of tenofovir on Caco-2 cells (at 2nd, 7th and 14th day of culture) after 24 h of exposure to drug (NT- non treated cells, TX 1%- cells treated with Triton-X 1% (v/v)). Viability was calculated as a percentage of the control (cells with medium only). The data represent the mean ± SD, n=3; each experiment was performed in triplicate.

In cells cultured for 2 days, cell viability decreased by 21% at the highest tested concentration of tenofovir. LDH release was not significantly different to control; below 2% of the control for any tested concentration. In cells cultured for 7 days, the concentration range between 0 – 157.8 µM did not produce any toxicity; cell viability was in the range of 98.3 – 106.8%. The highest concentration of tenofovir reduced cell viability by 17% and LDH release was below 1.5% of the control. In cells cultured for 14 days, tenofovir did not produce any reduction in cell viability even in the highest concentration. The maximum LDH release did not exceed 0.5% of the control. Tenofovir was tested for any interference with LDH

using the standard LDH provided by the manufacturer and did not present any interference.

Selection of dapivirine concentration for transport studies

Dapivirine showed a dose-dependent toxicity profile. The highest tested concentration, 100 µM reduced cell viability by 90.8 ± 1.7%, 79.9 ± 2.5% and 62.6 ± 8.5% at the 2nd, 7th and 14th day of culture, respectively (Figure 22). In cells cultured for 2 days, the concentration range between 0 – 30 µM did not reduce cell viability compare to control and LDH release was below 4% of the control.

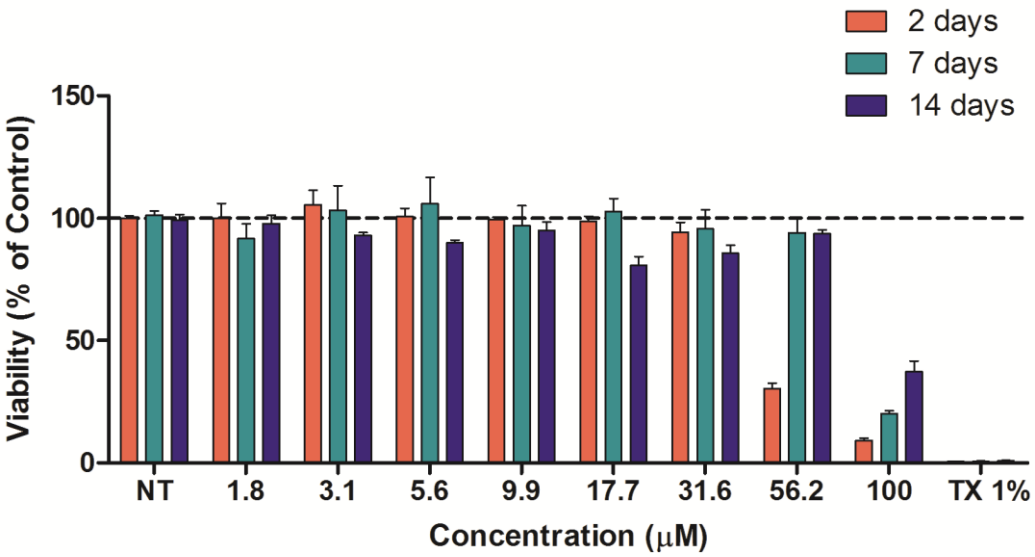


Figure 22. The effect of different concentrations of dapivirine on Caco-2 cells (cultured for 2, 7, or 14 days) after 24 h of exposure (NT- non treated cells, TX 1%- cells treated with Triton-X 1% (v/v)). Viability was calculated as a percentage of the control (cells with medium only). The data represent the mean ± SD, n=3; each experiment was performed in triplicate.

However, dapivirine concentration at range of 50 - 100 µM reduced cell viability by 70% and LDH release was statistically significant, reaching up to 44% of the control. LDH release showed a strong negative correlation with effects on cell viability measured using the MTT assay with Pearson's correlation coefficient value of -0.99 and -0.96 for the evaluations conducted using Caco-2 cells cultured for 2 or 7 days (Figure 23). At the 7th and 14th day of culture, only the highest concentration of dapivirine reduced cell viability and increased LDH release (above 45% of the control). The concentration range of 0 – 50 µM did not reduce cell viability (93 - 94% of the control).

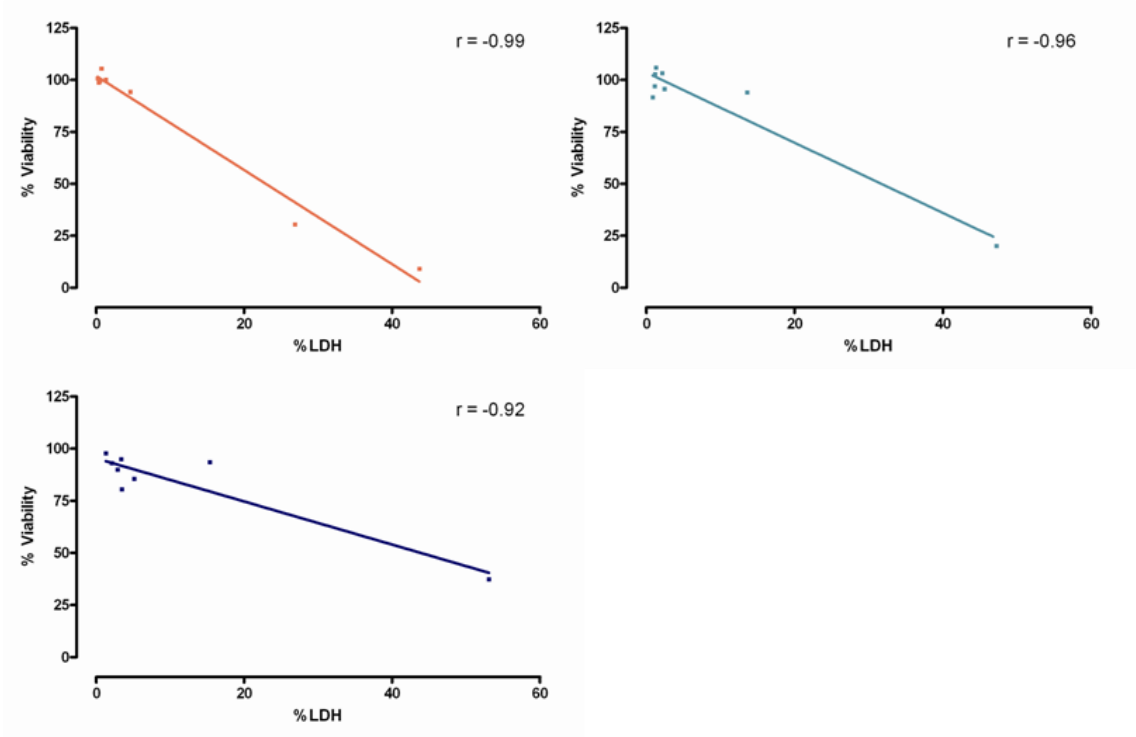


Figure 23. The correlation between cellular LDH release and metabolic activity of Caco-2 cells cultured for 2 (orange), 7 (green) or 14 (blue) days and exposed to Digoxin for 24 h. The data represent the mean, n=3; each experiment was performed in triplicate, r-Pearson correlation.

Selection of darunavir concentration for transport studies

Darunavir produced a concentration-dependent reduction in cell viability only in Caco-2 cells cultured for 2 days, with no effect on cells cultured for 7 or 14 days (Figure 24). In cells cultured for 2 days, cell viability decreased by 44% compared to control at the highest concentration of darunavir tested, however there was corresponding effect on LDH release (all values below 5%). None of the darunavir concentrations used reduced the viability of cells cultures for 7 or 14 days in culture, with all viability measurements remaining above 96%. LDH release was not significantly different to control with release values below 5%. To ensure that further transport experiments were performed in non-toxic conditions, darunavir till 150 µM concentration was used for transport experiment.

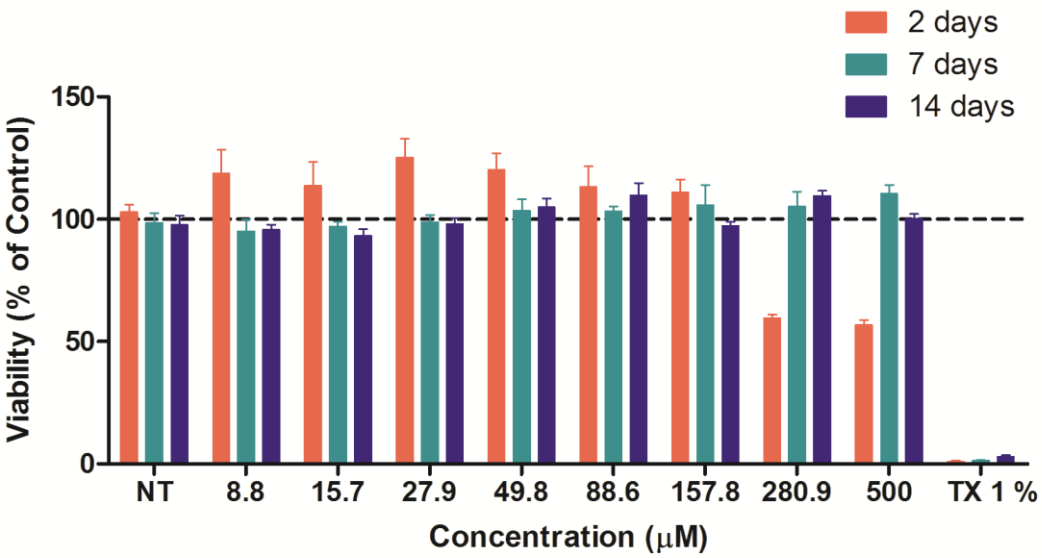


Figure 24. The effect of different concentration of Darunavir on Caco-2 cells (cultured for 2, 7, or 14 days) after 24 h of exposure (NT- non treated cells, TX 1%- cells treated with triton X 1% (v/v)). Viability was calculated as a percentage of the control (cells with medium only). The data represent the mean ± SD, n=3; each experiment was performed in triplicate.

3.1.5. Caco-2 cell permeability and P-gp transporter activity

Before investigating the permeability of antiretroviral drugs across Caco-2 cell monolayers, it was important to measure the permeability of ^{14}C-mannitol and ^{3}H-digoxin, used as negative and positive controls for the transporter p-glycoprotein, respectively. Additionally, ^{14}C-mannitol functioned as a paracellular marker to provide a reference measure of the barrier properties of the monolayers. Absorptive (A-B) and secretory (B-A) digoxin (Figure 25a) and mannitol (Figure 25b) flux was determined and linearity of flux (dQ/dt) for both compounds was >0.99. The mass balance (recovery) for mannitol in all assays was >97.3 % and for digoxin was >96.7 % (Table 7). Absorptive and secretory apparent permeability for mannitol was 0.18 ± 0.04 × 10^{-6} cm/s and 0.19 ± 0.05 × 10^{-6} cm/s, respectively. For digoxin, 10 µM, absorptive and secretory permeability was 0.5 ± 0.1 × 10^{-6} cm/s and 8.4 ± 3.2 × 10^{-6} cm/s, respectively (Figure 26a). The efflux ratio ($ER=P_{app\ (B-A)}/P_{app\ (A-B)}$) for mannitol and digoxin was 1.1 ± 0.2 and 16.5 ± 1.0, respectively (Figure 26b). At the beginning and at the end of the experiment the TER was measured and no substantial change in TER was observed (all values were within 85 % of the control).

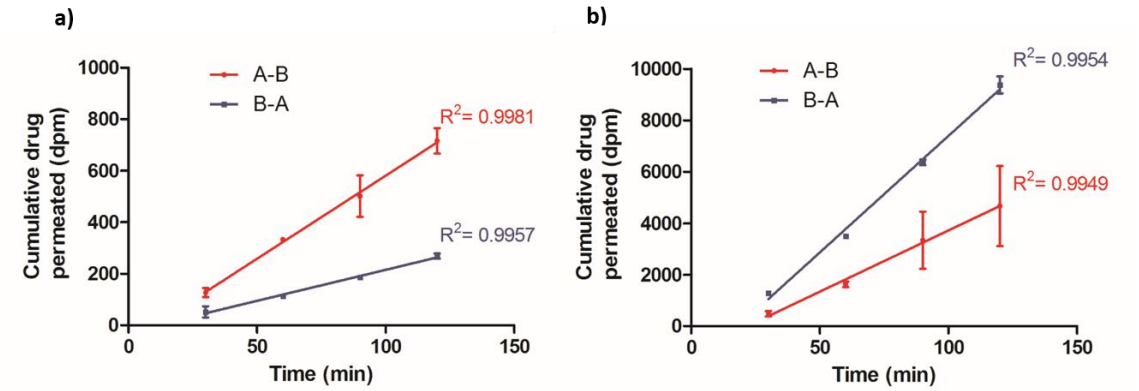


Figure 25. Flux of a) Digoxin 10 µM b) C^{14}-Mannitol with respect to time in both apical-to-basolateral (red line) and basolateral-to-apical (blue line) directions across Caco-2 cell monolayers over 120 min. Samples were collected for analysis every 30 min. Data represent the mean ± standard deviation from three independent studies, each performed in triplicate.

Table 7. Total recovery of mannitol and digoxin after 2h incubation period at the apical side of Caco-2 cell monolayers. Data represent mean ± SD (n=3).

Compound	Total recovery (%)
Mannitol	97.3 ± 4.2
Digoxin	96.7 ± 5.6

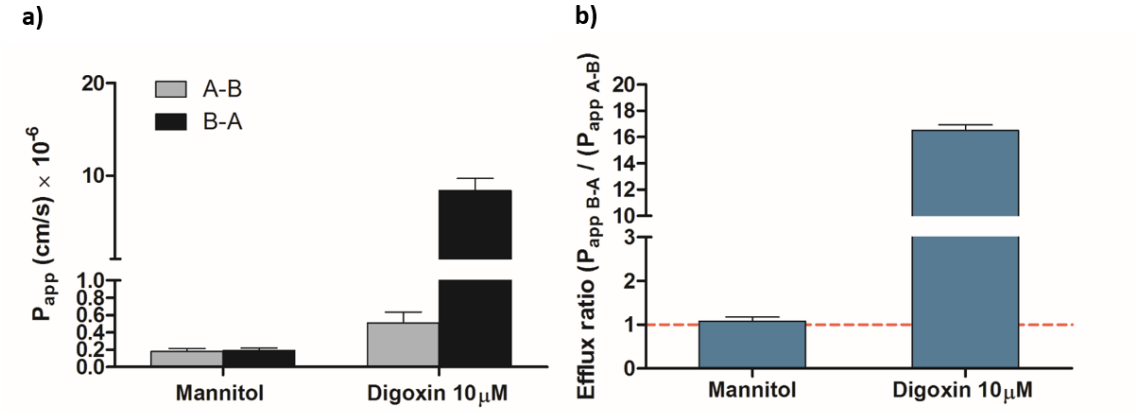


Figure 26. Permeability of mannitol and digoxin. a) Apparent permeability of ^{14}C-mannitol and ^{3}H-digoxin 10 µM across Caco-2 cells in apical-to-basolateral and basolateral-to-apical direction. **b)** Efflux ratio ($ER=P_{app(B-A)}/P_{app(A-B)}$) measured in Caco-2 cell monolayer for ^{14}C-mannitol and ^{3}H-digoxin 10 µM. Data represent mean ± SEM, n=6; each experiment performed in triplicate. Grey bars indicate transport in absorptive direction, black bars indicate transport in secretory directions.

Acceptance criteria for drug transport assays were developed to ensure that results were robust, reproducible and the method was standardised. Acceptance criteria were based on, passage number, days in culture of the monolayer, TER values, recovery of the drug, linearity of the cumulative drug transport and permeability of mannitol (used in each tested well as paracellular marker) (Table 8). Values that were out of the range of acceptance criteria were excluded from further calculations (a non-significant amount of values were excluded from data set).

Table 8. Acceptance criteria for drug transport assay.

Passage number	Passage 54-64
Monolayer age	21^{st}-28^{th} day of culture
TER values	$>1250\ \Omega\ cm^2$ $\pm$ 15% deviation from initial value
Drug recovery	$100 \pm 15\%$
Linearity of cumulative drug transport	$r^2 > 0.97$
Mannitol permeability	$< 0.3 \times 10^{-6}$ cm/s

To confirm P-gp transporter activity in Caco-2 cells, the effect of p-glycoprotein transport inhibitors on the bidirectional transport of digoxin (P-gp substrate) was tested. With increasing concentration of verapamil and CsA, the efflux ratio of digoxin gradually reduced, approaching approximately 1.9 and 7.4, respectively, at the highest concentration (10 µM) of the inhibitors (Figure 27a and 27b). Inhibition by known P-glycoprotein inhibitors provided evidence that the digoxin efflux is transporter mediated, with P-glycoprotein at least partially responsible. During the experiment, ^{14}C-mannitol was used as a paracellular marker and its permeability was unaffected by the presence of P-gp inhibitors. Comparable

effects were found in cell accumulation assays, digoxin uptake was enhanced in the presence of verapamil 10 µM by 201 ± 16% and in the presence of CsA by 181 ± 26% (Figure 28a and 28b). For both P-gp inhibitors the enhanced accumulation of digoxin was concentration dependent.

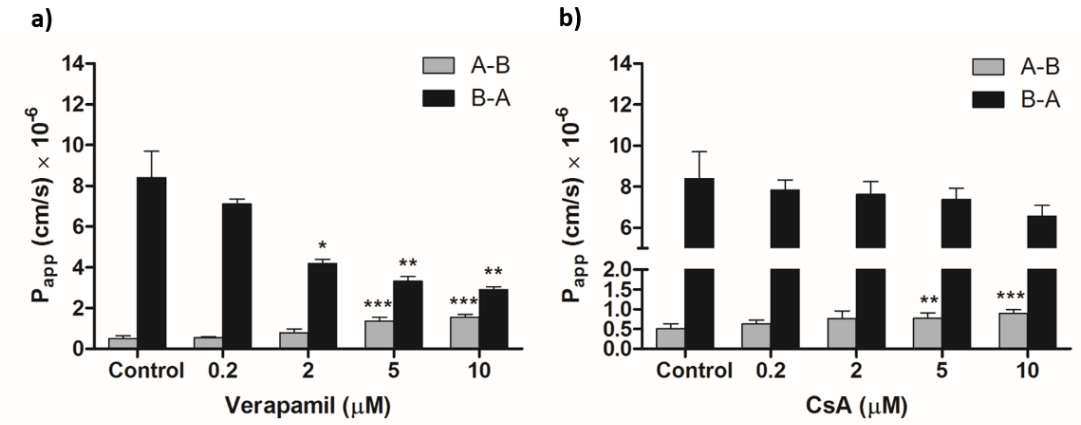


Figure 27. Effect of co-administering varying concentration of a) verapamil 0.2 – 10 µM b) CsA 0.2 – 10 µM on the absorptive and secretory permeability of digoxin 10 µM across Caco-2 cell monolayers. Data represent mean ± SD, n=3; each experiment performed in triplicate. Grey bars indicate transport in absorptive direction, black bars indicate transport in secretory directions.

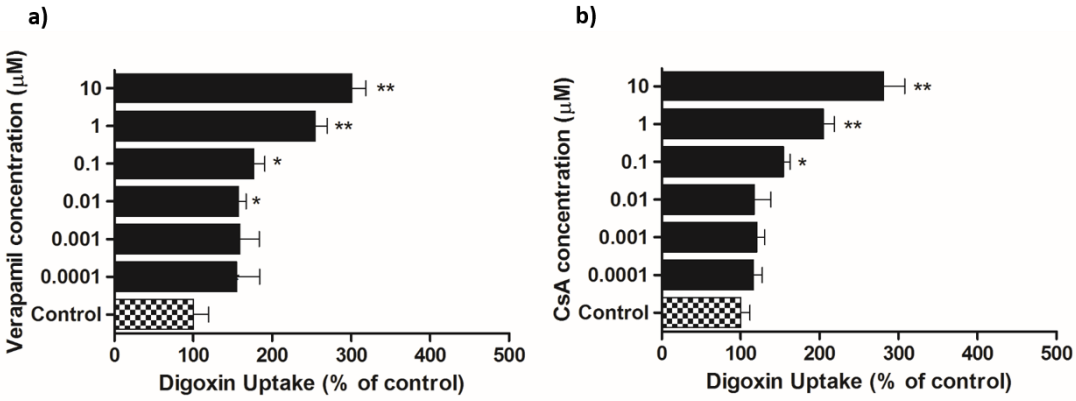


Figure 28. Effect of varying concentration of a) verapamil 0.0001 – 10 µM, b) CsA 0.0001 – 10 µM on the accumulation of digoxin 10 µM by Caco-2 cells in 48-well plates. Data represents mean ± SEM from three independent studies each performed with six replicates per data point (** $p<0.01$; * $p<0.05$).

The bioavailability of compounds can be affected by administration of certain GRAS (generally recognize as safe) excipients, an effect that may be mediated through transporter interactions. In this study the role of PEG 200 and PEG 400 on digoxin permeability across Caco-2 cell monolayers was investigated (Figure 29). During the experiment, mannitol transport and TER were measured to confirm cell monolayer integrity in the absence and presence of 1% (v/v) PEG 200 and 400. TER values were not significantly different compared to control (digoxin 10 µM with ^{14}C-mannitol), all values above 1400 Ω cm^2. Mannitol permeability was measured in the presence of excipients and no significant difference was observed.

When the transport of digoxin 10 µM was measured in the presence of PEG 200 1% (v/v) the absorptive and secretory transport remained unaffected with an efflux ratio of 15.5 ± 1.2 compared to control 16.5 ± 1.0. When verapamil was added to the experiment (PEG 200 1% (v/v) and verapamil 10 µM) the efflux ratio was reduced to 3.1 ± 0.8. In the presence of PEG 400 1% (v/v) alone the efflux ratio of digoxin was reduced by 85% to 2.5 ± 1.0, and when verapamil was added to the experiment (PEG 400 1% (v/v) and verapamil 10 µM) the efflux ratio was abolished completely (ER = 1.4).

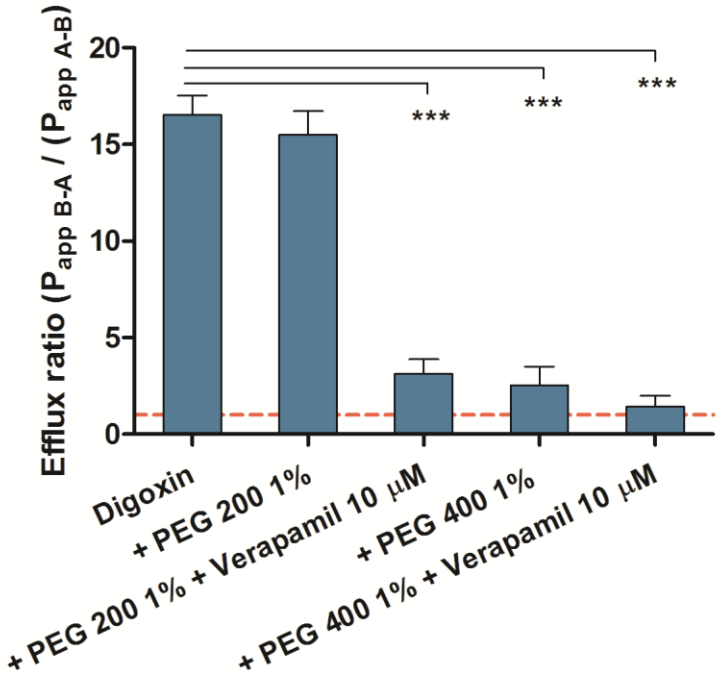


Figure 29. Efflux ratio measured in Caco-2 cell monolayers for digoxin 10 µM and digoxin 10 µM in the presence of: PEG 200 1% (v/v), PEG 400 1% (v/v), PEG 200 1% (v/v) with verapamil 10 µM and PEG 400 1% (v/v) with verapamil 10 µM. Data represent mean ± SD, from three independent studies each performed in triplicate.

3.2. Tenofovir, dapivirine and darunavir transport across Caco-2 cell monolayers

3.2.1. Tenofovir transport across Caco-2 cell monolayers

As a part of all transport experiments, TER measurements and mannitol permeability were used to evaluate the integrity of Caco-2 cell monolayers. When exposed to varying concentration of tenofovir, the permeability of mannitol was not significantly different from the tenofovir-free control (absorptive $0.18 \pm 0.05 \times 10^{-6}$ cm/s and secretory $0.17 \pm 0.03 \times 10^{-6}$ cm/s) and initial TER values were above 1450 Ω cm^2. Absorptive and secretory permeability of mannitol in Caco-2 cell monolayers exposed to tenofovir were $0.17 \pm 0.03 \times 10^{-6}$ cm/s and $0.18 \pm 0.04 \times 10^{-6}$ cm/s, respectively. TER values were measured at the beginning (t=0 min) and at the end (t=120 min) of the tenofovir transport experiments, and TER values did not decrease to more than 91 ± 4% from the initial reading in the A-B direction and to 91 ± 5% in the B-A direction (Figure 30a). When absorptive and secretory flux of tenofovir 0.1 µM was measured over 120 min, the linearity of flux was 0.9997 (absorptive flux) and 0.9996 (secretory flux) (Figure 30b). Flux was also determined for the higher concentrations of tenofovir (up to 100 µM) and linearity was above 0.99 in both transport directions.

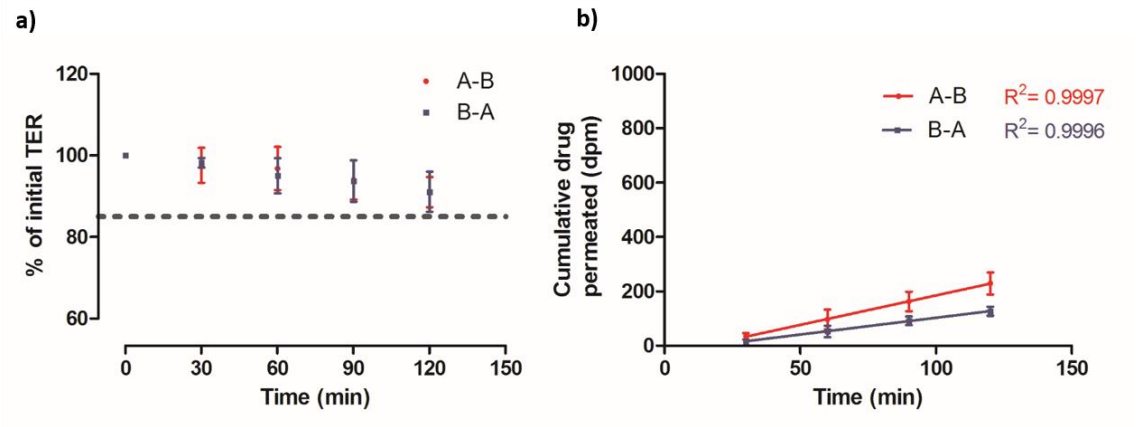


Figure 30. Maintenance of TER during tenofovir exposure and tenofovir flux across Caco-2 cell monolayers. a) The percentage change from the initial TER values of Caco-2 cell monolayers during experiments measuring tenofovir transport in absorptive (red) and secretory (blue) directions. TER values were measured at t=0 (initial TER) and 30, 60, 90 and 120 min after the start of the experiments. b) Flux of tenofovir 0.1 µM with respect to time in both absorptive (red line) and secretory (blue line) directions across Caco-2 cell monolayers over 120 min. Data represent the mean ± standard deviation from three independent studies, each performed in triplicate.

Mannitol mass balance (total recovery %) was measured in all inserts (Caco-2 cell monolayers) exposed to varying concentration of tenofovir and was in the range of 95.9 ± 3.6% in the absorptive direction and 95.8 ± 5.0% in the secretory direction (Table 9). After 120 min of the absorptive transport experiments, mannitol accumulation inside the cells was 1.9 ± 0.6%, and when the compound was applied into basolateral chamber and its appearance was measured in apical chamber, accumulation of the drug inside the cells was only 0.5 ± 0.1%. Total recovery of tenofovir in both direction was concentration-independent in the range of 0.1-100 µM and the mean recovery was greater than 95%.

The intracellular accumulation of tenofovir inside Caco-2 cells was measured after 120 min of transport experiment was 0.44 - 0.88% of the initial concentration of the drug applied into apical chamber or 0.26 – 0.67% of the initial concentration of drug applied into the basolateral chamber (Table 9). Intracellular accumulation of tenofovir was concentration independent irrespective of which side of the monolayer the tenofovir was applied.

Table 9. Recovery of mannitol and varying concentrations of tenofovir after 120 min absorptive or secretory permeability assays across Caco-2 cell monolayers (total recovery, recovery from receiver chamber and intracellular, i.e. cell monolayer). Recovery of mannitol was measured simultaneously with varying concentration of tenofovir and was pooled because the presence of tenofovir had no effect on mannitol recovery or permeability. Data represent the mean ± standard deviation from at least three independent studies, each performed in triplicate.

Compound		Total recovery (%)	% compound	
			Receiver compartment	Caco-2 cell monolayer
apical to basolateral direction				
Mannitol		95.97 ± 3.55	1.82 ± 0.21	1.92 ± 0.58
Tenofovir	0.1 µM	95.75 ± 3.06	1.19 ± 0.08	0.61 ± 0.11
	1 µM	96.92 ± 2.02	1.22 ± 0.07	0.70 ± 0.18
	10 µM	96.65 ± 3.62	1.18 ± 0.04	0.62 ± 0.10
	100 µM	96.18 ± 1.75	1.14 ± 0.05	0.63 ± 0.16
basolateral to apical direction				
Mannitol		95.80 ± 5.01	1.53 ± 0.11	0.47 ± 0.10
Tenofovir	0.1 µM	96.56 ± 3.24	1.05 ± 0.01	0.52 ± 0.15
	1 µM	95.69 ± 3.13	1.03 ± 0.02	0.47± 0.15
	10 µM	97.36 ± 5.14	1.04 ± 0.01	0.49 ± 0.10
	100 µM	97.48 ± 2.81	1.04 ± 0.01	0.36 ± 0.09

The apparent permeabilities of tenofovir (at a range of concentrations) across Caco-2 cell monolayers in absorptive and secretory directions are shown in Figure 31. The results showed that tenofovir permeability was not significantly different to that measured for mannitol. With increased concentration, absorptive transport decreased insignificantly whereas secretory transport remained at the same level. Absorptive and secretory permeability for the lowest tested concentration of tenofovir (0.1 µM) was 0.15 ± 0.04 × 10^{-6} cm/s and 0.14 ± 0.02 × 10^{-6} cm/s, respectively. For the highest concentration tested (100 µM) the respective permeabilities were 0.10 ± 0.02 × 10^{-6} cm/s and 0.14 ± 0.04 × 10^{-6} cm/s. The efflux ratio was around unity, varying from ER = 0.9 at 0.1 µM tenofovir to ER = 1.4 at 10 and 100 µM (Figure 31b).

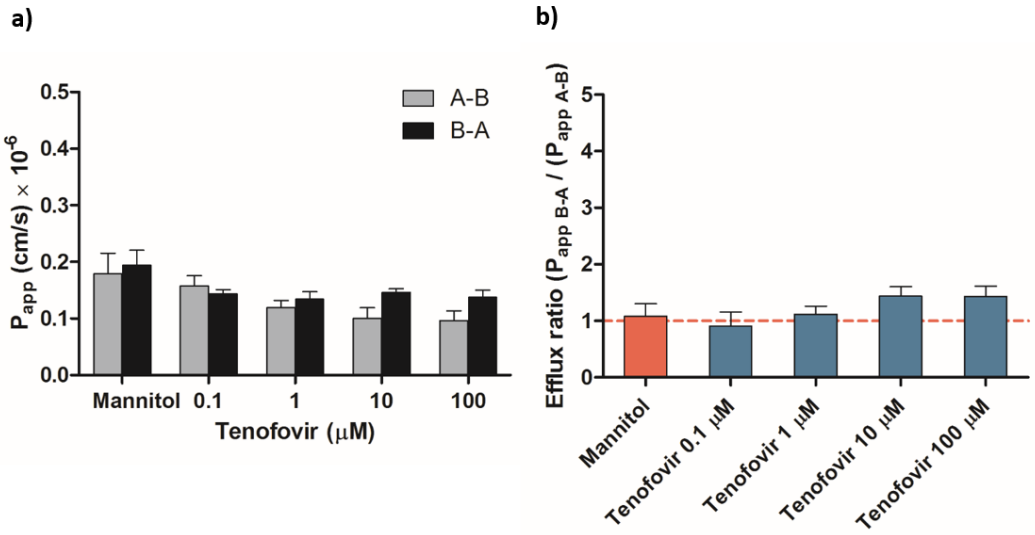


Figure 31. Permeability of varying concentration of tenofovir (0.1 - 100 µM). a) Absorptive and secretory permeability of varying concentrations of tenofovir, plus mannitol control (used as paracellular marker) across Caco-2 cell monolayers. b) Efflux ratio of mannitol and varying concentrations of tenofovir in Caco-2 cell monolayers. Data represent mean ± SD from three independent experiments, all p values > 0.05.

In order to identify any influence of the ABC transporters on tenofovir transport the effect of several inhibitors on drug permeability and cell accumulation were investigated (Figure 32). Tenofovir 100 µM flux in both directions was measured in the presence of P-gp inhibitors including verapamil (0.1-10 µM), GF120918 (0.1-10 µM), haloperidol (0.1-50 µM) and the ratio of tenofovir permeability in secretory to absorptive directions was not significantly different to that ne measured for tenofovir 100 µM alone (Figure 32a). Intracellular accumulation of tenofovir was unaffected by the presence of the P-gp inhibitors, CsA (0.01 and 10 µM), verapamil (0.01 and 10 µM), haloperidol (1 and 75 µM) and GF120918 (0.1 µM) or MRP-2 inhibitor bromsulphthalein (75 µM) (Figure 32b).

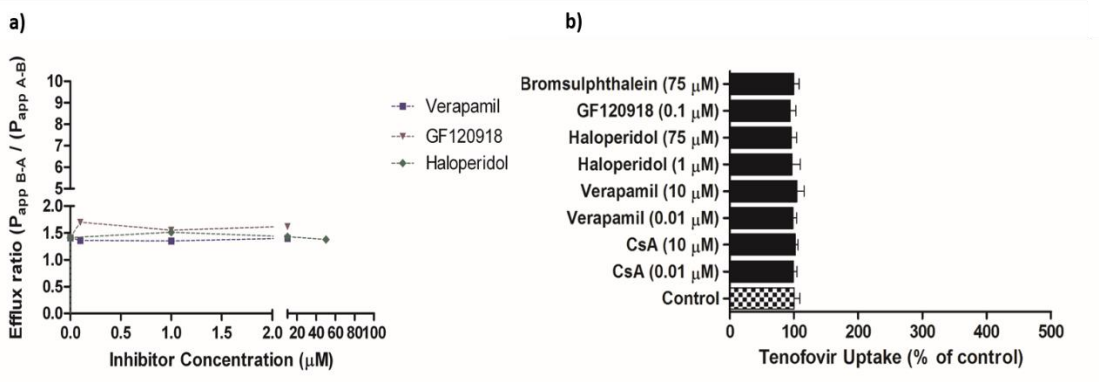


Figure 32. Influence of transporter inhibitors on tenofovir permeability and cell uptake. a) The effect of inhibitors on the efflux ratio of tenofovir 100 µM in Caco-2 cell monolayers. Data represent mean ± SD from three independent studies, each performed in triplicate (all p values > 0.05). b) The effect of transporter inhibitors on the accumulation of tenofovir 100 µM by Caco-2 cells in 48-well plates. Data represent mean ± SEM from at least three independent studies, each performed with six replicates per data point (all p values > 0.05).

3.2.2. Dapivirine transport across Caco-2 cell monolayers

Measurement of dapivirine permeability in Caco-2 cell monolayers using the same drug transport conditions as those for tenofovir proved unreliable. Preliminary experiments yielded apparent permeability coefficients in the absorptive and secretory directions of 2.91 ± 0.96 × 10^{-6} cm/s and 5.41 ± 1.04 × 10^{-6} cm/s, respectively. However, poor recovery of the drug (54 ± 7%) led to rejection of these due to uncertainties arising from loss of drug in the assay (Table 10, Figure 33a). It was noted that the drug accumulation inside the cells was very high >45% using the standard system.

The addition of BSA 4% did not improve the total recovery of the drug (56 ± 4%), but reduced the proportion of drug accumulated inside Caco-2 cell monolayers (Table 10). The permeability of dapivirine 1 µM when BSA 4% was added to the receiver chamber was higher compared to standard system and equivalent in both directions: 13.2 ± 1.5 × 10^{-6} cm/s and 13.6 ± 1.4 × 10^{-6} cm/s in absorptive and secretory directions, respectively (Figure 33b). In both conditions mannitol recovery was >93 % and TER reading >87% of the pre-experiment value.

Table 10. Recovery of dapivirine and mannitol after 2 h absorptive permeability assay in Caco-2 cells in the presence of different transport medium in the receiver chamber (total recovery and recovery of drug transported from the donor chamber; i.e. receiver chamber and cell monolayer). Data represent mean ± SD from three independent studies, each performed in triplicate.

Transport medium		Total recovery (%)	% compound	
Donor	Receiver fluid		Receiver compartment	Caco-2 cell monolayer
HBSS	**HBSS**	**Apical to basolateral direction**		
Mannitol		93.82 ± 3.87	1.89 ± 0.42	0.89 ± 0.22
Dapivirine 0.1 µM		54.39 ± 7.17	3.32 ± 0.79	45.16 ± 4.76
HBSS	**+ 4% BSA**	**Apical to basolateral direction**		
Mannitol		97.67 ± 2.21	1.17 ± 0.24	0.62 ± 0.10
Dapivirine 0.1 µM		56.15 ± 4.20	7.25 ± 1.42	34.15 ± 4.21
HBSS	**+ Poloxamer 407 0.2 % (w/v)**	**Apical to basolateral direction**		
Mannitol		96.91 ± 2.53	1.53 ± 0.38	1.19 ± 0.54
Dapivirine 0.1 µM		**89.76 ± 4.09**	41.49 ± 3.57	26.47 ± 3.93

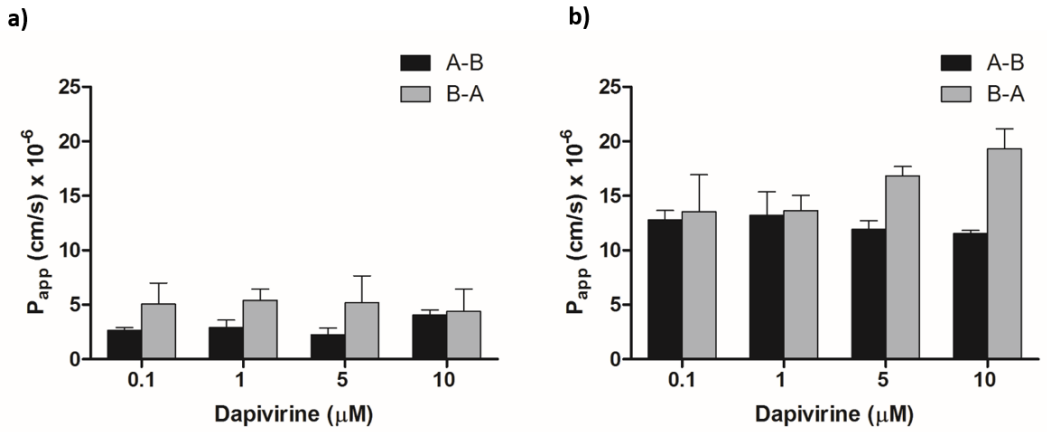


Figure 33. Permeability of varying concentration of dapivirine in the presence of different transport solutions a) donor: HBSS, receiver: HBSS, b) donor: HBSS, receiver: HBSS + 4% BSA. Data represent the mean ± standard deviation from three independent studies, each performed in triplicate.

The addition of Poloxamer 407 0.2 % (w/v) in the receiver compartment improved recovery (89.8 ± 4.1 %) and allowed the permeability over the full dapivirine concentration range to be measured in both absorptive and secretory directions. Poloxamer 407 0.2% w/v did not interfere with efflux pump transporters or tightness of monolayer, as demonstrated unchanged findings for the control compounds; digoxin and mannitol. Absorptive and secretory permeability values for mannitol co-transported with dapivirine were 0.24 ± 0.04 × 10^{-6} cm/s and 0.27 ± 0.05 × 10^{-6} cm/s, respectively. Resistance was measured at the beginning (t=0 min) and at the end (t=120 min) of the dapivirine transport experiments, and TER values were greater than 87% of the initial reading when permeability was determined in the A-B direction and 89% of the initial reading when permeability was determined in the B-A direction (Figure 34a). Absorptive and secretory flux of dapivirine 1 µM was measured over 120 min and linearity of flux was 0.989 (absorptive transport) and 0.993 (secretory transport) (Figure 34b). Flux was also determined for the higher concentrations of dapivirine (up to 10 µM) and linearity was above >0.978 in all cases.

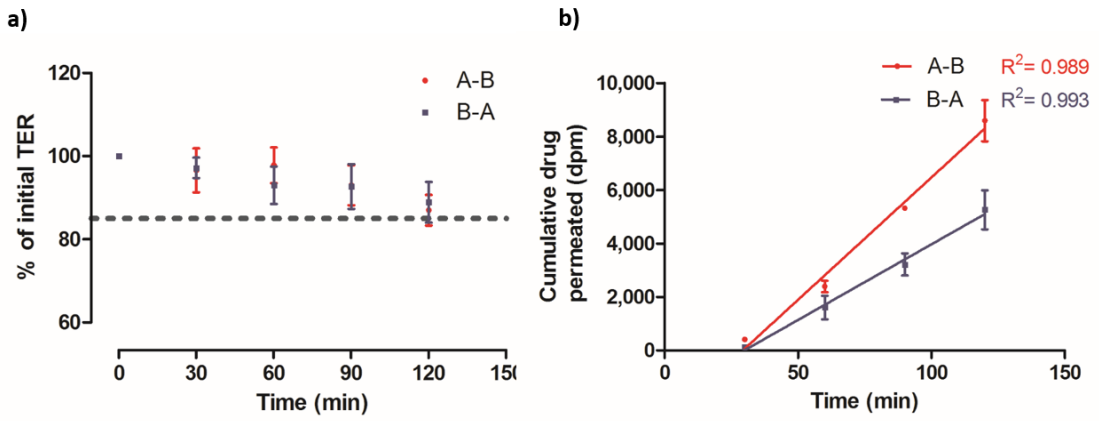


Figure 34. Maintenance of TER during dapivirine exposure and dapivirine flux across Caco-2 cell monolayers. a) The percentage of the initial TER values measured during dapivirine transport across Caco-2 cell monolayers in the absorptive (red dots) and secretory (blue squares) directions with respect to time. TER values were measured at t=0 (initial TER) and after 30, 60, 90 and 120 min of the start of the experiments. b) Flux of dapivirine 1 µM with respect to time in the absorptive (red line) and secretory (blue line) directions across Caco-2 cell monolayers over 120 min. Data represent the mean ± standard deviation from three independent studies, each performed in triplicate.

The apparent permeability of varying concentrations of dapivirine across Caco-2 cell monolayers in absorptive and secretory directions under optimised culture conditions are shown in Figure 35. The results showed that dapivirine permeability was high in absorptive and secretory directions, was concentration independent and statistically equivalent in both directions. Absorptive and secretory permeability for the lowest tested concentration of dapivirine (0.1 µM) was 32.2 ± 1.9 × 10^{-6} cm/s and 30.7 ± 5.5 × 10^{-6} cm/s, respectively and for the highest tested concentration (10 µM) was 30.2 ± 3.8 × 10^{-6} cm/s and 38.2 ± 12.7 × 10^{-6} cm/s. The efflux ratio varied from ER = 0.8 at 1 µM dapivirine to 1.1 at 10 µM (Figure 35b).

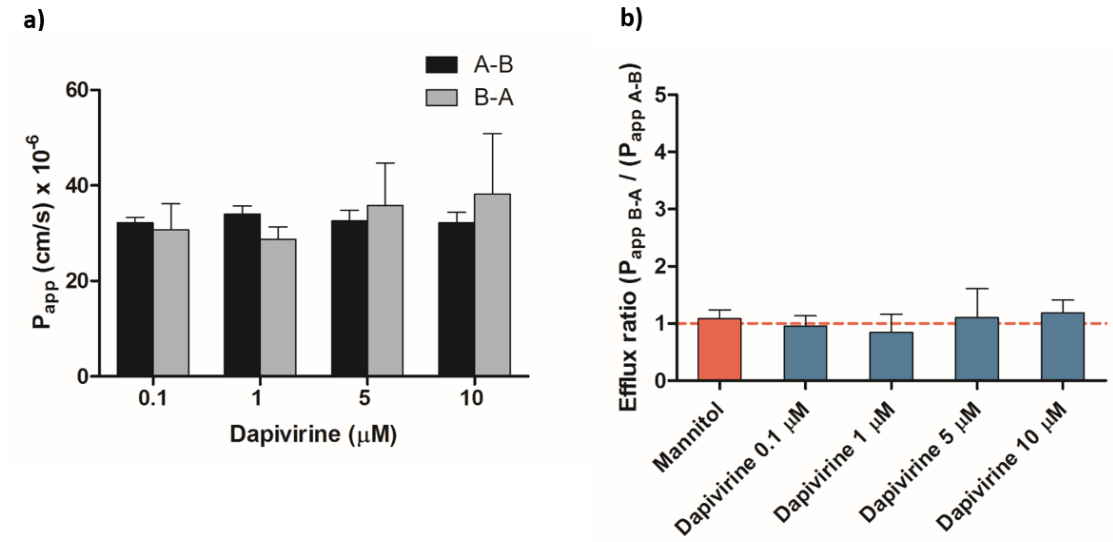


Figure 35. Permeability of varying concentrations of dapivirine (0.1 - 10 µM) (transport solution: donor: HBSS, receiver: HBSS supplemented with Poloxamer 407 0.2 % (w/v)). a) Absorptive and secretory permeability of dapivirine across Caco-2 cell monolayers. b) Efflux ratio of mannitol and dapivirine across Caco-2 cell monolayers. Data represents mean ± SD from three independent experiments, all p values > 0.5.

Permeability and intracellular accumulation of dapivirine were tested in the presence of varying concentrations of different inhibitors to investigate any importance of efflux transporters in drug transport across Caco-2 cell monolayers (Figure 36 and Figure 37). Dapivirine 10 µM flux in absorptive and secretory permeability was investigated in the presence of verapamil (0.1-10 µM), haloperidol (1-50 µM) and GF120918 (0.1-10 µM) and the efflux ratio of dapivirine in the presence of inhibitors was calculated (Figure 36). In the presence of 10 µM verapamil the absorptive and secretory permeability of dapivirine 10 µM decreased slightly, but not significantly to 22.2 ± 5.0 × 10^{-6} cm/s and 22.6 ± 4.7 × 10^{-6} cm/s, respectively (Figure 36a). A range of haloperidol and GF120918 concentrations on dapivirine permeability showed moderate, but not significant decrease in the absorptive permeability of dapivirine, but neither inhibitors influenced the secretory permeability (Figure 36b and c). The efflux ratio of dapivirine in the presence of inhibitors was no different to the ratio calculated for dapivirine only (Figure 36d).

Intracellular accumulation of dapivirine 10 µM was unaffected by the presence of CsA (0.01 µM), verapamil (0.01 and 10 µM), haloperidol (1 and 75 µM), GF120918 (0.1 µM) and bromsulphthalein (75 µM) (Figure 37). There was a slight, but not statistically significant increase in dapivirine accumulation in the presence of CsA (10 µM).

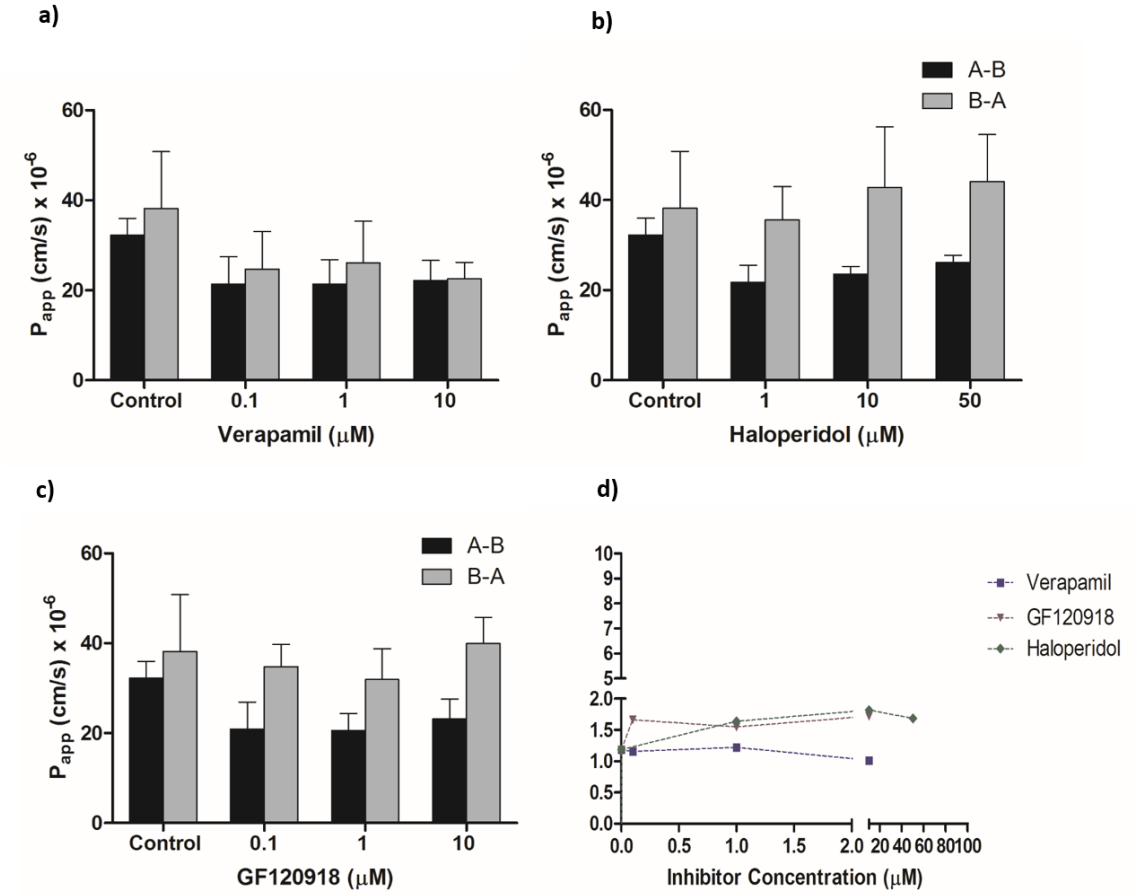


Figure 36. Influence of transporter inhibitors on the permeability of dapivirine 10 µM across Caco-2 cell monolayers. The effect of a) verapamil 0.1-10 µM, b) haloperidol 1-50 µM, and c) GF120918 0.1-10 µM on absorptive and secretory permeability of dapivirine across Caco-2 cell monolayers. d) The effect of inhibitors on the efflux ratio of dapivirine 10 µM in Caco-2 cells. Data represent mean ± SD from three independent studies, each done in triplicate (all p values >0.05).

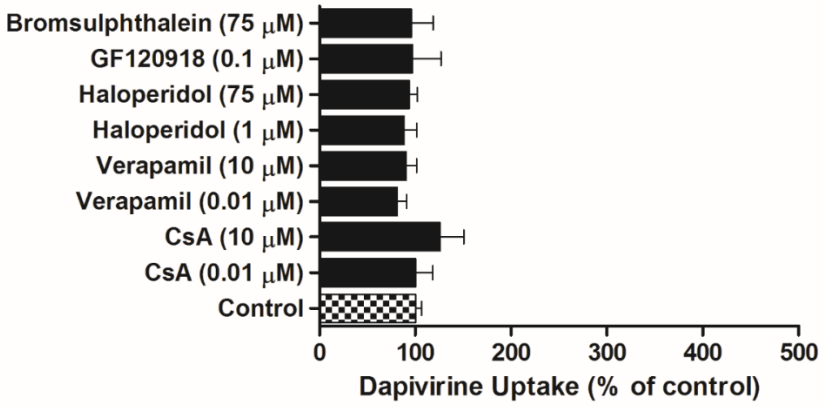


Figure 37. Effect of transporter inhibitors on the accumulation of dapivirine 10 μM by Caco-2 cells in 48-well plates after 21 days in culture. Data represent mean ± SEM from three independent studies, each performed at least with six replicates per data point (all p values >0.05).

3.2.3. Darunavir transport across Caco-2 cell monolayers

The drug transport of varying concentrations of darunavir and any influence of transporter inhibitors on darunavir permeability were investigated. Beforehand, to measure any significant effect of darunavir on Caco-2 cell monolayer integrity, TER measurements were taken at the beginning (t=0 min) and at the end (t=120 min) of transport experiments conducted in absorptive and secretory directions (Figure 38a). When the highest darunavir concentration investigated was applied into apical chamber, the TER decreased to 92 ± 4% of the initial reading by the end of the experiment and similar decrease to 93 ± 4%, was observed when the compound was added into the basolateral chamber. TER values derived from subsequent transport experiments were expressed as an average as no significant difference was observed for varying concentrations of darunavir. The P_{app} for mannitol across Caco-2 cell monolayers treated with darunavir was equivalent in absorptive and secretory directions, with a permeability of 0.21 ± 0.04 × 10^{-6} cm/s and 0.23 ± 0.05 × 10^{-6} cm/s, respectively and an efflux ratio equal to 1.1 ± 0.1. Apical to basolateral and basolateral to apical flux of darunavir 0.1 μM was measured over 120 min and linearity of flux was 0.9999 (A-B direction) and 0.9996 (B-A direction) (Figure 38b). Flux was determined for the higher concentrations of darunavir (up to 100 μM) and linearity was above 0.991 in both directions.

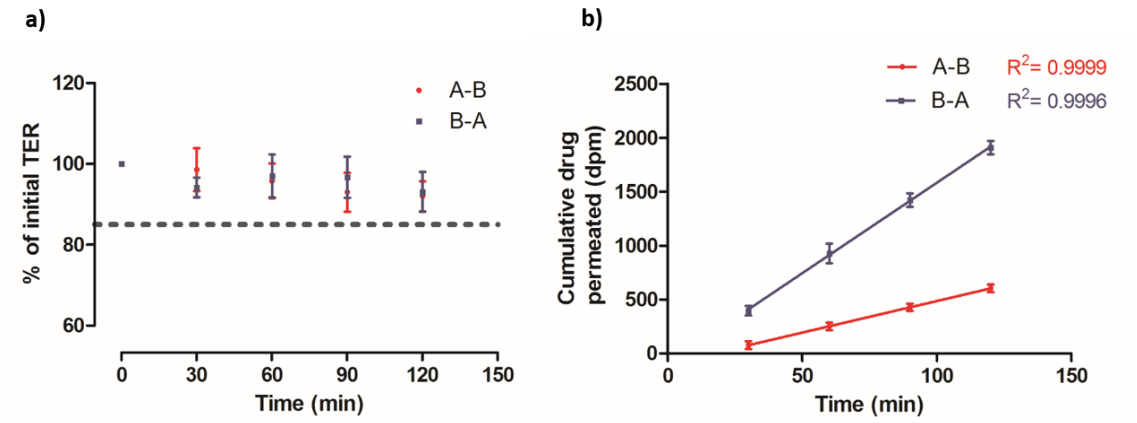


Figure 38. Maintenance of TER during darunavir exposure and darunavir flux across Caco-2 cell monolayers. a) The percentage of the initial TER values measured during darunavir transport across Caco-2 cell monolayers in absorptive (red dots) and secretory (blue squares) directions at different time-points. TER values were measured at t=0 (initial TER) and at 30, 60, 90 and 120 min after the start of the experiments. b) Flux of darunavir 0.1 µM with respect to time in both absorptive (red line) and secretory (blue line) directions across Caco-2 cell monolayers over 120 min. Data represent the mean ± standard deviation from three independent studies, each performed in triplicate.

For each the transport experiment, total recovery of mannitol and darunavir was measured (Table 11). Total recovery of mannitol was not influenced by the presence of varying concentrations of darunavir and was in the range of 98 ± 5% in the absorptive direction and 98 ± 3% in the secretory direction. For darunavir, total mass balance recovered from transport experiments in the absorptive and secretory directions was concentration-independent with the mean recovery above 96%. When darunavir was applied into apical or basolateral chamber, accumulation of the compound inside the cells after 120 min was in the range of 0.9 – 2.0% or 0.6 - 2.9%, respectively. The proportion of compound appearing in the receiver compartment was concentration dependent in A-B direction. The proportion of darunavir (concentration range of 0.1 - 10 µM) appearing in the receiver compartment was two-fold greater when drug was applied in the basolateral side compared to darunavir applied in the apical chamber.

Table 11. Recovery of mannitol and darunavir after absorptive and secretory permeability assays in Caco-2 cell monolayers (total recovery, recovery from receiver chamber and intracellular, i.e. cell monolayer). Recovery of mannitol was measured simultaneously with varying concentration of darunavir and was calculated as an average because tested concentrations of darunavir did not influence mannitol recovery or its permeability. Data represent the mean ± standard deviation from at least three independent studies, each performed in triplicate.

Compound		Total recovery (%)	% compound	
			Receiver compartment	Caco-2 cell monolayer
apical to basolateral direction				
Mannitol		97.82 ± 5.24	1.84 ± 0.39	0.95 ± 0.21
Darunavir	0.1 µM	97.05 ± 5.06	8.52 ± 1.32	1.56 ± 0.39
	1 µM	98.04 ± 5.62	8.92 ± 1.33	1.41 ± 0.28
	10 µM	98.38 ± 3.66	9.71 ± 1.07	1.52 ± 0.30
	100 µM	96.47 ± 4.68	12.07 ± 2.50	1.04 ± 0.14
basolateral to apical direction				
Mannitol		97.73 ± 2.99	1.58 ± 0.29	0.34 ± 0.11
Darunavir	0.1 µM	97.52 ± 2.18	19.57 ± 0.64	1.32 ± 0.75
	1 µM	96.85 ± 3.06	18.07 ± 0.89	1.12± 0.23
	10 µM	98.87 ± 2.88	20.62 ± 2.31	2.04 ± 0.84
	100 µM	95.02 ± 3.45	14.66 ± 2.73	0.97 ± 0.19

The transepithelial transport of varying concentrations of darunavir was measured in absorptive and secretory directions (Figure 39a). The bidirectional transport of darunavir was concentration dependent, indicating the presence of energy dependent active transport mechanism. Absorptive permeability of darunavir slightly increases from 5.9 ± 0.5 × 10^{-6} cm/s at 0.1 µM to 7.4 ± 1.8 × 10^{-6} cm/s at 100 µM, whereas secretory transport decreases from 41.3 ± 3.7 × 10^{-6} cm/s at 0.1 µM to 29.4 ± 3.3 × 10^{-6} cm/s at 100 µM. The efflux ratio decreased from 7.0 to 4.0 with increasing concentration of darunavir (from 0.1 to 100 µM) (Figure 39b). The secretory transport of darunavir 10 µM across Caco-2 cell monolayers was 6-fold grater compare to the absorptive permeability (40.4 ± 3.5 × 10^{-6} cm/s and 6.4 ± 0.9 × 10^{-6} cm/s, respectively).

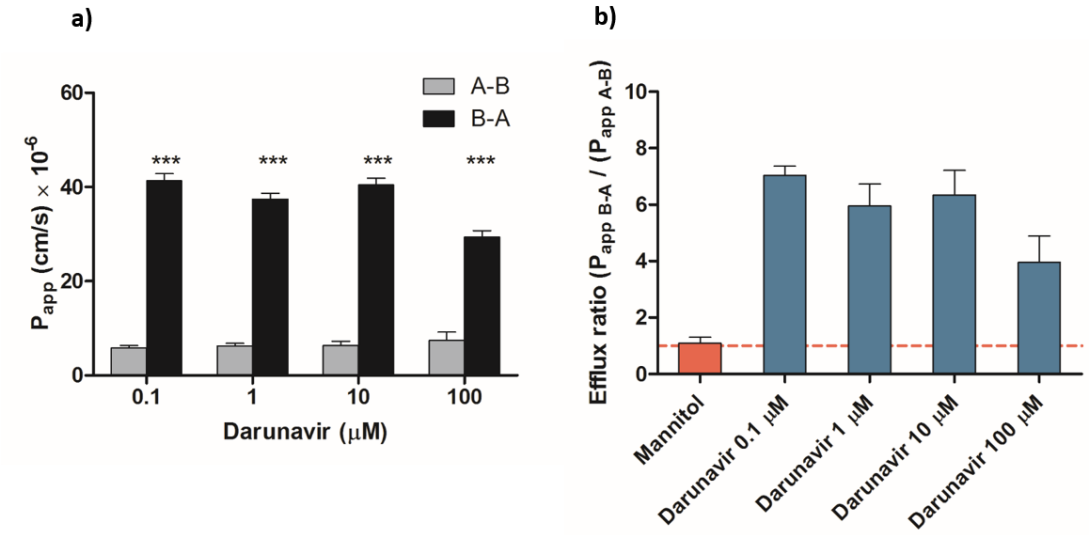


Figure 39. Permeability of darunavir 0.1 - 100 µM. a) Absorptive and secretory permeability of varying concentrations of darunavir b) Efflux ratio of mannitol (used as paracellular marker) and varying concentration of darunavir in Caco-2 cell monolayers. Data represents mean ± SD from three independent experiments, *** p values < 0.001.

To determine the identity and role of energy dependent active transport mechanisms involved in darunavir transport across Caco-2 cell monolayers, several ABC- transporter inhibitors were evaluated for their influence on darunavir permeability and accumulation (Figures 40-43). During these experiments, [^{3}H]-mannitol was incorporated as a marker for cell layer integrity and the bidirectional flux of this control compound was unaeffected by the presence of any inhibitor. The bidirectional permeability of darunavir (10 µM) was significantly affacted by P-gp inhibitors including verapamil, CsA, GF120918 and haloperidol in concentration-dependent manner (Figure 40 and Figure 42).

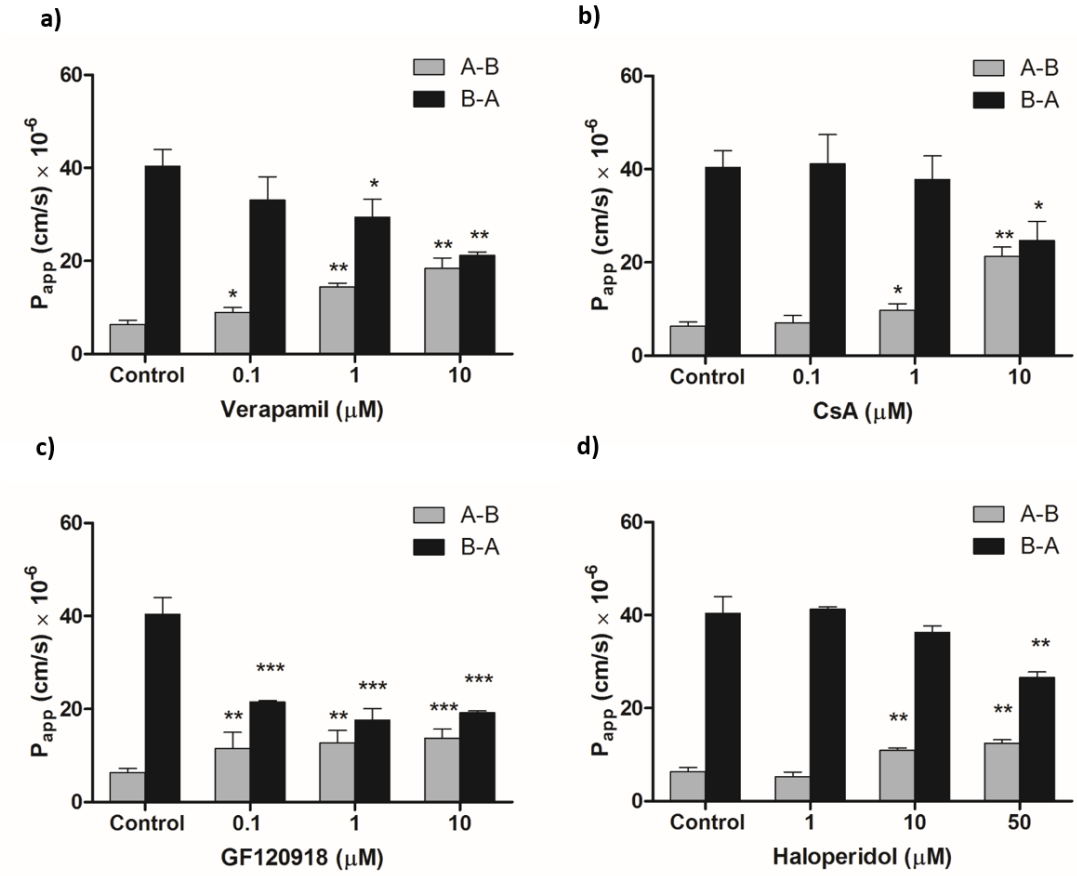


Figure 40. Influence of P-gp transporter inhibitors on darunavir permeability. The effect of varying concentration of P-gp inhibitors a) verapamil 0.1-10 µM, b) CsA 0.1-10 µM, c) GF120918 0.1-10 µM, and d) haloperidol 1-50 µM on darunavir 10 µM absorptive and secretory permeability across Caco-2 cell monolayers. Data represent mean ± SD from three independent studies, each performed in triplicate (***p<0.001, **p<0.01, *p<0.05).

The transport rate of darunavir 10 µM increased almost 3-fold (from 6.4 ± 0.9 × 10^{-6} cm/s to 18.4 ± 2.3 × 10^{-6} cm/s) in the absorptive direction with increasing concentrations of verapamil up to 10 µM. Transport in the secretory direction decreased concommitantly from 40.4 ± 3.5 × 10^{-6} cm/s to 21.2 ± 0.7 × 10^{-6} cm/s. These changes in permeabiliy were reflected in a reduction in ER to 1.2. Similary, incubation of darunavir (10 µM) with range of CsA concentrations between 0.1- 10 µM reduced ER to 1.2 ± 0.1. Strong modulation of darunavir absorptive and secretory transport by the selective P-glycoprotein transporter inhibitor GF120918 was concentration-dependent, with even the lowest concentration of GF120918 (0.1 µM) significantly reducing ER to 1.8 by decreasing secretory permeability, while increasing absorptive permeability by more than 2 fold. At 10 µM GF120918, secretory transport of darunavir decreased from 40.4 ± 3.5 × 10^{-6} cm/s to 19.2 ± 0.5 × 10^{-6} cm/s and absorptive transport increased up to 13.8 ± 1.9 × 10^{-6} cm/s. Haloperidol had moderate influence on darunavir transport and only the highest concentration, 50 µM, decreased significantly the secretory permeability, reducing the ER to 2.1. Additionally, darunavir was tested across Caco-2 cell monolayers after MRP-2 transporter inhibition by bromosulphthalein, which is shown in Figure 41a and Figure 42. All tested concentrations of the MRP-2 inhibitor showed modest but significant increase only in absorptive darunavir permeability, whereas the highest concentration of bromosulpthalein (50 µM) had significant effect on bidirectional transport of compound, decreasing ER to 4.1 ± 0.4. The role of the BCRP transporter in darunavir active transport was also investigated (Figure 41b and 42). When a range of Ko 143 concentrations (0.1-10 µM) were co-incubated with darunavir no modulation of the transport was observed, i.e. there was no influence on absorptive or secretory permeability of darunavir.

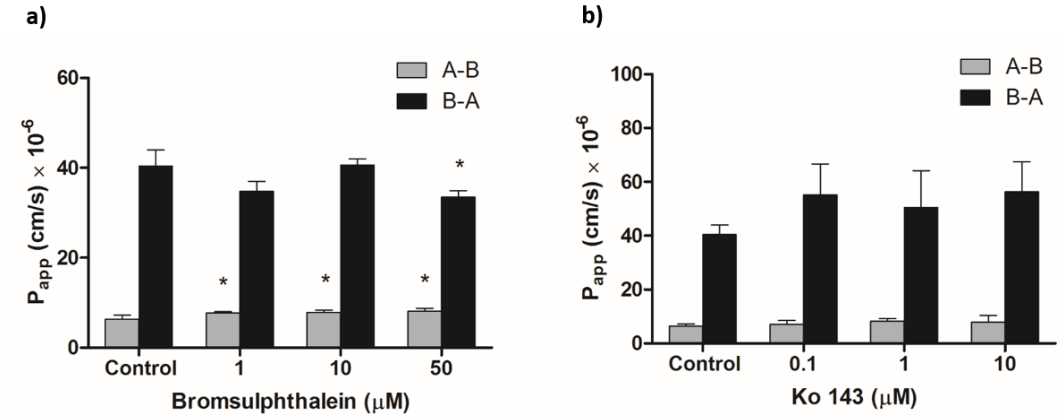


Figure 41. Influence of MRP-2 and BCRP transporter inhibitors on darunavir permeability. The effect of varying concentration of a) MRP-2 inhibitor-bromsulphthalein (1-50 μM), b) BCRP inhibitor- Ko 143 (0.1-10 μM) on darunavir 10 μM absorptive and secretory permeability across Caco-2 cell monolayers. Data represent mean ± SD from three independent studies, each performed in triplicate (*p<0.05).

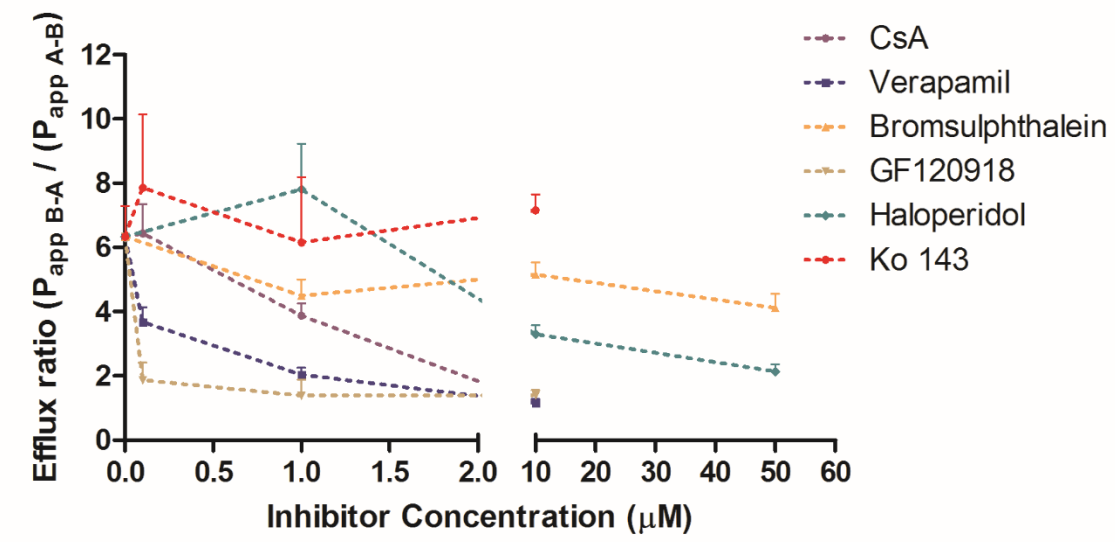


Figure 42. Influence of transporter inhibitors on darunavir permeability. The effect of various inhibitors on the efflux ratio of darunavir 10 μM in Caco-2 cell monolayers. Data represent mean ± SD from three independent studies, each performed in triplicate.

To further examine the involvement of ABC transporters in darunavir active transport, the concentration and temperature dependent effect on darunavir accumulation was investigated (Figure 43). Permeability and cell accumulation data showed similar trends. Incubation for 30 min with P-gp inhibitor, CsA at 10 µM enhanced darunavir accumulation inside the cells by 3.6-fold, however a lower concentration of CsA (0.01 µM) did not affect cellular accumulation. Incubation with GF120918 concentrations of 0.1 and 1 µM increased darunavir uptake by almost 2-fold and 3-fold, respectively. Verapamil 0.01 µM had moderate effect on darunavir cell uptake, whereas higher concentration of 10 µM significantly, enhanced accumulation by 1.8-fold. In the presence of MRP-2 inhibitor at concentration of 75 µM, darunavir cell uptake was enhanced by 1.8 fold, while lower concentration had no effect. Darunavir cell accumulation was temperature dependent (data not shown) and was completely abolished at a temperature of 4°C.

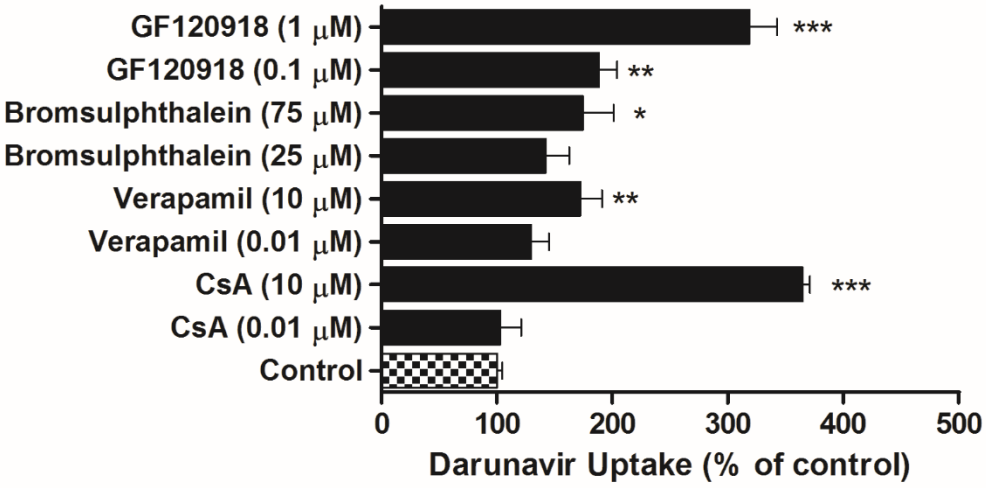


Figure 43. Effect of transporter inhibitors on the accumulation of darunavir 10 µM by Caco-2 cells cultured for 21 days in 48-well plates. Data represent mean ± SEM from three independent studies, each performed at least with six replicates per data point (***$p<0.001$, **$p<0.01$, *$p<0.05$).

3.2.4. Effect of co-administrations of tenofovir, dapivirine and darunavir on permeability in Caco-2 cell monolayers

To investigate the potential drug-drug interaction between tenofovir, darunavir and dapivirine when co-formulated as two drugs or in the triple combination, co-transport of these drug combinations was evaluated over a range of concentrations (0.1 µM – 100 µM) to look for inter-dependency in their permeability. The apparent permeability of each drug in Caco-2 cell monolayers in absorptive and secretory directions was measured in the presence of a second ARV drug (double combinations) then in the presence of both other ARV drugs (triple combination). During all experiments, TER measurements and mannitol permeability were evaluated to verify integrity of Caco-2 cell monolayers. For all tested combinations, TER values and mannitol permeability were unaffected and were in the range of acceptance criteria.

Drug transport of tenofovir in double and triple combinations

The apical to basolateral and basolateral to apical flux of tenofovir 100 µM was measured in the presence of dapivirine in concentrations of 0.1, 1 and 10 µM (Figure 44a). The presence of dapivirine did not have any significant influence on tenofovir transport. At the highest concentration of dapivirine, a small increase in secretory transport of tenofovir from $0.14 \pm 0.04 \times 10^{-6}$ cm/s to $0.15 \pm 0.05 \times 10^{-6}$ cm/s was observed, but the change was not significant. Co-administration with darunavir (1 – 100 µM) had no impact on either absorptive or secretory permeability of tenofovir (Figure 44b). To measure any potential changes in transport of tenofovir when formulated as a triple formulation, Caco-2 cells were first incubated for 30 min with buffer solution containing dapivirine 10 µM and darunavir 10 µM or dapivirine 1 µM and darunavir 10 µM and after the incubation period a test solution containing ^{14}C-tenofovir 100 µM, dapivirine 10 µM and darunavir 10 µM or ^{14}C-tenofovir 100 µM, dapivirine 1 µM and darunavir 10 µM was added to the donor compartment. The appearance of tenofovir in the receiver compartment was measured at appropriate time points. The absorptive permeability of tenofovir was slightly but not significantly increased in the presence of dapivirine 10 µM and darunavir 10 µM (from $0.10 \pm 0.02 \times 10^{-6}$ cm/s to $0.14 \pm$

0.04 × 10^{-6} cm/s) (Figure 45). It was noted that when dapivirine 10 µM with tenofovir was tested in the double combination (Figure 44a) there was no effect on the absorptive permeability of tenofovir. Tenofovir absorptive and secretory flux was unaffected by the presence of dapivirine 1 µM and darunavir 10 µM (Figure 45).

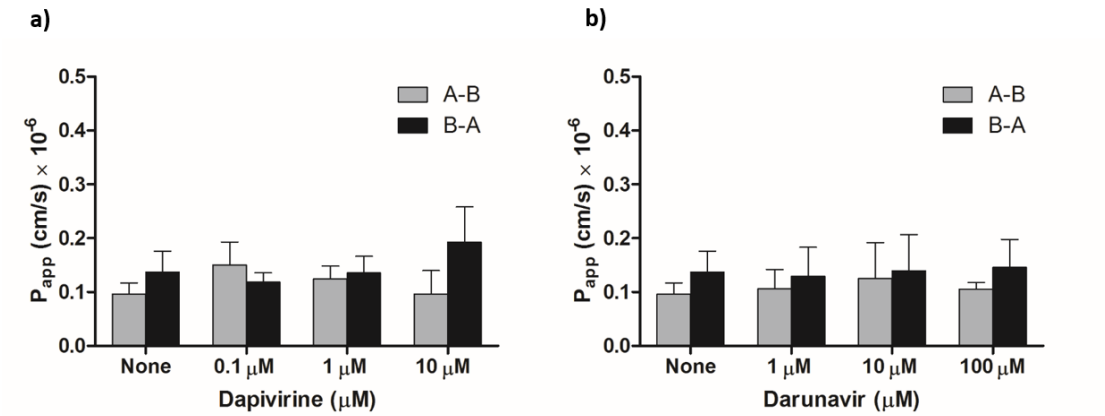


Figure 44. Drug transport of tenofovir in double combinations. Effect of varying concentrations of a) dapivirine (0.1 – 10 µM) b) darunavir (1 – 100 µM) on tenofovir 100 µM absorptive and secretory permeability across Caco-2 cell monolayers. Data represents mean ± SD, from three independent studies done in triplicate.

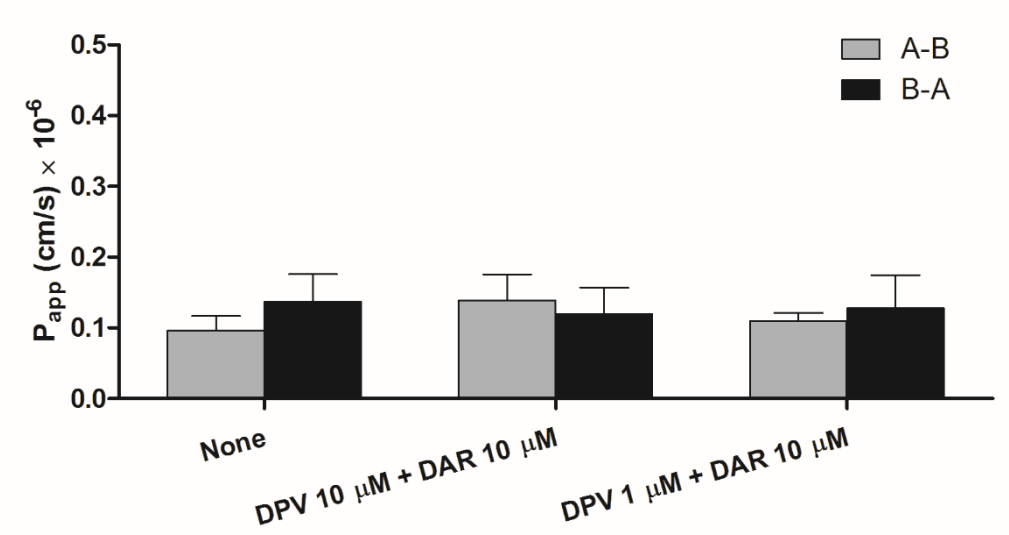


Figure 45. Drug transport of tenofovir in triple combination. Effect of varying drug compositions; dapivirine 10 µM + darunavir 10 µM and dapivirine 1 µM + darunavir 10 µM on tenofovir 100 µM absorptive and secretory permeability across Caco-2 cell monolayers. Data represents mean ± SD, from three independent studies performed in triplicate. DPV - dapivirine, DAR – darunavir.

Drug transport of dapivirine in double and triple combinations

The absorptive and secretory transport of dapivirine 10 µM was tested in the presence of tenofovir (1 – 100 µM) and darunavir (1 – 100 µM) (Figure 46a and 46b). None of the tested combinations had any impact on absorptive or secretory permeability of dapivirine across Caco-2 cell monolayers. The dapivirine flux in absorptive and secretory directions in triple combination was also unaffected by the presence of tenofovir and darunavir (Figure 47).

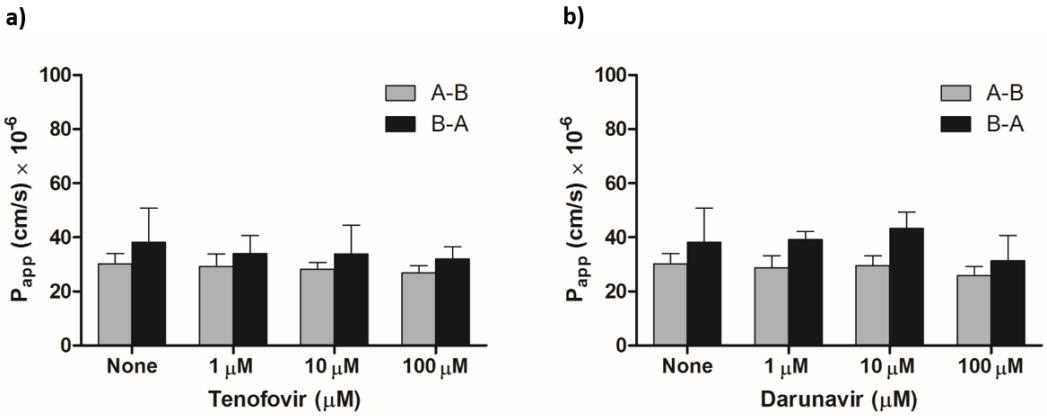


Figure 46. Drug transport of Dapivirine in double combinations. Effect of varying concentrations of a) tenofovir (1 – 100 µM) b) darunavir (1 – 100 µM) on dapivirine 10 µM absorptive and secretory permeability across Caco-2 cell monolayers. Data represents mean ± SD, from three independent studies done in triplicate.

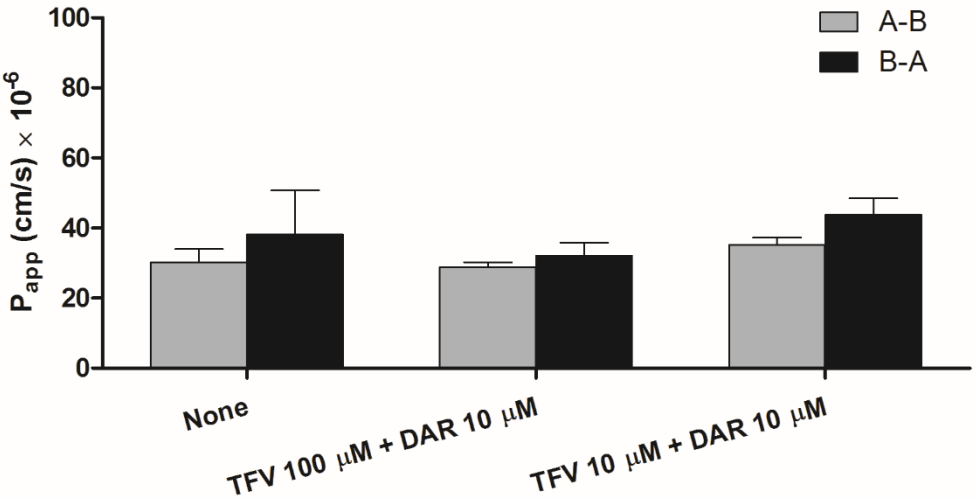


Figure 47. Drug transport of dapivirine in triple combination. Effect of varying drug compositions; tenofovir 100 µM + darunavir 10 µM and tenofovir 10 µM + darunavir 10 µM on dapivirine 10 µM absorptive and secretory permeability across Caco-2 cell monolayers. Data represents mean ± SD, from three independent studies performed in triplicate. TFV - tenofovir, DAR – darunavir.

Drug transport of darunavir in double and triple combinations

The absorptive and secretory permeability of darunavir 10 µM was tested in the presence of tenofovir (1 – 100 µM) and dapivirine (0.1 – 10 µM) (Figure 48a and 48b). In the presence of tenofovir or dapivirine, darunavir permeability in absorptive and secretory directions was not affected. However, when darunavir was co-administrated with tenofovir 100 µM and dapivirine 1 µM, the absorptive and secretory permeability appeared to increase, albeit this was not statistically significant (Figure 49). No effect was observed at lower concentrations: i.e. tenofovir 10 µM and dapivirine 1 µM.

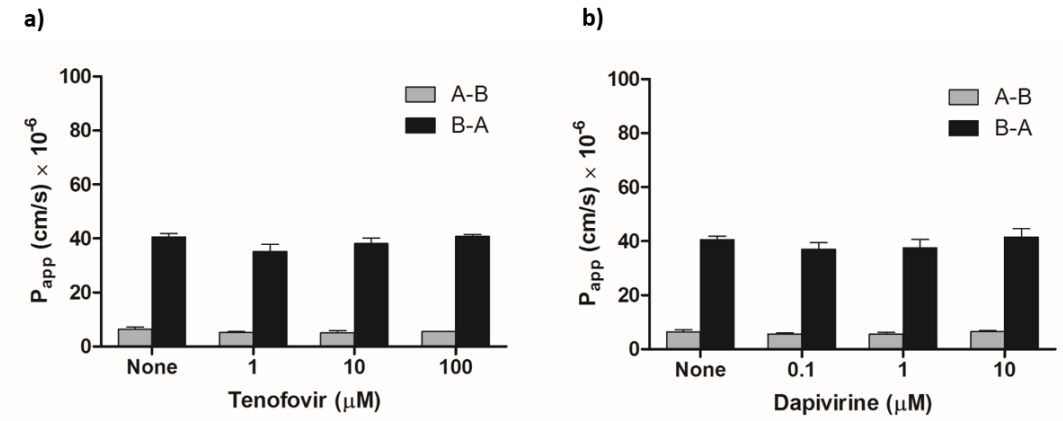


Figure 48. Drug transport of darunavir in double combinations. Effect of varying concentrations of a) tenofovir (1 – 100 µM) b) dapivirine (0.1 – 10 µM) on darunavir 10 µM absorptive and secretory permeability across Caco-2 cell monolayers. Data represents mean ± SD, from three independent studies done in triplicate.

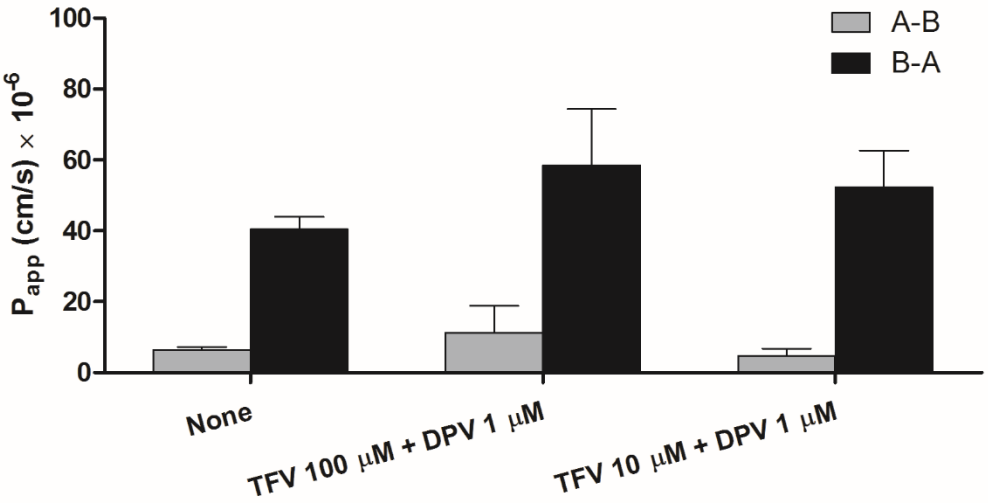


Figure 49. Drug transport of darunavir in triple combination. Effect of varying drug compositions; tenofovir 100 µM + dapivirine 1 µM and tenofovir 10 µM + dapivirine 10 µM on darunavir 10 µM absorptive and secretory permeability across Caco-2 cell monolayers. Data represents mean ± SD, from three independent studies done in triplicate. TFV - tenofovir, DPV – dapivirine.

Accumulation of ARVs drugs in double combinations

Intracellular uptake of tenofovir, dapivirine and darunavir was investigated in the presence of each other in a matrix inlcuding all the double combinations, over a range of concentrations (0.001 µM – 100 µM) (Figure 50). Similar trends to drug transport data were observed. Co-administration did not significantly alter the intracellular acumulation of any of the ARV drugs by Caco-2 cells.

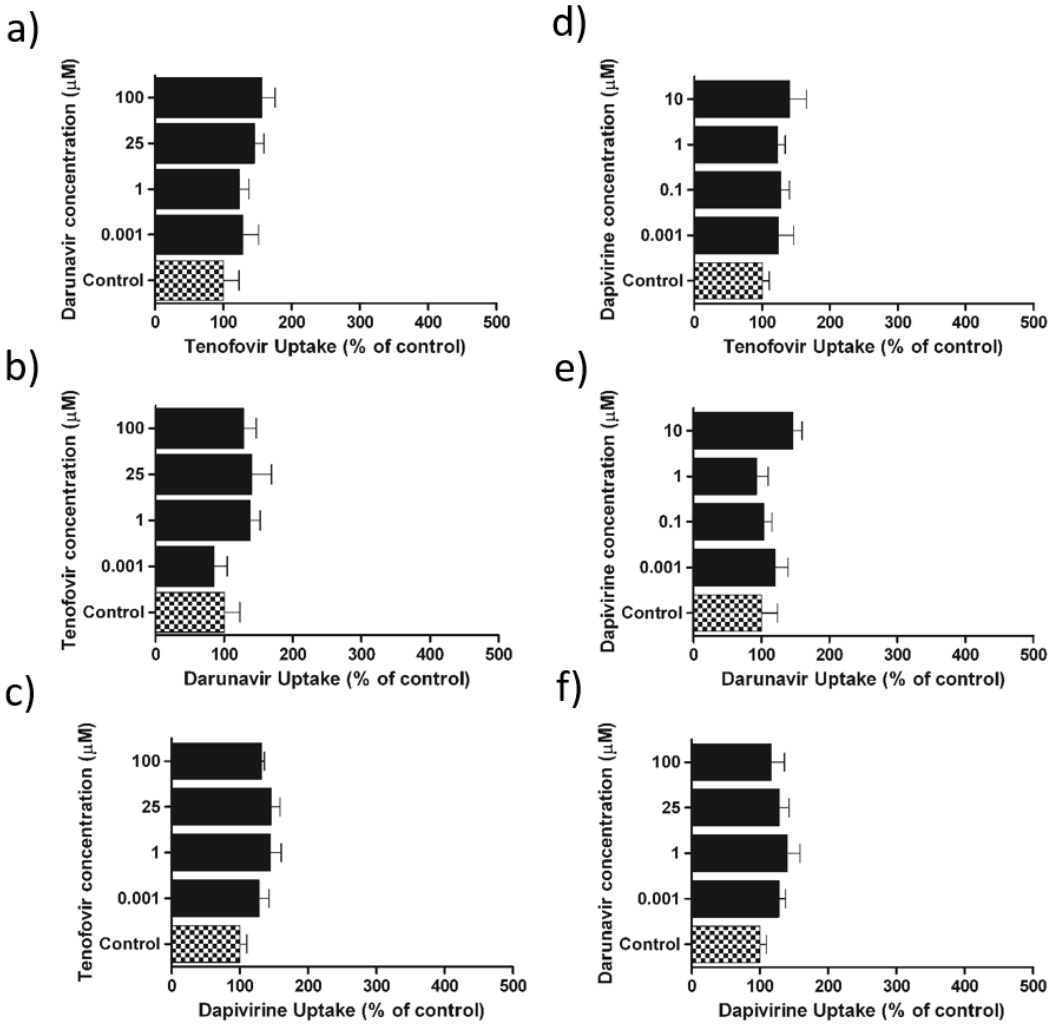


Figure 50. Intracellular accumulation of individual ARVs drugs when co-formulated into double combinations. Effect of varying concentration of a) darunavir (0.001 – 100 µM) on tenofovir 100 µM accumulation, b) tenofovir (0.001 – 100 µM) on darunavir 10 µM accumulation, c) tenofovir (0.001 – 100 µM) on dapivirine 10 µM accumulation, d) dapivirine (0.001 – 10 µM) on tenofovir 100 µM accumulation, e) dapivirine (0.001 – 10 µM) on darunavir 10 µM accumulation, f) darunavir (0.001 – 100 µM) on dapivirine 10 µM accumulation inside Caco-2 cells after 60 min incubation grown in 48 well plates for 21 - 28 days. Values represent the mean ± SEM from at least three independent studies, each performed with six replicaes per data point (all p values >0.05).

3.2.5. Permeability of tenofovir and darunavir in inflamed Caco-2 cell monolayers and the effect of film formulations on secretion of selected interleukins

In topical microbicide development the situation whereby formulations are applied to inflamed mucosa and drug permeability under these circumstances is the most relevant measure. A model of the inflamed epithelium was produced by challenging the Caco-2 cell monolayer with interleukin (IL)-1β and investigating the effect on the permeability of tenofovir and darunavir. Conversely, to check for inflammatory effects of the prospective microbicide formulation Caco-2 cell monolayers were exposed to the ARV drugs and darunavir film formulation and with interleukin secretion was measured as an indicator of irritation/inflammation.

The Caco-2 cell monolayers were exposed to varying concentration of IL-1 β (0.1 – 25 ng/ml) for 24 h. Afterwards, cells were washed and the drug transport assays for tenofovir 100 µM and darunavir 10 µM were performed as described earlier. After 24 h of stimulation with IL-1 β, the level of IL-8 was measured (Figure 51). The secretion of IL-8 was used to evaluate cell layer response to pro-inflammatory stimulus. The amount of the IL-8 secreted by untreated differentiated Caco-2 cells was 4.76 ± 0.85 pg/ml and after stimulation with IL-1 β 0.1, 10 and 25 ng/ml the secretion increased significantly by 2-fold, 6.5-fold and 19-fold (p<0.001, compared to unstimulated control). The secretion of IL-6 was also measured in untreated cells and was 0.9 ± 0.25 pg/ml, however there was no significant increase by exposure to IL-1 β.

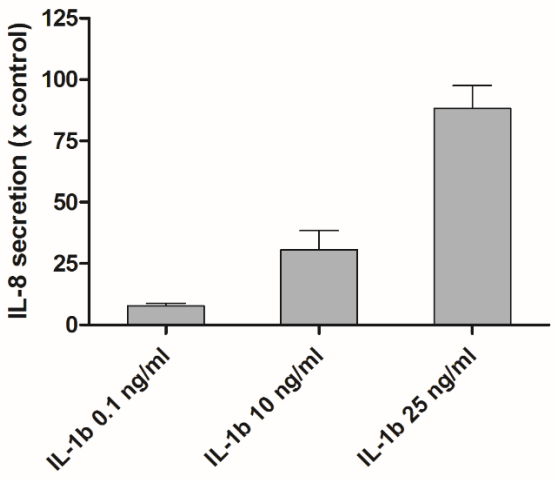


Figure 51. IL-8 secretion by Caco-2 cell monolayers exposed IL-1 β (inflammatory stimuli) in range of concentrations between 0.1 and 25 ng/ml IL-1 β. Data represents the mean ± SD from at least three independent experiments, performed in duplicate.

TER measurements were taken before and after the exposure to inflammatory stimuli and only incubation with the highest concentration of stimuli produced a modest reduction in the TER (by 13.2 ± 5.2 %) compared to the initial TER reading. There was no further reduction in TER reading after the ARV drugs were added or at the end of the drug transport experiments. The bidirectional transport of tenofovir 100 µM and darunavir 10 µM across Caco-2 cell monolayers is shown in Figure 52. For both antiretroviral drugs, neither the absorptive nor the secretory permeability was influenced by the Caco-2 cell monolayers being exposed to inflammatory stimuli.

Caco-2 cell monolayers were exposed to tenofovir 100 µM, darunavir 10 µM and the darunavir film formulation (film immersed in 500 µM of medium) for 24 h of exposure and there was no change from baseline or difference between the tested drugs in terms of secretion of IL-8 (3.15 ± 0.78 pg/ml), IL-6 (1.72 ± 0.93 pg/ml), IL-10 or TNFα (undetectable).

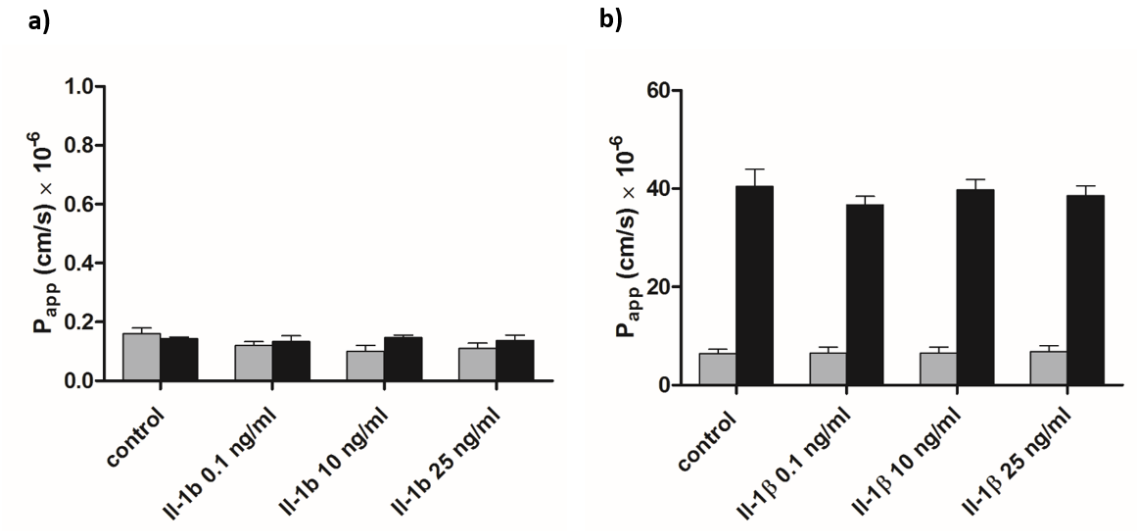


Figure 52. Permeability of tenofovir and darunavir across Caco-2 cells after being exposed to inflammatory stimuli. Apparent permeability in absorptive (grey bars) and secretory (black bars) directions for a) tenofovir 100 µM, b) darunavir 10 µM across untreated cells (control) and cells exposed for 24h to IL-1β 0.1, 10 and 25 ng/ml. Data represents the mean ± SD from three independent studies, performed in duplicates.

3.3. Effect of formulations on ARV permeability in Caco-2 cell monolayers

3.3.1. Effect of GRAS excipients used in formulation on modulating tenofovir, dapivirine and darunavir permeability across Caco-2 cell monolayers

To measure the effect of different classes of excipient commonly used in topical microbicide formulations, the transport of tenofovir, darunavir and dapivirine across Caco-2 cell monolayers in the presence of PEG 200 1% (v/v), PEG 400 1 % (v/v), Polysorbate 80 1% (v/v), HPMC-50 5% (v/v), PEG 1000 1% (v/v) and Poloxamer 407 0.2 % (v/w) was performed. Before investigating the effect of excipients on the ARV drug transport, the TER readings and mannitol permeability were assessed in the presence of formulation excipients. The changes in TER readings were not significant and did not decrease by more than 15 % compared to control for any excipient at the concentrations used. Initial TER values were above 1450 $\Omega \times cm^2$ and mannitol permeability in the absorptive and secretory directions was unaffected by the presence of the excipients; i.e. all values were around 0.2×10^{-6} cm/s. The absorptive and secretory transport of tenofovir 100 µM across Caco-2 cell monolayers in the presence of various excipients are shown in Figure 53. Changes in bidirectional transport of tenofovir were not considered as significant compared to untreated cells (control) for any tested excipient (all p values > 0.05). Total recovery of tenofovir in the presence of excipients was unchanged compare to control.

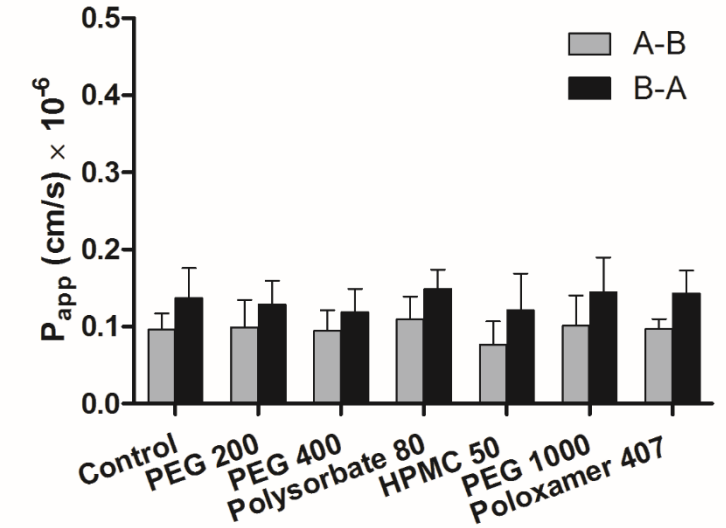


Figure 53. Influence of excipients on tenofovir 100 µM permeability. The effect of PEG 200 1 % (v/v), PEG 400 1% (v/v), polysorbate 80 1% (v/v), HPMC-50 5% (v/v), PEG 1000 1% (v/v) and poloxamer 407 0.2 % (v/w) on tenofovir transport in absorptive and secretory directions across Caco-2 cell monolayers. Data represents mean ± SD, from three independent studies, performed in duplicates.

Dapivirine 10 µM bidirectional transport was tested across Caco-2 cells in the presence of the same excipients (Figure 54). A control solution of dapivirine 10 µM was prepared in HBSS solution supplemented with 1 % (v/v) HEPES. As mentioned previously, dapivirine total recovery in the HBSS without a solubilising agent was below 60% and drug transport was unreliable, however to estimate the influence of different excipients on the dapivirine permeability, this system was used as a screen. Excipients including PEG 200, PEG 400, HPMC 50 and PEG 1000 did not improve the total recovery of dapivirine and changes in absorptive and secretory flux in the presence of these excipients were not significant compare to control (all p values >0.05). Polysorbate 80 1% v/v was the only excipient in these experiments to have a significant effect on the transport of dapivirine by increasing absorptive permeability from 4.3 ± 0.5 × 10^{-6} cm/s to 25.3 ± 4.1 × 10^{-6} cm/s (although it should be noted that in the presence of Poloxamer 0.2 % (v/w), absorptive permeability was 30.2 ± 3.8 × 10^{-6} cm/s) and secretory transport from 5.1 ± 1.4 × 10^{-6} cm/s to 28.2 ± 0.5 × 10^{-6} cm/s (in the presence of Poloxamer 0.2 % (v/w) secretory permeability was 38.16 ± 12.67 × 10^{-6} cm/s) (p<0.001). Additionally total recovery of dapivirine was improved to 83.1 ± 5.2%.

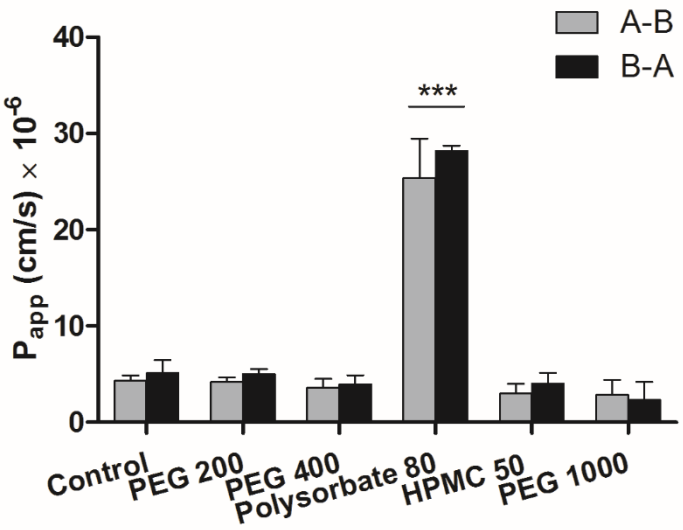


Figure 54. Influence of excipients on dapivirine 10 µM permeability. The effect of PEG 200 1 % (v/v), PEG 400 1% (v/v), polysorbate 80 1% (v/v), HPMC-50 5% (v/v) and PEG 1000 1% (v/v) on dapivirine transport in absorptive and secretory directions across Caco-2 cell monolayers. Data represent mean ± SD, from two independent studies, performed in duplicate (***p<0.001, ** p<0.01, *p<0.05).

The bidirectional permeability of darunavir 10 µM in the presence of excipients is shown in Figure 55. There was no significant change in the darunavir transport across Caco-2 cell monolayers in the presence of PEG 200, PEG 400, HPMC 50, PEG 1000 or Poloxamer 407 (p>0.05). The absorptive permeability of darunavir in the presence of PEG 400 1% increased to 10.1 ± 1.0 × 10^{-6} cm/s and permeability in the secretory direction decreased to 19.5 ± 3.9 × 10^{-6} cm/s with the efflux ratio approaching 1.9 (***p<0.001). In the presence of 1% v/v polysorbate 80 the absorptive permeability of darunavir increased significantly to 9.1 ± 0.9 × 10^{-6} cm/s (** p<0.01) and decreased slightly in the secretory direction to 19.5 ± 3.9 × 10^{-6} cm/s (* p<0.05). Darunavir recovery and mannitol permeability after 120 min in the presence of the excipients were unchanged.

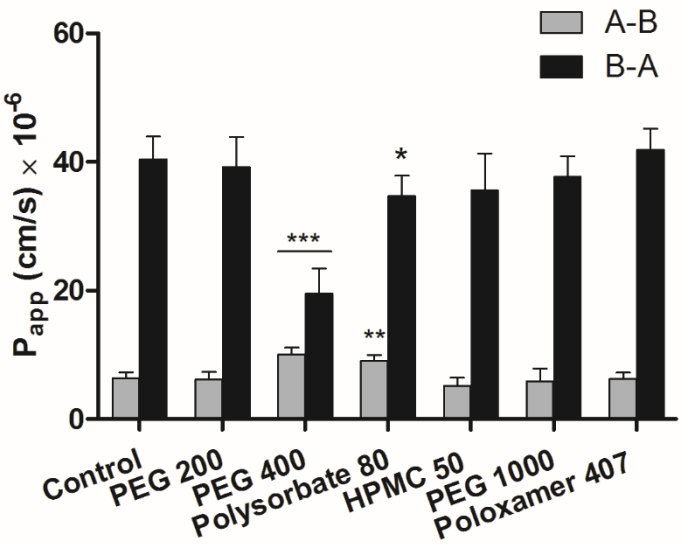


Figure 55. Influence of excipients on darunavir 10 µM permeability. The effect of PEG 200 1 % (v/v), PEG 400 1% (v/v), polysorbate 80 1% (v/v), HPMC-50 5% (v/v), PEG 1000 1% (v/v) and poloxamer 407 0.2 % (v/w) on darunavir transport in absorptive and secretory directions across Caco-2 cell monolayers. Data represent mean ± SD, from three independent studies performed in duplicate (***p<0.001, ** p<0.01, *p<0.05).

3.3.2. The impact of prototype formulations on drug absorption across Caco-2 cell monolayers

Validation evaluation of sensitive liquid chromatographic tandem mass spectrometry (LC-MS/MS) for analysis of darunavir film formulation

Peak shapes of darunavir and internal standard were consistent in all chromatograms with no interference from other peaks, or with no significant tailing. The retention time was in the range of 2.18 ± 0.02 min across all tested samples.

Calibration curves were produced from integrated peak area ratio of standards of known concentrations in the range of 0.01 – 10 µg/mL (Figure 56). The calibration curves for darunavir showed very good linearity with correlation coefficient of $R^2 \geq 1$.

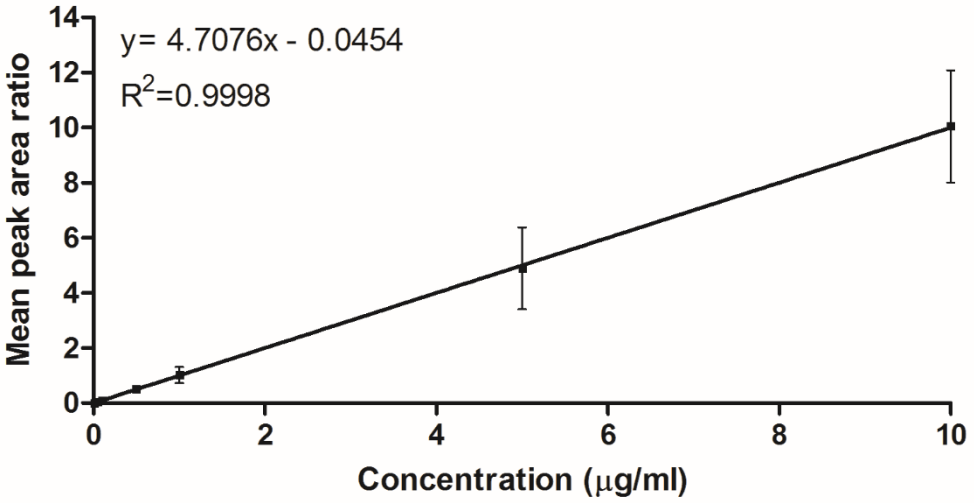


Figure 56. Calibration curve for darunavir in the range of 0.01 – 10 µg/mL. The linearity and range of 9 calibration curves ± SD (3 injections per sample). Data obtained are expressed as the mean ratio of darunavir/ IS peak area.

The limits of detection and quantifications were calculated using equation 6 and 7 and were in the ranges of 0.024 – 0.061 µg/mL and 0.068 – 0.143 µg/mL, respectively.

The accuracy and precision of the assay was compared using the ratio peak area (Table 12). Intra and inter-day variation was determined at seven concentration levels (n=9). Accuracy was within the accepted range of 85 – 115% and precision was < 20% CV [177]. The % CV for the intra-day and inter day calibration sets ranged from 3.3 – 11.3% and 3.8 – 13.1%, respectively. The % CV exceeded increased markedly (from <7% CV to ca. 13%) below 0.05 µg/mL.

Table 12. The intra and inter-day variation at the range of concentrations (0.01 – 10 µg/ml) of darunavir tested for LC-MS/MS system.

Concentration of darunavir (µg/ml)	Intra-day variation		Inter-day variation	
	% Accuracy	% Precision	% Accuracy	% Precision
0.01	109.43	11.28	114.43	13.17
0.05	108.21	5.10	114.81	6.04
0.1	102.41	3.31	104.37	3.75
0.5	101.45	4.10	103.76	4.48
1	100.98	4.47	102.40	5.59
5	96.43	6.38	97.87	3.85
10	98.46	3.99	100.50	4.63

Dissolution and transfer of darunavir from film formulation

Before investigating the dissolution and transfer of darunavir from the film formulation it was necessary to measure the effect of darunavir and placebo film formulations on Caco-2 cell viability and monolayer integrity. The viability of Caco-2 cells grown on inserts for 21-28 days to form the monolayer was measured. Cells were exposed to film formulations containing darunavir (0.0237 mg in 0.0314 cm^2 film) and placebo film (0.0314 cm^2) immersed in different volumes of HBSS solution (0, 28, 100, 500 µL) at the apical side of the Caco-2 cell monolayer for 180 min (Figure 57). During each experiment to evaluate the formulations, TER measurements were taken to measure the integrity of the cell monolayer (Figure 58 and 59). The cell viability was reduced by more than 40% when the darunavir film and placebo film formulations were placed directly onto the liquid-free apical surface of the cell monolayer (***, $p<0.001$). Similar results were obtained for darunavir film and placebo film formulation that were submersed in 28 µl of HBSS solution at the apical side of the membrane which reduced cell viability by more than 35% (**, $p<0.01$). TER values for both conditions (0 and 28 µL) and for both films (darunavir 0.0237mg/film and placebo film - both the same size of 0.0314 cm^2) dropped drastically by 90% from the initial reading in the first 3 min of the experiments and did not recover over the course of the experiment. Cell viability was reduced by approx. 25% when cells were exposed to darunavir and placebo films that were immersed in 100 and 500 µL of HBSS solution at the apical side of the membrane. There was no significant difference in cell viability between placebo film and film containing darunavir. However, the TER values were significantly affected by the presence of darunavir in the film composition. In the first 30 min, the darunavir films reduced TER by 40% from the pre-experiment reading and reached a plateau with TER value of 66 ± 11% by the end of the experiment. In contrast, the placebo film reduced the TER compared to the initial value by only 10% by the end of the experiment. The TER was not affected across cell monolayers exposed to placebo film or darunavir film that were immersed in 500 µl of HBSS solution at the apical side of the membrane.

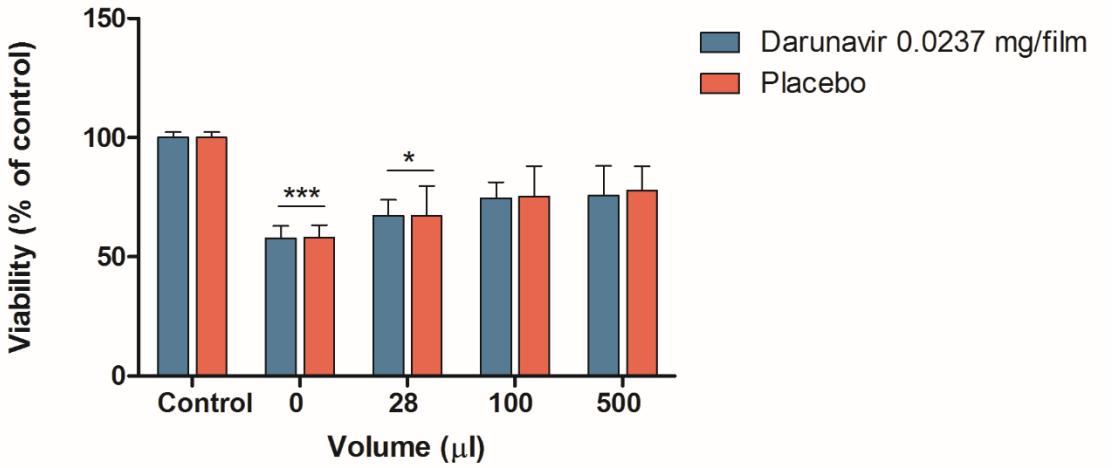


Figure 57. The effect of the film formulations (containing darunavir (blue bars) and placebo film (red bars) - 0.0314 cm² film) immersed in different volumes at the apical side of the membrane on Caco-2 cell viability. Viability (%) of control) was calculated as a percentage of the control MTT assay reading (control = cells exposed to medium only) over a range of concentrations. The data represents the mean ± SD, from three independent studies, performed in duplicates (***$p<0.001$, ** $p<0.01$, *$p<0.05$).

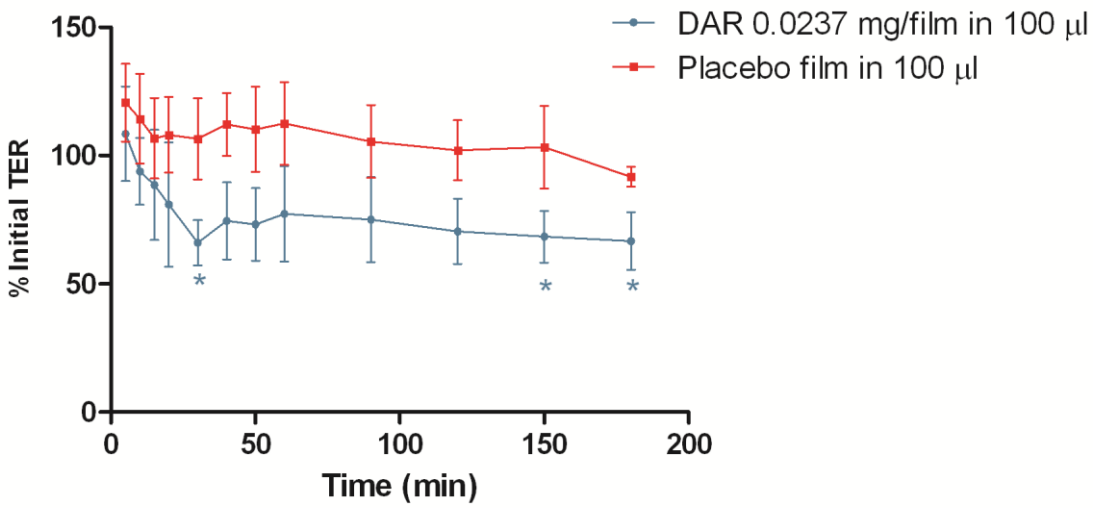


Figure 58. The variation of TER measurements in the presence of darunavir and placebo film immersed in 100 µL HBBS at the apical side of the membrane across Caco-2 cell monolayers. The % of the initial TER values were obtained for film formulation containing darunavir (blue dots) and placebo film (red squares) immersed in 100 µL HBSS solution at the apical side of the chamber. TER values were measured at t=0 (initial TER) and different time points till 180 min.

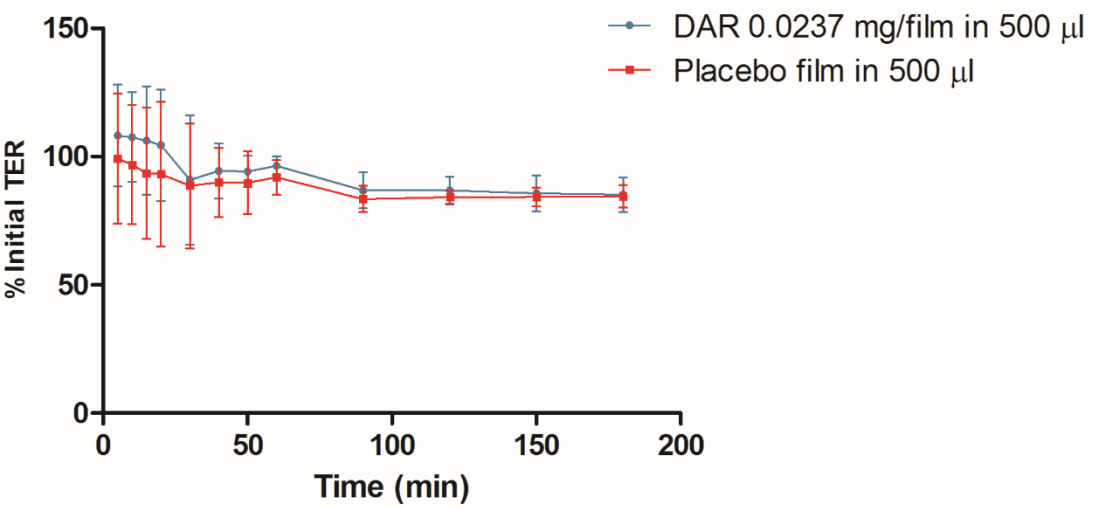


Figure 59. The variation of TER measurements in the presence of darunavir and placebo film immersed in 500 µL HBBS at the apical side of the membrane across Caco-2 cell monolayers. The % of the initial TER values were obtained for film formulation containing darunavir (blue dots) and placebo film (red squares) immersed in 500 µL HBSS solution at the apical side of the chamber. TER values were measured at t=0 (initial TER) and different time points till 180 min. The data represents the mean ± SD from three independent studies, performed in duplicate (**, $p<0.01$; *, $p<0.05$). .

Dissolution profiles and the transfer of darunavir (0.148 mg in 0.196 cm^2 film) from the film formulation that was immersed in different fluid volumes (0, 28, 100 and 500 µL) were performed across Caco-2 cell monolayers and are shown in Figure 60. Transfer of darunavir from the film immersed in 0 and 28 µL of the fluid at the apical side was rapid as 90 % of the total amount of the drug, was transferred after 180 min. Similarly, when film immersed in 100 µL more than 70 % of the total amount of the drug was transferred across Caco-2 cell monolayers. These tested conditions have shown rapid dissolution and transfer profile for the drug across Caco-2 cell monolayers, attributable to the disruption of cell monolayer integrity (as reflected in TER reduction). When the darunavir film was immersed in 500 µL of the solution at the apical side (biocompatible conditions), appearance in the receiver chamber was slower and by the end of the experiment around 35.2 ± 7.2 % of the total amount of the drug was transferred across Caco-2 cell monolayers.

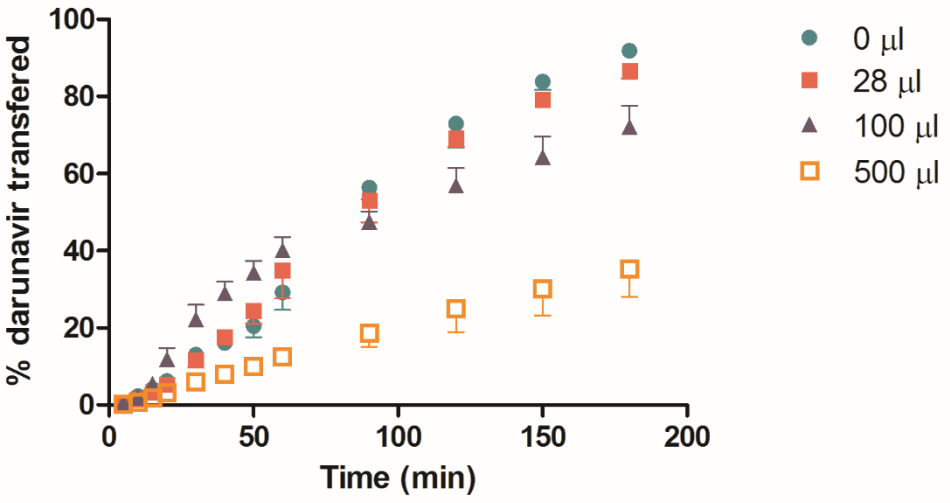


Figure 60. Dissolution and transfer of darunavir from film formulations (0.148 mg darunavir in 0.196 cm^2 film in 0, 28, 100 and 500 µL of HBSS solution) across Caco-2 cell monolayers or across cell-free system after placement at the apical side of the monolayer in the Transwell diffusion system. Data represent the mean ± SD from three independent studies. Note: error bars are within the data points.

The difference in dissolution profile of darunavir from film formulation immersed in 500 µL HBSS tested across cell-free system and Caco-2 system is shown in Figure 61. Different sizes of the film formulation (0.196 cm^2 of the film that contains 0.148 mg of darunavir and 0.0314 cm^2 of the film that contains 0.0237 mg of darunavir) were tested across the cell-free system (membrane only) and across Caco-2 cell monolayers. For both sizes of the film the dissolution profile and transfer of darunavir was a significantly different in the cell-free system compared to the Caco-2 cell system (***, $p<0.001$). Additionally, there is no significant change in the proportion of darunavir transferred across the cell-free system for both different sizes of the film containing different amounts of the drug. Interestingly, the proportion of the darunavir transferring across Caco-2 cell monolayers differs depending on the size of the film. The proportion of darunavir transferred across Caco-2 cell monolayers from 0.196 cm^2 by the end of the experiment was 35.2 ± 7.2%, whereas from 0.0314 cm^2 the proportion transferred was 15.5 ± 3.1 % from the total amount of darunavir.

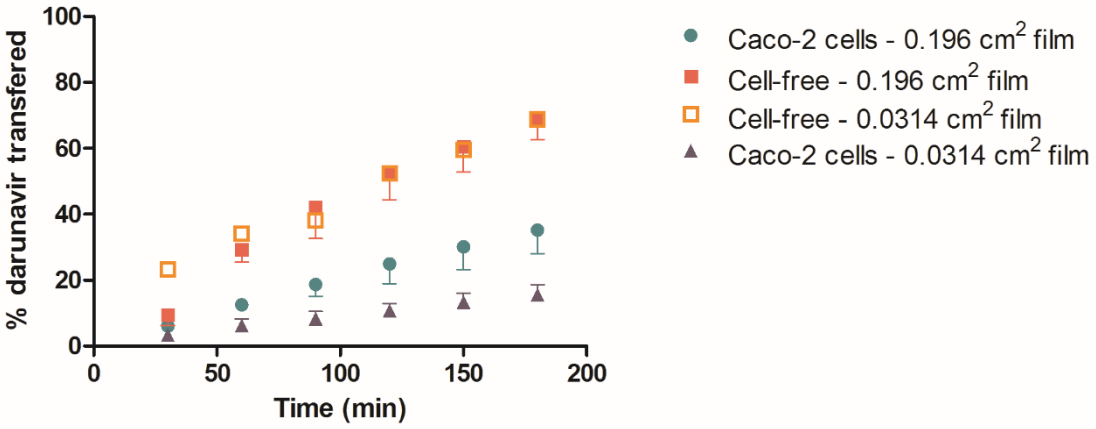


Figure 61. Dissolution and transfer of darunavir from a film formulations; 0.148 mg darunavir in 0.196 cm^2 film or 0.0237 mg darunavir loaded in 0.0314 cm^2 film immersed in 500 µL of HBSS solution in a Transwell diffusion system across Caco-2 cell monolayers or across cell-free system for 180 min time period. Data represent the mean ± SD from three independent studies. Note: error bars are within the data points.

The influence of P-gp and MRP-2 inhibitors on the darunavir dissolution/transfer profile across Caco-2 cell monolayers was investigated (Figure 62). The percentage of the darunavir transfered from film formulation across Caco-2 cell was equivalent to 35.2 ± 7.1% and was significantly lower compare to darunavir transfer in the presence of both inhibitors and the cell-free system (***, $p<0.001$). The percentage of darunavir transfered across the cell-free system was almost the same (64.4 ± 4.2%) as transfer across Caco-2 cell monolayers in the presence of verapamil 100 µM (60.6 ± 3.5%) and a similar effect was obtained in the presence of bromosulphalein, 51.1 ± 4.4%.

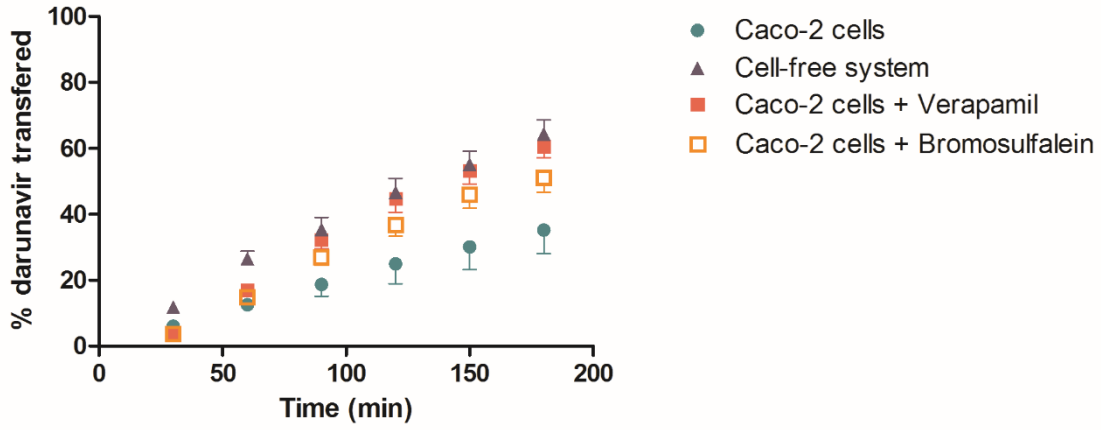


Figure 62. Dissolution and transfer of darunavir from a film formulations; 0.148 mg darunavir in 0.196 cm^2 film immersed in 500 µL of HBSS solution in the absence and in the presence of verapamil 100 µM and bromosulphalein 50 µM in a Transwell diffusion system across Caco-2 cell monolayers or across cell-free system. Data represent the mean ± SD from three independent studies. Note: error bars are within the data points.

3.4. Permeability of tenofovir and darunavir in *ex-vivo* colorectal tissue

To verify findings in Caco-2 cells, *ex-vivo* colorectal tissue segments of guinea-pigs, rats and rabbits were used to measure tenofovir and darunavir permeability across the colorectal tissue of different species in Ussing diffusion chambers in the presence of P-gp inhibitors GF120918 and/or verapamil and when the ARV drugs were co-administered. The Ussing chamber method allows absorptive and secretory transport to be measured across tissue segments (from animals or humans) to predict drug absorption in humans. The electrical parameters, potential difference (PD) and resistance (R), were measured simultaneously during the experiments to verify the viability and integrity of the intestinal segments mounted in the Ussing chamber. The permeability of the paracellular marker mannitol was measured concomitantly with ARV drug transport to confirm that the barrier function of the mucosa was maintained over the course of the experiments.

Potential difference and resistance values measured for colorectal mucosal segments in guinea-pig, rat and rabbit are shown in Figure 52. Before the start of the experiment the potential difference in the tissues varied according to species: guinea-pig tissue 4.4 – 6.4 mV, rat 5.5 – 6.6 mV, and rabbit 7.5 – 8.5 mV (Figure 63a). The potential difference of the mucosal segments was stable and typically exhibited a moderate decrease by the end of the experimental period. The resistance of the colorectal segments was calculated to be in the ranges: guinea-pigs 55 – 75 $\Omega \times cm^2$, rat between 72 – 92 $\Omega \times cm^2$, and rabbit 215 – 245 $\Omega \times cm^2$ (Figure 63b). The values of potential difference and resistance that changed by >25% of the initial reading were excluded from the further analysis.

The absorptive and secretory transport of mannitol was measured in different species (Table 13). The permeability values of mannitol across guinea-pig were $4.7 \pm 1.8 \times 10^{-6}$ cm/s and $4.9 \pm 1.5 \times 10^{-6}$ cm/s in absorptive and secretory directions, respectively. Likewise, no vectoral difference in mannitol transport was found for the rat (absorptive $2.9 \pm 1.2 \times 10^{-6}$ cm/s, secretory $3.1 \pm 1.6 \times 10^{-6}$ cm/s) or rabbit (absorptive $2.79 \pm 0.68 \times 10^{-6}$ cm/s, secretory $3.2 \pm 1.4 \times 10^{-6}$ cm/s)

colorectal mucosal segments, and permeability was similar in these species. Total recovery of mannitol in all Ussing chamber experiments was >95% and linearity of mannitol flux (dQ/dt) was >0.98.

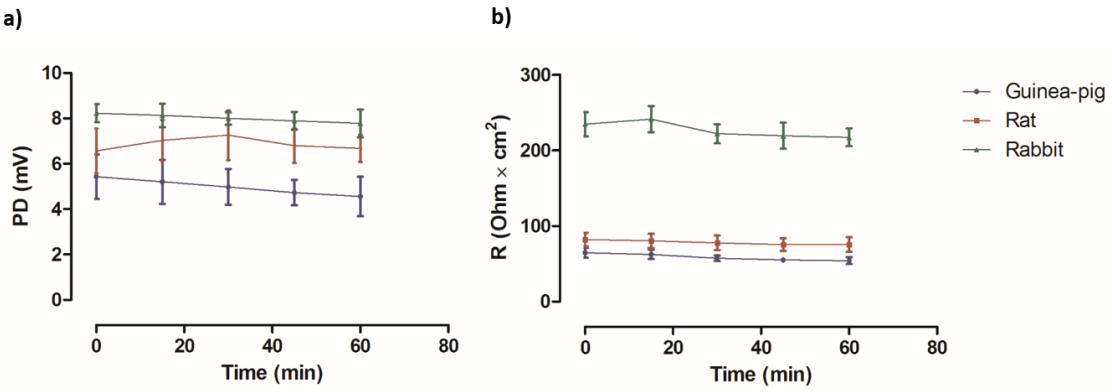


Figure 63. Electrical parameters in guinea-pig, rat and rabbit colorectal tissue segments. Changes in a) potential difference (PD) and b) trans-segmental resistance (R) in guinea-pig (blue dots), rat (red dots) and rabbit (green) colorectal tissue segments during 60 min of incubation in Ussing diffusion chambers. Data represents the mean ± SD from at least three independent experiments, performed in duplicate.

To verify the functionality of the P-gp transporter in guinea-pig and rat colorectal tissue segments, the effect of the P-gp protein inhibitor (verapamil) on the bidirectional transport of digoxin (P-gp substrate) was assessed (Table 13). The same experiments could not be performed for rabbit colorectal segments due to limited availability of tissue secondary to animal use for other experimental purposes, thus only selected parameters were tested. The permeability of digoxin (10 µM) across guinea-pig in absorptive direction was 2.67 ± 0.34 × 10^{-6} cm/s and in secretory direction was 7.84 ± 1.6 × 10^{-6} cm/s, i.e. an efflux ratio of 2.9 ± 0.4. In the presence of verapamil 100 µM, the absorptive permeability increased to 3.12 ± 0.43 × 10^{-6} cm/s and secretory permeability was reduced to 4.32 ± 1.4 × 10^{-6} cm/s (compare to control; **, p <0.01), i.e. a reduction in efflux ratio to 1.38. The permeability of digoxin across rat colorectal mucosal segments was lower in both directions compared to guinea-pig; the apical to basolateral permeability was 2.06 ± 0.32 × 10^{-6} cm/s and basolateral to apical permeability was 6.20 ± 1.39 × 10^{-6} cm/s. The efflux ratio for digoxin in rat was identical to that of guinea-pig, i.e. 2.9. In the presence of verapamil the efflux ratio of digoxin dropped markedly to 0.3 (***, p<0.001).

Table 13. Apparent permeability coefficient (P_{app}), efflux ratio and recovery of ^{14}C-mannitol, digoxin 10 µM and digoxin 10 µM in the presence of Verapamil 100 µM across guinea-pig, rat and rabbit colorectal mucosal segments. Data represents the mean ± SD from three independent studies, performed in duplicates.

	Guinea-pig colorectal mucosal segments			
	P_{app} (cm/s) $\times 10^{-6}$		Efflux ratio	Recovery (%)
	A to B	B to A		
Mannitol	4.7 ± 1.8	4.9 ± 1.5	~ 1.0	>97%
Digoxin 10 µM	2.7 ± 0.3	7.8 ± 1.6	~ 2.9	>96%
Digoxin + Verapamil 100 µM	3.1 ± 0.4	4.3 ± 1.4	~ 1.4	>96%
	Rat colorectal mucosal segments			
	P_{app} (cm/s) $\times 10^{-6}$		Efflux ratio	Recovery (%)
	A to B	B to A		
Mannitol	2.9 ± 1.2	3.1 ± 1.6	~ 1.1	>96%
Digoxin 10 µM	2.1 ± 0.3	6.2 ± 1.4	~ 2.9	>96%
Digoxin + Verapamil 100 µM	1.4 ± 0.4	0.4 ± 0.1	~ 0.3	>95%
	Rabbit colorectal mucosal segments			
	P_{app} (cm/s) $\times 10^{-6}$		Efflux ratio	Recovery (%)
	A to B	B to A		
Mannitol	2.7 ± 0.7	3.2 ± 1.4	~1.2	>95%

The permeability of tenofovir (100 µM) with and without the presence of verapamil (100 µM) was measured in rat colorectal tissue segments (Figure 64). The absorptive and secretory transport of tenofovir was equivalent, absorptive permeability 3.8 ± 1.8 × 10^{-6} cm/s and secretory permeability 3.3 ± 1.24 × 10^{-6} cm/s, and was not affected by verapamil (Figure 64). Additionally, the absorptive permeability of tenofovir in guinea-pig, rat and rabbit colorectal mucosal segments was not influenced by the other of P-gp inhibitor, GF120918 (1 µM) or darunavir (100 µM), confirming the conclusion from the cell culture experiments that tenofovir is passively transported (Figure 65). The total recovery of tenofovir across different species was >96% and the linearity of the flux was >0.987.

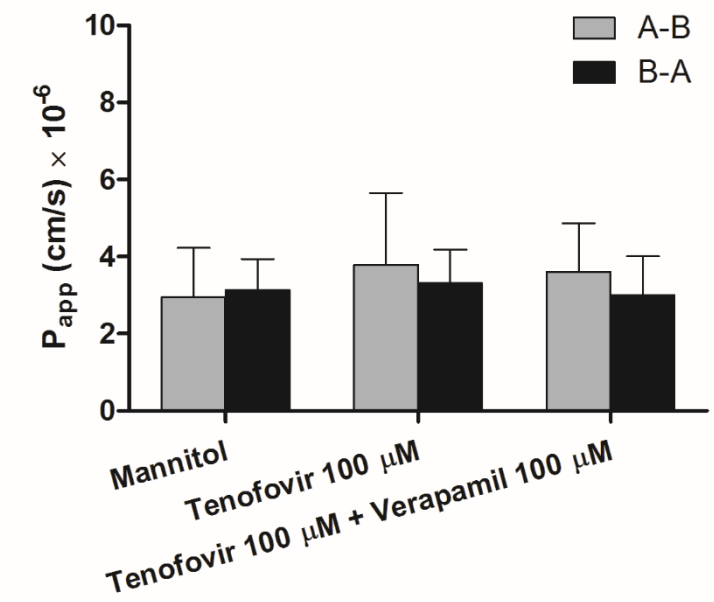


Figure 64. Mannitol and tenofovir transport across rat colorectal tissue segments. Apparent permeability coefficient in absorptive and secretory directions for ^{3}H-mannitol, ^{14}C-tenofovir 100 µM and tenofovir 100 µM in the presence of verapamil 100 µM in rat colorectal tissue segments in Ussing diffusion chambers. Data represent the mean ± SD from three independent studies, performed in duplicate.

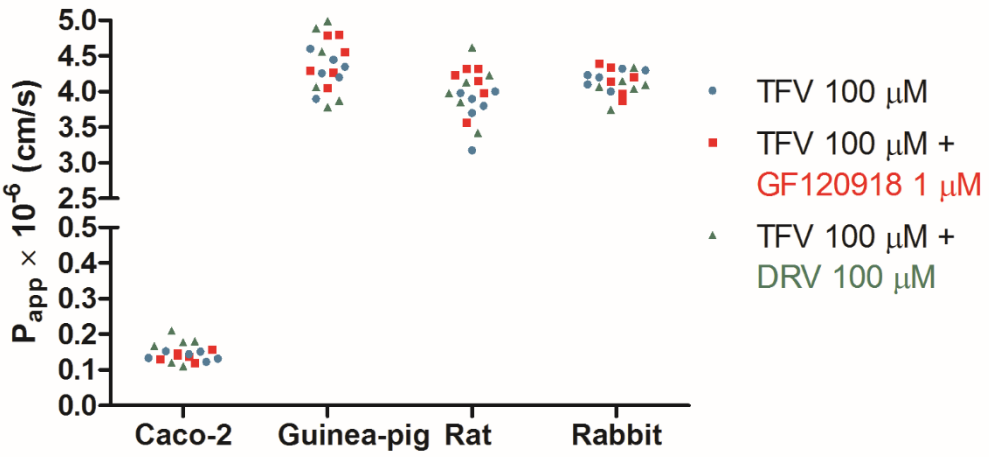


Figure 65. Tenofovir permeability in colo-rectal tissue segments. Absorptive permeability of tenofovir 100 µM in Caco-2 cell monolayer, guinea-pig, rat and rabbit colorectal mucosal segments. Data represent single measurements.

Darunavir (10 µM) transport was assessed in rabbit colorectal mucosal segments and found to have an efflux ratio of 4.9 ± 1.0. When darunavir was co-administrated with P-gp inhibitor GF120918 (1 µM) the efflux ratio decreased to 1.9 ± 0.6 (Figure 66). However, darunavir permeability in absorptive and secretory directions did not significantly change in the presence of tenofovir with efflux ratio 4.9 ± 1.0, suggesting that there is no drug-drug interaction between these two drugs in terms of drug absorption (Figure 66). The recovery of darunavir was >96.5% and linearity of the flux was >0.99 in all experiments.

Due to the limitations in solubility and recovery (<4%) of dapivirine in the tissue segments model and limitations with available animals, the apparent permeability in absorptive and secretory directions could not be determined.

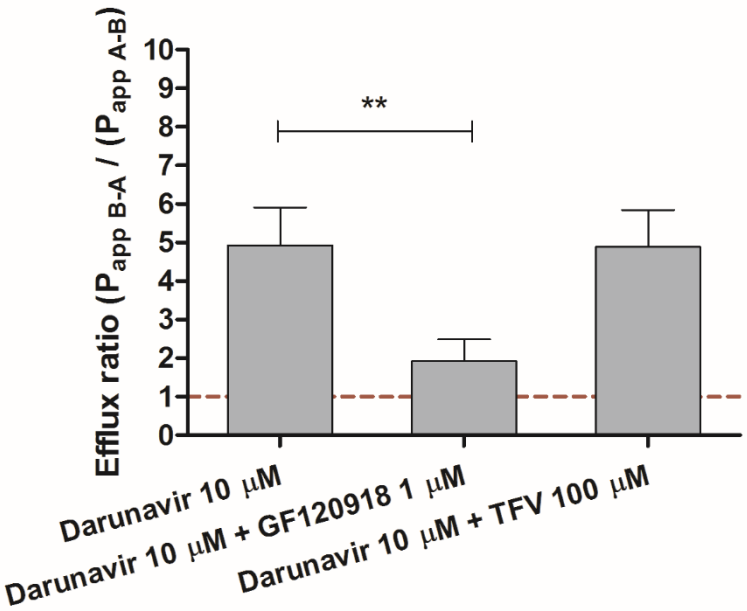
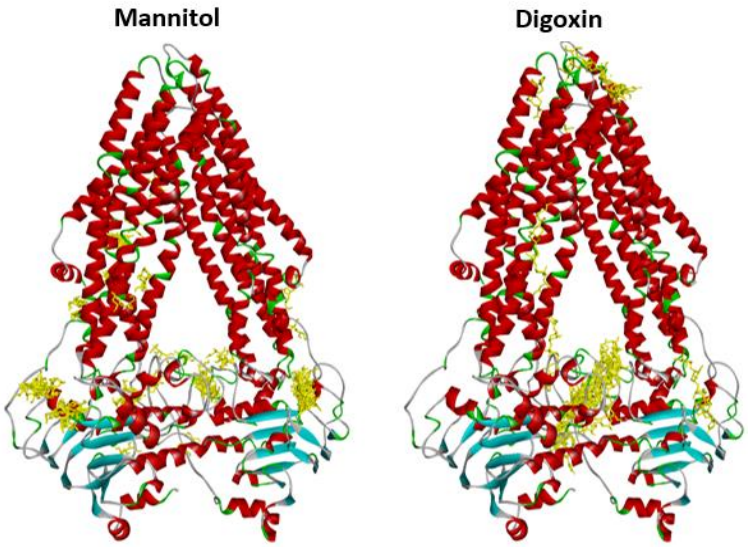


Figure 66. Darunavir transport across rabbit tissue segments. Efflux ratio of darunavir 10 μM in the presence of P-gp inhibitor GF120918 1 μM and tenofovir (TFV) 100 μM across rabbit excised colorectal mucosal segments. Data represents the mean ± SD from three independent studies (** p <0.01).

3.5. Molecular docking of ligands with P-glycoprotein

3.5.1. Molecular docking of mannitol and digoxin with P-glycoprotein

The best probable binding sites obtained by blind Smina molecular docking of mannitol and digoxin to the P-gp efflux protein are shown in Figure 67.



Complex	Mannitol	Digoxin
Affinity (kcal/mol)	-3.1 up to -5.6	-9.5 up to -12.5

Figure 67. Docking of mannitol (negative control; non-P-gp substrate) and digoxin (positive control; P-gp substrate) in yellow colour to a modelled P-gp transporter protein. The ranges of energy represent the affinities for corresponding ligand-protein structures.

The binding energy was calculated for each confirmation and was ranked and scored to give an estimation of the binding affinity between the compound and the target. The binding configurations that demonstrated the lowest binding free energy were considered as the most probable binding sites. First, mannitol and digoxin were tested to confirm the reliability of the model to calculate binding affinity between compounds and the P-gp structure. The compounds were selected on the basis of their transport characteristics in the *in-vitro* and *ex-vivo* models as a non P-gp substrate (mannitol) and P-gp substrate (digoxin). As expected from experimental data, mannitol demonstrated very weak binding affinity towards the

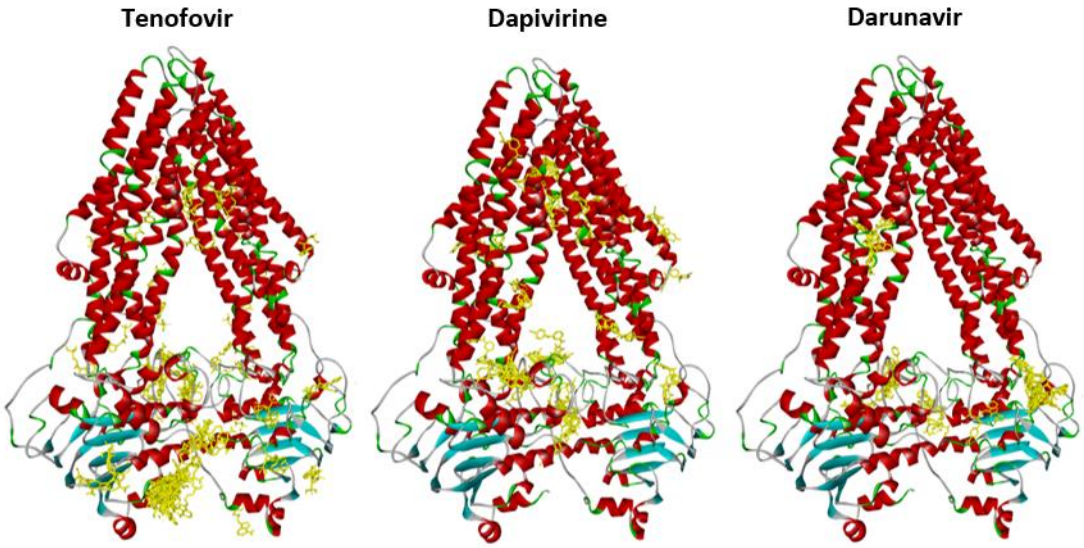
P-gp structure with affinity range of -3.1 to -5.6 kcal/mol, whereas digoxin showed very strong binding affinity -9.5 to -12.5 kcal/mol. GOLD molecular docking recognized the best 10 orientations for mannitol and digoxin into one SMINA-located binding site of the hydrophobic transmembrane domains. The scoring function was used to rank binding confirmations and the energy binding affinity was calculated for each pose (Table 14). GOLD docking scores are ranked based on contributions of hydrophobic interactions, Van der Waals forces and number of hydrogen bonds [178]. The types of binding interactions to the specific domains were characterized for the best pose in each system by Accelrys Discovery Studio 4.5. Mannitol and digoxin showed stronger affinity towards the hydrophobic transmembrane domain with a binding affinity of -5.4 and -9.8 kcal/mol, respectively.

Table 14. Gold molecular docking the best 10 poses for mannitol and digoxin in TMDs domain.

P-gp				Transmembrane domains (TMDs)			
Pose	**Ligand**	**Score**	**ΔG (kcal/mol)**	**Pose**	**Ligand**	**Score**	**ΔG (kcal/mol)**
1		7.621	-8.146	1		22.1622	-36.9891
2		7.4245	-7.5664	2		22.1472	-42.2183
3		7.166	-7.5334	3		19.9789	-32.9295
4		7.0313	-7.6439	4		19.5409	-40.5731
5		7.0222	-7.4953	5		19.1599	-39.4826
	Mannitol				**Digoxin**		
6		6.6417	-8.1101	6		19.0143	-38.1936
7		6.2636	-7.2625	7		18.2761	-43.0182
8		5.9542	-6.7886	8		16.7456	-35.5338
9		5.3556	-6.1394	9		14.6189	-32.4555
10		5.0336	-5.123	10		11.254	-39.0852

3.5.2. Molecular docking of tenofovir, darunavir and dapivirine with P-glycoprotein

The structures of tenofovir, dapivirine and darunavir were docked using blind Smina molecular docking to the P-gp protein structure and best probable binding sites are shown in Figure 68. Tenofovir showed very weak binding activity towards the P-gp structure, with an affinity very similar to mannitol of -2.5 to -5.4 kcal/mol. Dapivirine and darunavir had preferred binding sites in the hydrophobic transmembrane domains and nucleotide binding domains with strong binding affinity of -5.1 to -8.1 kcal/mol and -6.8 to -9.8 kcal/mol. Using GOLD molecular docking the best confirmation for Dapivirine was in the hydrophobic transmembrane domains with binding affinity of -8.1 kcal/mol, whereas tenofovir and darunavir demonstrated a binding affinity to the nucleotide binding domains of P-gp structure with an affinity of -5.4 and -9.8 kcal/mol, respectively. The best 10 poses for tenofovir, darunavir and dapivirine in the TMDs are presented in Table 15.



Complex	Tenofovir	Darunavir	Dapivirine
Affinity (kcal/mol)	-2.5 up to -5.4	-6.8 up to -9.8	-5.1 up to -8.1

Figure 68. Docking of tenofovir, darunavir and dapivirine (in yellow colour) to a P-gp efflux pump. The ranges of energy represent the affinities for corresponding ligand-protein structures.

Table 15. Gold molecular docking the best 10 poses for tenofovir, darunavir and dapivirine in TMDs domain.

P-gp Transmembrane domains (TMDs)											
Pose	**Ligand**	**Score**	**ΔG (kcal/mol)**	**Pose**	**Ligand**	**Score**	**ΔG (kcal/mol)**	**Pose**	**Ligand**	**Score**	**ΔG (kcal/mol)**
1		6.3388	-8.4867	1		19.7321	-29.9904	1		30.4412	-32.7465
2		6.2502	-8.2686	2		18.2316	-28.6928	2		30.1244	-32.71
3		6.2192	-8.2675	3		18.1351	-34.9968	3		29.849	-35.0679
4		5.9266	-8.2213	4		17.4117	-30.3808	4		29.6835	-32.6299
5		5.214	-7.8693	5		17.0055	-26.6538	5		29.6546	-33.0501
6	**Tenofovir**	4.6881	-7.0275	6	**Darunavir**	16.9706	-29.297	6	**Dapivirine**	29.6379	-32.5147
7		4.5497	-7.0753	7		14.6306	-27.4164	7		29.6356	-31.8528
8		4.2899	-6.7621	8		14.3581	-27.1663	8		28.9511	-30.7735
9		4.0351	-5.8804	9		13.6628	-26.0301	9		28.8146	-33.2587
10		2.545	-2.9341	10		11.7167	-23.3558	10		28.1827	-30.0587

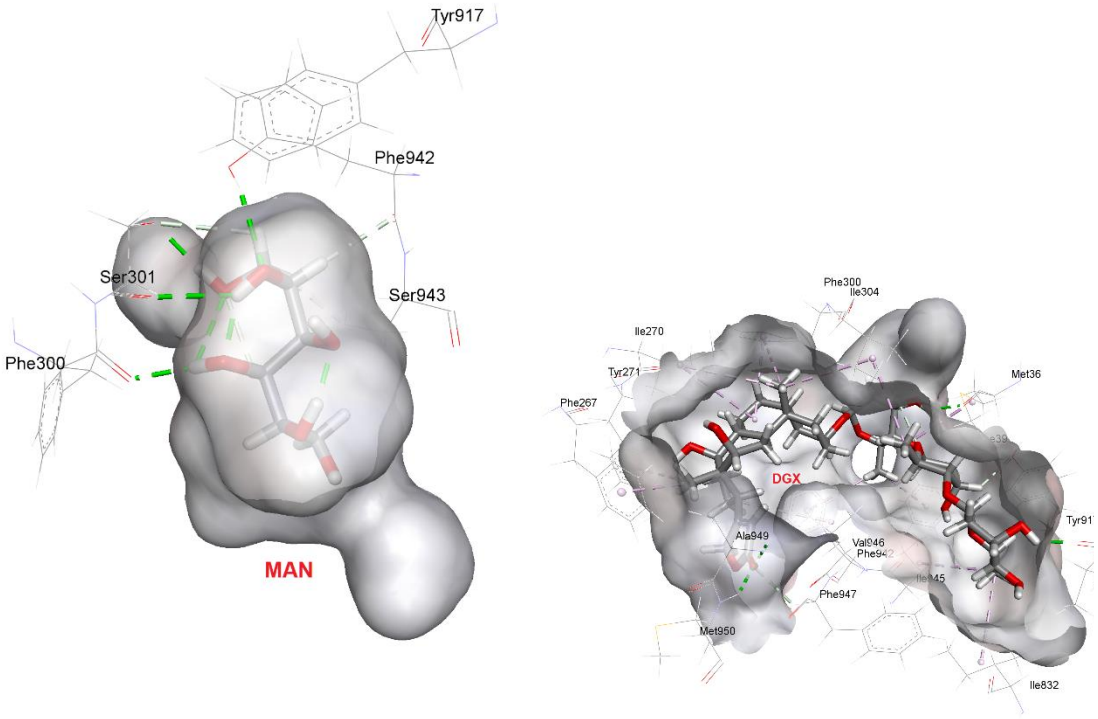
3.5.3. Molecular dynamics simulation of P-gp in complex with mannitol and digoxin

Molecular dynamics (MD) simulations were performed for mannitol, digoxin, darunavir and dapivirine to investigate the interactions between drugs and the P-gp protein structure in detail. Drug-protein complexes were subjected to MD stimulation to study their complex stability. Following 50 ns MD simulations for each drug, MM-PBSA/MM-GBSA calculations were implemented as post analysis to calculate the relative binding free energy for the ligand-protein complexes (Table 16 and Table 17). Mannitol and digoxin were tested and showed good correlation with the docking data. Mannitol showed very weak binding affinity with P-gp domains, forming a weak mannitol-P-gp complex with van der Waals interactions in the range of -29.90 ± 2.15 kcal/mol and ΔG_{PB} in the range of only -9.25± 2.39. Digoxin demonstrated a strong binding affinity towards P-gp structure. The contributions favouring the binding of digoxin are the van der Waals interaction in the range of -95.86 ± 4.23 kcal/mol, electrostatic energy in the range of -31.39 ± 6.16 and ΔG_{PB} in the range of -58.77 ± 5.76. The most important interactions between mannitol/digoxin in complexing with P-gp transporter are shown in Figure 69 and Figure 70.

Table 16. Average energy contributions to form of mannitol and digoxin complexes with P-gp.

Complex	Mannitol (kcal/mol)	Digoxin (kcal/mol)
ΔE_{ele}	-32.70 ± 4.36	-31.39 ± 6.16
ΔE_{vdw}	-29.90 ± 2.17	-95.86 ± 4.23
ΔE_{sol}	53.34 ± 3.01	68.48 ± 4.62
ΔG_{PB}	-9.25 ± 2.39	-58.77 ± 5.76
ΔG_{GB}	-17.87 ± 2.30	-74.72 ± 3.88

a) Mannitol b) Digoxin



Mannitol	Distance (Å)	Types	Digoxin	Distance (Å)	Types
:TYR917-:MAN:O1	2.34	Conventional Hydrogen Bond	:ALA949:H -:DGX:O5	2.38	Conventional Hydrogen Bond
:MAN:H10 -:SER301:OG	1.88	Conventional Hydrogen Bond	:MET950:H -:DGX:O5	2.28	Conventional Hydrogen Bond
: MAN:H8-:PHE300:O	2.03	Conventional Hydrogen Bond	:DGX:H40 -:MET36:O	2.09	Conventional Hydrogen Bond
:MAN:H12 -:SER301:O	2.62	Conventional Hydrogen Bond	:DGX:H59 -:THR909:O	1.95	Conventional Hydrogen Bond

Figure 69. Drug - P-gp transporter complexes in the transmembrane domain after MD simulation and the most important interactions determined by the 50 ns molecular simulation (a) mannitol, (b) digoxin.

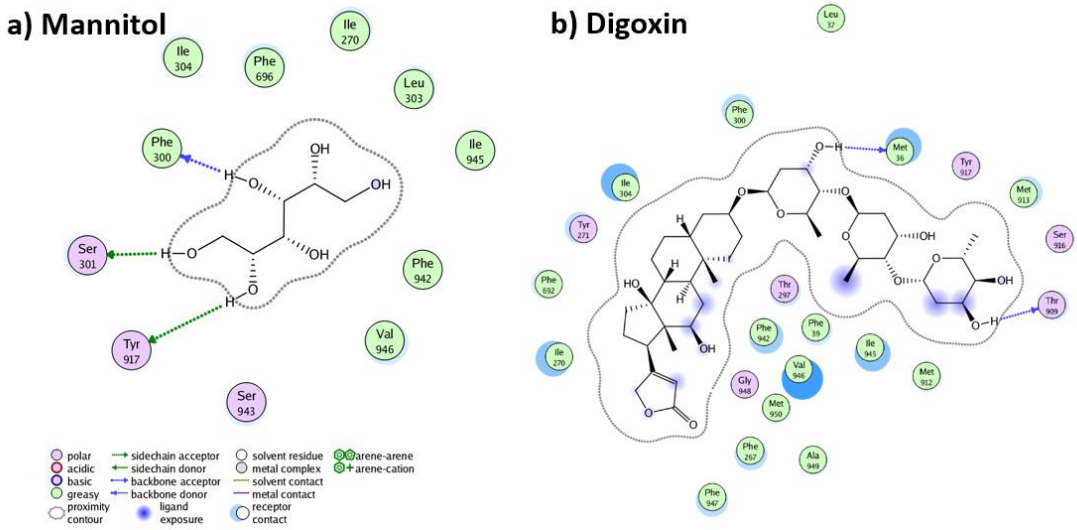


Figure 70. Most important interaction after 50 ns MD stimulation between a) mannitol b) digoxin and P-gp efflux pump.

3.5.4. Molecular dynamics simulation of P-gp in complex with dapivirine and darunavir

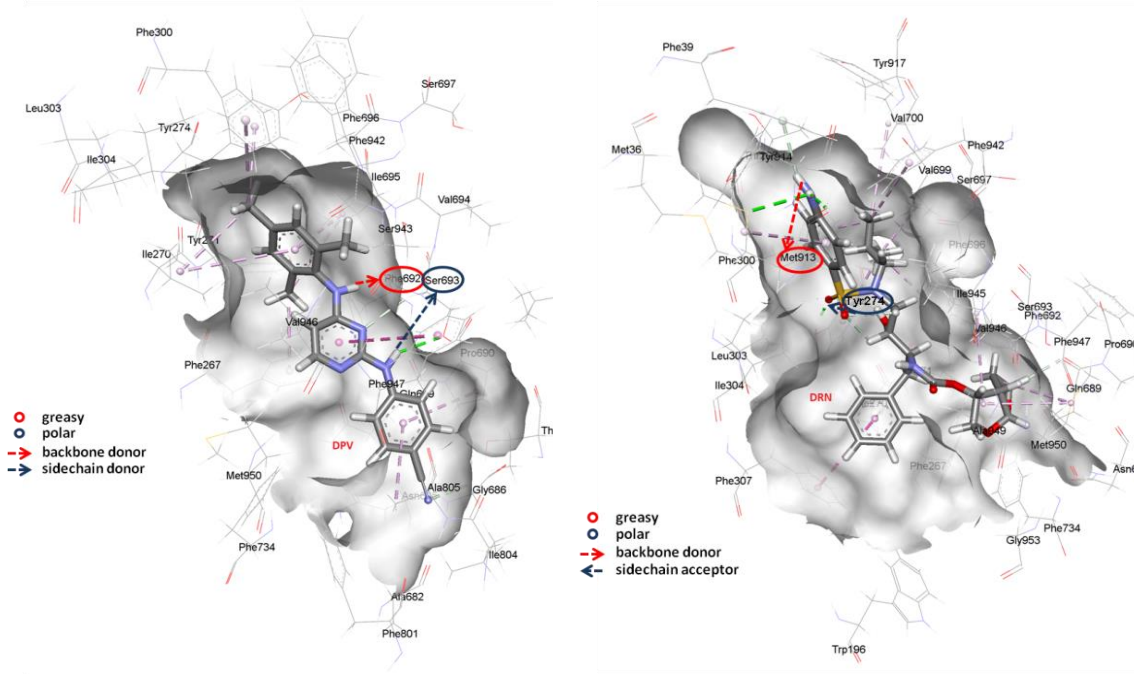
Since tenofovir showed good correlation between *in-silico*, *in-vitro* and *ex-vivo* models and did not interact with P-gp transporter, it was excluded from this analysis. Molecular docking for dapivirine and daurnavir identified a strong binding affinity for both compounds with P-gp domains. The contributions favouring the binding of dapivirine are the van der Waals interaction in the range of -55.54 ± 1.56 kcal/mol and ΔG_{PB} in the range of -38.24 ± 3.20 kcal/mol (Table 17). The contribution of interactions between darunavir and P-gp structure are ΔG_{PB} in the range of -36.84 ± 2.31 kcal/mol and the van der Waals interactions are in the range of -59.73 ± 2.57 kcal/mol (Table 17).

Table 17. Average energy contributions to form of dapivirine and darunavir complexes with P-gp.

Complex	Dapivirine (kcal/mol)	Darunavir (kcal/mol)
ΔE_{ele}	-12.90 ± 1.84	-22.36 ± 2.13
ΔE_{vdw}	-55.54 ± 1.56	-59.73 ± 2.57
ΔE_{sol}	30.20 ± 2.22	45.25 ± 3.35
ΔG_{PB}	-38.24 ± 3.20	-36.84 ± 2.31
ΔG_{GB}	-52.13 ± 2.68	-45.71 ± 2.19

Dapivirine created 14 binding interactions with the P-gp protein structure, in which close contact with Phe-692 and Ser-693 created strong conventional hydrogen bonds. Additionally, the compound formed strong carbon-hydrogen bonds with Gly-686 and Ser-693 (Figure 71a and 72b). Darunavir was found to create several strong possible binding interactions with the P-gp structure, such as very strong conventional hydrogen bonds with Tyr-274 and Met-913 (Figure 71b and Figure 72b).

a) Dapivirine b) Darunavir



Dapivirine	Distance (Å)	Types	Darunavir	Distance (Å)	Types
:DPV1240:H - :PHE692:O	1.88	Conventional Hydrogen Bond	:TYR274:HH - :DRN1240:O2	1.91	Conventional Hydrogen Bond
:DPV1240:H1 - :SER693:OG	2.44	Conventional Hydrogen Bond	:DRN1240:H4 - :MET913:SD	2.92	Conventional Hydrogen Bond
:GLY686:HA2 - :DPV1240:N1	2.88	Carbon Hydrogen Bond	:DRN1240:H4 - :MET913:O	2.19	Conventional Hydrogen Bond
:SER693:HA - :DPV1240:N	2.70	Carbon Hydrogen Bond	:DRN1240:H29 - :GLN689:O	2.44	Carbon Hydrogen Bond

Figure 71. Drug - P-gp transporter complexes in the transmembrane domain after MD simulation and the most important interactions determined by the 50 ns molecular simulation (a) dapivirine, (b) darunavir.

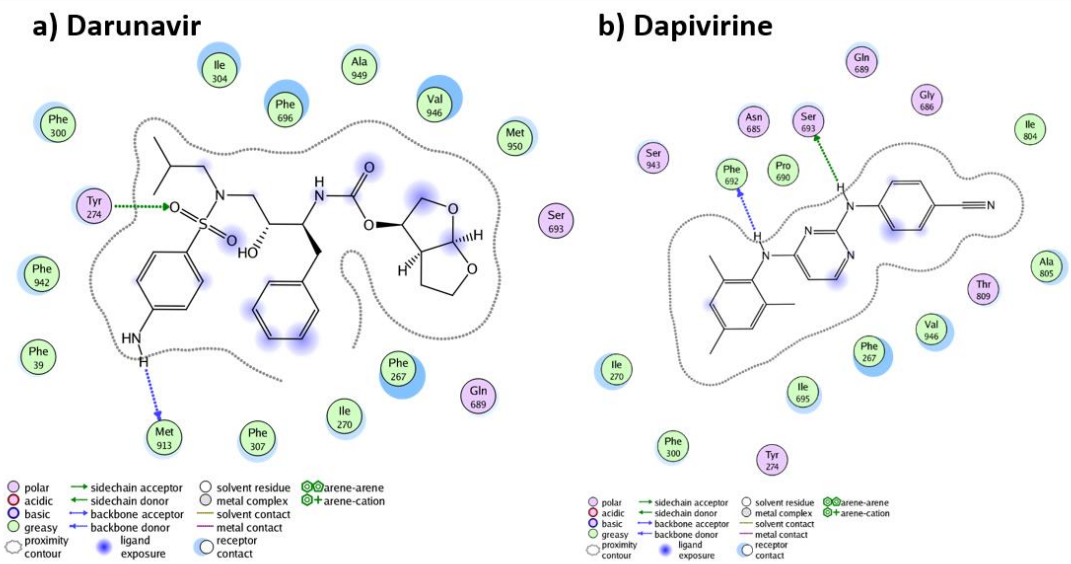


Figure 72. Most important interaction after 50 ns MD stimulation between a) darunavir b) dapivirine and P-gp efflux pump.

Stability of the drug-P-gp structure complexes was assessed with their RMSD values obtained through the MD trajectories (Figure 73). Dapivirine throughout the simulation period showed greater stability when compared to Darunavir and even to ligand-free form of the efflux pump (Figure 74).

In order to investigate the flexibility of residues during simulation, the atomic RMSF for Cα atoms was measured in the ligand-bound systems compared with the ligand-free P-gp (Figure 74). It has been shown that darunavir-P-gp (DRN_P-gp) structure complex was more flexible than dapivirine-P-gp (DPV_P-gp) complex. The fluctuations trend in the RMSF plot for dapivirine-P-gp was slightly closer to free P-gp, demonstrating greater stability of the complex compared to the darunavir- P-gp complex.

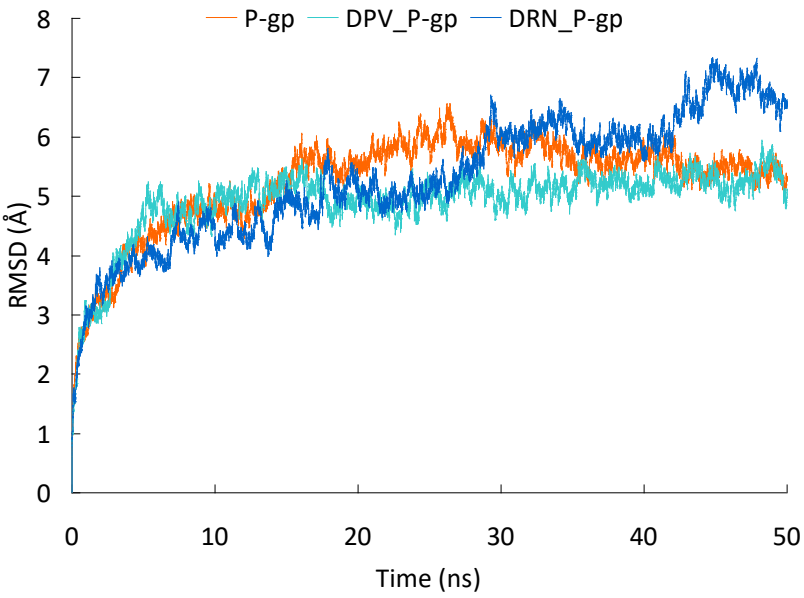


Figure 73. Time dependence of root-mean-square deviation (RMSD) (Å) of P-gp for the backbone atoms in the course of MD simulations in the complexes and ligand-free protein.

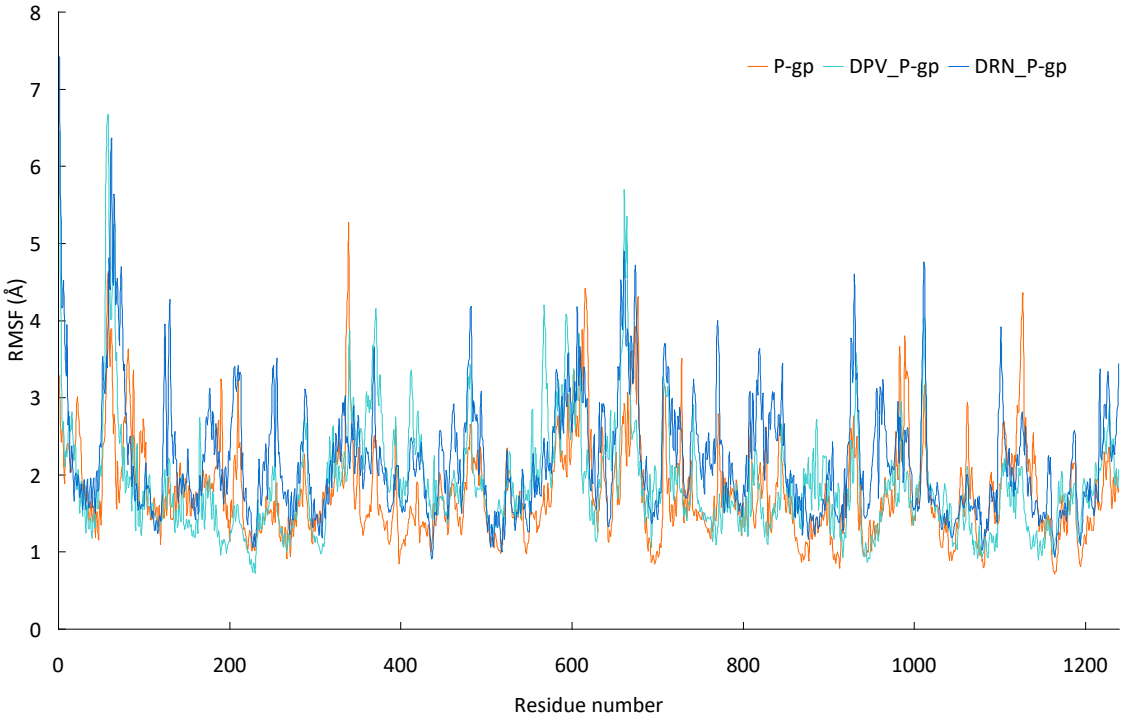


Figure 74. Atomic positional fluctuations (Å) of Cα atoms in the ligand-bound systems compared with the ligand-free P-gp.

Hydrogen bond analysis of MD trajectories with cut-off distance 3.5 Å and cut-off angle 180° showed that there is a permanent H-bond with occupancy over 70% in the dapivirine-P-gp complex. The interaction is formed between the oxygen atom of Ser-693 and the NH group of dapivirine that occupied 94% of MD trajectories (Figure 75).

In the case of the darunavir-P-gp complex, the H-bond between Tyr-274 and darunavir is the H-bond interaction with the highest occupancy 69%. Fluctuations in the distances of the most important hydrogen bonds in dapivirine-P-gp and darunavir-P-gp complexes are represented in Figure 75 and 76, respectively.

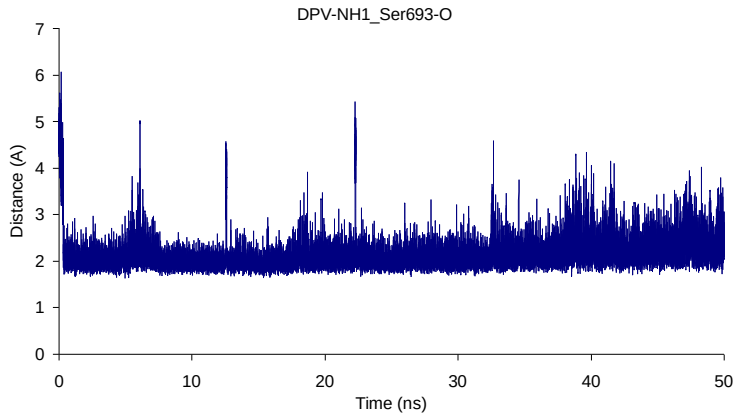


Figure 75. Fluctuations in the hydrogen bond distance between Dapivirine NH1 and Ser-693, during 50 ns MD trajectories.

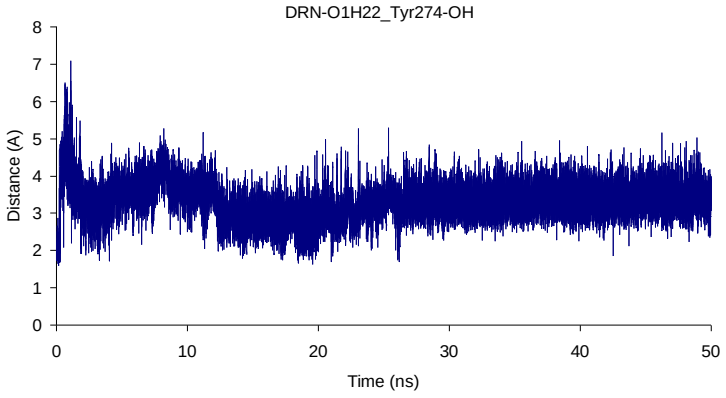


Figure 76. Fluctuations in hydrogen bond distance between Darunavir O1 and Tyr-274, during 50 ns MD trajectories.

Chapter Four
Discussion

4.1. General discussion

The interest in developing efficient and safe rectal topical microbicide over recent years can be attributed largely to improved understanding of the factors enabling efficient colorectal drug delivery combined with promising data obtained from products designed to prevent vaginal transmission of HIV that are far ahead (of their colorectal protective product counterparts) in drug development pipeline. The development of effective next-generation colorectal topical microbicides has focused on combination-based antiretroviral drug microbicides. The combination of two or more antiretroviral drugs with different mechanism of action provides a better chance of protection and fewer possibilities of developing resistance strains. However, as discussed earlier many of the classes of antiretroviral drugs proposed for use in combination can cause drug-drug interactions as a result of transporter interactions with implications for efficacy and toxicity. The drug disposition in cell and tissue compartments depends on several physiological and anatomical barriers such as the type of the cells, cell membrane, presence of mucus, protein binding, metabolizing enzymes and expression of protein transporters. The importance of drug transporters in the targeted tissue and cells and their role in pharmacodynamics, pharmacokinetics, drug-drug interactions and safety of several antiretroviral drugs are increasingly being recognised as important, especially the potential that transporters expressed in colorectal tissue could be highly relevant for topically applied microbicides for prevention of HIV. Understanding of the interplay of drug permeability and transporter-mediated transport will enable rationale design of effective formulations for microbicide combinations.

The differences in the anatomical and histopathological properties between the colorectal and vaginal compartments are likely to produce discrepancies in the disposition of topical microbicides and preclinical evaluation must be performed in adequate models of each of these tissues. Ideally, *in vitro* colorectal models should be physiologically reflective of the critical features of the biological barrier, i.e. should consist of monolayer of polarised cells that display the same characteristics as their *in vivo* counterpart. Additionally, the model should express protein transporters, enzymes, mucus and other biochemical characteristics at the same

level as native tissue. Besides an ideal model should give reproducible results, be cost effective, require only moderate levels of expertise to use and would provide detailed information relevant to *in vivo* system. However, to date, there is no ideal model that possesses all the necessary characteristics to mimic colorectal membranes in humans and it is crucial to use complimentary models to screen/predict drug transport before testing in clinical trials. Models used in pre-clinical evaluation include: *in silico* screening, cell-based model, excised segments from different animals or humans (Ussing chambers), *in situ* and *in vitro* intestinal perfusions and animal based studies. All these models have to be validated and performed under standardized laboratory conditions to provide reliable results.

Nevertheless, the influence of drug transporters on the transport of tenofovir, dapivirine and darunavir (proposed as double or triple topical microbicide formulations) across the colorectal epithelium has not been investigated to date. The aim of the thesis was to investigate the permeability of tenofovir, dapivirine and darunavir across colorectal epithelium (using cell-based and tissue-based) models, discern any role of transporters in regulating absorption using the selective inhibitors and explore the effect of co-administering the microbial agents and excipients on drug transport. To satisfy this aim, specific objectives were outlined; (1) to assess permeability of tenofovir, dapivirine and darunavir and to determine any potential interactions with transporters (especially ABC transporters) using Caco-2 cell monolayers; (2) to screen for drug-drug transporter interactions for tenofovir, darunavir and dapivirine in combination and potential transport modification by typical formulation excipients and a prototype darunavir film formulation; (3) to compare the transport of tenofovir and darunavir in Caco-2 cells to permeability in the excised colorectal tissue segments of animal species used in pre-clinical drug development; (4) to characterise the molecular interactions of tenofovir, dapivirine and darunavir with the P-gp efflux pump using *in silico* screening. These objectives will be discussed in detail in the subsequent sections of this discussion.

4.2. Tenofovir, dapivirine and darunavir transport across Caco-2 cell monolayers.

Caco-2 human colon adenocarcinoma cells slowly differentiate in culture and form a confluent epithelial cell monolayer and have been extensively used over the last thirty years as a model of the intestinal barrier [179]. It is less common to use Caco-2 cells as a model to study drug transport across colorectal epithelium, however a comprehensive comparison in a recent study of epithelial monolayer and transporter gene expression at the human colorectum with different colorectal cell lines such as HRA-16, SW1463, SW837, Caco-2 cells, concluded that Caco-2 cells are the most suitable model [120].

Although, Caco-2 cells are widely used, it has been reported in literature ([180], [181], [182], [183], [184], [185]) that there is variability in this model arising from cell and culture-related factors and it should be carefully monitored during the course of the study [186]. The differences between laboratories have been observed in variability of TER values, levels of expression of enzymes and transporters and permeability coefficient values. Additionally, even small changes in culture-related factors such as initial seeding density, culture time, passage number or medium supplements may led to significant differences in protein transporter expression. Therefore, Caco-2 cell culture needs to be carefully validated and during the time of culture it should be qualitatively controlled to provide consistent and reliable data.

During the course of this investigation, the Caco-2 cell model was validated and controlled during according to FDA recommendations and other scientific guidance ([187], [123], [188]) with the aim of reducing the likelihood of misleading results or poor data interpretation that can lead to false conclusions.

When establishing the method for growing Caco-2 cells on Transwell® inserts it is important to (i) visualise the morphology of the cell monolayers by confocal microscopy to verify that a single layer of cells is present rather than a multilayer formation, and (ii) confirm protein transporter expression by Western Blot. Additionally, it is important to verify the integrity of the cell monolayer (separately and together with the compound to be tested) using a hydrophilic

paracellular (fluid phase) marker such as mannitol which should demonstrate highly restricted permeability across cell monolayers and by measuring transcellular resistance (TER) using an epithelial voltohm meter. To monitor cell growth and epithelial barrier-like formation, TER measurement should be monitored over sequential days to follow the development of the monolayer and then after establishing the time period during which cell layers are stable, the TER should be checked routinely before and after the experiment.

The FDA draft drug-drug interaction guidance recommends that a known P-gp substrate is tested in bidirectional transport assays as a positive control to make verify that the Caco-2 cell model expresses functional P-gp expression when used for transport experiments [187]. For example, P-gp localization at the apical membrane will restrict the absorptive (A-B) permeability of substrate drugs and enhances the secretory (B-A) permeability. The efflux ratio ($ER=P_{app(B-A)}/P_{app(A-B)}$) has been recommended by FDA as a standard parameter to describe whether the test compound is a substrate of apical efflux transporters such as P-gp [187], [189]. A threshold value of ER >2, is often used to indicate that a drug is a P-gp substrate. When the ER value is between 1 and 2, this is regarded as less definitive regarding whether or not a drug is a substrate of P-gp. If the ER value decreases significantly in the presence of P-gp inhibitors (e.g. from the list recommended by FDA), then the tested drug is deemed to be a substrate of the efflux transporters [122]. P_{app} values depend on a variety of assay conditions. To help interpret P_{app} values for test drugs it is recommended that P_{app} of 'standard' compounds is measured as part of each experiment [129]. In order to check the functionality of the transporters in Caco-2 monolayer, it has been suggested that a low permeability substance, mannitol, and a compound with higher cellular permeability, e.g. digoxin, are measured along the test drugs [129]. The FDA has a recommended list of probe substrates for P-gp including, digoxin, vinblastine, quinidine, loperamide and talinolol. Digoxin has been confirmed to be a selective P-gp substrate and is sensitive for P-gp inhibition [190]. Additionally, FDA recommends confirmation of P-gp activity using selective inhibitors such as verapamil, cyclosporine A, GF120918 and saquinavir.

Potential toxicity of compounds is another aspect that must be checked before further investigation, as toxicity of compounds is one of the most

unpredictable characteristics of a molecule. As it has been reported, in many cases that non-toxicity of compounds in preclinical development does not necessarily correlate with findings obtained from clinical trials, where adverse effects may materialise and in the worst cases require withdrawal from clinical development or the market [191], [192]. There are many assays used *in vitro* for evaluating the toxicity of compounds such us trypan blue or fluorescent dye propidium iodide staining, activity of ATP, measuring oxidative stress or inflammatory cytokines level, however the most extensively used assays are MTT and LDH assays.

Optimizing in-vitro model conditions

In order to understand the interactions of compounds with cell monolayer, it is essential to define the suitability of the model and to evaluate the toxicity of tested compounds to exclude those affecting significantly cell viability. Caco-2 cell monolayers were cultured accordingly to the methods of Lakeram et al. [193]. Cells appeared to be similar at each passage when visualised using light microscopy. Cell monolayers were grown on permeable supports for 21-28 days to generate monolayers and to provide time for expression of transport proteins such as P-gp, MRP-2 and BCRP that are may influence drug permeability across Caco-2 cell monolayers [129]. Transporters can be detected by Western blot, but it only represents expression of the individual protein transporter, but does not necessary indicate its functionality. The transporter properties can be identified functionally by measuring the transport of substrates and/or inhibition of active transport by specific inhibitors. Caco-2 cells demonstrated the expression of investigated transporters. Additionally, confocal micrographs of Caco-2 cells showed formation of tight junctions between the cells and the absence of multilayer formation. To test monolayer integrity the TER was measured at each day of culture, plus before and after the experiment as an indication of the tightness of the cellular junctions. The TER values were high, $> 1490\ \Omega\ cm^2$, and after 21 days reached plateau. Other studies, e.g. those by Briske-Anderson et al., reported TER values in range $> 500\ \Omega\ cm^2$ with the same tendency to reached plateau after 21 days of culture. However, the passage number and differences between laboratory equipment and protocols may explain comparatively high TER values in this study, which are nonetheless acceptable [56]. In developing experimental conditions, cell viability

was evaluated after application of varying concentrations of DMSO. In this study, cell metabolism was reduced as the concentration of DMSO was increased from 0 to 10% v/v (Figure 19). However, at concentrations of up to 1% DMSO there was no observable evidence of cytotoxicity. These results are in agreement with a report from Krishna and colleagues who also observed no effect of cytotoxicity assays when using 1% DMSO [194]. For further drug transport studies each of the drugs were solubilized using 1% DMSO in preparation for experiments using hydrophobic antiretroviral drugs with low aqueous solubility. Cell viability and membrane damage were measured after exposure to varying concentrations of digoxin and antiretroviral drugs at different days of culture using MTT and LDH assay.

To assess the integrity and P-gp functionality of Caco-2 cell monolayers in this study, it was important to measure the permeability of mannitol used as negative control and digoxin as positive control. Mannitol was used to verify integrity of monolayer and absorptive permeability was in range $0.18 \pm 0.04 \times 10^{-6}$ cm/s. This was in agreement with previously reported studies that the value should be in range of 10^{-7} cm/s for this paracellular marker [195]. The initial solute flux profile obtained for these two compounds was linear ($r^2 > 0.99$). The values of ER of digoxin (10 µM) obtained under our experimental conditions were equivalent to 16.5 ± 1.0. These results are in the agreement with Ray et al and FDA recommendation which report that ER of digoxin tested at concentration between 0.1 and 10 µM varies between 4-14 [74].

The effect of competitive P-gp inhibitors on the absorptive (A-B) and secretory (B-A) flux of digoxin across the Caco-2 monolayers was measured. Two of the P-gp inhibitors recommended by FDA (verapamil with IC_{50} 2.1 µM and cyclosporine A with IC_{50} 1.3 µM) were used [190]. The efflux ratio of digoxin was reduced by the P-gp inhibitors in a concentration dependent manner. These studies suggest strongly that P-gp mediated efflux limits the absorptive permeability of digoxin across Caco-2 cell monolayers; similar results were reported by Ray and colleagues [74]. One of the possibilities to enhance solubility of hydrophobic drugs is to employ commonly used pharmaceutical excipients, such as PEG 400. It has been shown that PEG reduced P-gp transport activity by interaction with allosteric sites in P-gp pump or by blocking the binding site of P-gp. The permeability of mannitol and TER were checked to verify that PEG 400 1% (v/v) did not influence

paracellular transport. The P_{app} value of mannitol in the presence of PEG 400 did not change significantly compared to PEG-free control. However, PEG 400 1% (v/v) inhibited digoxin efflux in Caco-2 cells and reduced ER by 84%. This finding was in agreement with the results reported recently for the influence of PEG 400 on the ER of ranitidine, a P-gp substrate [196].

Correlation between lipophilicity and permeability across Caco-2 cell monolayers

Conclusions regarding membrane-drug interactions based only on the psychochemical properties of drugs is a simplification of a complex process of transport across epithelial monolayers that includes the interplay between passive and/ or active transport and drug properties. However, one of the most important psychochemical properties in predicting and understanding transcellular permeability is the lipophilicity of a compound. The lipophilicity is typically expressed as the octanol-water partition coefficient (log *P*) and gives indirect information regarding the extent to which passive transport is involved in a compound's permeability across epithelial monolayer. For compounds which are predominately transported by passive transport a strong relationship between permeability and lipophilicity is observed. However, complications occur when active transport is involved, leading to outliers in the correlation between permeability and lipophilicity [197].

In this study the correlation between lipophilicity and permeability of tested drugs was accurate. The absorptive permeability of our compounds ranked in accordance with their lipophilicity tenofovir< darunavir <dapivirine (Figure 77). However, the permeability of darunavir is lower than that of other drugs of similar log P.

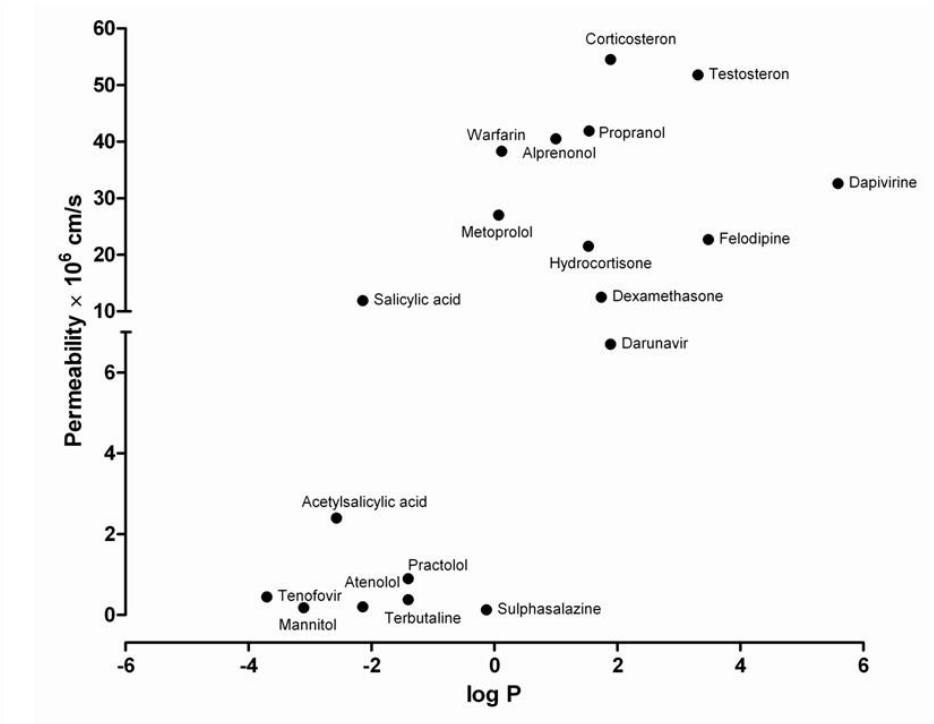


Figure 77. The absorptive permeability of tenofovir, darunavir and dapivirine in the context of reported permeability of drugs in Caco-2 monolayers in similar experiments as a function of octanol-water partition coefficients (n=3-6, each done in triplicate).

Tenofovir transport across Caco-2 cell monolayers

Tenofovir is one of the most commonly investigated antiretroviral drugs for application as an effective topical microbicide that has been tested in clinical trials. The hydrophilic properties of tenofovir may reduce the absorption of the drug due to limitations to permeation across the epithelial barrier in colorectal tissue. Hydrophilic drugs have characteristically low binding affinity to proteins present in colorectal tissue and this results in poor transport across the membrane. First results from the CAPRISA 004 clinical trial showed promising results for pericoitally dosed 1% tenofovir gel for vaginal administration, demonstrating that gel was effective against HIV-1 infection, and is a safe and acceptable product [139]. However, the more recent VOICE study had to discontinue as a clinical trial indicating that used once-daily 1% tenofovir gel was not effective against HIV transmission, revealing low concentration at targeted tissue [198] .

In this study, tenofovir permeability was tested in Caco-2 cell monolayers as an indication of its absorption and any influence of transporters in tenofovir distribution across epithelium. In agreement with *in vivo* data, the permeability of tenofovir in Caco-2 cells was low, being similar to permeability of mannitol (which is widely used as a paracellular marker). The permeability of tenofovir was equivalent in absorptive and secretory directions. Previous publications have suggested that ABC- efflux transporters such as P-gp, MRP2 or and BCRP might be involved in tenofovir transport across epithelia [73], [74], [75], [199]. However, in this study tenofovir exhibited very low penetration and intracellular accumulation in Caco-2 cell monolayers, which was not influenced by the presence of P-gp inhibitors, MRP-2 inhibitor or BCRP inhibitor. The bidirectional transport of tenofovir was unaffected by presence of efflux inhibitors. Tested concentrations of tenofovir were non-toxic, and did not affect the cell monolayer integrity and recovery of the drug was in the range of acceptance criteria. Our findings are in agreement with Ray and co-workers [74] and Neumanova and co-workers [200] suggesting that tenofovir traverses the mucosa via the paracellular route and is not a substrate for efflux transporters expressed in Caco-2 cell monolayers.

The low permeability of tenofovir concords with the findings of a cross over study comparing oral dosing (TDF ester) to topical application (non-esterified TFV) of 1% tenofovir vaginal gel. It was shown that after daily dosing of tenofovir

1% gel (40 mg) substantially lower (56-fold) systemic exposure of tenofovir was achieved compared to daily dosing of TDF (viread TM). Tenofovir demonstrated low efficiency after topical administration, it has been found to give a mM concentration levels in the vaginal fluid, whereas in the vaginal tissue concentration was in µM level [201]

One of the best way to improve the delivery of tenofovir would be co-formulation; it has been shown by Zidan and colleagues that incorporating tenofovir into proliposome formulations containing 5 and 15% of stearylamine enhances the permeability of tenofovir across Caco-2 cell monolayers by between 16.5 and 5.2-fold [202]. Proliposmome formulations exhibit show promising improvement of tenofovir permeation and could be suggested for further evaluation as a potential rectal microbicide formulation.

Dapivirine transport across Caco-2 cell monolayers

The highly lipophilic drug dapivirine, can be classified as drug class II in the Biopharmaceutical Classification System, indicated by low solubility and high permeability as defined by Amidon and co-workers [203]. Our results contradict those previously reported by Neves and co-workers and Lewi and co-workers describing dapivirine absorptive permeability across Caco-2 cell monolayers as equivalent to $3.28 \pm 0.16 \times 10^{-6}$ cm/s and $2.14 \pm 0.81 \times 10^{-6}$ cm/s, respectively [204], [205]. We found P_{app} values for dapivirine to be critically dependent on recovery, which when improved from <55% to > 89% in Caco-2 cell model changed P_{app} from $2.9 \pm 0.9 \times 10^{-6}$ cm/s to $34.2 \pm 0.31 \times 10^{-6}$ cm/s. The differences between the results might be related to the experimental procedure, as in both studies, the recovery of the dapivirine or paracellular marker used to measure monolayer integrity were not reported. Other factors that might influence the findings may include the use of different membrane supports, cell passages or initial seeding density as well as excipients used to improve recovery and solubility in the donor and receiver compartments. Grammen and colleagues also studied the absorptive permeability of dapivirine, albeit across a different cell line (HEC-1A cells) and have shown that after one hour of the incubation with apically administered dapivirine ≈21% of the applied dapivirine permeated across cell monolayers [206]. Whereas, in this study after two hours ≈42% of the applied dapivirine permeated

across Caco-2 cell monolayers into the receiver chamber. Similar results were obtained by Van Herrewege and colleagues, showing that 34-37% of the applied dapivirine permeated across a cervical cell line (ME-180) into the receiver compartment [207]. In this study, dapivirine showed very high intracellular accumulation, in range 26 – 45% of the applied dapivirine (depending on the sink condition and solubility used in the system). Similar results were obtained by Grammen and colleagues, where 56% of dapivirine was present inside HEC-1A cells [206]. The results from a Phase I trial which assessed a vaginal ring containing maraviroc and dapivirine revealed that the concentration of the hydrophobic drug dapivirine in the tissue were 1000 times higher than plasma concentration, whereas concentration of the hydrophilic drug maraviroc showed very low binding affinity to tissue proteins and was undetectable in plasma. Dapivirine, but not maraviroc showed a concentration-dependent inhibition in cervical tissue against HIV-1 infection [208]. Although dapivirine can be absorbed more efficiently compare to hydrophilic compounds (i.e higher accumulation of the drug inside the tissue) due to its hydrophobic properties, this distribution within the tissue might be problematic. As shown in study done by Akil and colleagues, dapivirine accumulation across excised human ectocervical tissue after release from a film formulation was mostly observed in upper part of the stroma, while there was significantly less in the deep part of the stroma [146].

Highly lipophilic compounds are often have poor recovery in experimental systems and which can cause problems in data interpretation and underestimation of drug transport across cell monolayers. Lipophilic drugs can exhibit high non-specific binding to Transwell surfaces and considerable retention by the Caco-2 cells affecting the final recovery if drug in this compartment is not quantified. Different methods to improve recovery of tested compound in Transwell system have been published. One of the most commonly recommended method is the use of 4% BSA in the receiver chamber which mimics *in vivo* conditions where drug is absorbed into blood which contains 4% albumin [209]. During the *in vivo* absorption mechanism, compounds after penetration across epithelium enters the blood circulation. Most of the hydrophobic molecules exist in a complex formed with serum proteins (such as albumin). Compounds that bind with the protein have enhanced solubility which might help produce sink conditions and increase their

permeation into the blood and provide with the necessary diffusion gradient to drive absorption. The use of 4% BSA might significantly reduce the binding of the compound both to cells and non-specific binding to the plastic of the Transwell chambers.

The absorptive and secretory transport of dapivirine was investigated in the presence of 4% BSA in the receiver compartment. The rates of mannitol transport were unaffected compared to those measured under standard experimental conditions, reflecting that mannitol does not bind to albumin. In contrast, addition of 4% BSA into receiver compartment did not improve significantly the recovery of dapivirine (in the absence of 4% BSA 55%, in the presence of BSA 56% of the applied drug). However, the use of BSA did increased significantly the permeability of dapivirine in both directions and reduced the intracellular level of dapivirine (from 45 to 34%).

Another approach to improve dapivirine recovery was to use excipients that solubilize poorly water-soluble compounds without affecting the permeability of mannitol and digoxin (used as controls) and create sink conditions. Poloxamer 407 0.2% (w/v) has been reported by the FDA guidance as an 'inactive' excipient for varying types of formulation (such as topical formulation, inhalation, suspension, oral solution or ophthalmic formulation) [210]. It has been shown by Shin and colleagues that Poloxamer 407 at a concentration of 22.5% (w/w) increased the water solubility of piroxicen by 11-fold [211]. It appears that Poloxamer 407 is more effective compared to some other surfactants such as polysorbate or polyol. Incorporation of Poloxamer 407 as a excipient in formulations facilitated the solubility of poorly water-soluble compounds (insulin, indomethacin, etc.) [212]. In this study, 0.2% (w/v) of Poloxamer 407 was used and this implementation significantly increased the recovery of the dapivirine to 89%. The enhanced recovery significantly increased the bidirectional transport of dapivirine, and by creating sink condition the intracellular accumulation of dapivirine decreased to 26%. Mannitol permeability and recovery were unaffected by the presence of the Poloxamer 407. Additionally, it had no impact on the TER values.

The high permeability of dapivirine can be attributed to passive diffusive transport enabled by the drug's lipophilicity, log P= 5.29. Dapivirine permeability was concentration independent and did not cause any significant upregulation in

the presence of MRP-2 or P-gp inhibitors. It has been observed that dapivirine permeability in the presence of verapamil and haloperidol exhibited greater variability in both absorptive and secretory directions, however the changes were not significant and it might be caused by dapivirine high lipophilicity.

Darunavir transport across Caco-2 cell monolayers

Darunavir is a protease inhibitor and many clinical studies have identified some of the protease inhibitors to be involved in drug-drug interactions by inhibition or induction of P-gp transporter [73].

This study aimed to explore whether transcellular transport of darunavir across Caco-2 cell monolayers is mediated by ABC - efflux transporters. A significant difference was observed between absorptive versus secretory permeability in Caco-2 cell monolayers. The secretory permeability of darunavir reduced over the concentration range studied (0.1-100 µM), indicating that the active transport component became saturated. This observation was strongly in agreement with reports of Lachau-Durand and co-workers that darunavir transport rates were strongly concentration-dependent [163]. With increasing concentration of darunavir, the absorptive permeability increased however the intracellular accumulation was unchanged. In all experiments cell monolayer integrity was evaluated by concommitant mannitol measurement and by TER readings. Both parameters were unchanged through all tested concentrations. The recovery of darunavir was in the range of acceptance criteria in all tested conditions.

Darunavir permeability was tested in the presence of P-gp inhibitors such as verapamil and GF120918, and both drugs significantly reduced the efflux ratio of darunavir by inhibiting P-gp mediated transport suggesting that darunavir efflux was mediated by the P-gp transporter. This observation was in agreement with studies by Holmstock and colleagues in which darunavir efflux was completely inhibited (6-fold increase of absorptive permeability) by the presence of GF120918 in Caco-2 cell monolayers [213]. To evaluate the role of BCRP transporter in modulating darunavir transport, the BCRP-inhibitor Ko 143 was used in the presence of darunavir across cell monolayers. Our finding suggested that BCRP was not involved in transcellular transport of darunavir as it did not influence

secretory or absorptive permeability of the drug at any tested concentrations. Similar findings were reported by Fujimoto and colleagues, who used Novobiocin as a typical BCRP inhibitor [76]. Further investigation included measuring the role of the MRP-2 transporter in darunavir transport. For this purpose varying concentrations of Bromosulphthalein (recommended as a specific MRP-2 inhibitor [214]) were used. It has been shown that MRP-2 plays a minor role in darunavir efflux across Caco-2 cell monolayers: bromosulphthalein had significant, but a comparatively weak effect on the apical-to basal transport of darunavir in Caco-2 cells. These observations were confirmed by darunavir accumulation in Caco-2 cells in uptake studies. Darunavir accumulation was inhibited by CsA 10 µM and GF120918 1 µM, increasing intracellular concentration of darunavir by more than 200% compared to the control. In the presence of bromosulphthalein, darunavir concentration increased by 75% compared to the control. These results demonstrate clearly the involvement of P-gp and to a lesser extent MRP2-mediated transport of darunavir across Caco-2 cells. These findings were in agreement with Fujimoto and colleagues who suggested that beside P-gp transporter, MRP (most probably MRP-2) was also involved in the transport of darunavir in Caco-2 cells [76].

Co-administration of tenofovir, dapivirine and darunavir across Caco-2 cell monolayers

To date, the potential for drug-drug interactions in the transport of co-administered tenofovir, dapivirine and darunavir has not been reported. However it is important to investigate any influence on drug permeability and cell/ tissue uptake when antiretroviral drugs are co-administered. Co-administration of two or more antiretroviral drugs and drugs that belong to different classes has previously been folund to upregulate protein transporter activity, and modify drug metabolism by enzymes / compound pharmacokinetics [73], [215]. For example co-administration of protease inhibitors such as darunavir, atazanvir, lopinavir/ritonavir with tenofovir disoproxil fumarate resulted in a 25-37% increase in tenofovir disoproxil fumarate exposure. *In-vitro* studies suggest that this upregulation was caused primarily by interaction with the P-gp transporter [73]. HAART combines at least three antiretroviral drugs in relatively high concentrations to achieve low viral activity [215]. So far, development of new generation of topical microbicides has featured antiretroviral drugs combinations such as tenofovir and dapivirine for vaginal rings [216] , films [217] and gels [218], tenofovir and nevirapine for vaginal rings, tenofovir and emtricitabine for vaginal gels [219], and dapivirine and maraviroc for vaginal rings [220].

Apart from the synergistic and additive roles of drug in terms of their antiretroviral activity, their effect on transporter activity can contribute to the safety and efficacy of topical microbicides. As an example it has been shown by Kakuda and colleagues, that exposure of maraviroc (well-known P-gp substrate), was reduced in the presence of etravirine, increased in the presence of darunavir-ritonavir, and increased when co-administered with etravirine - darunavir – ritonavir [221]. These results shows how modulation with different antiretroviral drugs can improve drug absorption. Thus the potential effects of co-administration of antiretroviral drugs on their trans-epithelial transport needs to be evaluated

In this study, varying combinations of tenofovir, dapivirine, and darunavir were tested for effects on their bi-directional transport across Caco-2 cell monolayers and accumulation inside Caco-2 cells. Using the Caco-2 cell drug

transport model, no significant influence on the trans-epithelial transport or cell uptake of co-administering the drugs in double or triple combinations was observed.

Permeability of tenofovir and darunavir across inflamed Caco-2 cell monolayers and effect of cell exposure to darunavir film formulation on secretion of selected interleukins by differentiated Caco-2 cells

Colorectal tissue might be inflamed by many factors that can cause modulation of the epithelial permeability. In order to develop an epithelial inflammation model, Caco-2 cells were exposed to varying concentration of inflammatory mediator IL-1 β. IL-1 β plays a major role in the induction and expansion of inflammatory conditions, and is released by various cell types such neutrophils, monocytes and macrophages. Most importantly, it leads to an increase in the activity and the secretion of IL-8, IL-6 or prostaglandin and can destroy the integrity of the epithelial barrier [222], [223]. The influenced of inflamed Caco-2 cell monolayers on the permeability of tenofovir and darunavir was investigated in this study. The effect of IL-1 β concentrations that caused inflammation of the cells were measured by increased secretion of IL-8 but without destroying the cell monolayer integrity. The permeability of tenofovir and darunavir was measured in Caco-2 cells under that exhibited an IL-8 inflammatory response. There was no significant difference observed in the drug transport across the inflamed cells compare to the non-inflamed model.

Exposure to topical microbicide formulations may trigger changes in the colorectal epithelium including the induction of irritation/inflammation that was not detected by the cell viability-based toxicity assays. At the beginning of the study, epithelial viability was measured in the presence of varying concentrations of tested compounds and only non-toxic concentrations of compounds were investigated to assess drug transport across Caco-2 cell monolayers. It has been demonstrated, that upon treatment with non-toxic concentrations (validated by cell viability) of some drugs and excipients can significantly increase the secretion of interleukins, leading to higher risk of HIV-1 infection as cytokines such as IL-8 attract HIV target cells [224]. Therefore, an assessment of interleukin secretion was

used as a sensitive technique in addition to the viability assays (MTT, LDH release) and integrity of epithelial layer (TER and paracellular marker) was also evaluated.

In this study, we evaluated the effect of 24 h exposure to darunavir film and tenofovir, darunavir solutions at concentrations that have been used in drug transport assay without affecting the cell monolayer integrity and cell viability. When interleukin secretion by differentiated Caco-2 cells was measured as an end-point, there was a correlation between mucosal non-toxicity and a lack of upregulation in the secretion of IL-8/IL-6. Tenofovir and darunavir solutions and darunavir film were demonstrated not to effect cell viability, monolayer integrity or interleukins secretion. Similar findings were reported by Gali and colleagues demonstrating that exposure to tenofovir (1- 1000 µM) did not increased secretion of IL-8 by Caco-2 cell monolayers [225].

4.3. Screening the impact of co-formulation on ARV drug absorption across Caco-2 cell monolayers.

Effect of GRAS excipients used in formulation on modulating tenofovir, dapivirine and darunavir permeability across Caco-2 cell monolayers

Generally recognized as safe (GRAS) excipients are extensively used in development of pharmaceutical formulations. It is well known that that some of the excipients used in formulations might influence transporter activity, act as wetting agents to improve the solubility, dissolution and absorption of non-soluble drugs, increase paracellular transport by opening tight junction or increase membrane fluidity [226], [227], [228], [229]. Excipients that inhibit efflux transporters, enhance the permeability or extend retention via mucoadhesion may play an important role in increasing intracellular concentration of compounds. Therefore, formulations developed as a topical microbicides (for rectal and vaginal use) containing different classes of antiretroviral drugs may modify drug pharmacokinetics by use of excipients that can modulate the absorption process and delivery of compound to the target tissue. Thus, excipients should be tested for safety and compatibility with tested drugs, to avoid adverse effects that might lead to increased risk of virus entry.

Pharmaceutical excipients such as pluronic P85, polysorbate 80, cremophor, vitamin E TPGS, PEG 300 and PEG 400 have been shown in many studies to inhibit P-gp transport [227], [230], [231]. A study by Ashiru-Oredope and colleagues revealed that PEG 400 exhibited a non-linear concentration dependence and at 1% (v/v) concentration inhibited the P-gp-mediated transport of ranitidine, whereas PEG 200 did not have any effect on the bidirectional transport of P-gp substrate across Caco-2 cell monolayers [196]. Another well known, non-ionic excipient Polysorbate 80 (Tween 80) demonstrated inhibition of P-gp mediated transport of rhodamine 123 across Caco-2 cell monolayers [227]. Additionally, Pluronic P85 and PEG 300 also inhibit MRPs transporters.

The effect of commonly used excipients in formulations, such as PEG 200 1% (v/v), PEG 400 1% (v/v), Polysorbate 80 % (v/v), PEG 1000 1% (v/v), HPMC-

50 5% (v/v), Poloxamer 407 0.2% (v/w) was investigated on bidirectional transport of tenofovir, darunavir and dapivirine across Caco-2 cell monolayers. In this study mannitol permeability and TER values were measured simultaneously to evulate cell monolayer integrity. The concentrations of excipients used in this study did not influence mannitol absorptive and secretory permeability across Caco-2 cell monolayers, and did not reduce TER readings by more than 15% from the initial reading. These results are in agreement with Rege and colleagues who demonstrated that mannitol permeability across Caco-2 cell monolayers was unaffected by the presence of Tween 80, HPMC and PEG 400 [228]. These findings concord with results presented by Ashiru-Oredope and colleagues that tested PEG 200 and 400 regarding mannitol permeability across Caco-2 cell monolayers [196]. The only inconsistency was with PEG 1000, which Grammen and colleagues found to decrease significantly TER reading across HEC-1A cells. However, this result might be explained by use of a higher concentration of PEG 1000 (20% (v/v)) and the different cell lines used in that study [206]. Paracellular permeability of mannitol provided an indication in our study that the tested excipients did not affect the barrier properties of the cell monolayers.

The trans-epithelial permeability of tenofovir in the presence of excipients listed above was similar that of the paracellular marker, mannitol. Co-administrations with excipients had no influence on absorptive nor secretory transport of tenofovir and produced no significant reduction in TER values. Importantly, Poloxamer 407 0.2% (v/w) did not influence the bidirectional transport of tenofovir or mannitol, suggesting that Poloxamer 407 was suitable for use as solubility enhancer when tenofovir will be co-administrated with dapivirine.

Dapivirine permeability was only significantly affected by the presence of Polysorbate 80 (a non-ionic surfactant) and Poloxamer 407. The absorptive and secretory transport was significantly increased with improved total recovery of the dapivirine in the presence of Polysorbate 80 with values comparable to those obtained when dapivirine was co-administered with Poloxamer 407. The improvement of recovery of dapivirine in the presence of Poloxamer 407 and Polysorbate 80 was explained by the fact that both excipients belong to non-ionic surfactants group that increases the solubility of compound. As mentioned above

Grammen and colleagues tested influence of PEG 1000 on dapivirine flux, demonstrating that flux across HEC-1A cells was significantly enhanced, however their TER was reduced to 35 – 80% of initial readings when PEG 1000 20% (v/v) was added, suggesting of disruption of the epithelial cell layer integrity, making interpretation of the data uncertain [206]. In our study none of the excipients: PEG 200, PEG 400, PEG 1000 or HPMC 50 influenced dapivirine transport across Caco-2 cell monolayers.

The bidirectional transport of darunavir in the presence of PEG 200, HPMC 50, PEG 1000 and Poloxamer 407 did not influence the absorptive or secretory permeability across Caco-2 cell monolayers. The influence of PEG 1000 concorded with that of Collnot and colleagues who showed that PEG 1000 does not influence P-gp activity as a rhodamine transport across Caco-2 cells was unaffected [232]. Similar findings were obtained in our study, demonstrating that darunavir (P-gp substrate) transport across Caco-2 cell monolayers was unaffected by PEG 1000. In contrast, incubation with PEG 400 inhibited significantly P-gp-mediated transport across Caco-2 cell monolayers, by increasing significantly the absorptive transport and decreasing significantly the secretory transport of darunavir. A similar but more moderate effect was found for darunavir transport in the presence of Polysorbate 80 with significantly increased absorptive transport and moderately decreased secretory transport across Caco-2 cells. Both observations concord with reports by Ashiru-Oredope and Rege demonstrating that PEG 400 1% (v/v) and Polysorbate 80 are inhibiting P-gp mediated transport [196], [227].

Screening the impact of co-formulations on ARV drug absorption across Caco-2 cell monolayers

Development of efficient, safe and active microbicide formulations should not only focus on inhibitory activity against HIV-1 virus infection, but also require a suitable pharmaceutical preparation that provides acceptable bioavailability and safety of microbicide containing antiretroviral drugs. Microbicide formulations developed so far include reservoir ring, aqueous gel, tablets and applied locally solid films, however most of these formulations were designed and tested for vaginal application. Different dosage forms should be developed to allow women/ men to

choose their preferred form of delivery [13]. Development of film formulations are especially recommended for compounds that are unstable in aqueous solution. Another advantages of using film formulations is that thin films are soluble in aqueous solution, do not leak, are discrete and have low-side effect potential. However, the only concern with this dosage form is the limitation that the absorption of drug from the film is dependent upon local hydration (vaginal/ rectal fluid) that can result in non-uniform the drug distribution in the targeted tissue. Further, it can lead to local irritation caused by mucosal contact with the solid film formulation, increasing the risk of viral entry. To date, film formulations have been developed for products containing several microbicides including dapivirine, IQP-0528 and co-formulation of dapivirine – tenofovir for vaginal applications [146], [233], [234], [235].

In this study we assessed a prototype darunavir film formulation as a rectal delivery system. To optimize the dissolution process and bioavailability of drug from a darunavir film formulation, we tested it across Caco-2 cell monolayers with drug concentrations analysed by LC-MS/MS. The film formulation was also evaluated for its compatibility when different volumes of the solution were present in the donor chamber to mimic the variation in local tissue hydration. Biocompatibility was assessed by measuring cell viability and monolayer integrity by TER readings.

A selective and high-throughput liquid chromatography – mass spectrometry assay was required for quantitative determination of low darunavir concentrations in this study. The LC-MS/MS technique used in this study was suitable for nano and micro-gram quantitation. The method was verified to be fit for the purpose of this study by validating the assay over the range of concentrations 0.01 – 10 µg/ml by evaluating linearity, accuracy, precision intra and inter-day variations and robustness [236]. Calibration curves exhibited excellent linearity and tested samples were within the limits of detection. The intra-day validation data showed instrument precision and good repeatability, accuracy data were within the accepted range of 85 - 115% and precision data were <20% CV at all concentration levels. Greater variation was observed at the lowest concentrations (0.01 and 0.05 µg/ml), however they were still in the range of acceptance criteria.

To measure compatibility of the film formulation with Caco-2 cells, darunavir film and placebo film were slowly immersed in different volumes of HBSS solution. With respect to previously reported thickness of mucus layer ([237], [238], [239]) and the presence of other fluids in colorectum [240], it was assumed that varying the volume between 0 - 500 µl of HBSS was suitable to test compatibility and dissolution profile of darunavir from film formulation. To ensure that topical formulations were safe, Caco-2 cell monolayers were exposed to the darunavir and placebo film formulations which were immersed in 0, 28, 100 and 500 µL at the apical side of the membrane for 180 min. During this time TER readings were taken to validate monolayer integrity. As mentioned before, one of the disadvantages of this dosage form was limitations imposed by poor local hydration (not enough fluid) that can lead to irritation (toxic effect) of the epithelium or can limit absorption of the drug. This concern was substantiated as application of the film directly into the cell monolayer and on the top of 28 µL HBSS at apical side of the monolayer led to collapse in TER (by 100% from the initial value), suggesting complete disruption of the monolayer. This finding was supported by results from the MTT assay, which revealed that for the both conditions cell viability reduced by 50% compared to the untreated control. Equivalent effects was obtained for darunavir film and placebo film suggesting that the dosage form induced the adverse effects when the film was applied directly to cell monolayer. In contrast, when darunavir and placebo films were immersed in 100 and 500 µL of HBSS at the apical side of the Caco-2 cell monolayers, the cell viability was reduced marginally, but non significantly compared to untreated cells. However, the TER of the cell monolayer was significantly reduced when darunavir film formulation was immersed in 100 µL of HBSS, whereas no effect on TER was observed when the placebo film was tested. These results suggest that darunavir concentration released from the film contributed to the disruption of the cell monolayer. When darunavir film and placebo films were immersed in 500 µL of HBSS no adverse effects on cell monolayers were detected. Additionally, in agreement with Garg and colleagues, the film formulation dispersed quite quickly during the first 10 min in 500 µL of HBSS solution [240].

The dissolution profile and transfer of darunavir across the cell monolayer were therefore measured under conditions where film is immersed in 500 µL of HBSS. Interestingly, the dissolution profile and transfer of darunavir from film formulation across Caco-2 cell monolayers was comparable with the transport of darunavir applied in solution (0.1 – 100 µM). More precisely, the % of appeared darunavir in the receiver compartment was concentration dependent in absorptive direction, reaching around 12% at the highest tested concertation (100 µM). The same trend was observed for film formulations, where the proportion of darunavir transferred across Caco-2 cell monolayers depends on the concentration of drug present in the film.

Another interesting correlation with transport of darunavir across cell monolayers after application in solution that the proportion of darunavir transferred from film formulation was sensitive to P-gp and MRP-2 inhibition, leading to 2-fold increase in absorptive transport. This dependency of darunavir transport on P-gp and MRP-2 transporters provides an opportunity to significantly increase darunavir absorption and improve darunavir efficacy.

4.4. Tissue permeability and drug-drug interactions of tenofovir and darunavir in intact *ex-vivo* colorectal tissue

The Ussing chamber is an *ex-vivo* technique for determining the apparent permeability in absorptive and secretory directions of compounds over tissue segments. Tissue may be obtained from rat, rabbit, dog, monkey and also recently humans. The method belongs to group of drug absorption-indicating techniques and permits well-defined transport and permeability measurements in a system that provides a more complex cellular heterogeneity and morphology that represents the mammalian intestine *in vivo* more closely than cell cultures.

The Ussing chamber technique provides good correlations with *in vivo* drug absorption in humans. Lennernäs has shown good correlation with the apparent permeability of human jejunum *in vivo* for passively transported compounds with low and high permeability with a particular high degree of accuracy [241]. Additionally, the method can be used to evaluate differences between regional absorption properties [242].

To reflect the heterogenous cellular coexistence typical of colorectal tissue and to confirm our *in-vitro* findings using an *ex-vivo* systems, tenofovir and darunavir permeability was measured in guinea-pig, rat and rabbit colorectal mucosal segments using the dual chamber Ussing system. The viability and integrity of the tissue are important factors were verified concomitantly alongside drug transport when using the Ussing chamber method, as this is critical for data reliability [243], [244]. Potential difference and resistance measured during the experiment provided values in agreement with those previously reported [244], [245], [246], [247], [248], [249], [250].

Mannitol was used as a paracellular marker in all experiments that used colorectal tissue segments. Mannitol permeability across rat colorectal mucosal segments was similar to that reported by Nejdfords and colleagues, but slightly higher than the absorptive permeability reported by Ungell and colleagues [245], [244]. The variation between the values might be caused by differences in the tissue segments and variability associated with the method.

Selected concentrations of tenofovir (100 µM) and darunavir (10 µM) were used to measure permeability in tissue segments. Tenofovir was transported by passive diffusion, with similar flux to the paracellular marker mannitol. Additionally, in accordance with *in-vitro* findings, bidirectional transport of tenofovir was unaffected by P-gp inhibition or co-administration with darunavir. In contrast, P-gp played an important role in transporting darunavir across the colorectal tissue segments. The absorptive and secretory permeability of darunavir were significantly inhibited by GF120918. Findings from these studies concorded with those found in the *in-vitro* system.

Despite some limitations (viability of the tissue, native or stripped tissue, differences between species, lack of vascular supply, etc.), *ex-vivo* models offer many advantages over *in-vitro* methods, including a preserved microenvironment at the mucosal membrane, regional differences in the expression of drug transporters and can be used as a secondary screening tool as more comparable to *in vivo* situation than other biological techniques [247], [251], [252].

The *in vitro* - *in vivo* correlation found in these studies, demonstrate the ability of cell-based and tissue-based models to predict the mechanism of transport across colo-rectal tissue. These drug absorptions models are capable of distinguishing absorption via passive transcellular absorption or active transport mediated by efflux transporters. Furthermore, these models are able to distinguish compounds based on their physicochemical characteristics such as the low absorption of hydrophilic compounds like tenofovir and mannitol and higher flux of hydrophobic compounds like darunavir.

4.5. Molecular docking of ligands with P-glycoprotein

The importance of ABC transporters in bioavailability and toxicity of drugs is well known and advanced methods are necessary to evaluated it in the early phases of the drug discovery process. Thus, *in silico* modelling is becoming important for the prediction of drug interaction with transporters at an early stage. A wide range of different computational techniques had been applied for this purpose ([253], [254]), however in this study structure-based modelling of drug-transporter interactions was used [255], [256], [257], [258]. Structure-based modelling provides information about ligand interactions with the protein structure of the transporter, commonly obtained by using X-ray crystallography. In the absence of crystal structure of human P-gp transporter, the structure of the mouse Mdr1/ P-gp ortholog has been used. The homology between mouse and human transporter is 87.3% which is high enough to expect the structure and affinities to be the same [90], [259].

Ligand-transporter interactions are characterised by computational docking experiments where interactions are scored. Scoring functions are physics-based molecular mechanics force fields that estimate the energy of the pose within the binding site. The various components involved in contributions to binding include solvent effects, conformational changes in the protein and ligand, free energy due to protein-ligand interactions, internal rotations, association energy of ligand and receptor to form a single complex and free energy due to changes in vibrational modes [260]. A negative energy indicates a more stable system and thus more likely binding interactions. Potential energy calculations (kcal/mol) for each ligand were taken to establish the preferred binding sites. Molecular dynamics simulations were carried out to predict the most preferred and stable interacting binding site after 50 ns of simulation.

Experimentally, tenofovir expressed low permeability across Caco-2 cell monolayers and did not exhibit any interactions with P-gp transporters in both cell-based and tissue-based models. These observations were supported by the results of the computational study using blind molecular docking and GOLD molecular docking which showed very weak binding affinity (-2.5 up to -5.4

kcal/mol) towards the P-gp efflux pump transporter. Mannitol was used as a non-substrate control, and similarly to tenofovir showed very weak binding affinity (-3.1 up to -5.6 kcal/mol) towards the transporter, whereas digoxin expressed strong binding affinity (-9.5 to -12.5 kcal/mol).

The blind molecular docking study showed a strong binding affinity for dapivirine to the P-gp transporter (-5.1 up to -8.1 kcal/mol), comparable to darunavir (-6.8 up to -9.8) which was a P-gp substrate in Caco-2 cell monolayers and colorectal tissue segments. It was confirmed by the GOLD molecular docking which showed that dapivirine has the highest binding affinity (-8.1 kcal/mol) towards the hydrophobic transmembrane domain. Interestingly, however, dapivirine transport or cell uptake when measured experimentally was passive and not modulated by any transport inhibitors or other transporter substrate. The stability of binding and relative binding free energy were investigated through 50 ns MD stimulation and the results confirmed the findings of the molecular docking study. Both dapivirine and darunavir exhibited good stability in the complex with P-gp transporter. The free energy of binding was found to be higher for dapivirine (ΔG_{PB}=-38.24 ± 3.20) than for darunavir (ΔG_{PB}=-36.84 ± 2.31), suggesting stronger interactions between dapivirine and the P-gp transporter. A possible explanation for the absence of active transport of dapivirine in Caco-2 cell monolayers is that fast passive diffusion and escape to the cytosol provides high accumulation of the drug inside the cell bypassing binding to P-gp within the cell plasma membrane [261] [262]. It has been reported by Al-Jayyoussi G. et al. [263] and Varma MV. et al. [264] that functional implication of the P-gp efflux transporter in biological barriers depends not only by compound binding affinity (e.g. hydrogen bonding potential, polar surface area, rotatable bond count) towards the transporter structure but also by interplay between the drug's transmembrane passive transport rate and compound's trans-barrier movement via paracellular absorption. Another possible explanation might be that dapivirine exhibited a false positive prediction in this model as it has more complex chemical structure compare to mannitol and digoxin used as a controls. Further investigation is necessary to determine the role of the P-gp transporter in dapivirine absorption using clinical evaluation, experimental systems and computational modelling.

The limitations of this study might be the resolution of the P-gp crystal structure (4.35 Å) used for computational modelling. High resolution of X-ray structure needs to be lower or equal to 1.50 Å and is likely to produce more accurate docking results. Whereas low resolution with values greater than 2.5 Å and might lead to errors in docking and simulations [265]. Models with higher resolution are developed using more experimental results, whereas models with lower resolution are more likely to be subjective and include a greater number of variation [266]. In our study *in silico* modelling wad used as an adjunct to the experimental results and gave an insight of the results on the atomic level. The crystal structure of protein was optimized at the beginning of the work using AMBER 12.0 package program to provide sufficient accuracy.

Chapter Five
Conclusion & Future Work

5.1. Conclusion

The implications of co-administering the antiretroviral drugs must be evaluated in order to determine any possible drug-drug interactions of biopharmaceutical relevance. At the start of this study a cell-based model was established for screening drug transport -modifying effects of microbicide formulation. It was important to characterise the cell-based model to be able to generate and interpret results correctly.

Using experimental models, selected specific inhibitors and substrates of efflux transporters were tested to understand the mechanism of tenofovir, dapivirine and darunavir transport. It was demonstrated that tenofovir and dapivirine did not interact with P-gp, MRP2 or BCRP transporters, whereas darunavir was shown to be a substrate of P-gp and MRP2. Experiments on rat, rabbit and guinea-pig colorectal tissue segments confirmed that tenofovir was passively transported, being concentration independent and unaffected by transporter inhibitors. Darunavir transport was strongly affected by the P-gp transporter and demonstrated high sensitivity to inhibition in the colorectal mucosa in the presence of inhibitors. The permeability of the compounds across cell-based models ranked in accordance with their lipophilicity; the most hydrophilic tenofovir (low permeability), darunavir (medium permeability) and the most hydrophobic dapivirine (high permeability). The mechanism of transport and interactions with ABC- efflux pump transporters concorded across *in-vitro*, *ex-vivo* and *in-silico* models for tenofovir and darunavir. Interestingly, no transporter effects were observed for dapivirine despite *in-silico* results indicating P-gp binding potential. This is an aspect that warrants further investigation. Hydrophilic compounds can be easily tested without any modifications across different models, whereas more hydrophobic compounds need modifications to experimental systems to obtain reliable data.

Furthermore, when the compounds were co-administrated and tested for any interactions, and it appeared that co-administration of tenofovir, dapivirine and darunavir in double and triple combinations did not lead to drug-drug interactions on trans-epithelial transport across Caco-2 cell monolayers. Double combination of

tenofovir and darunavir were co-administrated across colorectal tissue segments and similarly to cell-based model did not affect the transport of each other.

In summary, this thesis provides an understanding of underlying mechanism of tenofovir, dapivirine and darunavir transport across colorectal cell-based and tissue-based models, the role of efflux transporters, and insight into molecular interactions between compounds and P-gp transporter.

This increased understanding enables rational design of efficient and safe co-formulations of these antiretroviral drugs. Combination products that contain drugs affecting different stages in the viral replication cycle would be advantageous in developing efficient topical microbicide for colorectal use. Additionally the use of excipients could be employed to modulate the transporters function, drug absorption, solubility of drugs to modify drug concentration at the targeted tissue.

5.2. Future work

Future work to optimise combinatorial microbicide delivery for prevention of colorectal HIV infection would involve:

Further characterisation of molecular modelling

Dapivirine have shown contrary data between *in-vitro* and *in-silico* results and further understanding of these interactions is necessary. The controls that have been used in computational modelling (mannitol and digoxin) were too different in structures to act as a non-binding (mannitol – negative control) and binding (digoxin - positive control) ligands to P-gp transporter. Additional controls are needed that are more similar and relevant structurally to tested agents to confirm our findings and experimental testing might be needed. Additionally, the X-ray structure with higher resolution could be used for verifying obtained results.

Configuration of more complex cell culture models

More biorelevant cell models are requires to provide a more accurate representation of the biological barrier *in vivo*. Adding a mucus layer on the top of the cells and at basolateral chamber primary macrophages and dendritic cells would provide with more complex and relevant barrier to mimic colorectal environment. The transport of antiretroviral drugs could be investigated across co-culture model to bring new aspects into consideration.

Role of SLC transporters in tenofovir, dapivirine and darunavir transport across colorectal tissue models

Antiretroviral drugs are well known to interact with SLC transporters. The role of SLC transporters present in colorectal tissue would be investigated on the transport of tenofovir, darunavir and dapivirine.

Role of enzymes in metabolism of antiretroviral drugs and characterisation of any potential drug-drug interactions

Enzymes play an important role in disposition of antiretroviral drugs leading often to drug-drug interactions. The objective of this study would be to investigate metabolic degradation/ interactions of tenofovir, dapivirine and darunavir in mucosal homogenates of the colorectal tissue of rat, rabbit and human and across the individual sections of large intestine in order to assess its potential site-dependence. Furthermore, compounds would be incubated in the presence or absence of specific CYPs inhibitors to establish the role of CYPs in their metabolism.

Bibliography

[1] J. A. Turpin, "Topical microbicides to prevent the transmission of HIV: formulation gaps and challenges.," *Drug Deliv. Transl. Res.*, vol. 1, no. 3, pp. 194–200, Jun. 2011.

[2] UNAIDS, "Fact sheet 2016 | UNAIDS Report on the global AIDS epidemic 2016." [Online]. Available: http://www.unaids.org/en/resources/fact-sheet. [Accessed: 16-Aug-2016].

[3] A. E. Grulich and I. Zablotska, "Commentary: probability of HIV transmission through anal intercourse.," *Int. J. Epidemiol.*, vol. 39, no. 4, pp. 1064–5, Aug. 2010.

[4] R. F. Baggaley, R. G. White, and M.-C. Boily, "HIV transmission risk through anal intercourse: systematic review, meta-analysis and implications for HIV prevention.," *Int. J. Epidemiol.*, vol. 39, no. 4, pp. 1048–63, Aug. 2010.

[5] D. D. Richman, D. M. Margolis, M. Delaney, W. C. Greene, D. Hazuda, and R. J. Pomerantz, "The challenge of finding a cure for HIV infection.," *Science*, vol. 323, no. 5919, pp. 1304–7, Mar. 2009.

[6] J. Hu, M. B. Gardner, and C. J. Miller, "Simian immunodeficiency virus rapidly penetrates the cervicovaginal mucosa after intravaginal inoculation and infects intraepithelial dendritic cells.," *J. Virol.*, vol. 74, no. 13, pp. 6087–95, Jul. 2000.

[7] L. Wang, R. L. Schnaare, C. Dezzutti, P. A. Anton, and L. C. Rohan, "Rectal microbicides: clinically relevant approach to the design of rectal specific placebo formulations.," *AIDS Res. Ther.*, vol. 8, p. 12, Jan. 2011.

[8] J. L. Adams and A. D. M. Kashuba, "Formulation, pharmacokinetics and pharmacodynamics of topical microbicides.," *Best Pract. Res. Clin. Obstet. Gynaecol.*, vol. 26, no. 4, pp. 451–62, Aug. 2012.

[9] P. M. Gorbach, R. E. Weiss, E. Fuchs, R. A. Jeffries, M. Hezerah, S. Brown, A. Voskanian, E. Robbie, P. Anton, and R. D. Cranston, "The slippery slope: lubricant use and rectal sexually transmitted infections: a newly identified risk.," *Sex. Transm. Dis.*, vol. 39, no. 1, pp. 59–64, Jan. 2012.

[10] O. J. D'Cruz and F. M. Uckun, "Dawn of non-nucleoside inhibitor-based anti-HIV microbicides.," *J. Antimicrob. Chemother.*, vol. 57, no. 3, pp. 411–23, Mar. 2006.

[11] S. R. Tabet, C. Surawicz, S. Horton, M. Paradise, A. S. Coletti, M. Gross, T. R. Fleming, S. Buchbinder, R. C. Haggitt, H. Levine, C. W. Kelly, and C. L. Celum, "Safety and toxicity of nonoxynol-9 gel as a rectal microbicide.," *Sex. Transm. Dis.*, vol. 26, no. 10, pp. 564–71, Nov. 1999.

[12] D. M. Phillips, K. M. Sudol, C. L. Taylor, L. Guichard, R. Elsen, and R. A. Maguire, "Lubricants containing N-9 may enhance rectal transmission of HIV and other STIs.," *Contraception*, vol. 70, no. 2, pp. 107–10, Aug. 2004.

[13] R. J. Shattock and Z. Rosenberg, "Microbicides: topical prevention against HIV.," *Cold Spring Harb. Perspect. Med.*, vol. 2, no. 2, p. a007385, Feb. 2012.

[14] L. C. Rohan, B. J. Moncla, R. P. Kunjara Na Ayudhya, M. Cost, Y. Huang, F. Gai, N. Billitto, J. D. Lynam, K. Pryke, P. Graebing, N. Hopkins, J. F. Rooney, D. Friend, and C. S. Dezzutti, "In vitro and ex vivo testing of tenofovir shows it is effective as an HIV-1 microbicide.," *PLoS One*, vol. 5, no. 2, p. e9310, Jan. 2010.

[15] C. Grammen, P. Augustijns, and J. Brouwers, "In vitro profiling of the vaginal permeation potential of anti-HIV microbicides and the influence of formulation excipients.," *Antiviral Res.*, vol. 96, no. 2, pp. 226–33, Nov. 2012.

[16] H. Agashe, M. Hu, and L. Rohan, "Formulation and delivery of microbicides.," *Curr. HIV Res.*, vol. 10, no. 1, pp. 88–96, Jan. 2012.

[17] I. McGowan, "Rectal microbicide development.," *Curr. Opin. HIV AIDS*, vol. 7, no. 6, pp. 526–33, Nov. 2012.

[18] P. A. Anton, T. Saunders, J. Elliott, E. Khanukhova, R. Dennis, A. Adler, G. Cortina, K. Tanner, J. Boscardin, W. G. Cumberland, Y. Zhou, A. Ventuneac, A. Carballo-Diéguez, L. Rabe, T. McCormick, H. Gabelnick, C. Mauck, and I. McGowan, "First phase 1 double-blind, placebo-controlled, randomized rectal microbicide trial using UC781 gel with a novel index of ex vivo efficacy.," *PLoS One*, vol. 6, no. 9, p. e23243, Jan. 2011.

[19] C. S. Dezzutti, L. C. Rohan, L. Wang, K. Uranker, C. Shetler, M. Cost, J. D. Lynam, and D. Friend, "Reformulated tenofovir gel for use as a dual compartment microbicide.," *J. Antimicrob. Chemother.*, vol. 67, no. 9, pp. 2139–42, Sep. 2012.

[20] C. Herrera and R. J. Shattock, "Potential use of protease inhibitors as vaginal and colorectal microbicides.," *Curr. HIV Res.*, vol. 10, no. 1, pp. 42–52, Jan. 2012.

[21] P. J. Klasse, R. Shattock, and J. P. Moore, "Antiretroviral drug-based microbicides to prevent HIV-1 sexual transmission.," *Annu. Rev. Med.*, vol. 59, pp. 455–71, Jan. 2008.

[22] C. Herrera, M. Cranage, I. McGowan, P. Anton, and R. J. Shattock, "Reverse transcriptase inhibitors as potential colorectal microbicides.," *Antimicrob. Agents Chemother.*, vol. 53, no. 5, pp. 1797–807, May 2009.

[23] E. Bergogne-Berezin, "The suppository form of antibiotic administration: pharmacokinetics and clinical application," *J. Antimicrob. Chemother.*, vol. 43, no. 2, pp. 177–185, Feb. 1999.

[24] P. S. Fletcher, J. Elliott, J.-C. Grivel, L. Margolis, P. Anton, I. McGowan, and R. J. Shattock, "Ex vivo culture of human colorectal tissue for the evaluation of candidate microbicides.," *AIDS*, vol. 20, no. 9, pp. 1237–45, Jun. 2006.

[25] R. J. Shattock and J. P. Moore, "Inhibiting sexual transmission of HIV-1 infection.," *Nat. Rev. Microbiol.*, vol. 1, no. 1, pp. 25–34, Oct. 2003.

[26] J. R. Turner, "Intestinal mucosal barrier function in health and disease.," *Nat. Rev. Immunol.*, vol. 9, no. 11, pp. 799–809, Nov. 2009.

[27] J. M. Anderson, "Molecular Structure of Tight Junctions and Their Role in Epithelial Transport," *News Physiol Sci*, vol. 16, no. 3, pp. 126–130, Jun. 2001.

[28] A. L. Daugherty and R. J. Mrsny, "Transcellular uptake mechanisms of the intestinal epithelial barrier Part one," *Pharm. Sci. Technolo. Today*, vol. 2, no. 4, pp. 144–151, Apr. 1999.

[29] B. Deplancke and H. R. Gaskins, "Microbial modulation of innate defense: goblet cells and the intestinal mucus layer," *Am J Clin Nutr*, vol. 73, no. 6, p. 1131S–1141, Jun. 2001.

[30] K. Khanvilkar, M. D. Donovan, and D. R. Flanagan, "Drug transfer through mucus," *Adv. Drug Deliv. Rev.*, vol. 48, no. 2, pp. 173–193, 2001.

[31] M. E. V Johansson, J. M. H. Larsson, and G. C. Hansson, "The two mucus layers of colon are organized by the MUC2 mucin, whereas the outer layer is a legislator of host-microbial interactions.," *Proc. Natl. Acad. Sci. U. S. A.*, vol. 108 Suppl , no. Supplement_1, pp. 4659–65, Mar. 2011.

[32] C. Atuma, V. Strugala, A. Allen, and L. Holm, "The adherent gastrointestinal mucus gel layer: thickness and physical state in vivo," *Am J Physiol Gastrointest Liver Physiol*, vol. 280, no. 5, pp. G922–929, May 2001.

[33] K. Matsuo, H. Ota, T. Akamatsu, A. Sugiyama, and T. Katsuyama, "Histochemistry of the surface mucous gel layer of the human colon.," *Gut*, vol. 40, no. 6, pp. 782–9, Jun. 1997.

[34] M. J. Rathbone and J. Hadgraft, "Absorption of drugs from the human oral cavity," *Int. J. Pharm.*, vol. 74, no. 1, pp. 9–24, Aug. 1991.

[35] T. Pelaseyed, J. H. Bergström, J. K. Gustafsson, A. Ermund, G. M. H. Birchenough, A. Schütte, S. van der Post, F. Svensson, A. M. Rodríguez-Piñeiro, E. E. L. Nyström, C. Wising, M. E. V Johansson, and G. C. Hansson, "The mucus and mucins of the goblet cells and enterocytes provide the first defense line of the gastrointestinal tract and interact with the immune system.," *Immunol. Rev.*, vol. 260, no. 1, pp. 8–20, Jul. 2014.

[36] A. Wikman, J. Karlsson, I. Carlstedt, and P. Artursson, "A drug absorption model based on the mucus layer producing human intestinal goblet cell line HT29-H.," *Pharm. Res.*, vol. 10, no. 6, pp. 843–52, Jun. 1993.

[37] W. Rubas, M. E. Cromwell, Z. Shahrokh, J. Villagran, T. N. Nguyen, M. Wellton, T. H. Nguyen, and R. J. Mrsny, "Flux measurements across Caco-2 monolayers may predict transport in human large intestinal tissue.," *J. Pharm. Sci.*, vol. 85, no. 2, pp. 165–9, Feb. 1996.

[38] S. Tsukita, M. Furuse, and M. Itoh, "Multifunctional strands in tight junctions," *Nat. Rev. Mol. Cell Biol.*, vol. 2, no. 4, pp. 285–293, Apr. 2001.

[39] B. R. Stevenson and B. H. Keon, "The tight junction: morphology to molecules.," *Annu. Rev. Cell Dev. Biol.*, vol. 14, pp. 89–109, 1998.

[40] L. L. Mitic and J. M. Anderson, "Molecular architecture of tight junctions.," *Annu. Rev. Physiol.*, vol. 60, pp. 121–42, 1998.

[41] J. M. Brandner, "Tight junctions and tight junction proteins in mammalian epidermis," *Eur. J. Pharm. Biopharm.*, vol. 72, no. 2, pp. 289–294, 2009.

[42] E. FRÖMTER and J. DIAMOND, "Route of Passive Ion Permeation in Epithelia," *Nature*, vol. 235, no. 53, p. 9.

[43] O. Lacombe, J. Woodley, C. Solleux, J.-M. Delbos, C. Boursier-Neyret, and G. Houin, "Localisation of drug permeability along the rat small intestine, using markers of the paracellular, transcellular and some transporter routes," *Eur. J. Pharm. Sci.*, vol. 23, no. 4, pp. 385–391, 2004.

[44] D. W. Powell, "Barrier function of epithelia.," *Am. J. Physiol.*, vol. 241, no. 4, pp. G275–88, Oct. 1981.

[45] C. M. Van Itallie and J. M. Anderson, "Claudins and epithelial paracellular transport.," *Annu. Rev. Physiol.*, vol. 68, pp. 403–29, 2006.

[46] M. Kondoh, T. Yoshida, H. Kakutani, and K. Yagi, "Targeting tight junction proteins-significance for drug development," *Drug Discov. Today*, vol. 13, no. 3, pp. 180–186, 2008.

[47] P. Artursson and C. Magnusson, "Epithelial Transport of Drugs in Cell Culture. II: Effect of Extracellular Calcium Concentration on the Paracellular Transport of Drugs of Different Lipophilicities across Monolayers of Intestinal Epithelial (Caco-2) Cells," *J. Pharm. Sci.*, vol. 79, no. 7, pp. 595–600, Jul. 1990.

[48] M. Tomita, M. Hayashi, and S. Awazu, "Absorption-Enhancing Mechanism of EDTA, Caprate, and Decanoylcarnitine in Caco-2 Cells," *J. Pharm. Sci.*, vol. 85, no. 6, pp. 608–611, Jun. 1996.

[49] S. Citi, "Protein kinase inhibitors prevent junction dissociation induced by low extracellular calcium in MDCK epithelial cells," *J. Cell Biol.*, vol. 117, no. 1, pp. 169–178, Apr. 1992.

[50] J. M. Anderson and C. M. Van Itallie, "Physiology and Function of the Tight Junction."

[51] J. L. Gookin, J. A. Galanko, A. T. Blikslager, and R. A. Argenzio, "PG-mediated closure of paracellular pathway and not restitution is the primary determinant of barrier recovery in acutely injured porcine ileum," *Am. J. Physiol. - Gastrointest. Liver Physiol.*, vol. 285, no. 5, 2003.

[52] J. Linnankoski, J. Mäkelä, J. Palmgren, T. Mauriala, C. Vedin, A. Ungell, L. Lazorova, P. Artursson, A. Urtti, and M. Yliperttula, "Paracellular Porosity and Pore Size of the Human Intestinal Epithelium in Tissue and Cell Culture Models," *J. Pharm. Sci.*, vol. 99, no. 4, pp. 2166–2175, Apr. 2010.

[53] W. Rubas, M. E. Cromwell, Z. Shahrokh, J. Villagran, T. N. Nguyen, M. Wellton, T. H. Nguyen, and R. J. Mrsny, "Flux measurements across Caco-2 monolayers may predict transport in human large intestinal tissue.," *J. Pharm. Sci.*, vol. 85, no. 2, pp. 165–9, Feb. 1996.

[54] D. W. Powell, "Barrier function of epithelia," *Am J Physiol Gastrointest Liver Physiol*, vol. 241, no. 4, pp. G275–288, Oct. 1981.

[55] C. Hilgendorf, H. Spahn-Langguth, C. G. Regårdh, E. Lipka, G. L. Amidon, and P. Langguth, "Caco-2 versus Caco-2/HT29-MTX Co-cultured Cell Lines: Permeabilities Via Diffusion, Inside- and Outside-Directed Carrier-Mediated Transport," *J. Pharm. Sci.*, vol. 89, no. 1, pp. 63–75, 2000.

[56] M. J. Briske-Anderson, J. W. Finley, and S. M. Newman, "The Influence of Culture Time and Passage Number on the Morphological and Physiological Development of Caco-2 Cells," *Exp. Biol. Med.*, vol. 214, no. 3, pp. 248–257, Mar. 1997.

[57] I. Behrens, P. Stenberg, P. Artursson, and T. Kissel, "Transport of lipophilic drug molecules in a new mucus-secreting cell culture model based on HT29-MTX cells.," *Pharm. Res.*, vol. 18, no. 8, pp. 1138–45, Aug. 2001.

[58] J. D. Irvine, L. Takahashi, K. Lockhart, J. Cheong, J. W. Tolan, H. E. Selick, and J. R. Grove, "MDCK (Madin-Darby Canine Kidney) Cells: A Tool for Membrane Permeability Screening," *J. Pharm. Sci.*, vol. 88, no. 1, pp. 28–33, Jan. 1999.

[59] M. J. Cho, D. P. Thompson, C. T. Cramer, T. J. Vidmar, and J. F. Scieszka, "The Madin Darby canine kidney (MDCK) epithelial cell monolayer as a model cellular transport barrier.," *Pharm. Res.*, vol. 6, no. 1, pp. 71–7, Jan. 1989.

[60] E. Duizer, A. H. Penninks, W. H. Stenhuis, and J. P. Groten, "Comparison of permeability characteristics of the human colonic Caco-2 and rat small intestinal IEC-18 cell lines," *J. Control. Release*, vol. 49, no. 1, pp. 39–49, 1997.

[61] A. Steensma, H. P. J. . Noteborn, and H. A. Kuiper, "Comparison of Caco-2, IEC-18 and HCEC cell lines as a model for intestinal absorption of genistein, daidzein and their glycosides," *Environ. Toxicol. Pharmacol.*, vol. 16, no. 3, pp. 131–139, 2004.

[62] R. H. Turner, C. S. Mehta, and L. Z. Benet, "Apparent Directional Permeability Coefficients for Drug Ions: In Vitro Intestinal Perfusion Studies," *J. Pharm. Sci.*, vol. 59, no. 5, pp. 590–595, May 1970.

[63] P. S. Burton, R. A. Conradi, N. F. Ho, A. R. Hilgers, and R. T. Borchardt, "How structural features influence the biomembrane permeability of peptides.," *J. Pharm. Sci.*, vol. 85, no. 12, pp. 1336–40, Dec. 1996.

[64] A. Pagliara, M. Reist, S. Geinoz, P.-A. Carrupt, and B. Testa, "Evaluation and Prediction of Drug Permeation," *J. Pharm. Pharmacol.*, vol. 51, no. 12, pp. 1339–1357, Dec. 1999.

[65] C. A. Lipinski, F. Lombardo, B. W. Dominy, and P. J. Feeney, "Experimental and computational approaches to estimate solubility and permeability in drug discovery and development settings," *Adv. Drug Deliv. Rev.*, vol. 23, no. 1–3, pp. 3–25, Jan. 1997.

[66] G. M. Cooper, "Transport of Small Molecules." Sinauer Associates, 2000.

[67] P. Artursson, K. Palm, and K. Luthman, "Caco-2 monolayers in experimental and theoretical predictions of drug transport1PII of original article: S0169-409X(96)00415-2. The article was originally published in Advanced Drug Delivery Reviews 22 (1996) 67–84.1," *Adv. Drug Deliv. Rev.*, vol. 46, no. 1–3, pp. 27–43, Mar. 2001.

[68] M. Heyman, A. M. Crain-Denoyelle, S. K. Nath, and J. F. Desjeux, "Quantification of protein transcytosis in the human colon carcinoma cell line CaCo-2.," *J. Cell. Physiol.*, vol. 143, no. 2, pp. 391–5, May 1990.

[69] J. P. Kraehenbuhl and M. R. Neutra, "Molecular and cellular basis of immune protection of mucosal surfaces.," *Physiol. Rev.*, vol. 72, no. 4, pp. 853–79, Oct. 1992.

[70] B. Alberts, A. Johnson, J. Lewis, M. Raff, K. Roberts, and P. Walter, "Principles of Membrane Transport." Garland Science, 2002.

[71] A. Tsuji and I. Tamai, "Carrier-Mediated Intestinal Transport of Drugs," *Pharm. Res.*, vol. 13, no. 7, pp. 963–977, 1996.

[72] R. Whittam and K. P. Wheeler, "Transport Across Cell Membranes," *Annu. Rev. Physiol.*, vol. 32, no. 1, pp. 21–60, Mar. 1970.

[73] O. Kis, K. Robillard, G. N. Y. Chan, and R. Bendayan, "The complexities of antiretroviral drug-drug interactions: role of ABC and SLC transporters.," *Trends Pharmacol. Sci.*, vol. 31, no. 1, pp. 22–35, Jan. 2010.

[74] A. S. Ray, T. Cihlar, K. L. Robinson, L. Tong, J. E. Vela, M. D. Fuller, L. M. Wieman, E. J. Eisenberg, and G. R. Rhodes, "Mechanism of active renal tubular efflux of tenofovir.," *Antimicrob. Agents Chemother.*, vol. 50, no. 10, pp. 3297–304, Oct. 2006.

[75] J. Weiss, D. Theile, N. Ketabi-Kiyanvash, H. Lindenmaier, and W. E. Haefeli, "Inhibition of MRP1/ABCC1, MRP2/ABCC2, and MRP3/ABCC3 by nucleoside, nucleotide, and non-nucleoside reverse transcriptase inhibitors.," *Drug Metab. Dispos.*, vol. 35, no. 3, pp. 340–4, Mar. 2007.

[76] H. Fujimoto, M. Higuchi, H. Watanabe, Y. Koh, A. K. Ghosh, H. Mitsuya, N. Tanoue, A. Hamada, and H. Saito, "P-glycoprotein mediates efflux transport of darunavir in human intestinal Caco-2 and ABCB1 gene-transfected renal LLC-PK1 cell lines.," *Biol. Pharm. Bull.*, vol. 32, no. 9, pp. 1588–93, Sep. 2009.

[77] O. Kis, J. A. Zastre, M. T. Hoque, S. L. Walmsley, and R. Bendayan, "Role of drug efflux and uptake transporters in atazanavir intestinal permeability and drug-drug interactions.," *Pharm. Res.*, vol. 30, no. 4, pp. 1050–64, Apr. 2013.

[78] K. C. Brown, S. Paul, and A. D. M. Kashuba, "Drug interactions with new and investigational antiretrovirals.," *Clin. Pharmacokinet.*, vol. 48, no. 4, pp. 211–41, Jan. 2009.

[79] M. Dean, A. Rzhetsky, and R. Allikmets, "The Human ATP-Binding Cassette (ABC) Transporter Superfamily," *Genome Res.*, vol. 11, no. 7, pp. 1156–1166, 2001.

[80] G. Szakács, J. K. Paterson, J. A. Ludwig, C. Booth-Genthe, and M. M. Gottesman, "Targeting multidrug resistance in cancer.," *Nat. Rev. Drug Discov.*, vol. 5, no. 3, pp. 219–34, Mar. 2006.

[81] F. J. Sharom, "ABC multidrug transporters: structure, function and role in chemoresistance," *Pharmacogenomics*, vol. 9, no. 1, pp. 105–127, Jan. 2008.

[82] J. E. Walker, M. Saraste, M. J. Runswick, and N. J. Gay, "Distantly related sequences in the alpha- and beta-subunits of ATP synthase, myosin, kinases and other ATP-requiring enzymes and a common nucleotide binding fold.," *EMBO J.*, vol. 1, no. 8, pp. 945–51, 1982.

[83] F. J. Sharom, R. Liu, Y. Romsicki, and P. Lu, "Insights into the structure and substrate interactions of the P-glycoprotein multidrug transporter from spectroscopic studies.," *Biochim. Biophys. Acta*, vol. 1461, no. 2, pp. 327–45, Dec. 1999.

[84] L. W. Hung, I. X. Wang, K. Nikaido, P. Q. Liu, G. F. Ames, and S. H. Kim, "Crystal structure of the ATP-binding subunit of an ABC transporter.," *Nature*, vol. 396, no. 6712, pp. 703–7, Dec. 1998.

[85] S. V Ambudkar, S. Dey, C. A. Hrycyna, M. Ramachandra, I. Pastan, and M. M. Gottesman, "Biochemical, cellular, and pharmacological aspects of the multidrug transporter.," *Annu. Rev. Pharmacol. Toxicol.*, vol. 39, pp. 361–98, 1999.

[86] L. Salphati, E. G. Plise, and G. Li, "Expression and activity of the efflux transporters ABCB1, ABCC2 and ABCG2 in the human colorectal carcinoma cell line LS513.," *Eur. J. Pharm. Sci.*, vol. 37, no. 3–4, pp. 463–8, Jun. 2009.

[87] A. H. Schinkel, J. J. Smit, O. van Tellingen, J. H. Beijnen, E. Wagenaar, L. van Deemter, C. A. Mol, M. A. van der Valk, E. C. Robanus-Maandag, and H. P. te Riele, "Disruption of the mouse mdr1a P-glycoprotein gene leads to a deficiency in the blood-brain barrier and to increased sensitivity to drugs.," *Cell*, vol. 77, no. 4, pp. 491–502, May 1994.

[88] S. V Ambudkar, C. Kimchi-Sarfaty, Z. E. Sauna, and M. M. Gottesman, "P-glycoprotein: from genomics to mechanism.," *Oncogene*, vol. 22, no. 47, pp. 7468–85, Oct. 2003.

[89] M. F. Rosenberg, R. Callaghan, R. C. Ford, and C. F. Higgins, "Structure of the multidrug resistance P-glycoprotein to 2.5 nm resolution determined by electron microscopy and image analysis.," *J. Biol. Chem.*, vol. 272, no. 16, pp. 10685–94, Apr. 1997.

[90] S. G. Aller, J. Yu, A. Ward, Y. Weng, S. Chittaboina, R. Zhuo, P. M. Harrell, Y. T. Trinh, Q. Zhang, I. L. Urbatsch, and G. Chang, "Structure of P-glycoprotein reveals a molecular basis for poly-specific drug binding.," *Science*, vol. 323, no. 5922, pp. 1718–22, Mar. 2009.

[91] A. E. Senior and S. Bhagat, "P-Glycoprotein Shows Strong Catalytic Cooperativity between the Two Nucleotide Sites †," *Biochemistry*, vol. 37, no. 3, pp. 831–836, Jan. 1998.

[92] D. A. P. Gutmann, A. Ward, I. L. Urbatsch, G. Chang, and H. W. van Veen, "Understanding polyspecificity of multidrug ABC transporters: closing in on the gaps in ABCB1.," *Trends Biochem. Sci.*, vol. 35, no. 1, pp. 36–42, Jan. 2010.

[93] P. D. W. Eckford and F. J. Sharom, "ABC efflux pump-based resistance to chemotherapy drugs.," *Chem. Rev.*, vol. 109, no. 7, pp. 2989–3011, Jul. 2009.

[94] P. D. W. Eckford and F. J. Sharom, "ABC efflux pump-based resistance to chemotherapy drugs.," *Chem. Rev.*, vol. 109, no. 7, pp. 2989–3011, Jul. 2009.

[95] Z. E. Sauna and S. V. Ambudkar, "Evidence for a requirement for ATP hydrolysis at two distinct steps during a single turnover of the catalytic cycle of human P-glycoprotein," *Proc. Natl. Acad. Sci.*, vol. 97, no. 6, pp. 2515–2520, Mar. 2000.

[96] S. P. Cole, G. Bhardwaj, J. H. Gerlach, J. E. Mackie, C. E. Grant, K. C. Almquist, A. J. Stewart, E. U. Kurz, A. M. Duncan, and R. G. Deeley, "Overexpression of a transporter gene in a multidrug-resistant human lung cancer cell line.," *Science*, vol. 258, no. 5088, pp. 1650–4, Dec. 1992.

[97] P. Borst, R. Evers, M. Kool, and J. Wijnholds, "A Family of Drug Transporters: the Multidrug Resistance-Associated Proteins," *JNCI J. Natl. Cancer Inst.*, vol. 92, no. 16, pp. 1295–1302, Aug. 2000.

[98] Bakos E, T. Hegedüs, Z. Holló, E. Welker, G. E. Tusnády, G. J. Zaman, M. J. Flens, A. Váradi, and B. Sarkadi, "Membrane topology and glycosylation of the human multidrug resistance-associated protein.," *J. Biol. Chem.*, vol. 271, no. 21, pp. 12322–6, May 1996.

[99] G. D. Kruh and M. G. Belinsky, "The MRP family of drug efflux pumps," *Oncogene*, vol. 22, no. 47, pp. 7537–7552, Oct. 2003.

[100] M. G. Belinsky, L. J. Bain, B. B. Balsara, J. R. Testa, and G. D. Kruh, "Characterization of MOAT-C and MOAT-D, new members of the MRP/cMOAT subfamily of transporter proteins.," *J. Natl. Cancer Inst.*, vol. 90, no. 22, pp. 1735–41, Nov. 1998.

[101] E. Bakos, R. Evers, G. Szakacs, G. E. Tusnady, E. Welker, K. Szabo, M. de Haas, L. van Deemter, P. Borst, A. Varadi, and B. Sarkadi, "Functional Multidrug Resistance Protein (MRP1) Lacking the N-terminal Transmembrane Domain," *J. Biol. Chem.*, vol. 273, no. 48, pp. 32167–32175, Nov. 1998.

[102] Y. Toyoda, Y. Hagiya, T. Adachi, K. Hoshijima, M. T. Kuo, and T. Ishikawa, "MRP class of human ATP binding cassette (ABC) transporters: historical background and new research directions," *Xenobiotica*, vol. 38, no. 7–8, pp. 833–862, Aug. 2008.

[103] M. M. Gottesman, T. Fojo, and S. E. Bates, "Multidrug resistance in cancer: role of ATP-dependent transporters.," *Nat. Rev. Cancer*, vol. 2, no. 1, pp. 48–58, Jan. 2002.

[104] A. D. Mottino, T. Hoffman, L. Jennes, and M. Vore, "Expression and localization of multidrug resistant protein mrp2 in rat small intestine.," *J. Pharmacol. Exp. Ther.*, vol. 293, no. 3, pp. 717–23, Jun. 2000.

[105] J. König, D. Rost, Y. Cui, and D. Keppler, "Characterization of the human multidrug resistance protein isoform MRP3 localized to the basolateral hepatocyte membrane.," *Hepatology*, vol. 29, no. 4, pp. 1156–63, Apr. 1999.

[106] L. A. Doyle, W. Yang, L. V Abruzzo, T. Krogmann, Y. Gao, A. K. Rishi, and D. D. Ross, "A multidrug resistance transporter from human MCF-7 breast cancer cells.," *Proc. Natl. Acad. Sci. U. S. A.*, vol. 95, no. 26, pp. 15665–70, Dec. 1998.

[107] Z. Ni, Z. Bikadi, M. F. Rosenberg, and Q. Mao, "Structure and function of the human breast cancer resistance protein (BCRP/ABCG2).," *Curr. Drug Metab.*, vol. 11, no. 7, pp. 603–17, Sep. 2010.

[108] L. Lin, S. W. Yee, R. B. Kim, and K. M. Giacomini, "SLC transporters as therapeutic targets: emerging opportunities," *Nat. Rev. Drug Discov.*, vol. 14, no. 8, pp. 543–560, Jun. 2015.

[109] M. A. Hediger, M. F. Romero, J.-B. Peng, A. Rolfs, H. Takanaga, and E. A. Bruford, "The ABCs of solute carriers: physiological, pathological and therapeutic implications of human membrane transport proteinsIntroduction.," *Pflügers Arch. Eur. J. Physiol.*, vol. 447, no. 5, pp. 465–8, Feb. 2004.

[110] A. Schlessinger, S. W. Yee, A. Sali, and K. M. Giacomini, "SLC Classification: An Update," *Clin. Pharmacol. Ther.*, vol. 94, no. 1, pp. 19–23, Jul. 2013.

[111] L. R. Forrest, R. Krämer, and C. Ziegler, "The structural basis of secondary active transport mechanisms," *Biochim. Biophys. Acta - Bioenerg.*, vol. 1807, no. 2, pp. 167–188, Feb. 2011.

[112] J.-M. Scherrmann, "Transporters in Absorption, Distribution, and Elimination," *Chem. Biodivers.*, vol. 6, no. 11, pp. 1933–1942, Nov. 2009.

[113] G. Englund, F. Rorsman, A. Rönnblom, U. Karlbom, L. Lazorova, J. Gråsjö, A. Kindmark, and P. Artursson, "Regional levels of drug transporters along the human intestinal tract: co-expression of ABC and SLC transporters and comparison with Caco-2 cells.," *Eur. J. Pharm. Sci.*, vol. 29, no. 3–4, pp. 269–77, Dec. 2006.

[114] Y. Meier, J. J. Eloranta, J. Darimont, M. G. Ismair, C. Hiller, M. Fried, G. A. Kullak-Ublick, and S. R. Vavricka, "Regional distribution of solute carrier mRNA expression along the human intestinal tract.," *Drug Metab. Dispos.*, vol. 35, no. 4, pp. 590–4, Apr. 2007.

[115] A.-L. Ungell, "Drug Development and Industrial Pharmacy In Vitro Absorption Studies and Their Relevance to Absorption from the GI Tract," *Drug Dev. Ind. Pharm.*, vol. 23, no. 9, pp. 879–892, 1997.

[116] R. T. Borchardt, P. L. Smith, and G. Wilson, Eds., *Models for Assessing Drug Absorption and Metabolism*, vol. 8. Boston, MA: Springer US, 1996.

[117] Y. Iwata, M. Arisawa, R. Hamada, Y. Kita, M. Y. Mizutani, N. Tomioka, A. Itai, and S. Miyamoto, "Discovery of novel aldose reductase inhibitors using a protein structure-based approach: 3D-database search followed by design and synthesis.," *J. Med. Chem.*, vol. 44, no. 11, pp. 1718–28, May 2001.

[118] Z. Hayouka, A. Levin, M. Maes, E. Hadas, D. E. Shalev, D. J. Volsky, A. Loyter, and A. Friedler, "Mechanism of action of the HIV-1 integrase inhibitory peptide LEDGF 361–370," 2010.

[119] I. McGowan, "Rectal microbicides: a new focus for HIV prevention.," *Sex. Transm. Infect.*, vol. 84, no. 6, pp. 413–7, Nov. 2008.

[120] I. Mukhopadhya, G. I. Murray, S. Berry, J. Thomson, B. Frank, G. Gwozdz, J. Ekeruche-Makinde, R. Shattock, C. Kelly, F. Iannelli, G. Pozzi, E. M. El-Omar, G. L. Hold, and K. Hijazi, "Drug transporter gene expression in human colorectal tissue and cell lines: modulation with antiretrovirals for microbicide optimization.," *J. Antimicrob. Chemother.*, vol. 71, no. 2, pp. 372–86, Feb. 2016.

[121] B. Sarmento, F. Andrade, S. B. da Silva, F. Rodrigues, J. das Neves, and D. Ferreira, "Cell-based in vitro models for predicting drug permeability.," *Expert Opin. Drug Metab. Toxicol.*, vol. 8, no. 5, pp. 607–21, May 2012.

[122] H. Sun, E. C. Chow, S. Liu, Y. Du, and K. S. Pang, "The Caco-2 cell monolayer: usefulness and limitations.," *Expert Opin. Drug Metab. Toxicol.*, vol. 4, no. 4, pp. 395–411, Apr. 2008.

[123] I. Hubatsch, E. G. E. Ragnarsson, and P. Artursson, "Determination of drug permeability and prediction of drug absorption in Caco-2 monolayers.," *Nat. Protoc.*, vol. 2, no. 9, pp. 2111–9, Jan. 2007.

[124] F. Delie and W. Rubas, "A human colonic cell line sharing similarities with enterocytes as a model to examine oral absorption: advantages and limitations of the Caco-2 model.," *Crit. Rev. Ther. Drug Carrier Syst.*, vol. 14, no. 3, pp. 221–86, 1997.

[125] A. Zweibaum, M. Laburthe, E. Grasset, and D. Louvard, "Use of Cultured Cell Lines in Studies of Intestinal Cell Differentiation and Function," in *Comprehensive Physiology*, Hoboken, NJ, USA: John Wiley & Sons, Inc., 2011.

[126] A. Wikman-Larhed and P. Artursson, "Co-cultures of human intestinal goblet (HT29-H) and absorptive (Caco-2) cells for studies of drug and peptide absorption," *Eur. J. Pharm. Sci.*, vol. 3, no. 3, pp. 171–183, 1995.

[127] R. P. Donato, A. El-Merhibi, B. Gundsambuu, K. Y. Mak, E. R. Formosa, X. Wang, C. A. Abbott, and B. C. Powell, "Studying Permeability in a Commonly Used Epithelial Cell Line: T84 Intestinal Epithelial Cells," in *Methods in molecular biology (Clifton, N.J.)*, vol. 763, 2011, pp. 115–137.

[128] I. Hubatsch, E. G. E. Ragnarsson, and P. Artursson, "Determination of drug permeability and prediction of drug absorption in Caco-2 monolayers.," *Nat. Protoc.*, vol. 2, no. 9, pp. 2111–9, Jan. 2007.

[129] R. B. van Breemen and Y. Li, "Caco-2 cell permeability assays to measure drug absorption.," *Expert Opin. Drug Metab. Toxicol.*, vol. 1, no. 2, pp. 175–85, Aug. 2005.

[130] I. J. Hidalgo and J. Li, "Carrier-mediated transport and efflux mechanisms in Caco-2 cells," *Adv. Drug Deliv. Rev.*, vol. 22, no. 1–2, pp. 53–66, Nov. 1996.

[131] H. Suzuki and Y. Sugiyama, "Role of metabolic enzymes and efflux transporters in the absorption of drugs from the small intestine," *Eur. J. Pharm. Sci.*, vol. 12, no. 1, pp. 3–12, Nov. 2000.

[132] G. Minuesa, I. Huber-Ruano, M. Pastor-Anglada, H. Koepsell, B. Clotet, and J. Martinez-Picado, "Drug uptake transporters in antiretroviral therapy.," *Pharmacol. Ther.*, vol. 132, no. 3, pp. 268–79, Dec. 2011.

[133] C. G. Lee, M. M. Gottesman, C. O. Cardarelli, M. Ramachandra, K. T. Jeang, S. V Ambudkar, I. Pastan, and S. Dey, "HIV-1 protease inhibitors are substrates for the MDR1 multidrug transporter.," *Biochemistry*, vol. 37, no. 11, pp. 3594–601, Mar. 1998.

[134] L. Tong, T. K. Phan, K. L. Robinson, D. Babusis, R. Strab, S. Bhoopathy, I. J. Hidalgo, G. R. Rhodes, and A. S. Ray, "Effects of human immunodeficiency virus protease inhibitors on the intestinal absorption of tenofovir disoproxil fumarate in vitro.," *Antimicrob. Agents Chemother.*, vol. 51, no. 10, pp. 3498–504, Oct. 2007.

[135] T. Prueksaritanont, X. Chu, C. Gibson, D. Cui, K. L. Yee, J. Ballard, T. Cabalu, and J. Hochman, "Drug-drug interaction studies: regulatory guidance and an industry perspective.," *AAPS J.*, vol. 15, no. 3, pp. 629–45, Jul. 2013.

[136] "HIV/AIDS Guidelines - adultandadolescentgl.pdf." [Online]. Available: http://aidsinfo.nih.gov/contentfiles/lvguidelines/adultandadolescentgl.pdf. [Accessed: 21-Jul-2013].

[137] D. Vishnuvardhan, L. L. Moltke, C. Richert, and D. J. Greenblatt, "Lopinavir: acute exposure inhibits P-glycoprotein; extended exposure induces P-glycoprotein.," *AIDS*, vol. 17, no. 7, pp. 1092–4, May 2003.

[138] P. A. Pham and J. E. Gallant, "Tenofovir disoproxil fumarate for the treatment of HIV infection.," *Expert Opin. Drug Metab. Toxicol.*, vol. 2, no. 3, pp. 459–69, Jun. 2006.

[139] Q. Abdool Karim, S. S. Abdool Karim, J. A. Frohlich, A. C. Grobler, C. Baxter, L. E. Mansoor, A. B. M. Kharsany, S. Sibeko, K. P. Mlisana, Z. Omar, T. N. Gengiah, S. Maarschalk, N. Arulappan, M. Mlotshwa, L. Morris, and D. Taylor, "Effectiveness and safety of tenofovir gel, an antiretroviral microbicide, for the prevention of HIV infection in women.," *Science*, vol. 329, no. 5996, pp. 1168–74, Sep. 2010.

[140] J. van Gelder, S. Deferme, L. Naesens, E. De Clercq, G. van den Mooter, R. Kinget, and P. Augustijns, "Intestinal absorption enhancement of the ester prodrug tenofovir disoproxil fumarate through modulation of the biochemical barrier by defined ester mixtures.," *Drug Metab. Dispos.*, vol. 30, no. 8, pp. 924–30, Aug. 2002.

[141] M. Foggia, S. Nappa, G. Bonadies, M. Cotugno, G. Filippo, F. Borrelli, R. Orlando, and G. Borgia, "Tenofovir Disoproxil Fumarate in the Clinical Practice: An Overview," *Antiinfect. Agents Med. Chem.*, vol. 7, no. 4, pp. 285–295, Oct. 2008.

[142] J. J. Kohler, S. H. Hosseini, E. Green, A. Abuin, T. Ludaway, R. Russ, R. Santoianni, and W. Lewis, "Tenofovir renal proximal tubular toxicity is regulated by OAT1 and MRP4 transporters.," *Lab. Invest.*, vol. 91, no. 6, pp. 852–8, Jun. 2011.

[143] K. A. Lyseng-Williamson, N. A. Reynolds, and G. L. Plosker, "Tenofovir disoproxil fumarate: a review of its use in the management of HIV infection.," *Drugs*, vol. 65, no. 3, pp. 413–32, Jan. 2005.

[144] B. Devlin, J. Nuttall, S. Wilder, C. Woodsong, and Z. Rosenberg, "Development of dapivirine vaginal ring for HIV prevention.," *Antiviral Res.*, vol. 100 Suppl, pp. S3–8, Dec. 2013.

[145] Z. F. Rosenberg and B. Devlin, "Future strategies in microbicide development.," *Best Pract. Res. Clin. Obstet. Gynaecol.*, vol. 26, no. 4, pp. 503–13, Aug. 2012.

[146] A. Akil, B. Devlin, M. Cost, and L. C. Rohan, "Increased Dapivirine tissue accumulation through vaginal film codelivery of dapivirine and Tenofovir.," *Mol. Pharm.*, vol. 11, no. 5, pp. 1533–41, May 2014.

[147] S. Di Fabio, J. Van Roey, G. Giannini, G. van den Mooter, M. Spada, A. Binelli, M. F. Pirillo, E. Germinario, F. Belardelli, M.-P. de Bethune, and S. Vella, "Inhibition of vaginal transmission of HIV-1 in hu-SCID mice by the non-nucleoside reverse transcriptase inhibitor TMC120 in a gel formulation.," *AIDS*, vol. 17, no. 11, pp. 1597–604, Jul. 2003.

[148] Prezista, "PREZISTA (darunavir) HIGHLIGHTS OF PRESCRIBING INFORMATION." .

[149] S. De Meyer, H. Azijn, D. Surleraux, D. Jochmans, A. Tahri, R. Pauwels, P. Wigerinck, and M.-P. de Béthune, "TMC114, a novel human immunodeficiency virus type 1 protease inhibitor active against protease inhibitor-resistant viruses, including a broad range of clinical isolates.," *Antimicrob. Agents Chemother.*, vol. 49, no. 6, pp. 2314–21, Jun. 2005.

[150] Y. Koh, S. Matsumi, D. Das, M. Amano, D. A. Davis, J. Li, S. Leschenko, A. Baldridge, T. Shioda, R. Yarchoan, A. K. Ghosh, and H. Mitsuya, "Potent inhibition of HIV-1 replication by novel non-peptidyl small molecule inhibitors of protease dimerization.," *J. Biol. Chem.*, vol. 282, no. 39, pp. 28709–20, Sep. 2007.

[151] N. M. King, M. Prabu-Jeyabalan, E. A. Nalivaika, P. Wigerinck, M.-P. de Béthune, and C. A. Schiffer, "Structural and thermodynamic basis for the binding of TMC114, a next-generation human immunodeficiency virus type 1 protease inhibitor.," *J. Virol.*, vol. 78, no. 21, pp. 12012–21, Nov. 2004.

[152] Y. Koh, H. Nakata, K. Maeda, H. Ogata, G. Bilcer, T. Devasamudram, J. F. Kincaid, P. Boross, Y.-F. Wang, Y. Tie, P. Volarath, L. Gaddis, R. W. Harrison, I. T. Weber, A. K. Ghosh, and H. Mitsuya, "Novel bis-tetrahydrofuranylurethane-containing nonpeptidic protease inhibitor (PI) UIC-94017 (TMC114) with potent activity against multi-PI-resistant human immunodeficiency virus in vitro.," *Antimicrob. Agents Chemother.*, vol. 47, no. 10, pp. 3123–9, Oct. 2003.

[153] M. Rittweger and K. Arasteh, "Clinical pharmacokinetics of darunavir.," *Clin. Pharmacokinet.*, vol. 46, no. 9, pp. 739–56, Jan. 2007.

[154] D. Back, V. Sekar, and R. M. W. Hoetelmans, "Darunavir: pharmacokinetics and drug interactions.," *Antivir. Ther.*, vol. 13, no. 1, pp. 1–13, 2008.

[155] B. Clotet, N. Bellos, J.-M. Molina, D. Cooper, J.-C. Goffard, A. Lazzarin, A. Wöhrmann, C. Katlama, T. Wilkin, R. Haubrich, C. Cohen, C. Farthing, D. Jayaweera, M. Markowitz, P. Ruane, S. Spinosa-Guzman, E. Lefebvre, and POWER 1 and 2 study groups, "Efficacy and safety of darunavir-ritonavir at week 48 in treatment-experienced patients with HIV-1 infection in POWER 1 and 2: a pooled subgroup analysis of data from two randomised trials.," *Lancet (London, England)*, vol. 369, no. 9568, pp. 1169–78, Apr. 2007.

[156] J. C. R. Corrêa, D. M. D'Arcy, C. H. dos R. Serra, and H. R. N. Salgado, "A Critical Review of Properties of Darunavir and Analytical Methods for Its Determination," *Crit. Rev. Anal. Chem.*, vol. 44, no. 1, pp. 16–22, Jan. 2014.

[157] D. L. N. G. Surleraux, A. Tahri, W. G. Verschueren, G. M. E. Pille, H. A. De Kock, T. H. M. Jonckers, A. Peeters, S. De Meyer, H. Azijn, R. Pauwels, M.-P. De Bethune, N. M. King, M. Prabu-Jeyabalan, C. A. Schiffer, and P. B. T. P. Wigerinck, "Discovery and Selection of TMC114, a Next Generation HIV-1 Protease Inhibitor."

[158] M. Boffito, A. Winston, A. Jackson, C. Fletcher, A. Pozniak, M. Nelson, G. Moyle, I. Tolowinska, R. Hoetelmans, D. Miralles, and B. Gazzard, "Pharmacokinetics and antiretroviral response to darunavir/ritonavir and etravirine combination in patients with high-level viral resistance.," *AIDS*, vol. 21, no. 11, pp. 1449–55, Jul. 2007.

[159] V. Sekar, D. Kestens, S. Spinosa-Guzman, M. De Pauw, E. De Paepe, T. Vangeneugden, E. Lefebvre, and R. M. W. Hoetelmans, "The effect of different meal types on the pharmacokinetics of darunavir (TMC114)/ritonavir in HIV-negative healthy volunteers.," *J. Clin. Pharmacol.*, vol. 47, no. 4, pp. 479–84, Apr. 2007.

[160] M. Boffito, E. Acosta, D. Burger, C. V Fletcher, C. Flexner, R. Garaffo, G. Gatti, M. Kurowski, C. F. Perno, G. Peytavin, M. Regazzi, and D. Back, "Current status and future prospects of therapeutic drug monitoring and applied clinical pharmacology in antiretroviral therapy.," *Antivir. Ther.*, vol. 10, no. 3, pp. 375–92, 2005.

[161] S. De Meyer, H. Azijn, D. Surleraux, D. Jochmans, A. Tahri, R. Pauwels, P. Wigerinck, and M.-P. de Bethune, "TMC114, a Novel Human Immunodeficiency Virus Type 1 Protease Inhibitor Active against Protease Inhibitor-Resistant Viruses, Including a Broad Range of Clinical Isolates," *Antimicrob. Agents Chemother.*, vol. 49, no. 6, pp. 2314–2321, Jun. 2005.

[162] M. Rittweger and K. Arasteh, "Clinical pharmacokinetics of darunavir.," *Clin. Pharmacokinet.*, vol. 46, no. 9, pp. 739–56, 2007.

[163] S. Lachau-Durand, P. Annaert, K. Steemans, B. Willems, G. Mannens, A. Raoof, and W. Meuldermans, "Transport characteristics of the HIV protease inhibitor darunavir (TMC114) in Caco-2 monolayers."

[164] M. Vermeir, S. Lachau-Durand, G. Mannens, F. Cuyckens, B. van Hoof, and A. Raoof, "Absorption, metabolism, and excretion of darunavir, a new protease inhibitor, administered alone and with low-dose ritonavir in healthy subjects.," *Drug Metab. Dispos.*, vol. 37, no. 4, pp. 809–20, Apr. 2009.

[165] K. McKeage, C. M. Perry, and S. J. Keam, "Darunavir: a review of its use in the management of HIV infection in adults.," *Drugs*, vol. 69, no. 4, pp. 477–503, Jan. 2009.

[166] C. Herrera, M. Cranage, I. McGowan, P. Anton, and R. J. Shattock, "Colorectal microbicide design: triple combinations of reverse transcriptase inhibitors are optimal against HIV-1 in tissue explants.," *AIDS*, vol. 25, no. 16, pp. 1971–9, Oct. 2011.

[167] P. K. Smith, R. I. Krohn, G. T. Hermanson, A. K. Mallia, F. H. Gartner, M. D. Provenzano, E. K. Fujimoto, N. M. Goeke, B. J. Olson, and D. C. Klenk, "Measurement of protein using bicinchoninic acid.," *Anal. Biochem.*, vol. 150, no. 1, pp. 76–85, Oct. 1985.

[168] "Guidance for Industry Bioanalytical Method Validation," 2001.

[169] J. W. M. Nissink, C. Murray, M. Hartshorn, M. L. Verdonk, J. C. Cole, and R. Taylor, "A new test set for validating predictions of protein-ligand interaction.," *Proteins*, vol. 49, no. 4, pp. 457–71, Dec. 2002.

[170] T. Darden, D. York, and L. Pedersen, "Particle mesh Ewald: An N·log(N) method for Ewald sums in large systems," *J. Chem. Phys.*, vol. 98, no. 12, p. 10089, Jun. 1993.

[171] J.-P. Ryckaert, G. Ciccotti, and H. J. . Berendsen, "Numerical integration of the cartesian equations of motion of a system with constraints: molecular dynamics of n-alkanes," *J. Comput. Phys.*, vol. 23, no. 3, pp. 327–341, Mar. 1977.

[172] D. A. Case, T. E. Cheatham, T. Darden, H. Gohlke, R. Luo, K. M. Merz, A. Onufriev, C. Simmerling, B. Wang, and R. J. Woods, "The Amber biomolecular simulation programs.," *J. Comput. Chem.*, vol. 26, no. 16, pp. 1668–88, Dec. 2005.

[173] D. Sitkoff, K. A. Sharp, and B. Honig, "Accurate Calculation of Hydration Free Energies Using Macroscopic Solvent Models," *J. Phys. Chem.*, vol. 98, no. 7, pp. 1978–1988, Feb. 1994.

[174] W. Wang and P. A. Kollman, "Free energy calculations on dimer stability of the HIV protease using molecular dynamics and a continuum solvent model.," *J. Mol. Biol.*, vol. 303, no. 4, pp. 567–82, Nov. 2000.

[175] J. Weiser, P. S. Shenkin, and W. C. Still, "Approximate atomic surfaces from linear combinations of pairwise overlaps (LCPO)," *J. Comput. Chem.*, vol. 20, no. 2, pp. 217–230, Jan. 1999.

[176] V. Tsui and D. A. Case, "Theory and applications of the generalized Born solvation model in macromolecular simulations.," *Biopolymers*, vol. 56, no. 4, pp. 275–91, Jan. .

[177] US Food and Drug administration (FDA), "Guidance for Industry Q2B Validation of Analytical Procedures: Methodology," 1996. [Online]. Available: http://www.fda.gov/cder/guidance/index.htm. [Accessed: 10-Sep-2016].

[178] M. D. Cummings, R. L. DesJarlais, A. C. Gibbs, V. Mohan, and E. P. Jaeger, "Comparison of automated docking programs as virtual screening tools.," *J. Med. Chem.*, vol. 48, no. 4, pp. 962–76, Feb. 2005.

[179] et al Pinto M, Robine-Leon S, Appay M-D, "Enterocyte-like differentation and polarization of the human colon carcinoma cell line Caco-2 in culture.," *Biol Cell.*, vol. 47, pp. 323–330, 1983.

[180] P. Artursson and J. Karlsson, "Correlation between oral drug absorption in humans and apparent drug permeability coefficients in human intestinal epithelial (Caco-2) cells," *Biochem. Biophys. Res. Commun.*, vol. 175, no. 3, pp. 880–885, Mar. 1991.

[181] E. H. Kerns, *et al.,* "Combined Application of Parallel Artificial Membrane Permeability Assay and Caco-2 Permeability Assays in Drug Discovery," *J. Pharm. Sci.*, vol. 93, no. 6, pp. 1440–1453, Jun. 2004.

[182] I. Behrens, *et al.,* "Variation of Peptide Transporter (PepT1 and HPT1) Expression in Caco-2 Cells as a Function of Cell Origin," *J. Pharm. Sci.*, vol. 93, no. 7, pp. 1743–1754, 1995.

[183] E. Walter and T. Kissel, "Heterogeneity in the human intestinal cell line Caco-2 leads to differences in transepithelial transport," *Eur. J. Pharm. Sci.*, vol. 3, no. 4, pp. 215–230, 1995.

[184] I. Behrens and T. Kissel, "Do cell culture conditions influence the carrier-mediated transport of peptides in Caco-2 cell monolayers?," *Eur. J. Pharm. Sci.*, vol. 19, no. 5, pp. 433–442, 2003.

[185] P. Anderle, *et al.*, "P-Glycoprotein (P-gp) Mediated Efflux in Caco-2 Cell Monolayers: The Influence of Culturing Conditions and Drug Exposure on P-gp Expression Levels," *J. Pharm. Sci.*, vol. 87, no. 6, pp. 757–762, Jun. 1998.

[186] M. Natoli, B. D. Leoni, I. D'Agnano, M. D'Onofrio, R. Brandi, I. Arisi, F. Zucco, and A. Felsani, "Cell growing density affects the structural and functional properties of Caco-2 differentiated monolayer.," *J. Cell. Physiol.*, vol. 226, no. 6, pp. 1531–43, Jun. 2011.

[187] Fda, Cder, and Omalleys, "Guidance for Industry Drug Interaction Studies — Study Design, Data Analysis, Implications for Dosing, and Labeling Recommendations," 2012. [Online]. Available: http://www.fda.gov/Drugs/GuidanceComplianceRegulatoryInformation/Guidances/default.htm. [Accessed: 16-Sep-2016].

[188] W. Chen, F. Tang, K. Horie, and R. T. Borchardt, "Caco-2 cell monolayers as a model for studeis of drug transport across human intestinal epithelium.," in *Cell Culture Models of Biological Barriers: In vitro Test Systems for Drug Absorption and Delivery*, Claus-Michael Lehr, Ed. 2002, pp. 143–164.

[189] L. Zhang, J. M. Strong, W. Qiu, L. J. Lesko, and S.-M. Huang, "Scientific Perspectives on Drug Transporters and Their Role in Drug Interactions," *Mol. Pharm*, vol. 3, no. 1, pp. 62–69, 2006.

[190] C. for D. E. and Research, "Drug Interactions & Labeling - Drug Development and Drug Interactions: Table of Substrates, Inhibitors and Inducers." Center for Drug Evaluation and Research.

[191] S. Spring, "Guidance for Industry M3(R2) Nonclinical Safety Studies for the Conduct of Human Clinical Trials and Marketing Authorization for Pharmaceuticals."

[192] A. P. Li, "Screening for human ADME/Tox drug properties in drug discovery," *Drug Discov. Today*, vol. 6, no. 7, pp. 357–366, 2001.

[193] M. Lakeram, D. J. Lockley, D. J. Sanders, R. Pendlington, and B. Forbes, "Paraben transport and metabolism in the biomimetic artificial membrane permeability assay (BAMPA) and 3-day and 21-day Caco-2 cell systems.," *J. Biomol. Screen.*, vol. 12, no. 1, pp. 84–91, Feb. 2007.

[194] G. Krishna, K. Chen, C. Lin, and A. A. Nomeir, "Permeability of lipophilic compounds in drug discovery using in-vitro human absorption model, Caco-2.," *Int. J. Pharm.*, vol. 222, no. 1, pp. 77–89, Jul. 2001.

[195] *Cell Culture Models of Biological Barriers: In vitro Test Systems for Drug Absorption and Delivery (Google eBook)*. CRC Press, 2003.

[196] D. A. I. Ashiru-Oredope, N. Patel, B. Forbes, R. Patel, and A. W. Basit, "The effect of polyoxyethylene polymers on the transport of ranitidine in Caco-2 cell monolayers.," *Int. J. Pharm.*, vol. 409, no. 1–2, pp. 164–8, May 2011.

[197] P. V Balimane, S. Chong, and R. A. Morrison, "Current methodologies used for evaluation of intestinal permeability and absorption," *J. Pharmacol. Toxicol. Methods*, vol. 44, no. 1, pp. 301–312, Jul. 2000.

[198] J. M. Marrazzo, G. Ramjee, B. A. Richardson, K. Gomez, N. Mgodi, G. Nair, T. Palanee, C. Nakabiito, A. van der Straten, L. Noguchi, C. W. Hendrix, J. Y. Dai, S. Ganesh, B. Mkhize, M. Taljaard, U. M. Parikh, J. Piper, B. Mâsse, C. Grossman, J. Rooney, J. L. Schwartz, H. Watts, M. A. Marzinke, S. L. Hillier, I. M. McGowan, and Z. M. Chirenje, "Tenofovir-Based Preexposure Prophylaxis for HIV Infection among African Women," *N. Engl. J. Med.*, vol. 372, no. 6, pp. 509–518, Feb. 2015.

[199] R. Mallants, K. Van Oosterwyck, L. Van Vaeck, R. Mols, E. De Clercq, and P. Augustijns, "Multidrug resistance-associated protein 2 (MRP2) affects hepatobiliary elimination but not the intestinal disposition of tenofovir disoproxil fumarate and its metabolites.," *Xenobiotica.*, vol. 35, no. 10–11, pp. 1055–66.

[200] Z. Neumanova, L. Cerveny, M. Ceckova, and F. Staud, "Interactions of tenofovir and tenofovir disoproxil fumarate with drug efflux transporters ABCB1, ABCG2, and ABCC2; role in transport across the placenta.," *AIDS*, vol. 28, no. 1, pp. 9–17, Jan. 2014.

[201] C. W. Hendrix, *et al.,* "MTN-001: Randomized Pharmacokinetic Cross-Over Study Comparing Tenofovir Vaginal Gel and Oral Tablets in Vaginal Tissue and Other Compartments," *PLoS One*, vol. 8, no. 1, p. e55013, Jan. 2013.

[202] A. S. Zidan, C. B. Spinks, M. J. Habib, and M. A. Khan, "Formulation and transport properties of tenofovir loaded liposomes through Caco-2 cell model.," *J. Liposome Res.*, vol. 23, no. 4, pp. 318–26, Dec. 2013.

[203] G. L. Amidon, H. Lennernäs, V. P. Shah, and J. R. Crison, "A theoretical basis for a biopharmaceutic drug classification: the correlation of in vitro drug product dissolution and in vivo bioavailability.," *Pharm. Res.*, vol. 12, no. 3, pp. 413–20, Mar. 1995.

[204] J. das Neves, F. Araújo, F. Andrade, J. Michiels, K. K. Ariën, G. Vanham, M. Amiji, M. F. Bahia, and B. Sarmento, "In Vitro and Ex Vivo Evaluation of Polymeric Nanoparticles for Vaginal and Rectal Delivery of the Anti-HIV Drug Dapivirine.," *Mol. Pharm.*, vol. 10, no. 7, pp. 2793–2807, Jun. 2013.

[205] P. Lewi, E. Arnold, K. Andries, H. Bohets, H. Borghys, A. Clark, F. Daeyaert, K. Das, M.-P. de Béthune, M. de Jonge, J. Heeres, L. Koymans, J. Leempoels, J. Peeters, P. Timmerman, W. Van den Broeck, F. Vanhoutte, G. Van't Klooster, M. Vinkers, Y. Volovik, and P. A. J. Janssen, "Correlations between factors determining the pharmacokinetics and antiviral activity of HIV-1 non-nucleoside reverse transcriptase inhibitors of the diaryltriazine and diarylpyrimidine classes of compounds.," *Drugs R. D.*, vol. 5, no. 5, pp. 245–57, Jan. 2004.

[206] C. Grammen, P. Augustijns, and J. Brouwers, "In vitro profiling of the vaginal permeation potential of anti-HIV microbicides and the influence of formulation excipients.," *Antiviral Res.*, vol. 96, no. 2, pp. 226–33, Nov. 2012.

[207] Y. Van Herrewege, J. Michiels, A. Waeytens, G. De Boeck, E. Salden, L. Heyndrickx, G. van den Mooter, M.-P. de Béthune, K. Andries, P. Lewi, M. Praet, and G. Vanham, "A dual chamber model of female cervical mucosa for the study of HIV transmission and for the evaluation of candidate HIV microbicides.," *Antiviral Res.*, vol. 74, no. 2, pp. 111–24, May 2007.

[208] B. A. Chen, L. Panther, M. A. Marzinke, C. W. Hendrix, C. J. Hoesley, A. van der Straten, M. J. Husnik, L. Soto-Torres, A. Nel, S. Johnson, N. Richardson-Harman, L. K. Rabe, and C. S. Dezzutti, "Phase 1 Safety, Pharmacokinetics, and Pharmacodynamics of Dapivirine and Maraviroc Vaginal Rings: A Double-Blind Randomized Trial.," *J. Acquir. Immune Defic. Syndr.*, vol. 70, no. 3, pp. 242–9, Nov. 2015.

[209] G. Krishna, K. Chen, C. Lin, and A. A. Nomeir, "Permeability of lipophilic compounds in drug discovery using in-vitro human absorption model, Caco-2," *Int. J. Pharm.*, vol. 222, no. 1, pp. 77–89, Jul. 2001.

[210] R. C. Rowe BPharm, P. J. Sheskey, Rp. Technical Services Leader, and S. C. Owen, "Handbook of Pharmaceutical Excipients."

[211] S. C. Shin and C. W. Cho, "Physicochemical characterizations of piroxicam-poloxamer solid dispersion.," *Pharm. Dev. Technol.*, vol. 2, no. 4, pp. 403–7, Nov. 1997.

[212] G. Dumortier, J. L. Grossiord, F. Agnely, and J. C. Chaumeil, "A Review of Poloxamer 407 Pharmaceutical and Pharmacological Characteristics," *Pharm. Res.*, vol. 23, no. 12, pp. 2709–2728, Nov. 2006.

[213] N. Holmstock, P. Annaert, and P. Augustijns, "Boosting of HIV protease inhibitors by ritonavir in the intestine: the relative role of cytochrome P450 and P-glycoprotein inhibition based on Caco-2 monolayers versus in situ intestinal perfusion in mice.," *Drug Metab. Dispos.*, vol. 40, no. 8, pp. 1473–7, Aug. 2012.

[214] P. Matsson, J. M. Pedersen, U. Norinder, C. A. S. Bergström, and P. Artursson, "Identification of novel specific and general inhibitors of the three major human ATP-binding cassette transporters P-gp, BCRP and MRP2 among registered drugs.," *Pharm. Res.*, vol. 26, no. 8, pp. 1816–31, Aug. 2009.

[215] A. Tseng and M. Foisy, "Important Drug-Drug Interactions in HIV-Infected Persons on Antiretroviral Therapy: An Update on New Interactions Between HIV and Non-HIV Drugs.," *Curr. Infect. Dis. Rep.*, vol. 14, no. 1, pp. 67–82, Feb. 2012.

[216] T. J. Johnson, K. M. Gupta, J. Fabian, T. H. Albright, and P. F. Kiser, "Segmented polyurethane intravaginal rings for the sustained combined delivery of antiretroviral agents dapivirine and tenofovir.," *Eur. J. Pharm. Sci.*, vol. 39, no. 4, pp. 203–12, Feb. 2010.

[217] A. Akil, B. Devlin, M. Cost, and L. C. Rohan, "Increased Dapivirine Tissue Accumulation through Vaginal Film Codelivery of Dapivirine and Tenofovir," *Mol. Pharm.*, vol. 11, no. 5, pp. 1533–1541, May 2014.

[218] S. M. Schader, M. Oliveira, R.-I. Ibanescu, D. Moisi, S. P. Colby-Germinario, and M. A. Wainberg, "In vitro resistance profile of the candidate HIV-1 microbicide drug dapivirine.," *Antimicrob. Agents Chemother.*, vol. 56, no. 2, pp. 751–6, Feb. 2012.

[219] U. M. Parikh, C. Dobard, S. Sharma, M. Cong, H. Jia, A. Martin, C.-P. Pau, D. L. Hanson, P. Guenthner, J. Smith, E. Kersh, J. G. Garcia-Lerma, F. J. Novembre, R. Otten, T. Folks, and W. Heneine, "Complete protection from repeated vaginal simian-human immunodeficiency virus exposures in macaques by a topical gel containing tenofovir alone or with emtricitabine.," *J. Virol.*, vol. 83, no. 20, pp. 10358–65, Oct. 2009.

[220] S. M. Fetherston, P. Boyd, C. F. McCoy, M. C. McBride, K.-L. Edwards, S. Ampofo, and R. K. Malcolm, "A silicone elastomer vaginal ring for HIV prevention containing two microbicides with different mechanisms of action.," *Eur. J. Pharm. Sci.*, vol. 48, no. 3, pp. 406–15, Feb. 2013.

[221] T. N. Kakuda, S. Abel, J. Davis, J. Hamlin, M. Schöller-Gyüre, R. Mack, N. Ndongo, W. Petit, C. Ridgway, V. Sekar, S. Tweedy, and R. M. W. Hoetelmans, "Pharmacokinetic interactions of maraviroc with darunavir-ritonavir, etravirine, and etravirine-darunavir-ritonavir in healthy volunteers: results of two drug interaction trials.," *Antimicrob. Agents Chemother.*, vol. 55, no. 5, pp. 2290–6, May 2011.

[222] C. C. Schuerer-Maly, L. Eckmann, M. F. Kagnoff, M. T. Falco, and F. E. Maly, "Colonic epithelial cell lines as a source of interleukin-8: stimulation by inflammatory cytokines and bacterial lipopolysaccharide.," *Immunology*, vol. 81, no. 1, pp. 85–91, Jan. 1994.

[223] J. Van De Walle, A. Hendrickx, B. Romier, Y. Larondelle, and Y.-J. Schneider, "Inflammatory parameters in Caco-2 cells: effect of stimuli nature, concentration, combination and cell differentiation.," *Toxicol. In Vitro*, vol. 24, no. 5, pp. 1441–9, Aug. 2010.

[224] R. N. Fichorova, L. D. Tucker, and D. J. Anderson, "The molecular basis of nonoxynol-9-induced vaginal inflammation and its possible relevance to human immunodeficiency virus type 1 transmission.," *J. Infect. Dis.*, vol. 184, no. 4, pp. 418–28, Aug. 2001.

[225] Y. Gali, O. Delezay, J. Brouwers, N. Addad, P. Augustijns, T. Bourlet, H. Hamzeh-Cognasse, K. K. Ariën, B. Pozzetto, and G. Vanham, "In vitro evaluation of viability, integrity, and inflammation in genital epithelia upon exposure to pharmaceutical excipients and candidate microbicides.," *Antimicrob. Agents Chemother.*, vol. 54, no. 12, pp. 5105–14, Dec. 2010.

[226] P. Saha and J. H. Kou, "Effect of solubilizing excipients on permeation of poorly water-soluble compounds across Caco-2 cell monolayers," *Eur. J. Pharm. Biopharm.*, vol. 50, no. 3, pp. 403–411, 2000.

[227] B. D. Rege, J. P. Y. Kao, and J. E. Polli, "Effects of nonionic surfactants on membrane transporters in Caco-2 cell monolayers.," *Eur. J. Pharm. Sci.*, vol. 16, no. 4–5, pp. 237–46, Sep. 2002.

[228] B. D. Rege, L. X. Yu, A. S. Hussain, and J. E. Polli, "Effect of Common Excipients on Caco-2 Transport of Low-Permeability Drugs," *J. Pharm. Sci.*, vol. 90, no. 11, pp. 1776–1786, 2001.

[229] R. G. Strickley, "Solubilizing excipients in oral and injectable formulations.," *Pharm. Res.*, vol. 21, no. 2, pp. 201–30, Feb. 2004.

[230] J. Goole, D. J. Lindley, W. Roth, S. M. Carl, K. Amighi, J.-M. Kauffmann, and G. T. Knipp, "The effects of excipients on transporter mediated absorption.," *Int. J. Pharm.*, vol. 393, no. 1–2, pp. 17–31, Jun. 2010.

[231] H. Zhang, M. Yao, R. A. Morrison, and S. Chong, "Commonly used surfactant, Tween 80, improves absorption of P-glycoprotein substrate, digoxin, in rats.," *Arch. Pharm. Res.*, vol. 26, no. 9, pp. 768–72, Sep. 2003.

[232] E.-M. Collnot, C. Baldes, M. F. Wempe, J. Hyatt, L. Navarro, K. J. Edgar, U. F. Schaefer, and C.-M. Lehr, "Influence of vitamin E TPGS poly(ethylene glycol) chain length on apical efflux transporters in Caco-2 cell monolayers," *J. Control. Release*, vol. 111, no. 1, pp. 35–40, 2006.

[233] A. Akil, M. A. Parniak, C. S. Dezzutti, B. J. Moncla, M. R. Cost, M. Li, and L. C. Rohan, "Development and characterization of a vaginal film containing dapivirine, a non-nucleoside reverse transcriptase inhibitor (NNRTI), for prevention of HIV-1 sexual transmission," *Drug Deliv. Transl. Res.*, vol. 1, no. 3, pp. 209–222, Jun. 2011.

[234] A. S. Ham, S. R. Ugaonkar, L. Shi, K. W. Buckheit, H. Lakougna, U. Nagaraja, G. Gwozdz, L. Goldman, P. F. Kiser, and R. W. Buckheit, "Development of a combination microbicide gel formulation containing IQP-0528 and tenofovir for the prevention of HIV infection.," *J. Pharm. Sci.*, vol. 101, no. 4, pp. 1423–35, Apr. 2012.

[235] W. Zhang, M. A. Parniak, S. G. Sarafianos, M. R. Cost, and L. C. Rohan, "Development of a vaginal delivery film containing EFdA, a novel anti-HIV nucleoside reverse transcriptase inhibitor," *Int. J. Pharm.*, vol. 461, pp. 203–213, 2014.

[236] FDA, "Guidance for Industry Bioanalytical Method Validation," 2001. [Online]. Available: http://www.fda.gov/downloads/Drugs/Guidance/ucm070107.pdf. [Accessed: 19-Sep-2016].

[237] K. Matsuo, H. Ota, T. Akamatsu, A. Sugiyama, and T. Katsuyama, "Histochemistry of the surface mucous gel layer of the human colon.," *Gut*, vol. 40, no. 6, pp. 782–9, Jun. 1997.

[238] G. B. Hatton, V. Yadav, A. W. Basit, and H. A. Merchant, "Animal Farm: Considerations in Animal Gastrointestinal Physiology and Relevance to Drug Delivery in Humans.," *J. Pharm. Sci.*, vol. 104, no. 9, pp. 2747–76, Sep. 2015.

[239] F. J. O. Varum, F. Veiga, J. S. Sousa, and A. W. Basit, "Mucus thickness in the gastrointestinal tract of laboratory animals.," *J. Pharm. Pharmacol.*, vol. 64, no. 2, pp. 218–27, Feb. 2012.

[240] S. Garg, K. Vermani, A. Garg, R. A. Anderson, W. B. Rencher, and L. J. D. Zaneveld, "Development and Characterization of Bioadhesive Vaginal Films of Sodium Polystyrene Sulfonate (PSS), a Novel Contraceptive Antimicrobial Agent," *Pharm. Res.*, vol. 22, no. 4, pp. 584–595, Apr. 2005.

[241] H. Lennernäs, "Human jejunal effective permeability and its correlation with preclinical drug absorption models.," *J. Pharm. Pharmacol.*, vol. 49, no. 7, pp. 627–38, Jul. 1997.

[242] A. L. Ungell, S. Nylander, S. Bergstrand, A. Sjöberg, and H. Lennernäs, "Membrane transport of drugs in different regions of the intestinal tract of the rat.," *J. Pharm. Sci.*, vol. 87, no. 3, pp. 360–6, Mar. 1998.

[243] V. Rozehnal, D. Nakai, U. Hoepner, T. Fischer, E. Kamiyama, M. Takahashi, S. Yasuda, and J. Mueller, "Human small intestinal and colonic tissue mounted in the Ussing chamber as a tool for characterizing the intestinal absorption of drugs.," *Eur. J. Pharm. Sci.*, vol. 46, no. 5, pp. 367–73, Aug. 2012.

[244] A.-L. Ungell, S. Nylander, S. Bergstrand, Å. Sjöberg, and H. Lennernäs, "Membrane Transport of Drugs in Different Regions of the Intestinal Tract of the Rat," *J. Pharm. Sci.*, vol. 87, no. 3, pp. 360–366, 1998.

[245] P. Nejdfors, M. Ekelund, B. Jeppsso, "Mucosal in Vitro Permeability in the Intestinal Tract of the Pig, the Rat, and Man: Species- and Region-Related Differences," *Scand. J. Gastroenterol.*, vol. 35, no. 5, pp. 501–507, Jan. 2000.

[246] W. Rubas, N. Jezyk, and G. M. Grass, "Comparison of the Permeability Characteristics of a Human Colonic Epithelial (Caco-2) Cell Line to Colon of Rabbit, Monkey, and Dog Intestine and Human Drug Absorption," *Pharm. Res.*, vol. 10, no. 1, pp. 113–118, 1993.

[247] B. I. Polentarutti, A. L. Peterson, A. K. Sjöberg, E. K. Anderberg, L. M. Utter, and A. L. Ungell, "Evaluation of viability of excised rat intestinal segments in the Ussing chamber: investigation of morphology, electrical parameters, and permeability characteristics.," *Pharm. Res.*, vol. 16, no. 3, pp. 446–54, Mar. 1999.

[248] B. Hoffmann, I. Nagel, and W. Clauss, "Aldosterone regulates paracellular pathway resistance in rabbit distal colon," *J Comp Physiol B J. Comp. Syst. Biochem. Environ-Physiology B m Physiol.*, vol. 160, pp. 381–388, 1990.

[249] D. J. Brayden and A. W. Baird, "A distinctive electrophysiological signature from the Peyer's patches of rabbit intestine.," *Br. J. Pharmacol.*, vol. 113, no. 2, pp. 593–9, Oct. 1994.

[250] Y. Rojanasakul, L. Wang, M. Bhat, D. D. Glover, C. J. Malanga, and J. K. H. Ma, "The Transport Barrier of Epithelia: A Comparative Study on Membrane Permeability and Charge Selectivity in the Rabbit," *Pharm. Res.*, vol. 09, no. 8, pp. 1029–1034, 1992.

[251] E. Sjögren, J. Eriksson, C. Vedin, K. Breitholtz, and C. Hilgendorf, "Excised segments of rat small intestine in Ussing chamber studies: A comparison of native and stripped tissue viability and permeability to drugs," *Int. J. Pharm.*, vol. 505, no. 1, pp. 361–368, 2016.

[252] Å. Sjöberg, M. Lutz, C. Tannergren, C. Wingolf, A. Borde, and A.-L. Ungell, "Comprehensive study on regional human intestinal permeability and prediction of fraction absorbed of drugs using the Ussing chamber technique," *Eur. J. Pharm. Sci.*, vol. 48, no. 1, pp. 166–180, 2013.

[253] F. Montanari and G. F. Ecker, "Prediction of drug-ABC-transporter interaction--Recent advances and future challenges.," *Adv. Drug Deliv. Rev.*, vol. 86, pp. 17–26, Jun. 2015.

[254] P. Matsson and C. A. S. Bergström, "Computational modeling to predict the functions and impact of drug transporters.," *silico Pharmacol.*, vol. 3, no. 1, p. 8, Dec. 2015.

[255] M. A. Demel, O. Krämer, P. Ettmayer, E. E. J. Haaksma, and G. F. Ecker, "Predicting ligand interactions with ABC transporters in ADME.," *Chem. Biodivers.*, vol. 6, no. 11, pp. 1960–9, Nov. 2009.

[256] L. Chen, Y. Li, H. Yu, L. Zhang, and T. Hou, "Computational models for predicting substrates or inhibitors of P-glycoprotein.," *Drug Discov. Today*, vol. 17, no. 7–8, pp. 343–51, Apr. 2012.

[257] G. F. Ecker, T. Stockner, and P. Chiba, "Computational models for prediction of interactions with ABC-transporters.," *Drug Discov. Today*, vol. 13, no. 7–8, pp. 311–7, Apr. 2008.

[258] C. A. McDevitt and R. Callaghan, "How can we best use structural information on P-glycoprotein to design inhibitors?," *Pharmacol. Ther.*, vol. 113, no. 2, pp. 429–41, Feb. 2007.

[259] A. B. Ward, P. Szewczyk, V. Grimard, C.-W. Lee, L. Martinez, R. Doshi, A. Caya, M. Villaluz, E. Pardon, C. Cregger, D. J. Swartz, P. G. Falson, I. L. Urbatsch, C. Govaerts, J. Steyaert, and G. Chang, "Structures of P-glycoprotein reveal its conformational flexibility and an epitope on the nucleotide-binding domain.," *Proc. Natl. Acad. Sci. U. S. A.*, vol. 110, no. 33, pp. 13386–91, Aug. 2013.

[260] Ajay and M. A. Murcko, "Computational methods to predict binding free energy in ligand-receptor complexes.," *J. Med. Chem.*, vol. 38, no. 26, pp. 4953–67, Dec. 1995.

[261] T. J. Raub, "P-Glycoprotein Recognition of Substrates and Circumvention through Rational Drug Design," *Mol. Pharm.*, vol. 3, no. 1, pp. 3–25, Feb. 2006.

[262] P. V Desai, G. A. Sawada, I. A. Watson, and T. J. Raub, "Integration of in silico and in vitro tools for scaffold optimization during drug discovery: predicting P-glycoprotein efflux.," *Mol. Pharm.*, vol. 10, no. 4, pp. 1249–61, Apr. 2013.

[263] G. Al-Jayyoussi, D. F. Price, D. Francombe, G. Taylor, M. W. Smith, C. Morris, C. D. Edwards, P. Eddershaw, and M. Gumbleton, "Selectivity in the impact of P-glycoprotein upon pulmonary absorption of airway-dosed substrates: a study in ex vivo lung models using chemical inhibition and genetic knockout.," *J. Pharm. Sci.*, vol. 102, no. 9, pp. 3382–94, Sep. 2013.

[264] M. V. S. Varma and R. Panchagnula, "Enhanced oral paclitaxel absorption with vitamin E-TPGS: effect on solubility and permeability in vitro, in situ and in vivo.," *Eur. J. Pharm. Sci.*, vol. 25, no. 4–5, pp. 445–53, Jan. 2005.

[265] A. M. Davis, S. J. Teague, and G. J. Kleywegt, "Application and limitations of X-ray crystallographic data in structure-based ligand and drug design.," *Angew. Chem. Int. Ed. Engl.*, vol. 42, no. 24, pp. 2718–36, Jun. 2003.

[266] V. Mohan, A. C. Gibbs, M. D. Cummings, E. P. Jaeger, and R. L. DesJarlais, "Docking: successes and challenges.," *Curr. Pharm. Des.*, vol. 11, no. 3, pp. 323–33, 2005.